IEEE Photonics Journal
An IEEE Photonics Society Publication

Breakthroughs in Photonics 2011

Photonics Materials and Engineered Photonic Structures

Nanophotonics · Biophotonics · Silicon Photonics

Coherent Photon Sources · Solid State Lighting

Integrated Photonic Systems · Photovoltaics

Sensors, Imaging, and Visualization

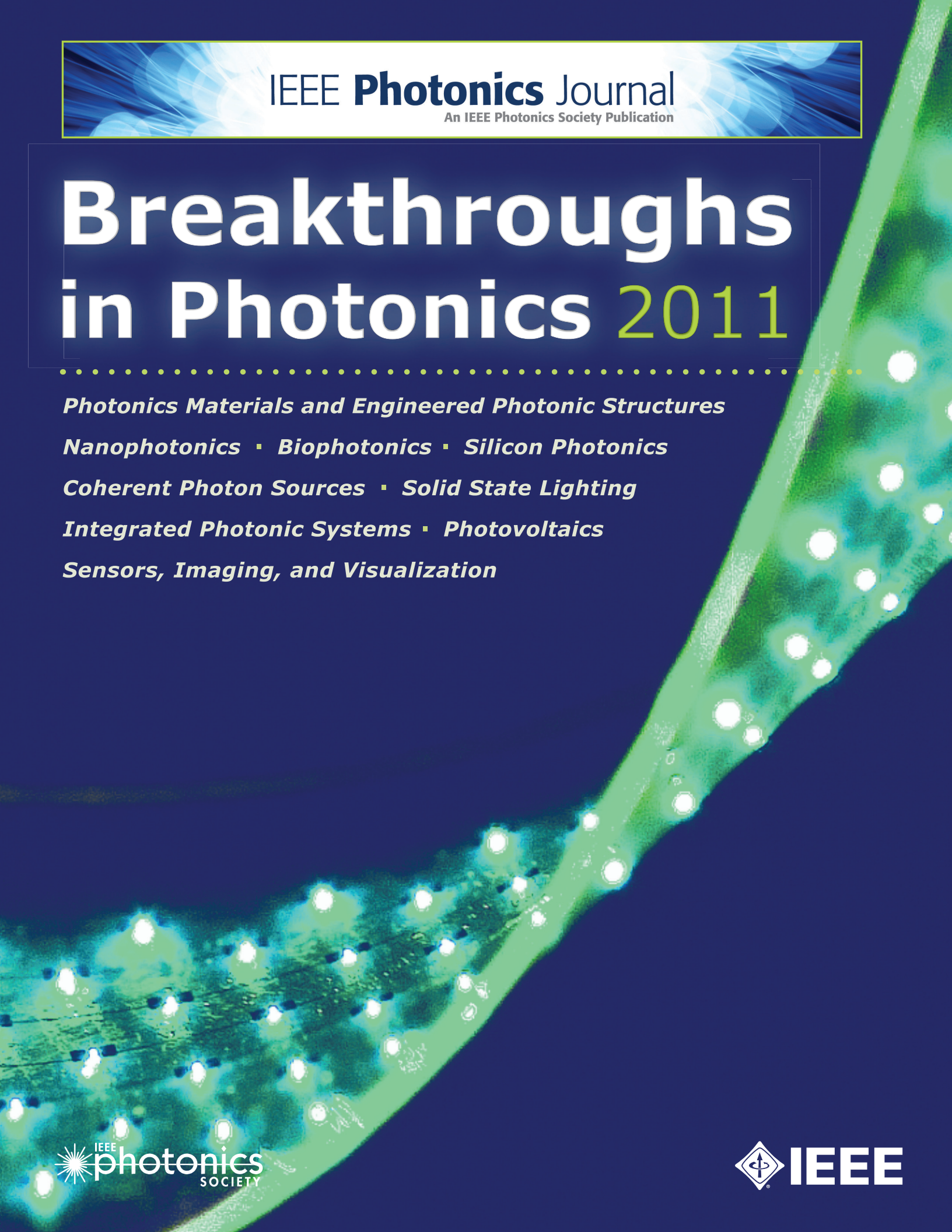

IEEE photonics SOCIETY

IEEE

Breakthroughs in Photonics 2011

Table of Contents

Solid-State Lightning

Photovoltaics

Sensors, Imaging and Visualization

Integrated Photonic Systems

Editorial

Breakthroughs in Photonics 2011

Breakthroughs in Photonics is a Special Issue of the IEEE PHOTONICS JOURNAL that contains a compilation of short reviews describing significant accomplishments in selected areas of Photonics within the last year.

Breakthroughs in Photonics 2011 is comprised of 19 invited comprehensive refereed reviews written by experts that cover progress in the following areas: ***Coherent Photon Sources, Photonics Materials and Engineered Photonic Structures, Nanophotonics, Biophotonics, Silicon Photonics, Solid-State Lighting, Photovoltaics, Sensors, Imaging and Visualization, and Integrated Photonic Systems***.

The selection of the topics that make up the Special Issue lies entirely with the Editorial Board of IEEE PHOTONICS JOURNAL. In a process that starts in December, the team identifies topics and experts in key areas of Photonics that mirror the scope of the JOURNAL. With the support of the editorial staff and the editorial office, *Breakthroughs in Photonics* is published online Open Access annually every April.

As a prelude to changes that are about to be implemented, I take this opportunity to announce that starting July 2012, IEEE PHOTONICS JOURNAL is moving to an "open access" publication model. Open access capabilities, coupled with an average time of 5 weeks from submission to online publishing, will provide authors with enhanced visibility and a much wider readership of their published articles.

I am grateful to the authors, the IEEE PHOTONICS JOURNAL editorial board and editorial staff, and IEEE Publications for their invaluable contributions to *Breakthroughs in Photonics 2011*.

Carmen S. Menoni, *Editor-In-Chief*

Breakthroughs in Semiconductor Lasers

Mark T. Crowley,[1] Vassilios Kovanis,[2] and Luke F. Lester,[1] *Senior Member, IEEE*

(Invited Paper)

[1]Center for High Technology Materials, University of New Mexico, NM 87106 USA
[2]Sensors Directorate, Air Force Research Laboratory, Wright-Patterson AFB, OH 45433 USA

DOI: 10.1109/JPHOT.2012.2190499

Manuscript received February 15, 2012; revised February 27, 2012; accepted March 6, 2012. Date of current version April 20, 2012. Corresponding author: M. T. Crowley (e-mail: mcrow80@unm.edu).

Abstract: The latest breakthroughs on the frontiers of semiconductor laser capabilities are presented. Achievements including the impressive advances in high-speed lasers with low pJ/bit energy consumption, high-power vertical external cavity surface emitting lasers (VECSELs), advances in III-nitrides, record-high temperature operation quantum dot lasers, the longest wavelength Type-I quantum well lasers to date, and the fascinating field of nanolasers with ultralow volume and threshold are all discussed.

Index Terms: Mid-infrared (IR) lasers, nanolasers, vertical cavity surface emitting lasers (VCSELs), semiconductor lasers, vertical external cavity surface emitting lasers (VECSELs), quantum dots (QDs), III-nitrides.

This review covers some of the most notable advances for semiconductor lasers in 2011. In particular, the latest results on high-power vertical external cavity surface emitting lasers (VECSELs) are reviewed with an emphasis on heat management. In terms of low-dimensional semiconductor lasers, the impressive performance of high-temperature ridge-waveguide quantum dot (QD) lasers is highlighted. Advances in the field of mid-IR lasers is also visited as well as breakthrough results pertaining to nanoscale lasers including bottom-up and top-down fabricated devices. Breakthroughs associated with the III-nitride material system are also addressed. First, we begin by reviewing the most significant results for high-speed and energy-efficient vertical cavity surface emitting lasers (VCSELs).

With what seems like an insatiable demand for faster access to information by modern society, so comes the inevitable need for the rapid and efficient transfer of data. It is expected that optical interconnects at the chip level are needed within a decade. The VCSEL is one of the candidates being touted as the light source to meet this challenge [1]. At the standard local area network (LAN) wavelength of 850 nm, high speeds reaching 40 Gbit/s have already been reported [2]. In parallel, there has been an impetus to move to longer wavelengths such as 980 nm an 1100 nm. Typically, VCSELs emitting at these wavelengths are based on compressively strained InGaAs quantum wells which have the advantage of higher differential gains and relaxation resonance frequencies and, therefore, the possibility of larger bandwidths. At 980 nm, the Technical University of Berlin has demonstrated error-free nominal data transmission rates of 40 Gbit/s up to temperatures of 85 °C, the highest data rates reported for VCSELs to date [3]. The origin of the improved performance has been cited as arising from a combination of several factors including optimized doping profiles and gain-cavity detuning, a binary GaAs bottom mirror and a shortened $\lambda/2$ cavity.

Currently, in terms of the energy-efficiencies required of optical interconnects in data centers, the International Technology Roadmap for Semiconductors demands lasers which exhibit a dissipated energy/bit in the region of ~100 fJ/bit (100 mW/Tb/s) [4]. Previous research has shown that sub 500 fJ/bit performances can be achieved using standard VCSEL technology at 980 nm and at 850 nm [5]. Research on such energy-efficient light sources in 2011 has been intense with Furukawa Electric Co. demonstrating 140-fJ/bit operation at a data rate of 10 Gbit/s at 1060 nm [6]. The real breakthrough in low power consumption VCSELs has been pioneered by a collaboration between the Technical University of Berlin and VI Systems GmbH from which the first sub 100 fJ/bit results have emerged. This result represents the most power efficient high-speed directly modulated light sources to date and were based on oxide confined GaAs-based VCSELs. The devices emit at 850 nm and operate at 17 Gb/s and the energy to data rate ratio ranges from 81–83 fJ/bit, while at 25 Gb/s, it becomes 99-117 fJ/bit for temperatures of 25 °C to 55 °C, respectively [5]. The impressive strides in energy-efficiency have been associated with reducing the operating currents through an optimization of the mirror doping profiles with a resultant reduction in the internal losses.

The lure of the VECSEL stems from its exceptional beam quality and high output powers coupled with a wavelength range spanning the infrared spectrum all the way to the visible [7]. The latter wavelengths are generated via nonlinear optical elements placed within the VECSEL cavity through frequency doubling and quadrupling. As a consequence of this flexibility, applications are wide, encompassing, for example, laser radar systems, chemical sensing and infrared countermeasures. Additionally, near-IR QD-based VECSELs can be used to provide high power at 1200–1280 nm [8], which is suitable for noninvasive selective photothermolysis of adipose tissue [9] or which can be frequency-doubled to reach red light for laser TV. In general, heat management has been the key focus in driving improvements in output power [7], [10]. The VECSEL is typically bonded using indium solder to a high thermal conductivity heat spreader such as diamond. The highest power to date of 100 W, reported in 2011 was achieved through a collaboration between researchers at the University of Arizona and Phillips University in Marburg based on 1040-nm InGaAs quantum wells [11].

The VCSEL was the first laser with a wavelength scale optical mode. Now stellar progress has been accomplished worldwide in the miniaturization of lasers in just the past few years using metals to form the laser resonator. Due to the small size and strong confinement in these laser structures, certain familiar concepts in semiconductor-laser physics needed to be carefully examined to determine their validity or implications at the nanoscale; therefore a new generation of laser designers had to get educated on the fundamentals of laser quantum engineering[1] [12], [13]. A portion of these devices now show lasing in cavities significantly smaller than the wavelength of light in all three dimensions with the optical mode being much smaller than what is permitted by the diffraction limit. For instance, the first report of lasing in metallic nanostructures occurred in 2007 and now this research area has exploded with various groups reporting impressive results based on plasmonic and metal-cavity nanolasers [12], [14]. Electrical injection of metal cavity lasers with a dimension less than a wavelength in one or two dimensions has also been demonstrated. Other approaches for nanolasers including cavities based on coaxial waveguides have been realized with thresholdless lasing operation at ~1370 nm in a single mode coaxial cavity of subwavelength size at cryogenic temperatures [15]. Nanolasers formed from top-down or bottom-up processed wires fabricated in a variety of material systems have made notable progress in recent months. As shown in Fig. 1(a), top-down GaN nanowire lasers emitting at 370 nm have achieved single-mode operation for a cavity with a diameter of 130 nm and a length of 4.7 μm [16]. The optically pumped laser threshold is about 250 kW/cm^2. The bottom-up GaAs/InGaAs/GaAs nanopillars shown in Fig. 1(b) are encased in an InGaP shell and are arrayed to simultaneously form a photonic band gap and the laser gain region [17]. The lasers operate single-mode at room temperature with an optically pumped threshold of 625 W/cm^2. MOCVD-grown InGaAs nanopilllars lasers emitting at 950 nm have also been achieved on a silicon substrate [18]. These lasers, which are particularly

[1]Such developments were supported by the DARPA Nanoscale Architecture for Coherent Hyper-Optic Sources (NACHOS) program established by the late H. Temkin.

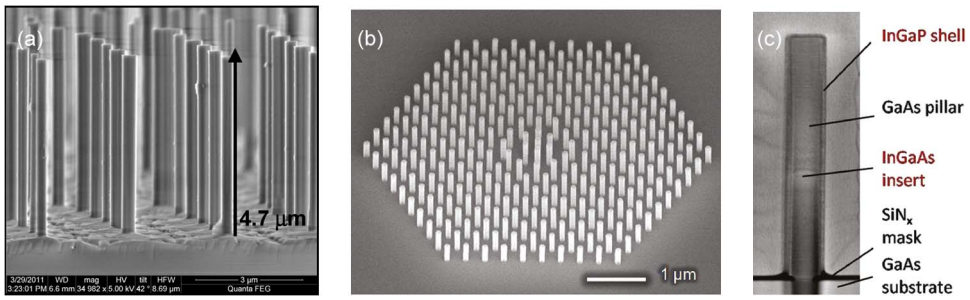

Fig. 1. (a) SEM of top-down GaN nanowire array (courtesy of Sandia National Labs), (b) bottom-up fabricated GaAs nanopillars and (c) cross-sectional STEM of a nanopillar showing the InGaAs insert located at the center of the pillar and InGaP shell (reprinted from [17] with permission from the ACS).

suited for high-density integration with CMOS electronics, depend on a helically propagating cavity mode in a subwavelength size cross-sectional pillar.

Historically, the emission wavelength range between 3–4 μm has been a graveyard for the semiconductor laser. Three different technologies currently compete in this arena including quantum cascade lasers (QCL), interband cascade lasers (ICL), and Type-I quantum well lasers, which are expertly compared in [19]. Progress in extending the wavelength of emission for Type-I quantum well lasers on GaSb substrates has been remarkable [20]. The most recent success comes from the Walter Schottky Institute which has achieved room temperature pulsed-mode lasing at 3.73 μm [21]. The authors attribute the extended wavelength performance to the use of quinternary AlGaInAsSb barriers around a 1.46% strained GaInAsSb quantum well. Potential applications include atmospheric monitoring for such gases as ozone, sulfur dioxide, and methane in the water-free absorption window. Strain-compensated InGaAs/AlAsSb QCLs on InP substrate have demonstrated wavelengths as short as 3.05 μm at 295K. For longer emission from 3.3–3.7 μm, QCLs have exhibited up to 20W output power at 285K, showing their clear advantage is output power in this wavelength range [22]. Regarding a viable source of THz radiation, THz QCLs operating significantly above the temperature limit (photon energy/Boltzmann constant) have been reported. These and other recent advances on Terahertz QCLs are extensively reviewed in [23].

GaN and its alloys have become the standard material system used for producing short-wavelength visible light-emitting devices; however, this material system has not come without its challenges. Charge separation effects have plagued InGaN QW lasers. Traditional c-plane InGaN QWs with large overlap design have been adopted for addressing the charge separation effect by exploiting staggered InGaN QWs [24]. Lasing performance comparable with the state-of-the-art conventional c-plane InGaN QW lasers has now also been attained in nonpolar/semipolar InGaN QW lasers [25]. There has been no electrically injected laser devices realized in the deep-UV to mid-UV laser wavelength regime ($\sim$220–320 nm). The challenges associated with these impediments are rooted in an insufficient understanding of the gain properties of the active region as well as challenges in material epitaxy. Nonetheless, in recent years, considerable theoretical progress has been made in understanding of the gain properties of high Al-content AlGaN QWs for deep UV lasers. Leveraging on these foundations, Taniyasu et al. have experimentally demonstrated a significant TE gain at deep-UV wavelengths based on AlN-delta-GaN QWs [26]. In related work, substantial results have been reported for current-injected GaN-based VCSELs based on a combination of hybrid dielectric DBRs and epitaxially grown DBRs [27].

Finally, one of the perpetual challenges since the inception of the semiconductor laser has been the ability to operate at high temperature. Recently, QD Laser Inc. has reported on a 1.2-mm-long QD edge-emitting ridge waveguide laser capable of ground state lasing up to 220 °C while at the same time maintaining 1 mW of output optical power [28]. This feat makes it the highest operating temperature for any commercially available semiconductor laser. The realization of such performance required a combination of a reduced dot dispersion and increased areal dot density. The device also featured high-reflectivity coatings on both laser facets. The optimized material epilayers

consisted of eight InAs QD layers, featuring a dot density of 5.9×10^{10} cm^{-2} in each stack, and included partially *p*-doped GaAs barriers. In addition, because the ground state and first excited state were separated by a large amount (80 meV), excited state lasing at very high temperatures was suppressed. Potential hot environment applications include oil and gas exploration, as well as incorporation in energy-efficient optical interconnects.

References

[1] F. Koyama, "Recent advances of VCSEL photonics," *J. Lightwave Technol.*, vol. 24, no. 12, pp. 4502–4513, Dec. 2006.

[2] P. Westbergh, J. S. Gustavsson, B. Kogel, A. Haglund, A. Larsson, A. Mutig, A. Nadtochiy, D. Bimberg, and A. Joel, "40 Gbit/s error free operation of oxide-confined 850 nm VCSEL," *Electron. Lett.*, vol. 46, no. 14, pp. 1014–1016, Jul. 2010.

[3] W. Hofmann, P. Moser, P. Wolf, A. Mutig, M. Kroh, and D. Bimberg, "44 Gb/s VCSEL for optical interconnects," presented at the Proc. OFC/NFOEC, Los Angeles, CA, Mar. 2011, Paper PDPC5.

[4] International Technology Roadmap for Semiconductors, 2007 ed. [Online]. Available: http://www.itrs.net/Links/2007ITRS/ExecSum2007.pdf

[5] P. Moser, W. Hofmann, P. Wolf, J. A. Lott, G. Larisch, A. Payusov, N. N. Ledentsov, and D. Bimberg, "81 fJ/bit energy-to-data ratio of 850 nm vertical-cavity surface-emitting lasers for optical interconnects," *Appl. Phys. Lett.*, vol. 98, no. 23, p. 231 106, Jun. 2011.

[6] S. Imai, K. Takaki, S. Kamiya, H. Shimizu, J. Yoshida, Y. Kawakita, T. Takagi, K. Hiraiwa, T. Suzuki, N. Iwai, T. Ishikawa, N. Tsukiji, and A. Kasukawa, "Recorded low power dissipation in highly reliable 1060-nm VCSELs for 'Green' optical interconnection," *IEEE J. Sel. Topics Quantum Electron.*, vol. 17, no. 6, pp. 1614–1620, Nov./Dec. 2011.

[7] R. G. Bedford, T. Dang, and D. Tomich, "Recent VECSEL developments for sensors applications," in *Proc. VECSELs II, Photon. West*, 2012, p. 82420W.

[8] A. R. Albrecht, A. Stintz, F. T. Jaeckel, T. J. Rotter, P. Ahirwar, V. J. Patel, C. P. Hains, L. F. Lester, K. J. Malloy, and G. Balakrishnan, "1220–1280-nm optically pumped InAs quantum Dot-based vertical external-cavity surface-emitting laser," *IEEE J. Sel. Topics Quantum Electron.*, vol. 17, no. 6, pp. 1787–1793, Nov./Dec. 2011.

[9] M. Wanner, M. Avram, D. Gagnon, M. C. Mihm, Jr., D. Zurakowski, K. Watanabe, Z. Tannous, R. R. Anderson, and D. Manstein, "Effects of non-invasive, 1210-nm laser exposure on adipose tissue: Results of a human pilot study," *Lasers Surg. Med.*, vol. 41, no. 6, pp. 401–407, Aug. 2009.

[10] S. Chatterjee, A. Chernikov, J. Herrmann, M. Scheller, M. Koch, B. Kunert, W. Stolz, S. W. Koch, T. L. Wang, Y. Kaneda, J. M. Yarborough, J. Hader, and J. V. Moloney, "Power scaling and heat management in high-power VECSELs," in *Proc. CLEO EUROPE/EQEC*, May 2011, p. 1.

[11] J. V. Moloney, J. Hader, T.-L. Wang, Y. Ying, Y. Kaneda, J. M. Yarborough, T. J. Rotter, G. Balakrishnan, C. Hains, S. W. Koch, W. Stolz, B. Kunert, and R. Bedford, "Power scaling of cw and pulsed IR and mid-IR OPSLs," in *Proc. SPIE*, 2011, vol. 7919, p. 79190S.

[12] C. Z. Ning, "Semiconductor nanolasers," *Phys. Stat. Sol. (B)*, vol. 247, no. 4, pp. 774–788, Apr. 2010.

[13] M. I. Stockman, "Nanoplasmonics: Past, present, and glimpse into future," *Opt. Exp.*, vol. 19, no. 22, pp. 22 029–22 106, Oct. 2011.

[14] M. T. Hill, "Status and prospects for metallic and plasmonic nano-lasers," *J. Opt. Soc. Amer. B.*, vol. 27, no. 11, pp. B36–B44, Nov. 2010.

[15] M. Khajavikhan, M. Katz, A. Simic, J. H. Lee, B. Slutsky, A. Mizrahi, V. Lomakin, and Y. Fainman, "Thresholdless nanoscale coaxial lasers," in *Proc. IEEE Photon. Conf.*, Arlington, VA, Oct. 2011. [Online]. Available: http://ieeexplore.ieee.org/stamp/stamp.jsp?tp=&arnumber=6110394

[16] J. B. Wright, Q. M. Li, T. S. Luk, I. Brener, G. T. Wang, K. R. Westlake, and L. F. Lester, "Single-mode lasing from top-down fabricated gallium nitride nanowires," in *Proc. IEEE Photon. Conf.*, Arlington, VA, Oct. 2011, pp. 529–530.

[17] A. C. Scofield, S.-H. Kim, J. N. Shapiro, A. Lin, B. Liang, A. Scherer, and D. L. Huffaker, "Bottom-up photonic crystal lasers," *Nano Lett.*, vol. 11, no. 12, pp. 5387–5390, Dec. 2011.

[18] R. Chen, T.-T. D. Tran, K. W. Ng, W. S. Ko, L. C. Chuang, F. G. Sedgwick, and C. Chang-Hasnain, "Nanolasers grown on silicon," *Nat. Photon.*, vol. 5, no. 3, pp. 170–175, Mar. 2011.

[19] A. Bauer, K. Röner, T. Lehnhardt, M. Kamp, S. Höfling, L. Worschech, and A. Forchel, "Mid-infrared semiconductor heterostructure lasers for gas sensing applications," *Semicond. Sci. Technol.*, vol. 26, no. 1, p. 014032, Jan. 2011.

[20] G. Belenky, L. Shterengas, G. Kipshidze, and T. Hosoda, "Type-I diode lasers for spectral region above 3 μm," *IEEE J. Sel. Topics Quantum Electron.*, vol. 17, no. 5, pp. 1426–1434, Sep./Oct. 2011.

[21] K. Vizbaras and M.-C. Amann, "Room-temperature 3.73 μm GaSb-based type-I quantum-well lasers with quinternary barriers," *Semicond. Sci. Technol.*, vol. 27, no. 3, p. 032001, Mar. 2012.

[22] D. G. Revin, J. P. Commin, S. Y. Zhang, A. B. Krysa, K. Kennedy, and J. W. Cockburn, "InP-based midinfrared quantum cascade lasers for wavelengths below 4 μm," *IEEE J. Sel. Topics Quantum Electron.*, vol. 17, no. 5, pp. 1417–1425, Sep./Oct. 2011.

[23] S. Kumar, "Recent progress in TeraHertz quantum cascade lasers," *IEEE J. Sel. Topics Quantum Electron.*, vol. 17, no. 1, pp. 38–47, Jan./Feb. 2011.

[24] H. Zhao, G. Liu, J. Zhang, J. D. Poplawsky, V. Dierolf, and N. Tansu, "Approaches for high internal quantum efficiency green InGaN light-emitting diodes with large overlap quantum wells," *Opt. Exp.*, vol. 19, no. Suppl. 4, pp. A991–A1007, Jul. 2011.

[25] R. M. Farrell, D. A. Haeger, P. S. Hsu, K. Fujito, D. F. Feezell, S. P. DenBaars, J. S. Speck, and S. Nakamura, "Determination of internal parameters for AlGaN-cladding-free m-plane InGaN/GaN laser diodes," *Appl. Phys. Lett.*, vol. 99, no. 17, p. 171 115, Oct. 2011.

[26] Y. Taniyasua and M. Kasu, "Polarization property of deep-ultraviolet light emission from C-plane AlN/GaN short-period superlattices," *Appl. Phys. Lett.*, vol. 99, no. 25, p. 251 112, Dec. 2011.
[27] T.-C. Lu, T.-T. Wu, S.-W. Chen, P.-M. Tu, Z.-Y. Li, C.-K. Chen, C.-H. Chen, H.-C. Kuo, S.-C. Wang, H.-W. Zan, and C.-Y. Chang, "Characteristics of current-injected GaN-based vertical-cavity surface-emitting lasers," *IEEE J. Sel. Topics Quantum Electron.*, vol. 17, no. 6, pp. 1594–1602, Nov./Dec. 2011.
[28] QD Laser Inc: Laser Focus World, *Quantum Dot Laser Operates at Startlingly High Temperatures,* vol. 47, p. 9, 2011.

Photonic Free-Electron Lasers

P. J. M. van der Slot, T. Denis, J. H. H. Lee, M. W. van Dijk, and K. J. Boller

(Invited Paper)

Laser Physics and Nonlinear Optics, Mesa+ Institute for Nanotechnology, Department of Science and Technology, University of Twente, 7500 Enschede, The Netherlands

DOI: 10.1109/JPHOT.2012.2190724
1943-0655/$31.00 ©2012 IEEE

Manuscript received February 16, 2012; revised March 7, 2012; accepted March 7, 2012. Date of current version April 20, 2012. This work was supported by the Dutch Technology Foundation STW, applied science division of NWO, and the technology program of the Dutch Ministry of Economic Affairs.
Corresponding author: P. J. M. van der Slot (e-mail: p.j.m.vanderslot@utwente.nl).

Abstract: A photonic free-electron laser (pFEL) produces coherent Cerenkov radiation from a set of parallel electron beams streaming through a photonic crystal. The function of the crystal is to slow down the phase velocity of a copropagating electromagnetic wave, such that also mildly relativistic electrons (of about 10-keV energy) can emit coherent Cerenkov radiation. Starting from spontaneous emission, the feedback of the radiation on the electrons results in bunching of the electrons on the scale of the radiation wavelength, and consequently, coherent radiation can build up. The frequency of the coherent mode is set by the electron velocity and wave dispersion of the photonic crystal and can, *a priori*, be continuously varied by varying the electron energy. The scale invariance of Maxwell's equation allows operation from Gigahertz to Terahertz and possible infrared (IR) frequencies without the need to increase the electron beam energy. Therefore, the pFEL is a very attractive, compact, and coherent radiation source that has the potential to significantly enhance the power available in the THz domain.

Index Terms: Free-electron lasers, photonic crystal, slow light, light source, oscillator.

Photonic crystals are structures with a periodically varying dielectric constant that show a strong interaction with light having a wavelength comparable to this periodicity [1]. Such a crystal allows an unprecedented control of light propagation and emission [2]–[4]. A most intriguing capability of photonic crystals is to shape the local density of electromagnetic states (LDOS) inside the crystal, which, e.g., can be used to suppress or enhance spontaneous emission [3]–[5] or be used to study fundamental strong-coupling cavity quantum electrodynamics experiments [6].

Of particular interest is the emission of Cerenkov radiation by a charged particle moving through a photonic crystal [7]. For example, it was shown that, contrary to ordinary Cerenkov emission in bulk material, distinctive, particle velocity dependent, radiation patterns are generated without a velocity threshold, which can be used for, e.g., particle detection. On the other hand, electron energy loss spectroscopy enables measurement of the photonic band structure and LDOS [8], [9]. Here, a low-energy electron beam from a transmission electron microscope is sent at various positions through a photonic crystal, and electrons lose energy through coupling to the crystal eigenmodes, among others via Cerenkov radiation [9]. Recently, spontaneous Cerenkov radiation was observed from a nanostructured light well [10], where a low-energy electron beam (20–40 keV) was sent through a 700-nm-diameter hole in a 1-D photonic crystal consisting of a stack of 11 alternating metal and dielectric layers, each having a thickness of 200 nm. By changing the electron beam energy, the

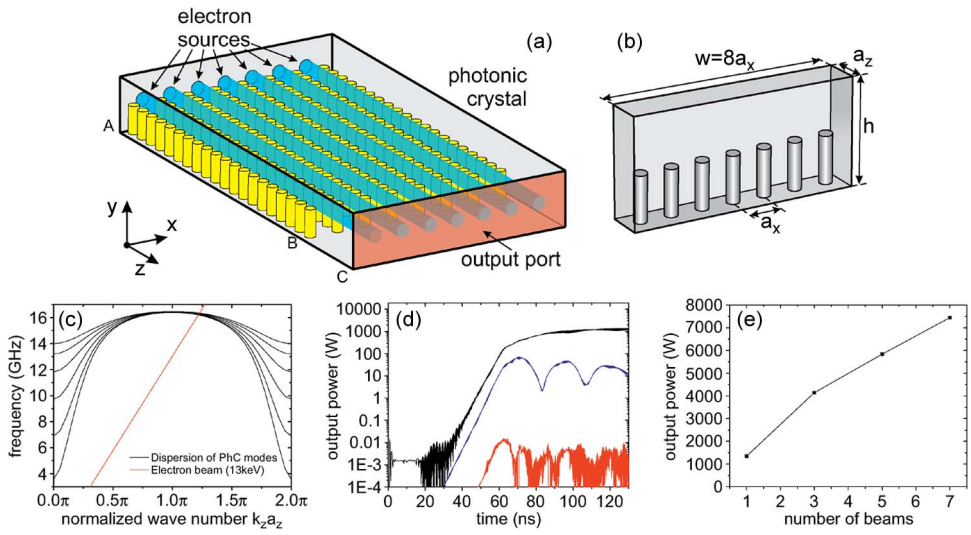

Fig. 1. (a) Schematic view of a pFEL oscillator. The photonic crystal consists of a 2-D array of round truncated posts in a rectangular waveguide. (b) Unit cell for the photonic crystal: $a_x = 4.2$ mm, $h = 8$ mm, and $a_z = 2.5$ mm. The height of the posts is 0.5 h, and the radius is 0.75 mm. (c) The band diagram calculated for the unit cell (b), showing only the lowest six modes. Also shown is the dispersion of a 13-keV electron beam. (d) Output power for the first three nonzero waveguide modes at the output port when the pFEL is pump with a single electron beam in the center. (e) Output power in the TE_{10} mode as a function of the number of electron beams. Current and voltage for each beam as in (d).

emission wavelength could be tuned from 750 to 840 nm. Due to the small current ($\leq$ 20 nA), only spontaneous radiation of about 0.2 nW was observed.

The concept of the photonic free-electron laser (pFEL) aims at the generation of coherent Cerenkov radiation from electrons streaming through straight and parallel vacuum channels in a photonic crystal [e.g., see Fig. 1(a)], which requires a sufficiently high total current and a sufficiently long crystal [10]. The pFEL allows scaling of the total current by providing many parallel electron beams without the need to increase the local current density in each individual beamlet. This not only controls the gain of the laser and allows scaling of the output power, but also, low-voltage ($\sim$10 kV), multibeam electron guns can be used that leads to compact devices, in contrast with other research [11]. Longitudinal coherence in each beamlet of a pFEL is established when the electron velocity approximately equals the phase velocity of a photonic crystal eigenmode, which possesses a longitudinal electric field component. This electric field component bunches the electrons on the scale of the radiation wavelength, thus providing longitudinal coherence in a way similar to the bunching in free-electron lasers [12], [13] and microwave tubes [13]. Transverse coherence is achieved by engineering the photonic crystal to provide coupling between neighboring channels, i.e., the electron beamlets communicate with each other through a common electromagnetic field. In this way, the bunching within the beamlets is phase locked, and despite the extended transverse interaction area, a coherent transverse field is developed, similar to the way supermodes are developed in coupled diode laser arrays [14].

Most pFEL devices use a photonic crystal similar to Fig. 1(a) with the unit cell shown in Fig. 1(b) [15]–[17]. The device of Fig. 1(a) allows multiple electron beams to propagate through the photonic crystal. The photonic crystal consists of a 2-D array of half-height cylindrical metal posts in a metallic rectangular waveguide. The half-height posts maximize the field strength of the resonant spatial harmonic at the position of the electron beam while, at the same time, maintaining a large tuning range [15] [see Fig. 1(c)]. A resonator is formed by a flat metallic mirror at location A and the partial reflecting mirror formed by the transition of the photonic crystal into an empty waveguide at location B. Alternatively, by tapering either the height of the posts or tapering the transverse distance between the posts in case of a single beam device, a low reflecting gain section can be realized [18]. Fig. 1(c) shows the band structure for the six lowest modes for the first Brillouin zone

calculated from the unit cell using an eigenmode solver (CST Microwave Studio). Also shown in Fig. 1(c) is the dispersion of a 13-kV electron beam. At the intersection point, the electron velocity equals the wave phase velocity and this point defines the approximate operating frequency of the device ($\sim$16.3 GHz). Note that for these settings the interaction is at the first spatial harmonic of the Bloch eigenmodes and that the interaction is of a backward-wave type. Also, from the wave dispersion, it is expected that the laser frequency tunes up with increasing electron accelerating voltage.

A particle-in-cell (PIC) simulation code is generally used to numerically analyze the performance of pFELs [15], [18], [19]. For the example shown in Fig. 1, several electron beams are injected into the resonator by placing electron sources on the surface of mirror A [see Fig. 1(a)]. The radiation that is coupled out of the resonator propagates to the nonreflecting waveguide port at C [see Fig. 1(a)]. Here, the radiation is decomposed into eigenmodes of the port. As a preliminary result of the PIC simulations (CST Particle Studio), Fig. 1(d) shows the temporal evolution of the three lowest *TE* eigenmodes of the port when the pFEL is driven by a single 13-kV, 1-A (32 A/cm^2) electron beam in the center. Initially, the output power in each mode is weak and noisy, but then, exponential growth ($\sim$1.5 dB/ns) over several orders of magnitude sets in. The fundamental TE_{10} mode is clearly dominant and saturates at a level of about 1.4 kW, and the mode suppression is then at least 20 dB. The output frequency is 15.88 GHz with a full width half maximum (FWHM) of 50 MHz. When the number of electron beams is increased from 1 to 7 by turning on two adjacent beams until all available electron beam channels are occupied, we observe an almost linear increase in output power of the fundamental TE_{10} mode, as is shown in Fig. 1(e). The center frequency, FWHM width, and mode suppression remain unchanged when the total beam current is increased from 1 to 7 A [19]. This preliminary result illustrates the possibility to scale the power of a pFEL by adding more electron beams in parallel, while maintaining a single coherent output mode, even when the output waveguide is strongly overmoded. A similar, single electron beam version that can be used to generate frequencies around 1 THz was studied in [15], where an output power of 75 mW was predicted using an 11.6-kV, 4-mA (200 A/cm^2) electron beam. In order to be compatible with current state-of-the-art cathode technology, this device requires electron beam compression and a high magnetic field ($\sim$0.8 T) for electron beam guiding, while only 0.2 T was used in the above example. Using multiple beams should greatly diminish the required electron density in a single beamlet, thereby simplifying electron gun design and beam guiding.

The scale invariance of Maxwell's equations [1] allows a direct translation of these results to different spectral regions. From the scale invariance it follows that the eigenmodes of the photonic crystal, and in particular the phase velocity, remain the same when the crystal is scaled down by a factor while the frequency of the mode is simultaneously increased by the same factor. Hence, the same electron beam energy is required to be resonant with the respective crystal eigenmodes, e.g., the 13-kV electron beam in the above example would produce 1.6 THz of radiation when the photonic crystal is reduced in size by a factor 100. Indeed, single beam pFEL [15], [18] and multiple beam pFEL [16] have been considered as sources for Terahertz radiation. For example, a single electron beam (10 kV, 5 mA, and 20 μm radius) was used in a design of a backward-wave amplifier to produce a calculated gain of 12 dB at 1 THz with a 100-μW input signal [18]. A multiple beam design is presented in [16]. This paper discusses the various subcomponents, e.g., electron gun, slow-wave structure (photonic crystal), output coupler, in more detail. Simulations predict an output power of 4–6 mW over a 100 GHz bandwidth from 600 to 700 GHz using a beam voltage of 3 to 6 kV and a total beam current of 45 mA. The electron gun produces a sheet electron beam and beam scrapers are used to create a total of 4 beamlets that propagate through the slow-wave structure. The device requires a guiding magnetic field of 1.1 T. Furthermore, scaling into the infrared has essentially been successful as was demonstrated in [10], although the output remained intrinsically below threshold, and only weak and incoherent radiation was observed. This is contrary to undulator based free-electron lasers where scaling by two orders of magnitude or more by changing the period of the undulator is not feasible, and operating it at increasingly higher frequencies requires higher electron beam energies [12], [20].

Here, we have considered Cerenkov radiation as the source of coherent radiation from electrons streaming through a photonic crystal. However, other interaction mechanisms to generate coherent radiation from electrons, e.g., the cyclotron [17], [21], or Smith-Purcell [22] interaction can be used as well. The fact that a low electron beam velocity can be used in combination with power and frequency scaling characteristics makes the pFEL a versatile, compact source of coherent radiation, with a great potential to significantly enhance the available power from Terahertz sources.

References

[1] J. Joannopoulos, S. Johnson, J. Winn, and R. Meade, *Photonic Crystals: Molding the Flow of Light,* 2nd ed. Princeton, NJ: Princeton Univ. Press, 2008.

[2] T. Baba, "Slow light in photonic crystals," *Nat. Photon.*, vol. 2, no. 8, pp. 465–473, Aug. 2008. [Online]. Available: http://dx.doi.org/doi:10.1038/nphoton.2008.146s

[3] E. Yablonovitch, "Inhibited spontaneous emission in solid-state physics and electronics," *Phys. Rev. Lett.*, vol. 58, no. 20, pp. 2059–2062, May 1987. [Online]. Available: http://link.aps.org/doi/10.1103/PhysRevLett.58.2059

[4] S. John, "Strong localization of photons in certain disordered dielectric superlattices," *Phys. Rev. Lett.*, vol. 58, no. 23, pp. 2486–2489, Jun. 1987. [Online]. Available: http://link.aps.org/doi/10.1103/PhysRevLett.58.2486

[5] P. Lodahl, A. van Driel, I. Nikolaev, A. Irman, K. Overgang, D. Vanmaekelbergh, and W. Vos, "Controlling the dynamics of spontaneous emission from quantum dots by photonic crystals," *Nature*, vol. 430, no. 7000, pp. 654–657, Aug. 2004. [Online]. Available: http://dx.doi.org/doi:10.1038/nature02772

[6] L. Sapienza, H. Thyrrestrup, S. Stobbe, P. Garcia, S. Smolka, and P. Lodahl, "Cavity quantum electrodynamics with Anderson-localized modes," *Science*, vol. 327, no. 5971, pp. 1352–1355, Mar. 2010. [Online]. Available: http://dx.doi.org/doi:10.1126/science.1185080

[7] C. Luo, M. Ibanescu, S. Johnson, and J. Joannopoulos, "Cerenkov radiation in photonic crystals," *Science*, vol. 299, no. 5605, pp. 368–371, Jan. 2003. [Online]. Available: http://dx.doi.org/doi:10.1126/science.1079549

[8] F. J. García de Abajo, A. G. Pattantyus-Abraham, N. Zabala, A. Rivacoba, M. O. Wolf, and P. M. Echenique, "Cherenkov effect as a probe of photonic nanostructures," *Phys. Rev. Lett.*, vol. 91, no. 14, pp. 143902-1–143902-4, Sep. 2003. [Online]. Available: http://link.aps.org/doi/10.1103/PhysRevLett.91.143902

[9] F. J. García de Abajo, "Optical excitations in electron microscopy," *Rev. Mod. Phys.*, vol. 82, no. 1, pp. 209–275, Feb. 2010. [Online]. Available: http://link.aps.org/doi/10.1103/RevModPhys.82.209

[10] G. Adamo, K. F. MacDonald, Y. H. Fu, C.-M. Wang, D. P. Tsai, F. J. García de Abajo, and N. I. Zheludev, "Light well: A tunable free-electron light source on a chip," *Phys. Rev. Lett.*, vol. 103, no. 11, pp. 113901-1–113901-4, Sep. 2009. [Online]. Available: http://link.aps.org/doi/10.1103/PhysRevLett.103.113901

[11] V. Baryshevsky, K. Batrakov, and V. Stolyarsky, "Application of volume diffraction grating for terahertz lasing in volume FEL (VFEL)," *Nucl. Instrum. Methods Phys. Res. A, Accel. Spectrom. Detect. Assoc. Equip.*, vol. 507, no. 1/2, pp. 93–96, Jun. 2003. [Online]. Available: http://www.sciencedirect.com/science/article/pii/S0168900203008453

[12] B. McNeil and N. Thompson, "X-ray free-electron lasers," *Nat. Photon.*, vol. 4, no. 12, pp. 814–821, Nov. 2010. [Online]. Available: http://dx.doi.org/doi:10.1038/nphoton.2010.239

[13] L. Schächter, *Beam-Wave Interaction in Period and Quasi-Periodic Structures,* 2nd ed. Heidelberg, Germany: Springer-Verlag, 2011.

[14] E. Kapon, J. Katz, and A. Yariv, "Supermode analysis of phase-locked arrays of semiconductor lasers," *Opt. Lett.*, vol. 9, no. 4, pp. 125–127, Apr. 1984. [Online]. Available: http://www.opticsinfobase.org/abstract. cfm?URI=ol-9-4-125

[15] M. Mineo and C. Paoloni, "Double-corrugated rectangular waveguide slow-wave structure for terahertz vacuum devices," *IEEE Trans. Electron Devices*, vol. 57, no. 11, pp. 3169–3175, Nov. 2010. [Online]. Available: http://dx.doi.org/doi:10.1109/TED.2010.2071876

[16] L. Ives, C. Kory, M. Read, J. Neilson, M. Caplan, N. Chubun, S. Schwartzkopf, and R. Witherspoon, "Development of backward wave oscillators for terahertz applications," in *Proc. SPIE*, 2003, vol. 5070, pp. 71–82. [Online]. Available: http://dx.doi.org/10.1117/12.506905

[17] L. Lei and E. Jerby, "Two-dimensional cyclotron-resonance maser array: Spectral measurements with one and two electron beams," *Phys. Rev. E*, vol. 59, no. 2, pp. 2322–2329, Feb. 1999. [Online]. Available: http://link.aps.org/doi/10.1103/PhysRevE.59.2322

[18] C. Paoloni, A. Di Carlo, F. Brunetti, M. Mineo, G. Ulisse, A. Durand, V. Krozer, M. Kotiranta, A. Fiorello, M. Dispenza, A. Secchi, V. Zhurbenko, F. Bouamrane, T. Bouvet, S. Megtert, E. Tamburri, C. Cojocaru, and A. Gohier, "Design and fabrication of a 1 THz backward wave amplifier," *Terahertz Sci. Technol.*, vol. 4, no. 4, pp. 149–163, Dec. 2011. [Online]. Available: http://www.tstnetwork.org/December2011/tst-v4n4-149Design%20and%20Fabrication.pdf

[19] T. Denis, J. Lee, M. van Dijk, P. van der Slot, and K. Boller, *Manuscript in Preparation.*

[20] S. Biedron and S. Milton, "Next generation light sources in 2010," *IEEE Photon.*, vol. 3, no. 2, pp. 249–254, Apr. 2011. [Online]. Available: http://dx.doi.org/doi:10.1109/JPHOT.2011.2147410

[21] E. Jerby, A. Kesar, M. Korol, L. Lei, and V. Dikhtyar, "Cyclotron-resonance-maser arrays," *IEEE Trans. Plasma Sci.*, vol. 27, no. 2, pp. 445–455, Apr. 1999. [Online]. Available: http://dx.doi.org/doi:10.1109/27.772272

[22] V. Baryshevsky, K. Batrakov, A. Gurinovich, I. Ilienko, A. Lobko, P. Molchanov, V. Moroz, P. Sofronov, and V. Stolyarsky, "Progress of the volume fel (vfel) experiments in millimeter range," *Nucl. Instrum. Methods Phys. Res. A, Accel. Spectrom. Detect. Assoc. Equip.*, vol. 507, no. 1/2, pp. 137–140, Jul. 2003. [Online]. Available: http://www.sciencedirect.com/science/article/pii/S016890020300857X

Integrated Optical Resonators: Progress in 2011

Amir Arbabi and Lynford L. Goddard

(Invited Paper)

Department of Electrical and Computer Engineering, Micro and Nanotechnology Laboratory, University of Illinois at Urbana-Champaign, Urbana, IL 61801 USA

DOI: 10.1109/JPHOT.2012.2189380

Manuscript received February 15, 2012; accepted February 24, 2012. Date of current version April 20, 2012. This work was supported by University of Illinois startup funds and National Science Foundation CAREER award ECCS-1055941. Corresponding author: L. L. Goddard (e-mail: lgoddard@illinois.edu).

Abstract: We present a review of the research on integrated optical resonators published in 2011. In particular, we focus on microdisk and microring devices and discuss high-quality factor resonators, methods to tune and trim the resonance wavelength, as well as device applications in optical communications, frequency comb generation, all-optical signal processing, sensing, and single-mode lasers.

Index Terms: Waveguide devices, tunable filters, nanophotonics, four-wave mixing, sensors, integrated nanophotonic systems.

High-quality factor (Q) resonators are useful for a variety of on-chip applications. To achieve high Q, bending and scattering losses must be minimized; therefore, waveguide design and fabrication optimization are necessary. In 2011, Si_3N_4 thin core waveguides were demonstrated with losses as small as 1.1 dB/m at 1310 nm for 5-mm-radius rings (corresponding to intrinsic Q of 2.8×10^7) [1]. Using a thin core and wide waveguide, the sidewall scattering loss, which was the main factor in the total loss, was reduced. Etch-less fabrication techniques were another approach for reducing sidewall roughness. Nezhad *et al.* [2] used patterned hydrogen silsesquioxane (HSQ) ebeam resist as a mask for local oxidation of silicon-on-insulator (SOI) and defined waveguides with 0.35 dB/cm (intrinsic Q of 1.57×10^6) in a 150 μm radius microring resonator (MRR). In another work, Luo *et al.* realized 0.8 dB/cm loss in a 50 μm radius SOI MRR (intrinsic Q of 5.1×10^5) by pattering a thermally grown oxide and using it as a mask to locally oxidize a silicon layer underneath [3].

High Q and large optical intensity enhancement inside integrated resonators comes with high sensitivity of their resonance wavelengths to the geometrical dimensions and fabrication errors. Although high sensitivity is useful for sensing, most other applications require accurate positioning of the resonance wavelengths. Novel methods for trimming and tuning the cavity resonances were introduced and demonstrated in 2011. Real-time trimming and monitoring of resonance wavelengths of GaN/InGaN microdisk cavities by a few nanometers was demonstrated using selective photo-enhanced oxidation. Oxidation happened when a UV laser light illuminated the cavity immersed in deionized water. The water dissolved the oxide, reducing the size of the cavity and blue shifting the resonance wavelengths [4]. Thermal tuning was also used for making adaptive filters. Thermal tuning of the central wavelength of an SOI band pass interference filter by 4 nm, and its full-width at half-maximum (FWHM) by almost a factor of two is reported [5]. The filter was implemented by combining the drop port outputs of two MRRs. Three thermal heaters

were used to control the resonance wavelength of the detuned resonators and the relative phase of their drop port outputs. Wavelength referenced temperature tuning with 0.1 pm stability of an integrated resonator was introduced by Zhu *et al.*, which allows for doing spectroscopy in bands where only fixed wavelength nontunable lasers are available [6]. They reported measurement of the transmission spectrum of a whispering gallery microresonator using a fixed probe laser by changing the temperature of the resonator. A tunable pump laser scanning another resonance was used to rapidly change the temperature of the resonator. Sensitivity to environmental temperature was reduced since the resonances at pump and probe wavelength move at almost the same rate. Large tuning of resonance wavelengths of resonators usually involves mechanical movement or resonator shape deformation. Wiederhecker *et al.* used the optical gradient force in a suspended double wheel to tune its resonance by 32 nm with only 13 mW input power [7].

Small footprint, narrow bandwidth, and equidistant resonances of MRRs make them attractive for applications in optical communication and in particular wavelength-division multiplexing (WDM) systems. Integration of 80 SOI MRRs and implementation and characterization of two sets of reconfigurable second-order MRR filter banks for WDM applications were reported in 2011 [8]. Each set of filters contained 20 double MRR filters with 20 GHz bandwidth and 124 GHz spacing. Successful thermal tuning of 11 of the channels was demonstrated, and optical crosstalk smaller than -45 dB between the channels was achieved. Demodulation of non-return-to-zero differential phase-shift keying (NRZ-DPSK) signals using a single MRR was reported previously [9]. Ding *et al.* reported simultaneous demodulation of four WDM channels modulated at 40 Gbits/s using a single SOI MRR with a moderate Q [10]. Two waveguides were coupled to a MRR in the add-drop configuration and alternate-mark inversion (AMI) and duobinary (DB) signals were obtained from the through and drop ports, respectively. Balanced detection by using both AMI and DB signals was shown to improve the receiver sensitivity by about 3 dB, compared with detection using only the AMI signal. Although the demodulation of different channels is done in a single MRR, a wavelength demultiplexer is still required for separation of different channels.

Frequency comb generation has been one of the most successful applications of integrated microresonators in nonlinear optics. Small device size and very high repetition rate make integrated resonators attractive for this application. Generation of a broadband optical frequency comb in a single Si_3N_4 MRR functioning as an optical parametric oscillator (OPO) was demonstrated by Foster *et al.* [11]. The OPO uses the optical Kerr nonlinearity of Si_3N_4 and a cascaded four-wave mixing nonlinear process. With careful design of the waveguide core dimensions, proper anomalous group velocity dispersion was achieved, and a single continuous wave pump laser coupled to the resonator generated a broadband frequency comb spanning a 75 THz bandwidth. The equidistance of the generated comb frequencies over a bandwidth of 14.5 THz was verified using a novel method that was introduced in [11]. Investigation of the coherence of optical frequency combs generated in Si_3N_4 resonators was also reported [12]. A single wavelength pump laser was coupled with MRRs with loaded Q as high as 3×10^6, and the temporal coherence of the output frequency combs were studied. Relative phases of different frequency lines of a comb were adjusted using a programmable pulse shaper for achieving pulse compression. Autocorrelation of the output of the pulse shaper was measured and two different types of frequency combs with different coherence properties were identified. In one type, the generated side bands are one free spectral range (FSR) apart, and their amplitudes drop as their frequency difference with the pump wavelength increases. Such a frequency comb was found to have a high coherence and stable relative phases among different frequency lines. Another type of frequency comb was also identified with primary sidebands separated by a multiple of the FSR and secondary lines with smaller amplitudes and separated by one FSR filling the gap between the primary sidebands. Partial coherence was observed in this type of frequency comb. The physical process responsible for the existence and coherence properties of the two types of frequency combs is not yet known.

Novel applications of MRRs in all-optical signal processing were also reported in 2011. Using reduced Q MRRs (6.5×10^4), first and second-order temporal waveform integrators with temporal resolution of 1.9 ps were realized [13]. First-order integration was made possible due to the

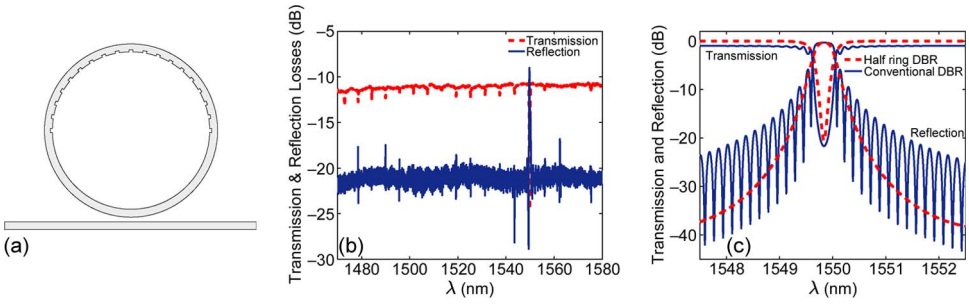

Fig. 1. (a) Schematic of a single wavelength reflector (half ring DBR). Modulation of the waveguide width on the top half of the ring forms a DBR that has its reflection nulls at all ring resonances, except for the one selected for reflection. (b) Measured transmission and reflection spectra of a half-ring DBR fabricated with Si_3N_4 core and SiO_2 cladding. (c) Extracted reflection and transmission spectra of the same device close to its reflection peak. Similar spectra for a 4.3-mm-long conventional DBR with the same reflectivity maximum and FWHM are also shown for comparison. Reprinted with permission from [21]. Copyright 2011, American Institute of Physics.

similarity of a part of the Lorentzian response of the MRR and the transfer function response of a first-order integrator. Second-order integration was achieved by passing the light twice through the same MRR. It was also shown that reduction of Q increases the temporal resolution of the integrators but reduces the integration window.

High Q MRRs have sharp resonance spectra. The center wavelength can be made sensitive to various environmental parameters and thus can be used as the readout for many different types of sensors. In 2011, research efforts vastly expanded the application space of MRRs for sensing as well as focused on improving parameters such as sensitivity and cost. Here, we discuss the results of a few sensor types: refractive index, biological, and acoustic. Scholten *et al.* fabricated high aspect ratio (85 μm tall by 2 μm wide) hollow SiO_x cylinders $(Q > 10^4)$ to form a microfluidic channel sensor where the fluid flows perpendicular to the wafer surface [14]. Hu and Dai used the Vernier effect in cascaded SOI MRRs and suspended the sensing ring to enhance the sensitivity to 4.6×10^5 nm/RIU and achieve a minimum detection limit of 4.8×10^{-6} [15]. For biosensing, Santiago-Cordoba *et al.* reported enhanced sensitivity for protein detection by coupling the evanescent field of a whispering gallery mode resonator to a layer of gold nanoparticles [16], while McClellan *et al.* showed how the health of a soybean leaf can be rapidly quantified in the field using silicon MRRs functionalized with antibodies [17]. Ling *et al.* demonstrated low-noise ultrasound detectors, with a noise equivalent pressure of 21.4 Pa over the 1–75 MHz range, using imprinted polymer MRRs with $Q = 4 \times 10^5$ and a diameter of $D = 60$ μm [18].

Two degenerate counter propagating modes exist at each resonance wavelength of a MRR. These two degenerate modes are uncoupled in an ideal resonator, but a small perturbation can couple them and cause reflection. Engineering this mode coupling for realizing frequency selective reflective devices was theoretically investigated by us [19], and fast numerical simulation and design methods were developed [20]. More recently, we validated these new theoretical models by experimentally realizing a small footprint (30 μm radius) single wavelength reflector with peak power reflectivity of 92.3% and greater than 7.8 dB suppression at adjacent ring resonances across a 100-nm measurement window [21]. A device schematic is shown in Fig. 1(a). Selective coupling of counter propagating modes, i.e., at the 1549.9 nm resonance only, was achieved by patterning a distributed Bragg reflector (DBR) on the inner wall of the MRR's top half. Measured transmission and reflection spectra of the device are shown in Fig. 1(b). The zoomed in view of the extracted spectra of the same device close to its reflectivity peak in Fig. 1(c) shows faster roll-off and no side modes compared with a 4.3 mm conventional linear DBR. This reflective MRR device can be used as a laser mirror for narrow linewidth single-mode semiconductor lasers.

In summary, we highlighted some of the research in 2011 into improving design, fabrication, and performance and the emerging applications of integrated optical resonators.

References

[1] M. Tien, J. F. Bauters, M. J. R. Heck, D. T. Spencer, D. J. Blumenthal, and J. E. Bowers, "Ultra-high quality factor planar Si_3N_4 ring resonators on Si substrates," *Opt. Exp.*, vol. 19, no. 20, pp. 13551–13556, Jul. 2011. [Online]. Available: http://www.opticsexpress.org/abstract.cfm?URI=oe-19-14-13551

[2] M.P. Nezhad, O. Bondarenko, M. Khajavikhan, A. Simic, and Y. Fainman, "Etch-free low loss silicon waveguides using hydrogen silsesquioxane oxidation masks," *Opt. Exp.*, vol. 19, no. 20, pp. 18827–18832, Sep. 2011. [Online]. Available: http://www.opticsexpress.org/abstract.cfm?URI=oe-19-20-18827

[3] L. Luo, G. S. Wiederhecker, J. Cardenas, C. Poitras, and M. Lipson, "High quality factor etchless silicon photonic ring resonators," *Appl. Phys. Lett.*, vol. 19, no. 7, pp. 6284–6289, Mar. 2011. [Online]. Available: http://www.opticsexpress.org/abstract.cfm?URI=oe-19-7-6284

[4] I. Aharonovich, N. Niu, F. Rol, K. J. Russell, A. Woolf, H. A. R. El-Ella, M. J. Kappers, R. A. Oliver, and E. L. Hu, "Controlled tuning of whispering gallery modes of GaN/InGaN microdisk cavities," *Appl. Phys. Lett.*, vol. 99, no. 11, pp. 111111-1–111111-3, Sep. 2011. [Online]. Available: http://apl.aip.org/resource/1/applab/v99/i11/p111111_s1

[5] Y. Ding, M. Pu, L. Liu, J. Xu, C. Peucheret, X. Zhang, D. Huang, and H. Ou, "Bandwidth and wavelength-tunable optical bandpass filter based on silicon microring-MZI structure," *Opt. Exp.*, vol. 19, no. 7, pp. 6462–6470, Mar. 2011. [Online]. Available: http://www.opticsexpress.org/abstract.cfm?URI=oe-19-7-6462

[6] J. Zhu, Ş. K. Özdemir, L. He, and L. Yang, "Optothermal spectroscopy of whispering gallery microresonators," *Appl. Phys. Lett.*, vol. 19, no. 17, pp. 171101-1–171101-3, Oct. 2011. [Online]. Available: http://apl.aip.org/resource/1/applab/v99/i17/p171101_s1

[7] G. S. Wiederhecker, S. Manipatruni, S. Lee, and M. Lipson, "Broadband tuning of optomechanical cavities," *Opt. Exp.*, vol. 19, no. 3, pp. 2782–2790, 2011. [Online]. Available: http://www.opticsexpress.org/abstract.cfm?URI=oe-19-3-2782

[8] M. S. Dahlem, C. W. Holzwarth, A. Khilo, F. X. Kärtner, H. I. Smith, and E. P. Ippen, "Reconfigurable multi-channel second-order silicon microring-resonator filterbanks for on-chip WDM systems," *Opt. Exp.*, vol. 19, no. 17, pp. 306–316, Jan. 2011. [Online]. Available: http://www.opticsexpress.org/abstract.cfm?URI=oe-19-1-306

[9] L. Zhang, J. Yang, M. Song, Y. Li, B. Zhang, R. G. Beausoleil, and A. E. Willner, "Microring-based modulation and demodulation of DPSK signal," *Opt. Exp.*, vol. 15, no. 18, pp. 11564–11569, Sep. 2007. [Online]. Available: http://www.opticsexpress.org/abstract.cfm?URI=oe-15-18-11564

[10] Y. Ding, J. Xu, C. Peucheret, M. Pu, L. Liu, J. Seoane, H. Ou, X. Zhang, and D. Huang, "Multi-channel 40 Gb/s NRZ-DPSK demodulation using a single silicon microring resonator," *J. Lightw. Technol.*, vol. 29, no. 5, pp. 677–684, Mar. 2011. [Online]. Available: http://jlt.osa.org/abstract.cfm?URI=jlt-29-5-677

[11] M. A. Foster, J. S. Levy, O. Kuzucu, K. Saha, M. Lipson, and A. L. Gaeta, "Silicon-based monolithic optical frequency comb source," *Opt. Exp.*, vol. 19, no. 15, pp. 14233–14239, Jul. 2011. [Online]. Available: http://www.opticsexpress.org/abstract.cfm?URI=oe-19-15-14233

[12] F. Ferdous, H. Miao, D. E. Leaird, K. Srinivasan, J. Wang, L. Chen, L. T. Varghese, and A. M. Weiner, "Spectral line-by-line pulse shaping of on-chip microresonator frequency combs," *Nat. Photon.*, vol. 5, no. 12, pp. 770–776, Dec. 2011. [Online]. Available: http://dx.doi.org/10.1038/nphoton.2011.255

[13] M. Ferrera, Y. Park, L. Razzari, B. E. Little, S. T. Chu, R. Morandotti, D. J. Moss, and J. Azaña, "All-optical 1st and 2nd order integration on a chip," *Opt. Exp.*, vol. 19, no. 23, pp. 23153–23161, Nov. 2011. [Online]. Available: http://www.opticsexpress.org/abstract.cfm?URI=oe-19-23-23153

[14] K. Scholten, X. Fan, and E. T. Zellers, "Microfabricated optofluidic ring resonator structures," *Appl. Phys. Lett.*, vol. 99, no. 14, pp. 141108-1–141108-3, Oct. 2011. [Online]. Available: http://apl.aip.org/resource/1/applab/v99/i14/p141108_s1

[15] J. Hu and D. Dai, "Cascaded-ring optical sensor with enhanced sensitivity by using suspended Si-Nanowires," *IEEE Photon. Technol. Lett.*, vol. 23, no. 13, pp. 842–844, Jul. 2011. [Online]. Available: http://ieeexplore.ieee.org/xpls/abs_all.jsp?arnumber=5741827&tag=1

[16] M. A. Santiago-Cordoba, S. V. Boriskina, F. Vollmer, and M. C. Demirel, "Nanoparticle-based protein detection by optical shift of a resonant microcavity," *Appl. Phys. Lett.*, vol. 99, no. 7, pp. 073701-1–073701-3, Aug. 2011. [Online]. Available: http://apl.aip.org/resource/1/applab/v99/i7/p073701_s1

[17] M. S. McClellan, L. L. Domier, and R. C. Bailey, "Label-free virus detection using silicon photonic microring resonators," *Biosens. Bioelectron.*, vol. 31, no. 1, pp. 388–392, Jan. 2012. [Online]. Available: http://www.sciencedirect.com/science/article/pii/S0956566311007445

[18] T. Ling, S. Chen, and L. J. Guo, "High-sensitivity and wide-directivity ultrasound detection using high Q polymer microring resonators," *Appl. Phys. Lett.*, vol. 98, no. 20, pp. 204103-1–204103-3, May 2011. [Online]. Available: http://apl.aip.org/resource/1/applab/v98/i20/p204103_s1

[19] Y. M. Kang, A. Arbabi, and L. L. Goddard, "Engineering the spectral reflectance of microring resonators with integrated reflective elements," *Opt. Exp.*, vol. 18, no. 16, pp. 16813–16825, Jul. 2010. [Online]. Available: http://www.opticsexpress.org/abstract.cfm?URI=oe-18-16-16813

[20] A. Arbabi, Y. M. Kang, and L. L. Goddard, "Cylindrical coordinates coupled mode theory," *IEEE J. Quantum Electron.*, vol. 46, no. 12, pp. 1769–1774, Dec. 2010. [Online]. Available: http://ieeexplore.ieee.org/xpls/abs_all.jsp?arnumber=5638355

[21] A. Arbabi, Y. M. Kang, C. Lu, E. Chow, and L. L. Goddard, "Realization of a narrowband single wavelength microring mirror," *Appl. Phys. Lett.*, vol. 99, no. 9, pp. 091105-1–091105-3, Aug. 2011. [Online]. Available: http://apl.aip.org/resource/1/applab/v99/i9/p091105_s1

Nonlinear Photonic Structures

Patrick Rose and Cornelia Denz

(Invited Paper)

Institut für Angewandte Physik and Center for Nonlinear Science (CeNoS),
Westfälische Wilhelms-Universität Münster, 48149 Münster, Germany

DOI: 10.1109/JPHOT.2012.2190590

Manuscript received February 18, 2012; revised February 27, 2012; accepted March 6, 2012. Date of current version April 20, 2012. Corresponding author: C. Denz (e-mail: denz@uni-muenster.de).

Abstract: In photonics, the investigation of structured nonlinear systems is an active and vivid research area. Their ability to control the dispersion and diffraction properties of light allows tailoring light in its spectral, temporal, and spatial features. Manipulating the spatial features, i.e., overcoming diffraction, is an actual and challenging issue that is of utmost importance for further information processing tasks. With this contribution, we highlight some of the most recent publications in this field. Among others, we discuss the progress in complex photonic lattice generation as well as the guiding and control of discrete spatial solitons—entities that no longer spread during propagation. We also emphasize the importance of photonic lattices as optical analogies to quantum mechanical systems and review current results on Anderson localization of light.

Index Terms: Nonlinear photonics, photonic lattices, band gap structures, spatial solitons, parity-time (PT) symmetry, Anderson localization.

Driven by the increasing requirements for digital information transmission and processing bandwidth, photonics research continuously provides new concepts for the engineering, guiding, or storing of light. In particular, the introduction of an artificial periodicity of the refractive index of a material and thus a structured potential can lead—in analogy to semiconductors—to dramatically modified propagation properties due to the appearance of band gap structures. In this context, many groups have published significant results during the last year, and in this contribution, we will review some of these works that advanced discrete spatial optics considerably.

In the field of artificial materials, photonic crystal structures with their artificial periodicity of the dielectric constant or the refractive index, respectively, and their unique transmission and reflection spectra revealing band gaps provide maybe the most influential concept in order to tailor light propagation. Whereas in the last 15 years special emphasis was set on the control of the spectral features of light, recently, the spatial features of light and its spatial frequencies came into view. By using materials that change their refractive index properties due to light whereupon light itself reacts on the modified material environment, this approach even allows for the control of light by light itself. Nonlinear effects to tailor the refractive index of the material are an indispensable ingredient of the success of this technique. Among them, photorefractive crystals are promising examples and, after illuminating with structured low intensity lattice writing light waves—a technique known as optical induction of photonic lattices [1]—can be used as an ideal model system to demonstrate a multitude of groundbreaking propagation effects [2].

In the course of 2011, several novel strategies have been presented [3] in order to overcome simple lattice geometries like hexagonal lattices studied in these systems so far. Among others, the

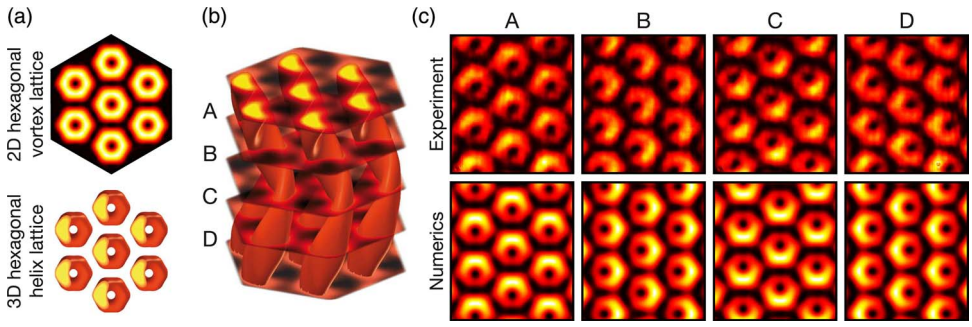

Fig. 1. (a) Intensity distribution of the 2-D hexagonal vortex lattice and top view of the corresponding 3-D helix lattice, (b) plot of the isointensity surfaces of the hexagonal helix lattice at 60% of the maximum intensity, and (c) comparison of experimental (top row) and numerical (bottom row) images for the planes A–D marked in (b).

idea to control the phase relation of different components in the spectrum of discrete nondiffracting beams led us to the demonstration of nondiffracting kagome [4] and graphene lattices [5]. Also, an analysis of nonlinear wave dynamics in the latter ones has been provided [6].

In the same way, the creation of 3-D helical lattices was a challenge for discrete photonics until we found a modification to the optical induction approach and used 2-D vortex lattices as a basis for the first construction of helix lattice waves [7]. Fig. 1 exemplarily illustrates the hexagonal helix lattice and its connection to the corresponding 2-D vortex lattice [7]. The analysis of different planes in the direction of propagation clearly verifies the helical structure of the complex 3-D intensity distribution.

The impressive capabilities of such photonic lattices have been underlined once more by the presentation of a structure allowing for a negative Goos-Hänchen shift [8]. While this application already illustrates the significant influence of structured materials on light and light propagation, the introduction of defects into an otherwise periodic potential adds other important features as an analysis of nonlinear beam deflection in lattices with negative defects shows [9]. In addition, the experimental realization of a true reflectionless potential that facilitates complete transmission for incident beams and, at the same time, supports localized modes is very interesting [10].

In particular, the occurrence of photonic band gaps in periodic structures offers unique possibilities to control the propagation of light. Since the pioneering work by Christodoulides *et al.* on discrete solitons in nonlinear photonic lattices [1], [2], many researchers have developed this field further. An important actual aspect is steering of discrete solitons. In 2011, a concept for positioning these localized structures based on linear defects has been introduced [11]. By dragging the defects, the attached solitons can be moved and positioned. Another work investigated two approaches for the control of soliton refraction in optical lattices [12] and could demonstrate the influence of both shape and position of individual waveguides on the soliton transmission.

Also, the interaction between solitons is of particular interest. Here, we want to highlight the detailed investigation of coupled dark-bright states, including corresponding experimental realizations [13]. The authors show that these two structures can coexist as a solitonic entity. Furthermore, it was demonstrated that two in-phase bright gap solitons—in contrast to solitons in homogeneous media—can repel each other while out-of-phase solitons show mutual attraction [14]. This anomalous interaction of spatial gap solitons in optically induced photonic lattices is also an important result since it emphasizes once more the importance of phase as a control parameter.

In the same sense, discrete vortex solitons being clusters of coupled bright states with distinct phase relations have been discussed for several years. In 2011, we contributed a work showing that surface vortex solitons in the two-beam counterpropagating geometry allow for a stable propagation of such vortex states, and we studied their orbital angular momentum transfer [15]. Configurations showing more than one phase singularity are referred to as multivortex solitons. Recently, researchers from the Australian National University introduced discrete multivortex solitons in a set of

nonlinear oscillators and found stable multivortex solitons supporting complex vortex dynamics [16]. They revealed that the vortices in this configuration can show spiraling trajectories or even topological charge flipping providing an all-optical discrete vortex switch [17].

Localization in the temporal domain is an important and actual aspect of photonic lattices as well. Combined with a spatial localization, this leads to the concept of so-called light bullets being nondispersive and nondiffractive at the same time. While this idea has been discussed for years, at the end of 2010 finally a first experimental realization providing 3-D nonlinear light bullets in arrays of coupled waveguides has been published [18]. During 2011, the authors added a detailed discussion about the evolution dynamics of these intriguing entities of light [19].

Moreover, due to formal similarities to quantum mechanical systems, discrete photonic structures also can serve as a versatile platform for the demonstration of optical analogies to quantum mechanical effects like quantum interference [20]. In this scope, currently a lot of interest surrounds questions related to parity-time (PT) symmetry in optics [21]. This property has been analyzed in detail for honeycomb photonic lattices [22] and the authors found a dispersion relation identical to tachyons. Furthermore, solitons were found in PT symmetric nonlinear photonic lattices as well [23]. Utilizing PT symmetry considerations, researchers from the United States presented another particularly interesting structure that acts as a unidirectional invisible medium [24]. In this way, light coming from one side passes the medium completely undisturbed, while light incident from the opposite side is strongly affected.

However, PT symmetry is only one analogy photonic structures can provide. At the beginning of 2011, we presented an experimental study on Pendellösung oscillations and interband Landau-Zener transitions based on resonant coupling between high-symmetry points of 2-D photonic lattices [25]. Also, Rabi oscillations in subwavelength structures have been investigated [26], and anharmonic Bloch oscillations facilitating second-order coupling were observed [27].

All these publications underline the possibilities of discrete optics to visualize important effects and therewith to deepen the understanding in multiple physical areas. This is particularly true for the field of Anderson localization. Since the first experimental observation of light localized in a perturbed periodic lattice [28], many researchers investigated Anderson localization in optical systems and, during 2011, again, multiple intriguing results have been published—among them the finding of localization in porous media [29]. Furthermore, it has been shown that partially coherent waves can experience this localization effect [30].

In this field, we recently contributed, on the one hand, an analysis of Anderson localization near the boundaries of a photonic lattice [31] and, on the other hand, of the crossover from 2-D to 1-D configurations in the linear and the nonlinear regime [32]. Since Anderson localization heavily relies on statistics, the properties of the underlying lattice play an important role. Notably, the introduction of disorder into quasi-periodic lattices was found to enhance wave transport [33], while characteristically, mobility was expected to decrease with increasing disorder.

Another intriguing concept of random structures introduced in 2011 is the idea of amorphous photonic lattices [35]. These materials lack Bragg peaks but, nevertheless, show band gaps and therewith raise many open questions.

All these significant scientific results show that photonics research in general and the investigation of photonic lattice structures in particular is a very active and vivid field. Many researchers from all over the world contribute on a daily basis to the constant progress. Naturally, we could not honor all important contributions of the last year in this short review. However, we hope to stimulate further research in this area contributing to the successful history of nonlinear photonics.

References

[1] N. K. Efremidis, S. Sears, D. N. Christodoulides, J. W. Fleischer, and M. Segev, "Discrete solitons in photorefractive optically induced photonic lattices," *Phys. Rev. E*, vol. 66, p. 046602, 2002.

[2] J. W. Fleischer, M. Segev, N. K. Efremidis, and D. N. Christodoulides, "Observation of two-dimensional discrete solitons in optically induced nonlinear photonic lattices," *Nature*, vol. 422, pp. 147–150, 2003.

[3] Y. V. Kartashov, S. Lopez-Aguayo, V. A. Vysloukh, and L. Torner, "Stripe-like quasi-nondiffracting optical lattices," *Opt. Exp.*, vol. 19, no. 10, pp. 9505–9511, May 2011.
[4] M. Boguslawski, P. Rose, and C. Denz, "Nondiffracting kagome lattice," *Appl. Phys. Lett.*, vol. 98, no. 6, pp. 061111-1–061111-3, Feb. 2011.
[5] M. Boguslawski, P. Rose, and C. Denz, "Increasing the structural variety of discrete nondiffracting wave fields," *Phys. Rev., A*, vol. 84, no. 8, pp. 013832-1–013832-8, 2011.
[6] O. Bahat-Treidel and M. Segev, "Nonlinear wave dynamics in honeycomb lattices," *Phys. Rev. A*, vol. 84, pp. 021802-1–021802-4, 2011.
[7] J. Becker, P. Rose, M. Boguslawski, and C. Denz, "Systematic approach to complex periodic vortex and helix lattices," *Opt. Exp.*, vol. 19, no. 10, pp. 9848–9862, 2011.
[8] M. C. Rechtsman, Y. V. Kartashov, F. Setzpfandt, H. Trompeter, L. Torner, T. Pertsch, U. Peschel, and A. Szameit, "Negative Goos-Hänchen shift in periodic media," *Opt. Lett.*, vol. 36, no. 22, pp. 4446–4448, Nov. 2011.
[9] J. Wang, Z. Ye, A. Miller, Y. Hu, C. Lou, P. Zhang, Z. Chen, and J. Yang, "Nonlinear beam deflection in photonic lattices with negative defects," *Phys. Rev. A*, vol. 83, no. 3, pp. 033836-1–033836-6, 2011.
[10] A. Szameit, F. Dreisow, M. Heinrich, S. Nolte, and A. A. Sukhorukov, "Realization of reflectionless potentials in photonic lattices," *Phys. Rev. Lett.*, vol. 106, no. 19, p. 193903, May 2011.
[11] V. A. Brazhnyi and B. A. Malomed, "Dragging two-dimensional discrete solitons by moving linear defects," *Phys. Rev. E*, vol. 84, no. 1, pp. 016608-1–016608-8, Jul. 2011.
[12] J. E. Prilepsky, S. A. Derevyanko, and S. A. Gredeskul, "Controlling soliton refraction in optical lattices," *Phys. Rev. Lett.*, vol. 107, no. 8, pp. 083901-1–083901-5, Aug. 2011.
[13] R. Dong, C. E. Rüter, D. Kip, J. Cuevas, P. G. Kevrekidis, D. Song, and J. Xu, "Dark-bright gap solitons in coupled-mode one-dimensional saturable waveguide arrays," *Phys. Rev. A*, vol. 83, no. 6, pp. 063816-1–063816-10, Jun. 2011.
[14] S. Liu, Y. Hu, P. Zhang, X. Gan, F. Xiao, C. Lou, D. Song, J. Zhao, J. Xu, and Z. Chen, "Anomalous interactions of spatial gap solitons in optically induced photonic lattices," *Opt. Lett.*, vol. 36, no. 7, pp. 1167–1169, 2011.
[15] D. Jovic, C. Denz, and M. Belic, "Vortex solitons at the boundaries of photonic lattices," *Opt. Exp.*, vol. 19, no. 27, pp. 26 232–26 238, Dec. 2011.
[16] D. Leykam and A. S. Desyatnikov, "Discrete multivortex solitons," *Opt. Lett.*, vol. 36, no. 24, pp. 4806–4808, Dec. 2011.
[17] A. S. Desyatnikov, M. R. Dennis, and A. Ferrando, "All-optical discrete vortex switch," *Phys. Rev. A*, vol. 83, no. 6, pp. 063822-1–063822-5, 2011.
[18] S. Minardi, F. Eilenberger, Y. V. Kartashov, A. Szameit, U. Röpke, J. Kobelke, K. Schuster, H. Bartelt, S. Nolte, L. Torner, F. Lederer, A. Tünnermann, and T. Pertsch, "Three-dimensional light bullets in arrays of waveguides," *Phys. Rev. Lett.*, vol. 105, no. 26, pp. 263901-1–263901-4, 2010.
[19] F. Eilenberger, S. Minardi, A. Szameit, U. Röpke, J. Kobelke, K. Schuster *et al.,* "Evolution dynamics of discrete-continuous light bullets," *Phys. Rev. A*, vol. 84, no. 1, pp. 013836-1–013836-10, 2011.
[20] S. Longhi, "Quantum interference in photonic lattices with defects," *Phys. Rev. A*, vol. 83, no. 3, pp. 033821-1–033821-7, Mar. 2011.
[21] C. E. Rüter, K. G. Makris, R. El-Ganainy, D. N. Christodoulides, M. Segev, and D. Kip, "Observation of parity-time symmetry in optics," *Nature Phys.*, vol. 6, no. 3, pp. 192–195, 2010.
[22] A. Szameit, M. C. Rechtsman, O. Bahat-Treidel, and M. Segev, "PT-symmetry in honeycomb photonic lattices," *Phys. Rev. A*, vol. 84, no. 2, pp. 021806-1–021806-5, Aug. 2011.
[23] F. K. Abdullaev, Y. V. Kartashov, V. V. Konotop, and D. A. Zezyulin, "Solitons in PT-symmetric nonlinear lattices," *Phys. Rev. A*, vol. 83, no. 4, pp. 041805-1–041805-4, Apr. 2011.
[24] Z. Lin, H. Ramezani, T. Eichelkraut, T. Kottos, H. Cao, and D. N. Christodoulides, "Unidirectional invisibility induced by PT-symmetric periodic structures," *Phys. Rev. Lett.*, vol. 106, no. 21, pp. 213901-1–213901-4, May 2011.
[25] B. Terhalle, A. S. Desyatnikov, D. N. Neshev, W. Krolikowski, C. Denz, and Y. S. Kivshar, "Dynamic diffraction and interband transitions in two-dimensional photonic lattices," *Phys. Rev. Lett.*, vol. 106, no. 8, pp. 083902-1–083902-4, Feb. 2011.
[26] B. Alfassi, O. Peleg, N. Moiseyev, and M. Segev, "Diverging rabi oscillations in subwavelength photonic lattices," *Phys. Rev. Lett.*, vol. 106, no. 7, pp. 073901-1–073901-4, Feb. 2011.
[27] F. Dreisow, G. Wang, M. Heinrich, R. Keil, A. Tünnermann, S. Nolte, and A. Szameit, "Observation of anharmonic Bloch oscillations," *Opt. Lett.*, vol. 36, no. 20, pp. 3963–3965, Oct. 2011.
[28] T. Schwartz, G. Bartal, S. Fishman, and M. Segev, "Transport and Anderson localization in disordered two-dimensional photonic lattices," *Nature*, vol. 446, pp. 52–55, Mar. 2007.
[29] F. Riboli, P. Barthelemy, S. Vignolini, F. Intonti, A. D. Rossi, S. Combrie, and D. S. Wiersma, "Anderson localization of near-visible light in two dimensions," *Opt. Lett.*, vol. 36, no. 2, pp. 127–129, Jan. 2011.
[30] D. Capeta, J. Radic, A. Szameit, M. Segev, and H. Buljan, "Anderson localization of partially incoherent light," *Phys. Rev. A*, vol. 84, no. 1, pp. 011801-1–011801-4, Jul. 2011.
[31] D. M. Jovic, Y. S. Kivshar, C. Denz, and M. R. Belic, "Anderson localization of light near boundaries of disordered photonic lattices," *Phys. Rev. A*, vol. 83, no. 3, pp. 033813-1–033813-5, Mar. 2011.
[32] D. M. Jovic, M. R. Belic, and C. Denz, "Transverse localization of light in nonlinear photonic lattices with dimensionality crossover," *Phys. Rev. A*, vol. 84, no. 4, pp. 043811-1–043811-5, Oct. 2011.
[33] L. Levi, M. Rechtsman, B. Freedman, T. Schwartz, O. Manela, and M. Segev, "Disorder-enhanced transport in photonic quasicrystals," *Science*, vol. 332, no. 6037, pp. 1541–1544, Jun. 2011.
[34] M. V. Ivanchenko, T. V. Laptyeva, and S. Flach, "Anderson localization or nonlinear waves: A matter of probability," *Phys. Rev. Lett.*, vol. 107, no. 24, p. 240 602, Dec. 2011.
[35] M. Rechtsman, A. Szameit, F. Dreisow, M. Heinrich, R. Keil, S. Nolte, and M. Segev, "Amorphous photonic lattices: Band gaps, effective mass, and suppressed transport," *Phys. Rev. Lett.*, vol. 106, no. 19, p. 193 904, 2011.

Semiconductor Nanolasers

D. Saxena, S. Mokkapati, and C. Jagadish

(Invited Paper)

Department of Electronic Materials Engineering, Research School of Physics and Engineering, Australian National University, Canberra, ACT 0200, Australia

DOI: 10.1109/JPHOT.2012.2189201
1943-0655/$31.00 ©2012 IEEE

Manuscript received February 6, 2012; accepted February 19, 2012. Date of current version April 20, 2012. This work was supported by the Australian Research Council. Corresponding author: D. Saxena (e-mail: dhruv.saxena@anu.edu.au).

Abstract: Recent progress in the field of semiconductor nanolasers is discussed. New designs have emerged that eliminate the need for a conventional Fabry–Perot cavity, bringing down the physical dimensions of the lasers below the diffraction limit. Semiconductor nanolasers are critical components for nanophotonics and offer possible integration with Si nanoelectronics.

Index Terms: Semiconductor nanowire lasers, nanolasers, plasmonic lasers.

The current electronic circuits/devices have reached their ultimate speeds, as they are only limited by inherent resistance-capacitive (RC) delay times. Photonic devices can overcome these limitations. However, photonic circuits/devices need to shrink in dimensions to the nanoscale to be compatible with current day electronic devices. Photonic devices that offer the possibility of integration with Si electronics are especially interesting as these devices would be compatible with current electronics industry practices and would enable us to reap the benefits of both electronics and photonics. A laser is an inherent part of any photonic circuit, and this paper describes the recent progress in the field of semiconductor nanolasers.

Defect free direct bangdap semiconductor nanowires can be grown on Si substrates, unlike planar epitaxial layers, in spite of lattice mismatch between the substrate and the nanowire material. These nanowires are efficient light emitters and form interesting candidates for integration of efficient light emitters with Si technology. In addition, semiconductor nanowires offer tiny footprints and scalability, which has great potential for future high density optoelectronics. Semiconductor nanowire lasers have subwavelength diameters and are typically only a few micrometers long. The nanowire behaves like a Fabry–Perot cavity, with gain provided by the direct band gap semiconductor material. However, the guided modes in a nanowire are evanescent in nature and become less confined as nanowire diameter is reduced. This imposes severe size restrictions for a nanowire laser in order to attain low lasing thresholds.

The laser size can be further reduced by replacing the semiconductor Fabry–Perot cavity with metallic cavities. Metallic cavities provide the necessary positive feedback through light confinement by excitation of surface plasmon polaritons (SPPs). SPPs confine light in regions much smaller than the wavelength of light and thus bring down the laser sizes below the diffraction limit. Recently, a new concept, i.e., "lasing Surface Plasmon Amplification by Stimulated Emission of Radiation (SPASER)," was proposed [1], which uses amplification of localized surface plasmons (LSPs) to create a nanolaser. We will discuss the recent progress in semiconductor nanowire lasers, metal cavity nanolasers, and SPASERs in further detail.

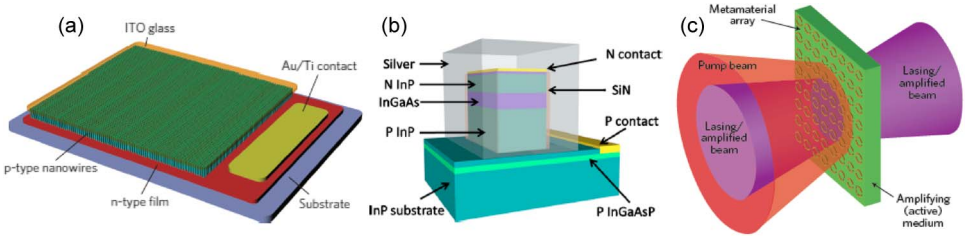

Fig. 1. (a) Schematic of electrically pumped nanowire laser device, with p-type ZnO nanowires sandwiched between ITO top contact and n-type ZnO film. Adapted by permission from Macmillan Publishers Ltd.: Nature Nanotechnology [10] © 2011. (b) Schematic of the metal cavity semiconductor nanolaser operating in continuous wave mode at 260 K. Device size is 1.1 μm wide $\times$ 2.15 μm long $\times$ 1.55 μm high. Reprinted with permission from [16] © 2011, American Institute of Physics. (c) Proposed design for a lasing SPASER which uses a metamaterial array. Adapted by permission from Macmillan Publishers Ltd.: Nature Materials [21] © 2010.

Nanowire Lasers

Nanowires can be grown from a variety of semiconductor materials and in a number of different structures, such as core only, core-shell, radial heterostructures, and axial superlattice structures [2]. In the last decade, lasing from nanowires of various materials, such as nitrides [3]–[5], II-VI compounds [6]–[10], III-V compounds [11], and ternary alloys [12], [13], has been reported. The majority of these demonstrations have achieved lasing by optical pumping at low temperatures. To achieve room-temperature lasing with electrical injection of carriers is a major challenge.

The first demonstration of electrically driven nanowire lasing at room temperature was in single CdS nanowires [7]. In the setup, n-type CdS nanowires were laid side-on upon a heavily doped p-type silicon substrate and Ti/Au was deposited over the nanowire with an Al_2O_3 barrier in between for electrical insulation. Electroluminescence from the nanowire end was observed at room temperature and superlinear increase in intensity was observed for injection current values above 200 μA.

A more recent demonstration of electrically pumped room-temperature lasing was in ZnO nanowires [10]. Although room temperature lasing in ZnO nanowires had been shown several years ago [6], electrical pumping was difficult to achieve due to issues with controllable p-type doping. In this paper, in Fig. 1(a), ZnO nanowires doped with Sb were grown on n-type ZnO thin film. Electrical contact to the nanowires was accomplished by embedding the nanowires in a thin layer of polymer and then depositing indium tin oxide (ITO) on top. The bottom contact was made by depositing Au/Ti on the n-type ZnO thin film. Fabry–Perot cavity modes were observed from the ZnO nanowires in both photoluminescence and electroluminescence experiments. The threshold current for lasing in this device was $\sim$48 mA. This is promising for the development of practical ultraviolet nanolasers, though further work is necessary to realize electrically pumped single nanowire lasers.

The recent demonstration of room temperature lasing in InGaAs/GaAs core-shell nanopillars[1] grown on Si [13] is a promising accomplishment toward the monolithic integration of nanolasers with Si. In this paper, the InGaAs/GaAs heterostructures were grown on silicon without the use of metal catalysts, under conditions that are compatible with complementary metal–oxide–semiconductor (CMOS) technology. Lasing was achieved by optically pumping with an external laser, and a lasing threshold of $\sim$93 μJ cm^{-2} was measured at room temperature. The quality $\langle Q \rangle$ factor of the nanopillar cavity was estimated to be $\sim$206. Optical losses due to high tapering in the nanopillars and leakage to the high index Si substrate resulted in such a low Q factor. In such a cavity, low order Fabry–Perot modes which experience large loss cannot lase. Instead lasing was achieved for higher order whispering gallery modes, since they experience relatively lower losses. However, these modes in principle require larger diameter nanowires to propagate. Further work in growing high-quality III-V

[1]They were termed nanopillars because they were much wider ($\sim$600 nm) and shorter than most nanowires.

nanowires on silicon with minimum tapering is necessary to accomplish lower lasing thresholds and a smaller device footprint.

Metal Cavity Nanolasers

The dimensions of nanowire lasers described earlier are ultimately constrained by the diffraction limit. To reduce the optical mode size and laser cavity dimensions further, especially for nanolasers emitting in the infrared, metal-dielectric cavities have to be used. The metal also serves as an electrical contact and as a heat sink. This was demonstrated in [14], in which InP/InGaAs heterostructure nanopillars were clad with Au, and lasing was achieved by electrical pumping at low temperatures. The effective volume of the device was smaller than the diffraction limit. However, nonradiative recombinations, in particular Auger recombination, as a result of using Au limited the device functionality at room temperature. Instead, Ag, which has the lowest optical losses at infrared wavelengths, was used in the next demonstration, which achieved room-temperature lasing in metal–insulator–metal waveguide [15]. However, this device only had one dimension of the order of the wavelength of light (cross section 6 μm long $\times$ 310 nm wide) and required large pulsed currents (peak value $\sim$6 mA) for room-temperature lasing.

In the most recent demonstration of electrically pumped metal cavity nanolaser, continuous-wave operation at 260 K was achieved [16]. The structure comprised of n-InP/InGaAs/p-InP rectangular pillar which was encapsulated by Ag with a thin SiN layer in between for insulation; see Fig. 1(b). The total device volume was smaller than the cubic of the operating wavelengths in vacuum and the threshold current for lasing was $\sim$620 μA. Room temperature lasing with optical pumping in a metal-dielectric cavity smaller than the wavelength of emission in all three dimensions was also reported in [17] for InGaAsP active region. In another example, named nanopatch laser [18], lasing at cryogenic temperatures was observed in a small patch of metal/semiconductor/metal sandwich. Again InGaAsP was used as the semiconductor gain material.

There are other possible metal cavity nanolaser structures, with optical mode volumes below the diffraction limit, which have been demonstrated recently [19], [20]. Plasmonic crystal defect nanolasers [19] are similar to photonic crystal defect lasers except, that a plasmonic crystal defect cavity, with dimensions much smaller than a photonic crystal defect cavity, is used to localize SPPs to a volume much smaller than the diffraction limit of light. In the other demonstration [20], a plasmonic cavity is formed by GaN nanorods on Au/SiO_2 substrate. Both these structures demonstrated lasing when optically pumped at low temperatures.

Lasing SPASERs

This idea of a SPASER was first proposed by Bergman and Stockman in 2003 [1]. Unlike metallic cavities that support SPPs, it is possible to excite highly confined LSPs in arrays of nanostructured metals by coupling the metal to a semiconductor gain medium [21], see Fig. 1(c). The LSPs are amplified through emission in the semiconductor and generate intense localized optical fields. Coupling the amplified surface plasmons to radiative modes results in a "lasing SPASER." The first demonstrations of a SPASER device with subwavelength confinement of light in all three dimensions was in 2009, using a dye gain medium [22] and a II-VI semiconductor gain medium [23]. These semiconductors however either have low lifetimes and/or are not compatible with current optoelectronics industrial processes.

Semiconductor nanolasers have certainly opened up opportunities for chip-scale integration, as a result of small device volumes, electrical operation and possible integration with Si. However, there are still further improvements to be made, especially in the fabrication process, in order to reduce surface damage, attain high-quality structures and high Q factor nanostructures. These are important considerations for devices to work at room temperature with lower threshold current. Also, efficient coupling of light from a subwavelength size laser cavity to waveguides and plasmonic circuits on Si has yet to be demonstrated. Further work is also required to demonstrate lasing SPASERS with III-V semiconductor gain materials.

References

[1] D. J. Bergman and M. I. Stockman, "Surface plasmon amplification by stimulated emission of radiation: Quantum generation of coherent surface plasmons in nanosystems," *Phys. Rev. Lett.*, vol. 90, no. 2, p. 027402, Jan. 2003.

[2] O. Hayden, R. Agarwal, and W. Lu, "Semiconductor nanowire devices," *Nano Today*, vol. 3, no. 5/6, pp. 12–22, Oct.–Dec. 2008.

[3] J. C. Johnson, H.-J. Choi, K. P. Knutsen, R. D. Schaller, P. Yang, and R. J. Saykally, "Single gallium nitride nanowire lasers," *Nat. Mater.*, vol. 1, no. 2, pp. 106–110, Oct. 2002.

[4] S. Gradecak, F. Qian, Y. Li, H.-G. Park, and C. M. Lieber, "GaN nanowire lasers with low lasing thresholds," *Appl. Phys. Lett.*, vol. 87, no. 17, pp. 173111-1–173111-3, Oct. 2005.

[5] J. Heo, "Monolithic single GaN nanowire laser with photonic crystal microcavity on silicon," *Appl. Phys. Lett.*, vol. 98, no. 2, pp. 021110-1–021110-3, Jan. 2011.

[6] M. H. Huang, S. Mao, H. Feick, H. Yan, Y. Wu, H. Kind, E. Weber, R. Russo, and P. Yang, "Room-temperature ultraviolet nanowire nanolasers," *Science*, vol. 292, no. 5523, pp. 1897–1899, Jun. 8, 2001.

[7] X. Duan, Y. Huang, R. Agarwal, and C. M. Lieber, "Single-nanowire electrically driven lasers," *Nature*, vol. 421, no. 6920, pp. 241–245, Jan. 2003.

[8] M. A. Zimmler, J. Bao, F. Capasso, S. Muller, and C. Ronning, "Laser action in nanowires: Observation of the transition from amplified spontaneous emission to laser oscillation," *Appl. Phys. Lett.*, vol. 93, no. 5, pp. 051101-1–051101-3, Aug. 2008.

[9] Y. Xiao, C. Meng, P. Wang, Y. Ye, H. Yu, S. Wang, F. Gu, L. Dai, and L. Tong, "Single-nanowire single-mode laser," *Nano Lett.*, vol. 11, no. 3, pp. 1122–1126, Mar. 2011.

[10] S. Chu, G. Wang, W. Zhou, Y. Lin, L. Chernyak, J. Zhao, J. Kong, L. Li, J. Ren, and J. Liu, "Electrically pumped waveguide lasing from ZnO nanowires," *Nat. Nanotechnol.*, vol. 6, no. 8, pp. 506–510, Jul. 2011.

[11] B. Hua, J. Motohisa, Y. Kobayashi, S. Hara, and T. Fukui, "Single GaAs/GaAsP coaxial core-shell nanowire lasers," *Nano Lett.*, vol. 9, no. 1, pp. 112–116, Jan. 2009.

[12] A. Pan, W. Zhou, E. S. P. Leong, R. Liu, A. H. Chin, B. Zou, and C. Z. Ning, "Continuous alloy-composition spatial grading and superbroad wavelength-tunable nanowire lasers on a single chip," *Nano Lett.*, vol. 9, no. 2, pp. 784–788, Feb. 2009.

[13] R. Chen, T.-T. D. Tran, K. W. Ng, W. S. Ko, L. C. Chuang, F. G. Sedgwick, and C. Chang-Hasnain, "Nanolasers grown on silicon," *Nat. Photon.*, vol. 5, no. 3, pp. 170–175, 2011.

[14] M. T. Hill, Y.-S. Oei, B. Smalbrugge, Y. Zhu, T. de Vries, P. J. van Veldhoven, F. W. M. van Otten, T. J. Eijkemans, J. P. Turkiewicz, H. de Waardt, E. J. Geluk, S.-H. Kwon, Y.-H. Lee, R. Notzel, and M. K. Smit, "Lasing in metallic-coated nanocavities," *Nat. Photon.*, vol. 1, no. 10, pp. 589–594, 2007.

[15] M. T. Hill, M. Marell, E. S. P. Leong, B. Smalbrugge, Y. Zhu, M. Sun, P. J. van Veldhoven, E. J. Geluk, F. Karouta, Y.-S. Oei, R. Nötzel, C.-Z. Ning, and M. K. Smit, "Lasing in metal–insulator–metal sub-wavelength plasmonic waveguides," *Opt. Exp.*, vol. 17, no. 13, pp. 11107–11112, Jun. 2009.

[16] K. Ding, Z. Liu, L. Yin, H. Wang, R. Liu, M. T. Hill, M. J. H. Marell, P. J. van Veldhoven, R. Notzel, and C. Z. Ning, "Electrical injection, continuous wave operation of subwavelength-metallic-cavity lasers at 260 K," *Appl. Phys. Lett.*, vol. 98, no. 23, pp. 231108-1–231108-3, Jun. 2011.

[17] M. P. Nezhad, A. Simic, O. Bondarenko, B. Slutsky, A. Mizrahi, L. Feng, V. Lomakin, and Y. Fainman, "Room-temperature subwavelength metallo-dielectric lasers," *Nat. Photon.*, vol. 4, no. 6, pp. 395–399, Jun. 2010.

[18] K. Yu, A. Lakhani, and M. C. Wu, "Subwavelength metal-optic semiconductor nanopatch lasers," *Opt. Exp.*, vol. 18, no. 9, pp. 8790–8799, Apr. 2010.

[19] A. M. Lakhani, M.-K. Kim, E. K. Lau, and M. C. Wu, "Plasmonic crystal defect nanolaser," *Opt. Exp.*, vol. 19, no. 19, pp. 18237–18245, Sep. 2011.

[20] C.-Y. Wu, C.-T. Kuo, C.-Y. Wang, C.-L. He, M.-H. Lin, H. Ahn, and S. Gwo, "Plasmonic green nanolaser based on a metal–oxide–semiconductor structure," *Nano Lett.*, vol. 11, no. 10, pp. 4256–4260, Oct. 2011.

[21] B. Luk'yanchuk, N. I. Zheludev, S. A. Maier, N. J. Halas, P. Nordlander, H. Giessen, and C. T. Chong, "The Fano resonance in plasmonic nanostructures and metamaterials," *Nat. Mater.*, vol. 9, no. 9, pp. 707–715, 2010.

[22] M. A. Noginov, G. Zhu, A. M. Belgrave, R. Bakker, V. M. Shalaev, E. E. Narimanov, S. Stout, E. Herz, T. Suteewong, and U. Wiesner, "Demonstration of a spaser-based nanolaser," *Nature*, vol. 460, no. 7259, pp. 1110–1112, Aug. 2009.

[23] R. F. Oulton, V. J. Sorger, T. Zentgraf, R.-M. Ma, C. Gladden, L. Dai, G. Bartal, and X. Zhang, "Plasmon lasers at deep subwavelength scale," *Nature*, vol. 461, no. 7264, pp. 629–632, Oct. 2009.

Advances in Imaging Beyond the Diffraction Limit

Alex M. H. Wong, *Student Member, IEEE*, and George V. Eleftheriades, *Fellow, IEEE*

(Invited Paper)

Department of Electrical and Computer Engineering, University of Toronto, Toronto, ON M5S 3G4, Canada

DOI: 10.1109/JPHOT.2012.2189615
1943-0655/$31.00 ©2012 IEEE

Manuscript received February 15, 2012; accepted February 22, 2012. Date of current version April 20, 2012. This work was sponsored by the National Science and Engineering Research Council of Canada.
Corresponding author: A. M. H. Wong (e-mail: alex.wong@utoronto.ca).

Abstract: Considerable research has been devoted to the development of imaging apparatus capable of high-resolution imaging beyond the diffraction limit. Innovative subdiffraction imaging systems have been proposed and successfully demonstrated. These systems either focus the electromagnetic near-field more tightly than a Hertzian dipole or resolve the electromagnetic far-field beyond Abbé's diffraction limit and, hence, can be termed subdiffraction imaging systems. This paper reviews major advances in the field of subdiffraction imaging in the year 2011, along the research fronts of superlenses, hyperlenses, metascreens, and superoscillations.

Index Terms: Imaging systems, subwavelength resolution, diffraction limit, metamaterials.

1. Superlens

Our review on progress in subdiffraction imaging in the year 2011 begins with the superlens, as it can be argued that Pendry's proposal of the superlens in year 2000 [1] revived research interest in the field of subdiffraction imaging. Pendry showed that a negative index slab (henceforth called the superlens) not only gives rise to negative refraction but can actually amplify evanescent waves and, thus, restore high-resolution details, which are inaccessible by classical imaging systems. In 2004, Grbic and Eleftheriades demonstrated superlensing for the first time with a 2-D microwave transmission-line metamaterial [2]. A year later, Fang *et al.* demonstrated optical subdiffraction imaging, following Pendry's suggestion of using a thin silver slab as a poor man's superlens for TE waves [3].

While the initial superlenses were restricted in terms of the object wave's polarization and direction of incidence, much effort has been directed toward making a 3-D, isotropic, polarization independent superlens. The transmission-line metamaterial emerged as a viable candidate (due to its low loss) for building such a superlens in the microwave regime. In 2009, Iyer and Eleftheriades extended the transmission-line superlens into 3-D in a volumetric fashion [4]; in 2011, Rudolph and Grbic used a transmission-line inspired platform to demonstrate the first 3-D, fully isotropic, polarization independent superlens [5]. They fabricated their superlens using a 3-D stereolithographic technique [see Fig. 1(a)] and showed that their superlens attained a field intensity focal width of approximately 0.17λ at an image distance of 0.15λ and at 1.51 GHz. A wide subdiffraction focusing bandwidth of over 13% has also been observed.

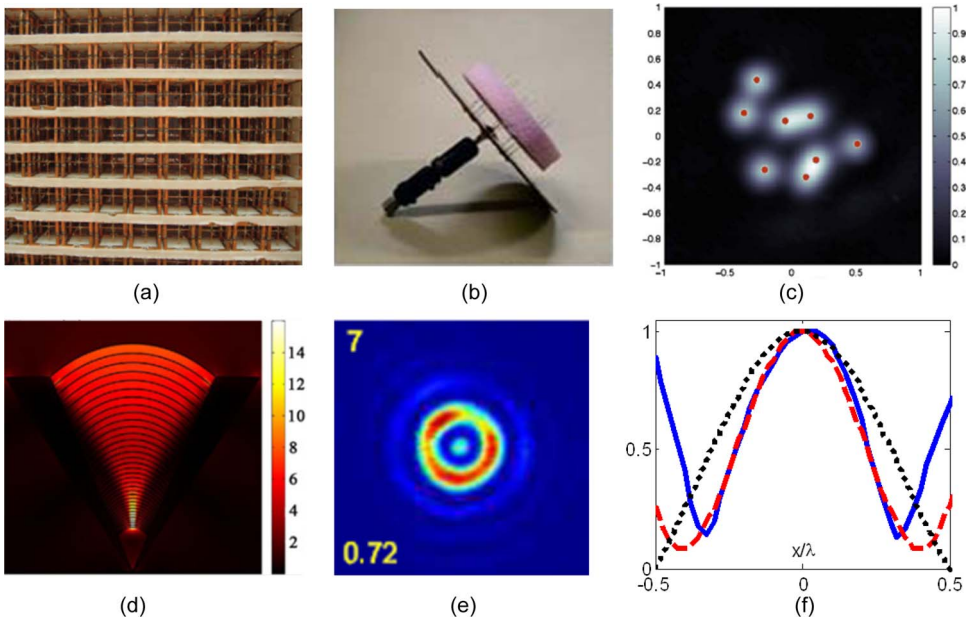

Fig. 1. Progress in subdiffraction imaging. (a) A frontal view of the microwave isotropic superlens [5, Fig. 6]. (b) A metascreen monopole array probe head inset of [17, Fig. 12]. (c) 2-D near-field subdiffraction imaging with the metascreen in (b). Most scatterers (labeled as red dots) are resolved with the metascreen, while a diffraction-limited probe failed to resolve any of them [17, Fig. 14(a)]. (d) Full-wave simulation of a trumpet hyperlens, showing subdiffraction electric field concentration at the bottom end of the trumpet [12, Fig. 4(d)]. (e) A measured superoscillatory focal pattern constructed by the optical eigenmode approach. The central peak has a spot width 72% of the diffraction limit (part of [25, Fig. 8]). (f) In-waveguide experimental subdiffraction focusing at a 5λ focal distance, comparing the measured (blue, solid), and simulated (red, dash) field profiles with the diffraction limit (black) (adapted from [22, Fig. 10]).

A related work by Kehr *et al.* [6] applies the superlensing effect to improve imaging resolution at mid-IR frequencies. Using a perovskite-based superlens, Kehr *et al.* demonstrated resolution improvement in a near-field scanning setup, compared to when the superlens was absent. The group demonstrated a resolution of $\lambda/14$ at the extreme near-field—at an image distance of 30 nm (around $\lambda/450$). While the involvement of a near-field probe and a reflective microscopic modality means the overall imaging system should not be considered as a simple superlens, the group distinguished probe-resonant effects from the superlensing effect and showed that superlensing was responsible for the observed resolution improvement.

2. Hyperlens and Related Developments

While the superlens forms an image of an object in the near field, the hyperlens images a near-field object into the far-field with subdiffraction resolution. Independently proposed by Jacob *et al.* [7] and by Salandrino and Engetha [8], the hyperlens is an anisotropic metamaterial exhibiting a hyperbolic dispersion property, which enables it to convert an object's evanescent waves into propagating waves, then image them into the far-field. The hyperlens has seen various developments in year 2011. Zhang *et al.* proposed theoretical extensions and designed a hyperlens with negative μ_ϕ and ρ_z [9]. They synthesized the necessary electromagnetic properties with an S-string-patterned metamaterial, performed simulations and experiments in the microwave range, and demonstrated a subdiffraction resolution of $\lambda/10$—an appreciable improvement over the initial optical demonstration where a resolution of about $\lambda/3$ was achieved [10].

On the optical front, the Wuhan University group of Zheng *et al.* [11] and the Lanzhou University group of Meng *et al.* [12] investigated using the hyperlens in reverse—to focus an impinging plane wave into a subdiffraction spot. The Wuhan group coupled an immersion lens with a traditional hyperlens, and showed through simulations that the system is capable of forming a focus with a spot

size of $\lambda/11$. The Lanzhou group proposed the trumpet hyperlens, which is a sectorized hyperlens with its layered curves redesigned with a transformation optics approach. They showed in simulation [see Fig. 1(b)] that their design funnels a normally incident plane wave toward a central spot down to 6 nm—or $\lambda/60$—in size. A successful experimental demonstration on this front would be of significant interest to the fields of subdiffraction imaging and lithography.

3. Metascreens

Besides efforts toward achieving subdiffraction imaging using metamaterials, there is also prevalent work toward forming subdiffraction focal spots—and subsequently images—with subwavelength structured surfaces, which we will collectively term metascreens. A metascreen is an electromagnetic surface upon which one can launch an electromagnetic wave, which evolves into a subdiffraction spot at a set distance away from the surface. The principle was first proposed by Merlin [13], and a working device was first proposed by Wong *et al.* [14] based on a near-field holographic point of view. The field of metascreens has since seen constant development. Grbic *et al.* summarized their research effort in a work in 2011 [15]. They solved an inverse electromagnetic problem to find the spatially varying surface impedance along the metascreen, then synthesized the impedance surface using current strips and current rings. With their metascreen, they calculated ultratight focusing to below $\lambda/15$, at a focal length of $\lambda/15$. Previous experiments on similar designs from Grbic *et al.* have yielded similar subdiffraction focusing results [16] in the microwave regime.

Markley and Eleftheriades adopted a different perspective to designing metascreens [17]. They employed a "shifted-beam" theory and designed the metascreen by optimizing the near-field interference of a 2-D antenna array. Using this approach, they proposed dipole and monopole arrays, and experimentally demonstrated focusing and imaging capabilities about 50% reduced from that of a diffraction-limited system [see Fig. 1(b) and (c)]. While their system resolution—experimentally found to be 0.25λ to 0.3λ—and their obtained focal widths are higher than in the work by Grbic *et al.*, these focal widths are obtained at a working distance of a quarter wavelength—much longer than the range considered by Grbic *et al.* and much improved over the working distance of most near-field probes. This work can be carried into the optical regime, with similar resolution improvement ratios achieved for 1-D subdiffraction imaging [18].

A related work from the group of Pan *et al.* should also be mentioned. In their work, a multistage plasmonic lens was proposed, which allowed the extraordinary transmission of ultraviolet light through a structured nanoscale aperture, thus forming a tight spot with an intensity full width and half maximum of 45 nm at 10 nm from the lens [19]. The resolution was then further improved to 22 nm due to the thermal threshold of the photoresist 10 nm away from the lens. Although the multistage plasmonic lens (which can be viewed as a form of metascreen) was diffraction-limited in the near-field sense according to the definition given in our abstract, it nonetheless greatly enhanced the transmitted power while maintaining, for the most part, the field localization of a same-shaped central aperture. It can thus be viewed as a use of the metascreen in a practical lithographic environment.

4. Superoscillation

Whereas superlenses, hyperlenses, and metascreens employ evanescent waves which limit either their object-to-device or their device-to-image distances, a newly emergent class of super-oscillation-based devices are unhindered by these distance limitations. Superoscillation refers to a wave phenomenon whereby within an interval of a waveform, rapid oscillations occur which exceed the waveform's highest constituent frequency. High-energy sidebands coexist with such super-oscillations. However, if one can tolerate the sidebands, one can record subdiffraction features with superoscillatory propagating waves, and thereby image them into the far-field.

Superoscillations were first studied as a mathematical property of the prolate spheroidal wave functions [20], which have been proposed as candidates to improve image resolution in a post-processing scheme [21]. Recently, Wong and Eleftheriades [22] related superoscillation and Schelkunoff's superdirectivity as dual effects in the spatial and spatial-frequency domains. Leveraging this analogy, Wong and Eleftheriades used methods of antenna design to synthesize

superoscillation waves, and demonstrated microwave subdiffraction focusing at a working distance of five wavelengths [see Fig. 1(f)] [22]. The periodic nature of their design allowed them to demonstrate superoscillation within a waveguide environment, which greatly compacted the lateral electrical size of their device. In a parallel stream of work, Huang and Zheludev numerically synthesized superoscillations using prolate spheroidal wave functions [23]. More recently, their collaboration with Baumgartl *et al.* resulted in a demonstration of optical subdiffraction focusing using a superoscillatory waveform constructed from optical eigenmodes, which in turn are formed from the superposition of Bessel beams [24], [25]. In their work, a subdiffraction field intensity lobe of 0.35λ was created at a focal length away from a focusing microscope objective [see Fig. 1(e)]. In a separate development, Makris and Psaltis theoretically and numerically studied the formation of diffraction-free superoscillatory waveforms, which directly beamed subdiffraction features into the far-field [26].

References

[1] J. B. Pendry, "Negative refraction makes a perfect lens," *Phys. Rev. Lett.*, vol. 85, no. 18, pp. 3966–3969, Oct. 2000.
[2] A. Grbic and G. V. Eleftheriades, "Overcoming the diffraction limit with a planar left-handed transmission-line lens," *Phys. Rev. Lett.*, vol. 92, no. 11, pp. 117403-1–117403-4, Mar. 2004.
[3] N. Fang, H. Lee, C. Sun, and X. Zhang, "Sub-diffraction-limited optical imaging with a silver superlens," *Science*, vol. 308, no. 5721, pp. 534–537, Apr. 2005.
[4] A. K. Iyer and G. V. Eleftheriades, "Free-space imaging beyond the diffraction limit using a Veselago-Pendry transmission-line metamaterial superlens," *IEEE Trans. Antennas Propag.*, vol. 57, no. 6, pp. 1720–1727, Jun. 2009.
[5] S. M. Rudolph and A. Grbic, "The design and performance of an isotropic negative-refractive-index metamaterial lens," in *Proc. URSI Gen. Assembly Sci. Symp.*, Aug. 13–20, 2011, pp. 1–4.
[6] S. C. Kehr, Y. M. Liu, L. W. Martin, P. Yu, M. Gajek, S. Y. Yang, C. H. Yang, M. T. Wenzel, R. Jacob, H. G. von Ribbeck, M. Helm, X. Zhang, L. M. Eng, and R. Ramesh, "Near-field examination of perovskite-based superlenses and superlens-enhanced probe-object coupling," *Nat. Commun.*, vol. 2, p. 249, Mar. 2011.
[7] Z. Jacob, L. V. Alekseyev, and E. Narimanov, "Optical hyperlens: Far-field imaging beyond the diffraction limit," *Opt. Exp.*, vol. 14, no. 18, pp. 8247–8256, Sep. 2006.
[8] A. Salandrino and N. Engheta, "Far-field subdiffraction optical microscopy using metamaterial crystals: Theory and simulations," *Phys. Rev. B*, vol. 74, no. 7, pp. 075103-1–075103-5, Aug. 2006.
[9] W. Zhang, H. Chen, and H. O. Moser, "Subwavelength imaging in a cylindrical hyperlens based on S-string resonators," *Appl. Phys. Lett.*, vol. 98, no. 7, pp. 073501-1–073501-3, Feb. 2011.
[10] Z. Liu, H. Lee, Y. Xiong, C. Sun, and X. Zhang, "Far-field optical hyperlens magnifying sub-diffraction-limited objects," *Science*, vol. 315, no. 5819, p. 1686, Mar. 2007.
[11] G. Zheng, R. Zhang, S. Li, P. He, H. Zhou, and Y. Shi, "A hyperlens-embedded solid immersion lens for beam focusing beyond the diffraction limit," *IEEE Photon. Technol. Lett.*, vol. 23, no. 17, pp. 1234–1236, Sep. 2011.
[12] Q. Meng, X. Zhang, L. Cheng, P. Cao, Y. Li, H. Zhang, and G. Wang, "Deep subwavelength focusing of light by a trumpet hyperlens," *J. Opt.*, vol. 13, no. 7, p. 075102, Jul. 2011, DOI:10.1088/2040-8978/13/7/075102.
[13] R. Merlin, "Radiationless electromagnetic interference: Evanescent-field lenses and perfect focusing," *Science*, vol. 317, no. 5840, pp. 927–929, Aug. 2007.
[14] A. M. H. Wong, C. D. Sarris, and G. V. Eleftheriades, "Metallic transmission screen for sub-wavelength focusing," *Electron. Lett.*, vol. 43, no. 25, pp. 1402–1404, Dec. 2007.
[15] A. Grbic, R. Merlin, E. M. Thomas, and M. F. Imani, "Near-field plates: Metamaterial surfaces/arrays for subwavelength focusing and probing," *Proc. IEEE*, vol. 99, no. 10, pp. 1806–1815, Oct. 2011.
[16] A. Grbic, L. Jiang, and R. Merlin, "Near-field plates: Subdiffraction focusing with patterned surfaces," *Science*, vol. 320, no. 5875, pp. 511–513, Apr. 2008.
[17] L. Markley and G. V. Eleftheriades, "Meta-screens and near-field antenna-arrays: A new perspective on subwavelength focusing and imaging," *Metamaterials*, vol. 5, no. 2/3, pp. 97–106, Jun.–Sep. 2011.
[18] Y. Wang, A. M. H. Wong, L. Markley, A. S. Helmy, and G. V. Eleftheriades, "Plasmonic meta-screen for alleviating the trade-offs in the near-field optics," *Opt. Exp.*, vol. 17, no. 15, pp. 12 351–12 361, Jul. 2009.
[19] L. Pan, Y. Park, Y. Xiong, E. Ulin-Avila, Y. Wang, L. Zeng, S. Xiong, J. Rho, C. Sun, D. B. Bogy, and X. Zhang, "Maskless plasmonic lithography at 22 nm resolution," *Sci. Rep.*, vol. 1, p. 175, Nov. 2011.
[20] D. Slepian and H. O. Pollak, "Prolate spheroidal wave functions, Fourier analysis and uncertainty I," *Bell Syst. Tech. J.*, vol. 40, pp. 43–63, 1961.
[21] C. W. Barnes, "Object restoration in a diffraction-limited imaging system," *J. Opt. Soc. Amer.*, vol. 56, no. 5, pp. 575–578, May 1966.
[22] A. M. H. Wong and G. V. Eleftheriades, "Sub-wavelength focusing at the multi-wavelength range using superoscillations: An experimental demonstration," *IEEE Trans. Antennas Propag.*, vol. 59, no. 12, pp. 4766–4776, Dec. 2011.
[23] F. M. Huang and N. I. Zheludev, "Super-resolution without evanescent waves," *Nano Lett.*, vol. 9, no. 3, pp. 1249–1254, Mar. 2009.
[24] J. Baumgartl, S. Kosmeier, M. Mazilu, E. T. F. Rogers, N. I. Zheludev, and K. Dholakia, "Far field subwavelength focusing using optical eigenmodes," *Appl. Phys. Lett.*, vol. 98, no. 18, pp. 181109-1–181109-3, May 2011.
[25] M. Mazilu, J. Baumgartl, S. Kosmeier, and K. Dholakia, "Optical eigenmodes; Exploiting the quadratic nature of the energy flux and of scattering interactions," *Opt. Exp.*, vol. 19, no. 2, pp. 933–945, Jan. 2011.
[26] K. G. Makris and D. Psaltis, "Superoscillatory diffraction-free beams," *Opt. Lett.*, vol. 36, no. 22, pp. 4335–4337, Nov. 2011.

Surface Plasmon Polaritons and Its Applications

Xiangang Luo[1] **and Lianshan Yan**[2]

(Invited Paper)

[1]State Key Laboratory of Optical Technologies for Micro-Nano Fabrication and Engineering, Institute of Optics and Electronics, Chinese Academy of Science, Chengdu 610209, China
[2]Center for Information Photonics and Communications, Southwest Jiaotong University, Chengdu 610031, China

DOI: 10.1109/JPHOT.2012.2189436
1943-0655/$31.00 ©2012 IEEE

Manuscript received February 13, 2012; revised February 22, 2012; accepted February 23, 2012. Date of current version April 20, 2012. Related work was supported by the National Basic Research Program of China under Grant 2011CB301800. Corresponding authors: X. G. Luo and L. Yan (e-mail: lxg@ioe.ac.cn; lsyan@home.swjtu.edu.cn).

Abstract: Surface plasmon polaritons (SPPs) have become one of the most rapidly expanding fields in photonics today. Exciting advances were made in research on SPPs in 2011. This review summarizes the significant progress and major achievements of super-resolution imaging, SPP lithography, SPP-assisted absorption, SPP-based antennas, light manipulation, and the current state-of-the-art in loss-compensation and process. The potential applications, future challenges, and opportunities are also discussed.

Index Terms: Nanostructures, nanophotonics, surface plamsmon polariton.

The unique properties of surface plasmon polaritons (SPPs) provide pathways to harnessing light in ways not possible with conventional optics. Many SPP-based achievements have been continuously emerging through deep research in 2011.

The first breakthrough is SPPs super-resolution imaging. The spatial resolution of conventional imaging systems is inherently restricted by diffraction limit. A hyperlens lens, following Pendry's perfectlens or superlens [1], was the first step toward magnifying subdiffraction-scale objects to the far-field with subdiffraction resolution imaging. Based on alternating stacks of metallic and dielectric films with nanoscale thickness, semispherical and cylindrical hyperlens designs were proposed to magnify nano-objects [2], [3]. Rahman *et al.* realized subwavelength optical imaging with an array of silver nanorods [4], while Robillard report on the subwavelength imaging capabilities of a photonic crystal (PC) flat lens consisting of triangular array of steel cylinders in methanol, all surrounded by water [5].

Despite many years of investigation into alternative lithographic techniques, no obvious replacements for optical approaches have been developed. With the help of SPPs, this trend will keep on going. The pioneering efforts for nanolithography with SPPs [6], [7] indicated that SPPs might provide one promising alternative to optical lithography and imaging with resolution far smaller than the wavelength without the need for complicated optics and expensive light sources. The most important challenge has been to achieve sufficient demagnification using SPPs lithography. Luo *et al.* proposed to apply a phase-shifting mask (PSM) that comprises chromium slits alternatively filled by Ag and PMMA to achieve $\sim\lambda/10$ ($\sim$35 nm) resolution ($\sim\lambda/6$ without the PSM) [8]. In fact, an entirely new SPPs lithographic scheme to realize lithographic imaging with a

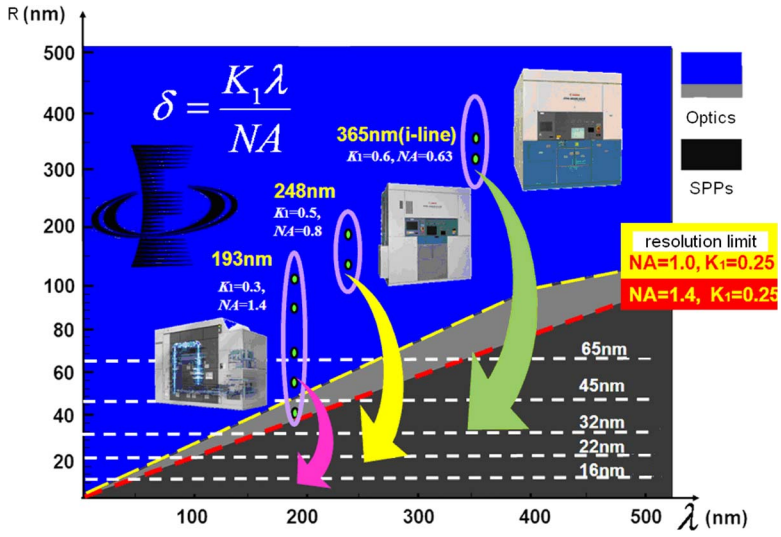

Fig. 1. Roads for SPPs nanolithography using UV light.

reduction-ratio beyond the diffraction limit has been demonstrated [9]. (Fig. 1 indicates the roadmap of SPPs nanolithography using UV light with increased resolution.) The latest experiment of SPPs lithography demonstrated printing of about 32 nm lines by demagnifying a mask pattern. Theoretical calculations predict SPPs lithography to achieve a spatial resolution beyond the 22-nm node [9]. Of course a number of engineering challenges will need to be addressed before this approach can be introduced into real world nanomanufacturing applications.

Another fascinating advance is the demonstration of the nearly complete light absorption in plasmonic structures [10]. This conversion can be realized utilizing specific micro-nano metallic structures to create desired surface impedance, resulting in complete coupling of the incident light into regions with large losses. Microcavity structures are introduced at the entrance and exit sides of a slit to realize the resonant field enhancement to enhance the optical absorption in subwavelength slits [11]. Truncated spherical voids nanostructured tungsten films are shown to have nearly perfect absorption with characteristics of broadband, polarization-independent and wide-incidence angle [12]. For tolerance to fabrication errors, quite recently, a broadband light harvesting nanostructures robust to edge bluntness is proposed and investigated [13]. Coherent perfect absorption of light is proposed and demonstrated in a planar intrinsic silicon slab when illuminated on both sides by two beams with equal intensities and correct relative phase [14]. Such a device is termed a coherent perfect absorber (CPA) and a "time-reversed laser." The coherent absorption enhancement can also be extended to strong scattering media [15]. Compared with the perfect absorbers (PAs) based on metamaterials or plasmonic structures [16], CPA provides additional tunability of absorption through the interplay of absorption and interference. The coherent control of absorption is potentially useful in transducers, modulators, or optical switches. Recently, Luo *et al.* proposed a ultrathin broadband nearly PA with symmetrical coherent illuminations to avoid the intrinsic narrow band problem of the CPA [17].

Optical antennas are an enabling technology for manipulating and controlling optical radiation at subwavelength or nanometer scales [18], [19], while also providing optimal control of transduction in the far-field. A detailed formalism allowing analytical calculations of the radiation properties for nanoantennas design (Yagi–Uda configurations) is given in [20]. In addition and more promising, optical antennas have also been explored to enhance the efficiency of photovoltaic devices, particularly for solar energy harvesting. Fan *et al.* identified the number of optical states as the major factor for light absorption, as well as the presence of the high-index material near the interface effectively raised the refractive index of the low-index material [21]. Most recently, Atwater's team generalized this idea by showing that cramming in more optical states can make thin-film absorbers

take up more light than usual, also providing a comprehensive study of various designs that potentially go beyond the ray-optic limit [22]. Enhanced radiation is the opposite side of light absorption, which is of great importance for light sources, such as light-emitting diodes (LEDs). Several notable demonstrations have been done to improve the efficiency of LEDs (or OLEDs) aided by the plasmonic structures [23]–[25].

Another application of optical antennas is biosensing [26]. Bartoli *et al.* experimentally demonstrated a plasmonic Mach–Zehnder interferometer (MZI, formed by patterning two parallel nanoslits in a thin metal film) integrated with a microfluidic chip for ultrasensitive biosensing [27], yielding enhanced refractive index sensitivities greater than 3500 nm/RIU and record high sensing figures of merit exceeding 200 in the visible region. Dregely *et al.* reported a palladium-based plasmonic PA at visible wavelengths and its application to hydrogen sensing [28]. Their design exhibits a reflectance $< 0.5\%$ and zero transmittance at 650 nm, and thus, the exposure to hydrogen gas causes a rapid and reversible increase in reflectance on a time scale of seconds.

Beam manipulation is another example taking advantage of the strong coupling of metallic structures with electromagnetic wave [29]. Since the pioneering work made by Ebbesen *et al.* [30], SPPs have been demonstrated to provide the opportunity to confine light into very small dimensions by means of surface corrugation, opening new opportunities for subwavelength optical devices [29]–[32]. Luo *et al.* present a design for a subwavelength hole array decorated with an electric resonance ring to realize angle-insensitive extraordinary optical transmission in the far-infrared regime [29]. Levy *et al.* propose and experimentally demonstrate the nanoscale focusing of surface plasmons by constructing an integrated plasmonic/photonic on chip nanofocusing device in silicon platform [33]. Palacios *et al.* analyzed both experimentally and theoretically the physical mechanisms that determine the optical transmission through deep subwavelength bull's eye structures [34]. In addition, various schemes of "lens" or beam focusing have been proposed [35]–[37].

In reality, the existence of SPPs not only depends on the strong dispersion of the metal, but also the specific pattern design on the metal surface [38]. In the Terahertz region, the spoof SPP's structure is designed to collimate light beams [39], which is composed of a 1-D array of L-shaped metallic elements horizontally attached to a metal surface. In the microwave region, another new radiation mode, surface polaritons radiation mode, was proposed to design a corrugated antenna, achieving higher aperture efficiency and stronger directivity with elements' space beyond a wavelength [40].

The intrinsic loss in metals is a fundamental challenge, which would dramatically limit the performance of plasmonic devices. Searching for materials with low loss has become one necessary step to realize optimal plasmonic properties for specific frequencies and applications [41]. Gain medium, amplifiers, and lasers based on SPPs have been studied for decades [42]. Various metallic structures such as planes, films, stripes, wires and particles, have been integrated with gain materials. In particular, Zayats *et al.* experimentally demonstrated suppressed absorptions and stimulated emission of SPP with more than 10 times efficiency compared with out-of-plane pumping [43]. Such approach may open up a possibility for active nanophotonic integration. Gather *et al.* demonstrated amplified spontaneous emission of long-range SPPs in planar metallic waveguides embedded in a fluorescent polymer with a net gain coefficient of 8 ± 2/cm for propagation up to 2 mm [44]. Plasmon laser [45] and loss compensated active metamaterials [46] are also proposed as alternatives.

No progress in SPPs research will be possible without further developments in fabrication. Surface roughness and other inhomogeneities have so far limited SPPs propagation in real plasmonic devices. Last year, Shalaev's group at Purdue University obtained a significant result showing how to create ultrathin, ultrasmooth and low-loss Ag films and silver–silica lamellar composite films [47]. They further developed a fabrication method for creating semicontinuous metal films with arbitrary thickness and a modeling technique for such films using realistic geometries [48].

Ultrasmooth patterned metals for SPPs have been realized by combined template stripping with precise patterned silicon substrates [49]. These achievements may remarkably improve the performance of superlens and hyperlens structures for high-resolution and subwavelength imaging. The properties of SPPs at the plasmon resonance frequency can also help develop various passive or

active (dynamic) nano-optic devices. Devices that have potential applications in telecommunications including optical interconnect or photonic integrated circuits are of great interests [50]–[53]. Recently Février demonstrated a total energy transfer from a TE mode to a transverse plasmon mode of a coupled metal nanoparticle chain at 1550 nm [54]. So-called "Giant coupling" effects happened from record coupling lengths as short as ~560 nm. Such a design opens the way for localized plasmon-based devices into photonic integrated circuits. Gjonaj *et al.* achieved active control (both the amplitude and phase) of the coherent properties of SPPs excited on a nanohole array [55]. Their observations revealed SPPs dressed with the Bloch modes of the periodic nanostructure (dressed plasmons DP). Actively controlling DP waves via programmable phase patterns offers the potential for high field confinement applicable in lithography, surface-enhanced Raman scattering, and plasmonic structured illumination microscopy. In addition, as evidenced by the nonlinear tunneling conduction between gold electrodes separated by a subnanometer gap under illumination, Ward *et al.* further proved that a strong confinement of the field with an enhancement factor exceeding 10^3 for interelectrode distances on the order of a few Angstroms does exist [56].

Within only one year, we have witnessed many remarkable breakthroughs. Without any doubt, SPPs have become an extremely exciting research area. The unique electromagnetic properties provided by SPPs have attracted considerable attention from researchers in multiple disciplines. In turn, the merging of knowledge and expertise across different areas will further drive the astounding advances of SPPs research. The advances in the field are so extensive and it is inevitably difficult to include all in this brief review. Important future practical applications of SPPs are strongly dependent on further theoretical and technological advanced in this area.

References

[1] J. B. Pendry, "Negative refraction makes a perfect lens," *Phys. Rev. Lett.*, vol. 85, no. 18, pp. 3966–3969, Oct. 2000.
[2] W. Zhang, H. Chen, and H. O. Moser, "Subwavelength imaging in a cylindrical hyperlens based on S-string resonators," *Appl. Phys. Lett.*, vol. 98, no. 7, pp. 073501–073503, Feb. 2011.
[3] D. Li, D. H. Zhang, C Yan, and Y. Wang, "Two-dimensional subwavelength imaging from a hemispherical hyperlens," *Appl. Opt.*, vol. 50, no. 31, pp. G86–G90, Nov. 2011.
[4] A. Rahman, Y. Hao, C. Parini, P. A. Belov, and S. Y. Kosulnikov, "Subwavelength optical imaging with an array of silver nanorods," *J. Nanophoton.*, vol. 5, p. 051601, 2011.
[5] J. Robillard, J. Bucay, P. A. Deymier, A. Shelke, K. Muralidharan, B. Merheb, J. O. Vasseur, A. Sukhovich, and J. H. Page, "Resolution limit of a photonic crystal superlens," *Phys. Rev. B*, vol. 83, no. 22, pp. 224301-1–224301-11, Jun. 2011.
[6] X. G. Luo and T. Ishihara, "Surface plasmon resonant interference nanolithography technique," *Appl. Phys. Lett.*, vol. 84, no. 23, pp. 4780–4782, Jun. 2004.
[7] N. Fang, H. Lee, C. Sun, and X. Zhang, "Sub-diffraction-limited optical imaging with a Silver Superlens," *Science*, vol. 308, no. 5721, pp. 534–537, Apr. 2005.
[8] N. Yao, Z. Lai, L. Fang, C. Wang, Q. Feng, Z. Zhao, and X. Luo, "Improving resolution of superlens lithography by phase-shifting mask," *Opt. Exp.*, vol. 19, no. 17, pp. 15 982–15 989, Aug. 2011.
[9] X. G. Luo, Q. Feng, K. Liu, L. Liu, Y. Liu, L. Pan, C. Wang, and H. Xing, "A method of demagnification projection for sub-diffraction imaging and lithography," China Patent 200 910 243 540.1, Aug. 4, 2010.
[10] T. V. Teperik, F. J. García de Abajo, A. G. Borisov, M. Abdelsalam, P. N. Bartlett, Y. Sugawara, and J. J. Baumberg, "Omnidirectional absorption in nano-structured metal surfaces," *Nature*, vol. 2, no. 5, pp. 299–301, May 2008.
[11] C. Min, L. Yang, and G. Veronis, "Microcavity enhanced optical absorption in subwavelength slits," *Opt. Exp.*, vol. 19, no. 27, pp. 26 850–26 858, Dec. 2011.
[12] X. G. Luo, M. Wang, C. Hu, M. Pu, C. Huang, Z. Zhao, and Q. Feng, "Truncated spherical voids for nearly omnidirectional optical absorption," *Opt. Exp.*, vol. 19, no. 21, pp. 20 642–20 649, Oct. 2011.
[13] Y. Luo, D. Y. Lei, S. A. Maier, and J. B. Pendry, "Broadband light harvesting nanostructures robust to edge bluntness," *Phys. Rev. Lett.*, vol. 108, no. 2, pp. 023901–023905, Jan. 2012.
[14] W. Wan, Y. Chong, L. Ge, H. Noh, A. D. Stone, and H. Cao, "Time-reversed lasing and interferometric control of absorption," *Science*, vol. 331, no. 6019, pp. 889–892, Feb. 2011.
[15] Y. D. Chong and A. D. Stone, "Hidden black: Coherent enhancement of absorption in strongly scattering media," *Phys. Rev. Lett.*, vol. 107, no. 16, p. 163901-1, Oct. 2011.
[16] X. G. Luo, M. Pu, C. Hu, M. Wang, C. Huang, Z. Zhao, C. Wang, and Q. Feng, "Design principles for infrared wide-angle perfect absorber based on plasmonic structure," *Opt. Exp.*, vol. 19, no. 18, pp. 17 413–17 420, Aug. 2011.
[17] M. B. Pu, Q. Feng, M. Wang, C. Hu, C. Huang, X. Ma, Z. Zhao, C. Wang, and X. Luo, "Ultrathin broadband nearly perfect absorber with symmetrical coherent illumination," *Opt. Exp.*, vol. 20, no. 3, pp. 2246–2254, Jan. 2012.
[18] L. Novotny and N. van Hulst, "Antennas for light," *Nat. Photon.*, vol. 5, no. 2, pp. 83–90, Feb. 2011.
[19] R. Adato, A. A. Yanik, and H. Altug, "On chip plasmonic monopole nano-antennas and circuits," *Nano Lett.*, vol. 11, no. 12, pp. 5219–5226, Dec. 2011.

[20] B. Stout, A. Devilez, B. Rolly, and N. Bonod, "Multipole methods for nanoantennas design: Applications to Yagi-Uda configurations," *J. Opt. Soc. Amer. B*, vol. 28, no. 5, pp. 1213–1223, May 2011.
[21] Z. Yu, A. Raman, and S. Fan, "Fundamental limit of nanophotonic light trapping in solar cells," *Proc. Nat. Acad. Sci. U.S.A.*, vol. 107, no. 41, pp. 17 491–17 496, Oct. 2010.
[22] D. M. Callahan, J. N. Munday, and H. A. Atwater, "Solar cell light trapping beyond the ray optic limit," *Nano Lett.*, vol. 12, no. 1, pp. 214–218, Jan. 2012.
[23] C.-Y. Cho, S.-J. Lee, J.-H. Song, S.-H. Hong, S.-M. Lee, Y.-H. Cho, and S.-J. Park, "Enhanced optical output power of green light-emitting diodes by surface plasmon of gold nanoparticles," *Appl. Phys. Lett.*, vol. 98, no. 5, pp. 051106-1–051106-3, Jan. 2011.
[24] Y. Kuo, S. Y. Ting, C. H. Liao, J. J. Huang, C. Y. Chen, C. Hsieh, Y. C. Lu, C. Y. Chen, K. C. Shen, C. F. Lu, D. M. Yeh, J. Y. Wang, W. H. Chuang, Y. W. Kiang, and C. C. Yang, "Surface plasmon coupling with radiating dipole for enhancing the emission efficiency of a light-emitting diode," *Opt. Exp.*, vol. 19, no. S4, pp. A914–A929, Jul. 2011.
[25] S. G. Zhang, X. W. Zhang, Z. G. Yin, J. X. Wang, J. J. Dong, H. L. Gao, F. T. Si, S. S. Sun, and Y. Tao, "Localized surface plasmon-enhanced electroluminescence from ZnO-based heterojunction light-emitting diodes," *Appl. Phys. Lett.*, vol. 99, no. 18, pp. 181116-1–181116-3, Oct. 2011.
[26] T. Chung, S.-Y. Lee, E. Y. Song, H. Chun, and B. Lee, "Plasmonic nanostructures for nano-scale bio-sensing," *Sensors*, vol. 11, no. 11, pp. 10 907–10 929, Nov. 2011.
[27] Y. Gao, Q. Gan, Z. Xin, X. Cheng, and F. J. Bartoli, "Plasmonic Mach–Zehnder interferometer for ultrasensitive on-chip biosensing," *ACS Nano*, vol. 5, no. 11, pp. 9836–9844, Dec. 2011.
[28] A. Tittl, P. Mai, R. Taubert, D. Dregely, N. Liu, and H. Giessen, "Palladium-based plasmonic perfect absorber in the visible and its applications to hydrogen sensing," *Nano Lett.*, vol. 11, no. 10, pp. 4366–4369, Oct. 2011.
[29] C. G. Hu, P. Mai, R. Taubert, D. Dregely, N. Liu, and H. Giessen, "Extraordinary optical transmission induced by electric resonance ring and its dynamic manipulation at far-infrared regime," *Opt. Exp.*, vol. 19, no. 19, pp. 18 109–18 115, Sep. 2011.
[30] H. J. Lezec, A. Degiron, E. Devaux, R. A. Linke, L. Martin-Moreno, F. J. Garcia-Vidal, and T. W. Ebbesen, "Beaming light from a subwavelength aperture," *Science*, vol. 297, no. 5582, pp. 820–822, Aug. 2002.
[31] M. Schnell, P. Alonso-González, L. Arzubiaga, F. Casanova, L. E. Hueso, A. Chuvilin, and R. Hillenbrand, "Nanofocusing of mid-infrared energy with tapered transmission lines," *Nat. Photon.*, vol. 5, no. 5, pp. 283–287, May 2011.
[32] J. Weiner, "The electromagnetics of light transmission through subwavelength slits in metallic films," *Opt. Exp.*, vol. 19, no. 17, pp. 16 139–16 153, Aug. 2011.
[33] B. Desiatov, I. Goykhman, and U. Levy, "Plasmonic nanofocusing of light in an integrated silicon photonics platform," *Opt. Exp.*, vol. 19, no. 14, pp. 13 150–13 157, Jul. 2011.
[34] S. Carretero-Palacios, "Mechanisms for extraordinary optical transmission through bull's eye structures," *Opt. Exp.*, vol. 19, no. 11, pp. 10 429–10 442, May 2011.
[35] G. Zheng, R. Zhang, S. Li, P. He, and H. Zhou, "A hyperlens-embedded solid immersion lens for beam focusing beyond the diffraction limit," *IEEE Photon. Technol. Lett.*, vol. 23, no. 17, pp. 1234–1236, Sep. 2011.
[36] Z. Fang, Q. Peng, W. Song, F. Hao, J. Wang, P. Nordlander, and X. Zhu, "Plasmonic focusing in symmetry broken nanocorrals," *Nano Lett.*, vol. 11, no. 2, pp. 893–897, Feb. 2011.
[37] T. Zentgraf, Y. Liu, M. H. Mikkelsen, J. Valentine, and X. Zhang, "Plasmonic Luneburg and Eaton lenses," *Nat. Nanotechnol.*, vol. 6, no. 3, pp. 151–155, Mar. 2011.
[38] J. B. Pendry, L. Martín-Moreno, and F. J. Garcia-Vidal, "Mimicking surface plasmons with structured surfaces," *Science*, vol. 305, no. 5685, pp. 847–848, Aug. 2004.
[39] D. Martin-Cano, O. Quevedo-Teruel, E. Moreno, L. Martin-Moreno, and F. J. Garcia-Vidal, "Waveguided spoof surface plasmons with deep-subwavelength lateral confinement," *Opt. Lett.*, vol. 36, no. 23, pp. 4635–4637, Dec. 2011.
[40] X. G. Luo, J. Cui, Q. Feng, C. Huang, X. Luo, and Z. Zhao, "A novel surface polaritions radiation mode on the periodic corrugation for highly efficient beaming," China Patent 200 910 244 248.1, Jun. 2, 2010.
[41] A. Boltasseva and H. A. Atwater, "Low-loss plasmonic metamaterials," *Science*, vol. 331, no. 6015, pp. 290–291, Jan. 2011.
[42] P. Berini and I. de Leon, "Surface plasmon-polariton amplifiers and lasers," *Nat. Photon.*, vol. 6, no. 1, pp. 16–24, Jan. 2012.
[43] A. V. Krasavin, T. P. Vo, W. Dickson, P. M. Bolger, and A. V. Zayats, "All-plasmonic modulation via stimulated emission of copropagating surface plasmon polaritons on a substrate with gain," *Nano Lett.*, vol. 11, no. 6, pp. 2231–2235, Jun. 2011.
[44] M. C. Gather, D. Danz, K. Meerholz, and K. Leosson, "Optical amplification of propagating surface plasmon polaritons," presented at the Conf. Lasers Electro-Optics/Quantum Electronics Laser Science, Baltimore, MD, 2011, Paper QFE5.
[45] R. M. Ma, R. F. Oulton, V. J. Sorger, G. Bartal, and X. Zhang, "Room-temperature sub-diffraction-limited plasmon laser by total internal reflection," *Nat. Mater.*, vol. 10, no. 2, pp. 110–113, Feb. 2011.
[46] X. J. Ni, S. Ishii, M. D. Thoreson, V. M. Shalaev, S. Han, S. Lee, and A. V. Kildishev, "Loss-compensated and active hyperbolic metamaterials," *Opt. Exp.*, vol. 19, no. 25, pp. 25 242–25 254, Nov. 2011.
[47] W. Q. Chen, M. D. Thoreson, S. Ishii, A. V. Kildishev, and V. M. Shalaev, "Ultra-thin ultra-smooth and low-loss silver films on a germanium wetting layer," *Opt. Exp.*, vol. 18, no. 5, pp. 5124–5134, Feb. 2010.
[48] M. D. Thoreson, J. Fang, A. V. Kildishev, V. M. Shalaev, V. P. Drachev, L. J. Prokopeva, P. Nyga, and U. K. Chettiar, "Fabrication and realistic modeling of three-dimensional metal-dielectric composites," *J. Nanophoton.*, vol. 5, no. 1, pp. 051503-1–051503-17, Jan. 2011.
[49] P. Nagpal, N. C. Lindquist, S.-H. Oh, and D. J. Norris, "Ultrasmooth patterned metals for plasmonics and metamaterials," *Science*, vol. 325, no. 5940, pp. 594–597, Jul. 2009.
[50] Y. Guo, L. Yan, W. Pan, B. Luo, K. Wen, Z. Guo, H. Li, and X. Luo, "A plasmonic splitter based on slot cavity," *Opt. Exp.*, vol. 19, no. 15, pp. 13 831–13 838, Jul. 2011.

[51] F. F. Hu, H. Yi, and Z. Zhou, "Band-pass plasmonic slot filter with band selection and spectrally splitting capabilities," *Opt. Exp.*, vol. 19, no. 6, pp. 4848–4855, Mar. 2011.
[52] X. Sun, L. Zhou, X. Li, Z. Hong, and J. Chen, "Design and analysis of a phase modulator based on a metal-polymer-silicon hybrid plasmonic waveguide," *Appl. Opt.*, vol. 50, no. 20, pp. 3428–3434, Jul. 2011.
[53] J. Tao, Q. J. Wang, and X. G. Huang, "All-optical plasmonic switches based on coupled nano-disk cavity structures containing nonlinear material," *Plasmonics*, vol. 6, no. 4, pp. 753–759, Dec. 2011.
[54] M. Février, P. Gogol, A. Aassime, R. Mégy, C. Delacour, A. Chelnokov, A. Apuzzo, S. Blaize, J. M. Lourtioz, and B. Dagens, "Giant coupling effect between metal nanoparticle chain and optical waveguide," *Nano Lett.*, vol. 12, no. 2, pp. 1032–1037, Feb. 2012.
[55] B. Gjonaj, J. Aulbach, P. M. Johnson, A. P. Mosk, L. Kuipers, and A. Lagendijk, "Optical control of plasmonic BLOCH modes on periodic nanostructures," *Nano Lett.*, vol. 12, no. 2, pp. 546–550, Feb. 2012.
[56] A. Garcia-Martin, D. R. Ward, D. Natelson, and J. C. Cuevas, "Field enhancement in subnanometer metallic gaps," *Phys. Rev. B*, vol. 83, no. 19, pp. 193404-1–193404-4, May 2011.

Optofluidics for Biophotonic Applications

F. Bragheri, R. Osellame, and R. Ramponi

(Invited Paper)

Istituto di Fotonica e Nanotecnologie-CNR, Dipartimento di Fisica-Politecnico di Milano, 20133 Milano, Italy

DOI: 10.1109/JPHOT.2012.2190725
1943-0655/$31.00 ©2012 IEEE

Manuscript received February 15, 2012; revised February 27, 2012; accepted March 6, 2012. Date of current version April 20, 2012. This work was supported by the European Commission through the FP7 project *microFLUID* (Contract ICT-224205) and by Regione Lombardia through the project *MINILAB* (ID MAN-18). Corresponding author: R. Osellame (e-mail: roberto.osellame@ifn.cnr.it).

Abstract: Optofluidics experienced significant developments in the past few years and is still proving to be a dynamic field of research with a particular focus on biological and chemical sensing applications. This paper reviews a selection of 2011 achievements concerning different aspects of the on-chip integration of photonics and microfluidics and, in particular, highlighting how the versatility and simple reconfigurability of the optofluidic approach can represent an added value in biophotonic applications.

Index Terms: Optofluidics, biophotonics, optofluidic sensor, optofluidic manipulation, lab-on-chip.

1. Introduction

Optofluidics defines a wide research field that is characterized by the synergic combination of optics and microfluidics; hence, the term can be applied either when light senses or modifies a fluid or when a fluid is used to define or tune the properties of a photonic device (e.g., laser activated fluids, liquid lenses or microfluidic microscope) [1], [2]. In biophotonic applications, the combination of microfluidics and optics is typically exploited to further increase the miniaturization of the devices toward an integrated optofluidic platform [3]. Such a platform would benefit from both aspects previously mentioned in the definition of optofluidics; on the one hand, small amounts of fluid can provide unprecedented reconfigurability of the photonic devices; on the other hand, the very high sensitivity of optical detection methods can provide relevant measurements even on small amounts of biological fluid samples (nano/picoliters), down to single molecule detection [4], [5]. Particular attention is dedicated to the integration of different functionalities on a single substrate to obtain a lab-on-chip microsystem that can address biochemical and biomedical assays in a cost-effective, miniaturized, and automated way. Here, we review a selection of results reported in 2011, by classifying them into four main areas of research: 1) lens-free optofluidic microscopes (OFMs); 2) fluidic tuning of photonic devices; 3) on-chip optofluidic sensors; 4) optofluidic micromanipulation of biosamples.

2. Discussion

One interesting research area concerns the development of low-cost lens-free imaging systems to replace the traditional bulky microscopes. The OFM is one such method [6], offering lens-less high-resolution imaging by using a suitable microfluidic flow to scan specimens across submicrometer

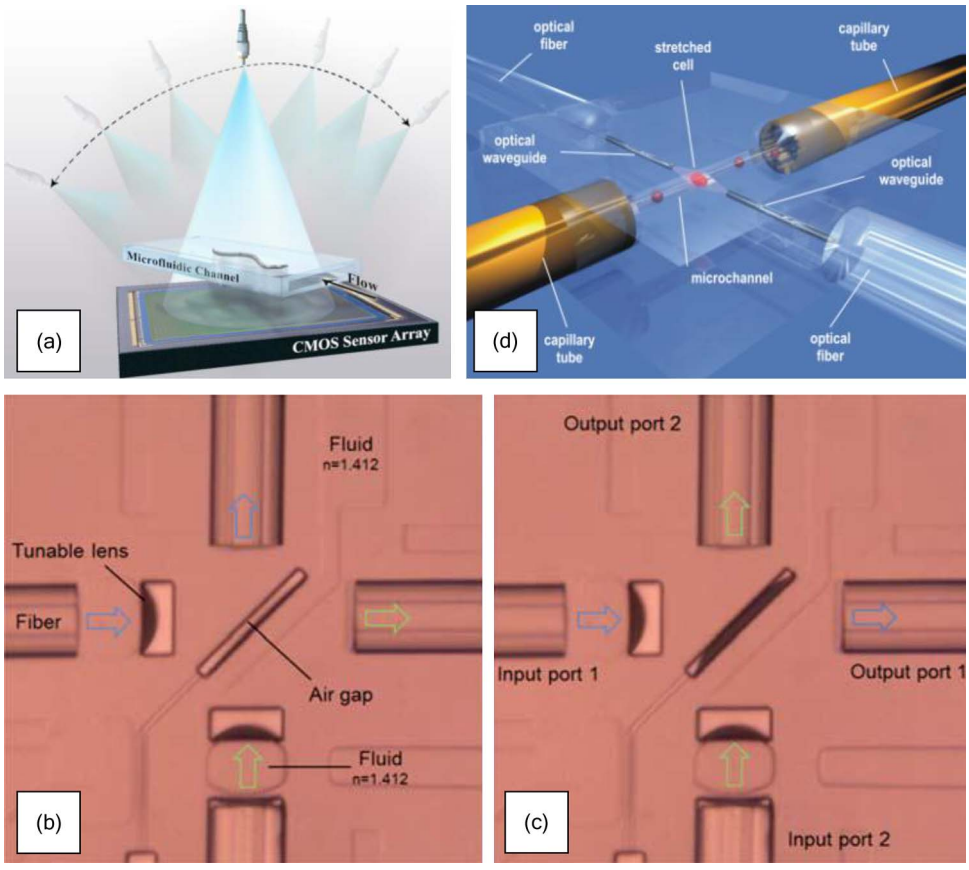

Fig. 1. (a) Schematic diagram of optofluidic tomographic microscopy setup [8] (courtesy of *Applied Physics Letters*). (b)–(c) Microscopy images of the pneumatically tunable 2 × 2 optofluidic switch for on-chip light routing controlled by compressed air, switching between exchange (b) and bypass (c) mode [14] (courtesy of Lab Chip). (d) 3-D rendering of the monolithic optical stretcher fabricated by femtosecond laser micromachining [25], [26] (courtesy of *Optics Express*).

apertures on a complementary metal–oxide–semiconductor (CMOS) image sensor. In 2011, a color imaging of blood samples to detect malaria has been reported [7]. Color illumination in a subpixel resolving OFM device yielded a resolution of 660 nm by using sequential red–green–blue (RGB) illumination to obtain a low-resolution sequence for each color and then combine them into a single high-resolution full-color image. A different approach has been reported in [8], [9] where the demonstration of optofluidic tomographic microscopy is shown. This on-chip tomographic imaging modality would be quite valuable for microfluidic lab-on-a-chip platforms where high-throughput 3-D imaging of the specimen is needed. A partially coherent light source is used to illuminate the objects flowing in a microfluidic channel directly placed on a digital sensor array. As sketched in Fig. 1(a) the light source is rotated to record lens-free holograms of the objects at different viewing directions. By capturing multiple frames at each illumination angle, pixel super-resolution techniques are utilized to reconstruct high-resolution transmission images.

A second important research area is that of fluidic tuning of optical components. In the past few years, there has been tremendous interest in the development of on-chip optical components such as lenses, mirrors, liquid waveguides, and light sources to be integrated with microfluidic components on a chip. As already mentioned, reconfigurability is a major advantage of optofluidics, where the optical properties of the device can be tuned by manipulating fluids. In [10], a novel method for building optofluidic microlenses with excellent flexibility, robustness, and simplicity has been reported. A compound microlens system is constructed with multiple lens elements self-aligned

together inside a monolithic polydimethylsiloxane (PDMS) microchip. The gas permeability of PDMS allows dead-end microchannels and microchambers to be completely filled with liquid, and the elasticity of PDMS ensures the deformation of thin membranes for tuning the lens. The tuning mechanism consists in discretely actuated pneumatic valves, integrated on-chip, which precisely adjusts the shape of the lenses. This method leads to high zoom ratio (7–8$\times$), wide tuning of the angle of view (15°–80°), large range of focal adjustment (from mm to cm), high numerical apertures (up to 0.44), and small lens-size (a few hundreds of micrometers in diameter). Another important component for biophotonic applications, e.g., fluorescence and Raman spectroscopy, is an optical spectral filter. In [11], on-chip optofluidic filters have been reported, where multiple spectral regions with high and low transmissions are achieved by tailoring three bottom layers of a liquid-core antiresonant reflecting optical waveguide (ARROW). High extinction (37 dB) was shown, using 4-mm-long optofluidic filters. In traditional optical systems, a prism is typically used to change the optical path of a collimated light beam or to perform light dispersion. A tunable optofluidic prism, based on two laminar flow streams with different refractive indices in a microfluidic triangular chamber, has been presented in [12]. This optofluidic prism provides new features, as its capability to transform from a symmetric to an asymmetric prism with the assistance of a third flow, and it might be useful in several applications as, for example, the precise deflection of an optical beam inside an integrated lab-on-a-chip system. Active devices have also been reported in 2011, such as an optofluidic modulator [13] and an optofluidic switch [14]. This latter device could play a key role in a reconfigurable optofluidic chip where several photonic circuits and microfluidic networks could be integrated. The authors presented a pneumatically tunable 2 $\times$ 2 optofluidic switch for on-chip light routing controlled by compressed air. The optical switching is realized in a PDMS chip with a tunable air-gap mirror that deflects the light, due to total internal reflection, in the exchange mode. When the device is subjected to high pressure, the air gap collapses and hence the light is switched to the bypass mode, as shown in Fig. 1(b) and (c). The device has a switching speed of more than 5 Hz and an extinction ratio of 8 dB. This switch can be integrated with other microfluidic circuits, and the authors demonstrated a simple reconfigurable optical waveguide circuit for dual-channel spectroscopy on a microfluidic chip.

A third area, in which research on optofluidics for biophotonic applications produced fruitful results in 2011, concerns the realization of integrated optofluidic sensors on a chip. Because of the variety of possible sensing techniques in the biological and biochemical field, this area saw achievements both in the exploitation of new technologies to fabricate optofluidic lab-on-chip devices and in the development of improved label-free sensing techniques. As new fabrication techniques are concerned, very interesting results were obtained by femtosecond laser micromachining. This technology allows the fabrication of both optical waveguides and microfluidic channels, and their 3-D integration; it has, therefore, great potential for the realization of optofluidic devices, as demonstrated by several examples reported in this 2011 review [15]. Further results have also been reported in 2011, where this technology has been exploited to fabricate optical waveguides on a commercial lab-on-chip to detect fluorescence from electrophoretically separated DNA molecules with an ultralow limit of detection [16]; this result paves the way to point-of-care, fast, and sensitive bioassays for detection of genetic diseases. A second example is the fabrication of a lab-on-a-chip that works as a compact and robust device for fast screening, real-time monitoring, and initial classification of algae [17], which is of importance when monitoring effects such as eutrophication, but also when assessing the water quality of watersheds. Concerning label-free sensing techniques, in [18], optofluidic intracavity spectroscopy (OFIS) is exploited to distinguish different types of cells by their optical properties. OFIS sensor chip combine microfluidic cell handling and a Fabry–Perot cavity to acquire transmission spectra that are qualitatively and quantitatively different for neoplastic and non-neoplastic cells. Neoplastic cells produce multimode transmission spectra, while non-neoplastic cells create only weak transmission peaks between bare cavity modes. Another spectroscopic label-free technique that is of great interest in this field of research is surface-enhanced Raman scattering (SERS). In [19], the use of a highly sensitive optical imaging technology using SERS-fluorescence in a dual modal nanoprobe is reported. Fluorescence imaging is used as a fast indicator of molecular recognition, while SERS imaging is subsequently used to determine the signature of specific molecular interactions. In this way, they demonstrated the use of fluorescence

and SERS sensing probes for targeting and imaging specific cancer markers in living cells. One of the main limitations in microfluidic platform for SERS detection is that the metal nanoparticles, which work as the Raman enhancers, are dispersed in solution. In [20], a novel active SERS platform based on optoelectrofluidics is presented, in which metal nanoparticles are spontaneously concentrated and assembled within the laser spot by optically induced electrokinetic mechanisms, resulting in the *in situ* enhancement of the SERS signal. What is interesting is that both the metal particle concentration and the Raman signal can be obtained with a single laser beam. A different sensor has been reported in [21], where a new device for measuring on-chip microfluidic pressure and flow rate using integrated optofluidic membrane interferometers (OMIs) is shown. The device is made of two layers of structured PDMS on a glass substrate by multilayer soft lithography. The OMI consists of a flexible air-gap optical cavity which, upon illumination by monochromatic light, generates interference patterns that depend on the pressure. Once the interference patterns are captured with a microscope and computer analyzed on the basis of a pattern recognition algorithm, a dynamic range of 0–10 psi with an accuracy of $\pm 2\%$ is achieved. By exploiting two OMI sensors it is possible to measure the flow rate in a channel. The exploitation of this sensor might be useful when a real time monitor of the flow of biological liquid samples is needed.

Finally, because of the importance that single cell methods are assuming in unraveling biological complexity [22], it is worth mentioning the application of optofluidics to optical manipulation and analysis of single particles/cells dispersed in liquids. In biological research and clinical medicine the possibility of sorting specific target cells from a heterogeneous population is of great importance. Two devices for single cell sorting are presented in [23] and [24], both based on the combination of microfluidics with optical tweezers. In the first paper sorting is conditioned to cell size or fluorescence and performed by means of moving optical tweezers. In the second paper the optical tweezers are exploited to trap and perform Raman spectral analysis on the cell; the outcome of the measurement is used to sort the cell by switching the flow between two outlet channels. Despite the low throughput of the systems both devices proved to be effective in discriminating different types of cells and might be used in the future for sorting rare progenitor cell populations in regenerative biology or to discriminate between normal blood cells and circulating tumor cells. A different approach in handling and analyzing single cells by integrating both fluidics and optics has been recently shown in [25] and [26], where a dual beam laser trap fabricated by means of femtosecond laser micromachining has been successfully used to trap and stretch one single red blood cell at a time to evaluate its mechanical properties. A high-throughput system for single cell manipulation has been presented in [27]. This microfluidic PDMS system is composed of one main channel with cell-trapping pockets and drain channels that also collect the single-cell content. The sequence of single-cell trapping and content extraction has been demonstrated with a 512-pocket device. In the future, this device could be applied to the quantification of the molecular weight variability in organelles like mitochondria. Most of the optofluidic approaches in micromanipulation are based on traditional optical tweezing techniques, which have proven to be inadequate in direct application to the handling of nanoscale materials. To overcome this limitation a relatively new research field is growing concerning nanomanipulation by means of near field photonics. As reviewed in [28], a number of research groups have demonstrated how the evanescent fields surrounding photonic structures like photonic waveguides, optical resonators, and plasmonic nanoparticles can be used to greatly enhance optical forces envisaging the possibility of exploiting these techniques into lab-on-a-chip devices for single molecule analysis, nanoassembly, and optical chromatography.

3. Conclusion

Research in optofluidics saw significant activity in 2011 and a broad variety of biophotonic applications. Integration seems to be the main drive as well as the search for high-performance and cost-effective solutions. This highly interdisciplinary field is continuously growing every year and can help life sciences to have a tangible impact on our everyday life.

References

[1] V. R. Horowitz, D. D. Awschalom, and S. Pennathur, "Optofluidics: Field or technique?" *Lab. Chip*, vol. 8, no. 11, pp. 1856–1863, Nov. 2008.

[2] D. Psaltis, S. R. Quake, and C. Yang, "Developing optofluidic technology through the fusion of microfluidics and optics," *Nature*, vol. 442, no. 7101, pp. 381–386, Jul. 2006.

[3] C. Monat, P. Domachuk, and B. J. Eggleton, "Integrated optofluidics: A new river of light," *Nat. Photon.*, vol. 1, pp. 106–114, Feb. 2007.

[4] X. Fan and I. M. White, "Optofluidic microsystems for chemical and biological analysis," *Nat. Photon.*, vol. 5, no. 10, pp. 591–597, Oct. 2011.

[5] H. Schmidt and A. R. Hawkins, "The photonic integration of non-solid media using optofluidics," *Nat. Photon.*, vol. 5, no. 10, pp. 598–604, Oct. 2011.

[6] X. Cui, L. M. Lee, X. Heng, W. Zhong, P. W. Sternberg, D. Psaltis, and C. Yang, "Lensless high-resolution on-chip optofluidic microscopes for Caenorhabditis elegans and cell imaging," *Proc. Nat. Acad. Sci.*, vol. 105, no. 31, pp. 10 670–10 675, Aug. 2008.

[7] S. A. Lee, R. Leitao, G. Zheng, S. Yang, A. Rodriguez, and C. Yang, "Color capable sub-pixel resolving optofluidic microscope and its application to blood cell imaging for malaria diagnosis," *PLoS ONE*, vol. 6, no. 10, pp. e26127/1–e26127/6, Oct. 2011.

[8] S. O. Isikman, W. Bishara, H. Zhu, and A. Ozcan, "Optofluidic tomography on a chip," *Appl. Phys. Lett.*, vol. 98, no. 6, p. 161 109, Apr. 2011.

[9] S. O. Isikman, W. Bishara, U. Sikora, O. Yaglidere, J. Yeah, and A. Ozcan, "Field-portable lensfree tomographic microscope," *Lab Chip*, vol. 11, no. 13, pp. 2222–2230, Jul. 2011.

[10] P. Fei, Z. He, C. Zheng, T. Chen, Y. Men, and Y. Huang, "Discretely tunable optofluidic compound microlenses," *Lab Chip*, vol. 11, no. 17, pp. 2835–2841, Aug. 2011.

[11] P. Measor, B. S. Phillips, A. Chen, A. R. Hawkins, and H. Schmidt, "Tailorable integrated optofluidic filters for biomolecular detection," *Lab Chip*, vol. 11, no. 5, pp. 899–904, Mar. 2011.

[12] S. Xiong, A. Q. Liu, L. K. Chin, and Y. Yang, "An optofluidic prism tuned by two laminar flows," *Lab Chip*, vol. 11, no. 11, pp. 1864–1869, Jun. 2011.

[13] J. G. Cuennet, A. E. Vasdekis, L. De Sio, and D. Psaltis, "Optofluidic modulator based on peristaltic nematogen microflows," *Nat. Photon.*, vol. 5, no. 4, pp. 234–238, Apr. 2011.

[14] W. Song and D. Psaltis, "Pneumatically tunable optofluidic 2 $\times$ 2 switch for reconfigurable optical circuit," *Lab Chip*, vol. 11, no. 14, pp. 2397–2402, 2011.

[15] R. Osellame, H. Hoekstra, G. Cerullo, and M. Pollnau, "Femtosecond laser microstructuring: An enabling tool for optofluidic lab-on-chips," *Laser Photon. Rev.*, vol. 5, no. 3, pp. 442–463, May 2011.

[16] C. Dongre, J. van Weerd, G. A. J. Besselink, R. Martinez Vazquez, R. Osellame, G. Cerullo, R. van Weeghel, H. H. van den Vlekkert, H. J. W. M. Hoekstra, and M. Pollnau, "Modulation-frequency encoded multi-color fluorescent DNA analysis in an optofluidic chip," *Lab Chip*, vol. 11, no. 4, pp. 679–683, Feb. 2011.

[17] A. Schaap, Y. Bellouard, and T. Rohrlack, "Optofluidic lab-on-a-chip for rapid algae population screening," *Biomed. Opt. Exp.*, vol. 2, no. 3, pp. 658–664, Mar. 2011.

[18] W. Wang, D. W. Kisker, D. H. Thamm, H. Shao, and K. L. Lear, "Optofluidic intracavity spectroscopy of canine hemangiosarcoma," *IEEE Trans. Biomed. Eng.*, vol. 58, no. 4, pp. 853–860, Apr. 2011.

[19] S. Lee, H. Chon, S. Y. Yoon, E. K. Lee, S. I. Chang, D. W. Lim, and J. Choo, "Fabrication of SERS-fluorescence dual modal nanoprobes and application to multiplex cancer cell imaging," *Nanoscale*, vol. 4, no. 1, pp. 124–129, 2012.

[20] H. Hwang, D. Han, Y. J. Oh, Y. K. Cho, K. H. Jeong, and J. K. Park, "In situ dynamic measurements of the enhanced SERS signal using an optoelectrofluidic SERS platform," *Lab Chip*, vol. 11, no. 15, pp. 2518–2525, 2011.

[21] W. Song and D. Psaltis, "Optofluidic membrane interferometer: An imaging method for measuring microfluidic pressure and flow rate simultaneously on a chip," *Biomicrofluidics*, vol. 5, no. 4, p. 044110, Dec. 2011.

[22] N. de Souza, "Single-cell methods," *Nat. Methods*, vol. 9, no. 1, p. 35, Jan. 2012.

[23] X. Wang, S. Chen, M. Kong, Z. Wang, K. D. Costa, R. A. Li, and D. Sun, "Enhanced cell sorting and manipulation with combined optical tweezer and microfluidic chip technologies," *Lab Chip*, vol. 11, no. 21, pp. 3656–3662, Nov. 2011.

[24] S. Dochow, C. Krafft, U. Neugebauer, T. Bocklitz, T. Henkel, G. Mayer, J. Albert, and J. Popp, "Tumour cell identification by means of Raman spectroscopy in combination with optical traps and microfluidic environments," *Lab Chip*, vol. 11, no. 8, pp. 1484–1490, 2011.

[25] N. Bellini, K. C. Vishnubhatla, F. Bragheri, L. Ferrara, P. Minzioni, R. Ramponi, I. Cristiani, and R. Osellame, "Femtosecond laser fabricated monolithic chip for optical trapping and stretching of single cells," *Opt. Exp.*, vol. 18, no. 5, pp. 4679–4688, Mar. 2010.

[26] F. Bragheri, L. Ferrara, P. Minzioni, I. Cristiani, K. Vishnubhatla, N. Bellini, R. Ramponi, and R. Osellame, "Single cell trapping and stretching in an optofluidic chip fabricated by femtosecond laser micromachining," in *CLEO/Europe EQEC Conf. Dig., OSA Tech. Dig. (CD)*, Munich, Germany, May 2011, Paper JSIV2_4.

[27] T. Arakawa, M. Noguchi, K. Sumitomo, Y. Yamaguchi, and S. Shoji, "High-throughput single-cell manipulation system for a large number of target cells," *Biomicrofluidics*, vol. 5, no. 1, p. 014114, Mar. 2011.

[28] D. Erickson, X. Serey, Y. Chenac, and S. Mandala, "Nanomanipulation using near field photonics," *Lab Chip*, vol. 11, no. 6, pp. 995–1009, Mar. 2011.

Breakthroughs in Nonlinear Silicon Photonics 2011

Yoshitomo Okawachi,[1] Alexander L. Gaeta,[1] and Michal Lipson[2]

(Invited Paper)

[1]School of Applied and Engineering Physics, Cornell University, Ithaca, NY 14853 USA
[2]School of Electrical and Computer Engineering, Cornell University, Ithaca, NY 14853 USA

DOI: 10.1109/JPHOT.2012.2189874

Manuscript received February 17, 2012; accepted February 24, 2012. Date of current version April 20, 2012. Corresponding author: A. L. Gaeta (e-mail: a.gaeta@cornell.edu).

Abstract: We present an overview of the recent developments in nonlinear silicon photonics. There were significant advances in devices exploiting the $\chi^{(2)}$ and $\chi^{(3)}$ nonlinearities. Here, we discuss parametric amplification, wavelength conversion, supercontinuum generation, parametric oscillation, and frequency comb generation in silicon-based devices.

Index Terms: Nonlinear optics, nanophotonics, silicon photonics, four-wave mixing (FWM).

1. Introduction

With the recent advances of fabrication and processing techniques, there has been significant progress in the development of silicon-based chip-scale devices for nonlinear optics. Efficient nonlinear optical processes require both large nonlinearities and low losses. The inherent large nonlinearity of silicon along with the high optical confinement that can be achieved due to the high refractive index contrast between the core and cladding allows for a significant enhancement in the effective nonlinearity, as compared with optical fibers [1]. This large effective nonlinearity combined with the improvement in linear propagation losses has allowed for extraordinarily compact nonlinear optical devices that previously might have required hundreds of meters of fiber.

In addition to the effective nonlinearity, the phase matching of the wavevectors associated with the interacting fields determines the efficiency of the nonlinear process. In order to achieve this phase matching, it is essential to engineer the effective dispersion of the nonlinear interaction. This dispersion depends on both the intrinsic material (material dispersion), which is fixed, and on the geometric properties of the medium (waveguide dispersion), which can be varied. In waveguide structures, the waveguide dispersion can be modified by engineering the cross section size and shape, allowing for the flexibility to tailor the net dispersion to be normal or anomalous to suit the particular nonlinear process [2]–[4].

In this review, we will focus on developments in 2011 related to silicon-based nonlinear optical devices utilizing the $\chi^{(2)}$ and $\chi^{(3)}$ nonlinearity. These devices have shown promise largely due to the fact that they are CMOS-process compatible, are low-cost, have low linear losses in the telecommunication window, and offer promise for fully integrated optoelectronic devices. In particular, we will discuss the advances in parametric amplification and wavelength conversion, supercontinuum generation, and parametric oscillation and frequency comb generation.

2. Parametric Amplification and Wavelength Conversion

In recent years, there has been significant research in dispersion-engineered silicon waveguides for broadband parametric amplification and wavelength conversion. Parametric four-wave mixing (FWM) is a nonlinear process that depends on the third-order nonlinearity $\chi^{(3)}$ in which two pump photons annihilate to create a signal and idler photon pair. To achieve efficient FWM, it is necessary to tailor the dispersion of the waveguide such that the pump wavelength is tuned near the zero-group velocity dispersion (GVD) point of the waveguide [5], [6]. CMOS-compatible silicon-based FWM devices have been demonstrated using silicon, silicon nitride, and high-index silica glass waveguides and, over the past few years, there have been numerous signal processing applications utilizing chip-scale FWM, including signal regeneration [7], an ultrafast oscilloscope [8], and a radio-frequency spectrum analyzer [9]. Further developments in 2011 include real-time dispersion monitoring for high-speed differential phase-shift keying signals [10], spectral phase interferometry for direct electric-field reconstruction (SPIDER) [11], and time integration of optical signals [12]. For further development of these FWM-based devices, higher efficiencies and larger operating bandwidths are critical. Previous FWM demonstrations have shown extremely broadband wavelength conversion spanning from 1241 to 2078 nm using a pump laser in the telecommunications C-band [13]. The efficiency of the FWM process pumped in the C-band is ultimately limited by two-photon absorption (TPA) and free-carrier absorption (FCA) induced by TPA. Various techniques have been utilized to circumvent the effects of FCA, such as the use of a reverse-biased $p-i-n$ diode for carrier removal [14]. However, the effects of TPA are unavoidable at telecommunication wavelengths, due to the proximity to the silicon band-edge [15], [16].

Another silicon-based material that has shown promise for large parametric amplification is hydrogenated amorphous silicon (a-Si:H) [17]. Unlike crystalline silicon, it is possible to change the material properties of a-Si:H with fabrication procedures. In 2011, Kuyken *et al.* [18] demonstrated 26.5 dB parametric gain in a-Si:H waveguides. This is made possible since the bandgap of a-Si:H is 1.61 eV, in contrast with 1.12 eV for crystalline Si, which corresponds to a half-bandgap wavelength near 1550 nm. For a-Si:H this significantly reduces the effects of nonlinear absorption, allowing for an improvement in the figure-of-merit, defined as the ratio of the real and imaginary parts of the nonlinear parameter, by a factor of 4, as compared with crystalline Si waveguides [19]. While material degradation from pump exposure currently limits the performance [19], the a-Si:H platform offers potential for efficient on-chip optical signal processing.

Alternatively, there has been significant effort to design crystalline Si waveguides for operation near and beyond 2.2 μm, which corresponds to half the bandgap energy of silicon. Previously, large amplification was demonstrated with a pulsed pump source [20], [21]. In 2011, Lau *et al.* [22] presented the first demonstration of broadband continuous wave parametric wavelength conversion pumped near 2 μm. The results indicate a maximum conversion bandwidth of 748 nm, which is limited only by the detection range of the spectrum analyzer used. Simulation results indicate a theoretical bandwidth of 936 nm. Additionally, Kuyken *et al.* [23] demonstrated 50-dB parametric gain using a pulsed pump at 2173 nm. They achieve $>$40 dB gain over a wavelength range exceeding 580 nm. Recent studies performed in 2011 by Hon *et al.* [24] and Gholami *et al.* [25] indicate that the third-order nonlinearity in silicon beyond 2.2 μm is comparable to that in the near-infrared region. With the further development of platforms that exhibit lower losses in the midinfrared region, including silicon-on-porous-silicon and silicon-on-sapphire [26]–[28], the operation wavelength range of parametric mixing devices should extend into the 3–5-μm midinfrared region. Silicon photonics technology extended into this regime will allow for the translation of well-developed telecommunications technology to the midinfrared and the development of innovative devices for applications including astronomy, biochemical sensing, free-space communications, and spectroscopy.

In addition, there have been studies of parametric nonlinear processes based on the $\chi^{(2)}$ nonlinearity. Since in centrosymmetric materials, such as silicon, the bulk $\chi^{(2)}$ contribution vanishes, it is necessary to break the bulk symmetry to observe a second-order nonlinear response. Two approaches have been demonstrated. One utilizes a technique to induce strain in a silicon waveguide. To achieve the strain, the silicon waveguide is clad with a straining Si_3N_4 layer, allowing

for an efficient phase matching for $\chi^{(2)}$ interactions. Cazzanelli *et al.* [29] demonstrate both sum-frequency generation and second harmonic generation (SHG) in the strained silicon waveguides. The second approach utilizes a silicon nitride ring resonator where the symmetry breaking occurs at the interface between silicon nitride core and silicon dioxide cladding. By satisfying the phase matching conditions and utilizing the cavity geometry, Levy *et al.* [30] demonstrate efficient SHG, generating a signal at 777 nm from a 1554 nm pump. In addition, $\chi^{(3)}$-based third-harmonic generation is observed in the nitride ring resonators. These demonstrations offer additional paths toward further extending the operational wavelength range of these integrated devices.

3. Supercontinuum Generation

Over the past decade rapid progress has been made in supercontinuum generation (SCG) with the utilization of photonic crystal fibers [31]. A variety of applications exist for SCG, including spectroscopy, frequency metrology, optical coherence tomography, gas sensing, and pulse compression. Recently, the use of chip-scale devices has attracted interest, due to its potential for integration and high-volume, low-cost fabrication. Supercontinuum generation has been previously demonstrated in chalcogenide [32] and lithium niobate [33] platforms and both achieve broad spectral bandwidths. However, neither platform is readily compatible with existing CMOS processes. Alternatively, there has been work done on SCG in high-index silica glass waveguides 45-cm in length, with spectra spanning 300 nm and centered at 1550 nm [34].

Due to its high nonlinearity, silicon is an ideal platform for SCG. However, the effects of TPA limit the continuum bandwidth that can be achieved when pumped near the silicon bandgap [35], [36]. In 2011, Kuyken *et al.* [37] demonstrated SCG in silicon spanning three-quarters of an octave from 1535 to 2525 nm. This broad bandwidth is achieved by placing the pump at wavelengths near the half-bandgap energy of silicon, minimizing the effects of TPA and FCA. Alternatively, SCG has been demonstrated in silicon nitride waveguides. Although the nonlinearity of silicon nitride is smaller than that of silicon, it is an ideal platform for nonlinear optics at communication wavelengths due to the fact that it is still CMOS-compatible and does not suffer from the effects of TPA. Halir *et al.* [38] have shown SCG spanning 1.6 octaves from 665 to 2025 nm. These demonstrations offer promise towards the realization of a chip-scale supercontinuum source.

4. Parametric Oscillation and Frequency Comb Generation

In addition to linear waveguide structures, 2011 saw significant developments in integrated resonator structures for nonlinear optical processes. The high confinement of the optical field in the silicon waveguide structures combined with the enhancement due to the cavity geometry enables significant enhancements in the effective nonlinearity and results in highly efficient parametric processes with moderate pump powers. When the FWM gain exceeds the round-trip cavity loss, optical parametric oscillation occurs where the signal and idler pair at the cavity modes oscillates. At higher powers, cascaded parametric oscillation occurs enabling the generation of a broadband frequency comb. While frequency comb generation utilizing mode-locked femtosecond lasers is a mature technology [39], there has been significant interest over the past few years in developing a compact comb source based on parametric oscillation in high quality (Q) factor microresonators pumped by a single-frequency laser [40]. In particular, recent demonstrations using a CMOS-compatible, monolithically integrated resonator structures in high-index silica glass [41] and silicon nitride [42] offer potential as platforms for environmentally robust, ultracompact, stabilized frequency comb generation that can be used in applications such as spectroscopy, gas sensing, on-chip clock distribution for high-speed optical networks, remote clock synchronization, and photonic analog-to-digital conversion.

In 2011, there were significant advances in silicon-nitride-based frequency comb generation, both in generation and characterization [43], [44]. To enable efficient phase-matching for FWM over a broad bandwidth, the resonator cross section is engineered to create a broad spectral range with anomalous GVD, and researchers [44] demonstrated a parametric frequency comb spanning an octave of optical bandwidth from 1170 to 2350 nm (see Fig. 1). In parametric frequency comb

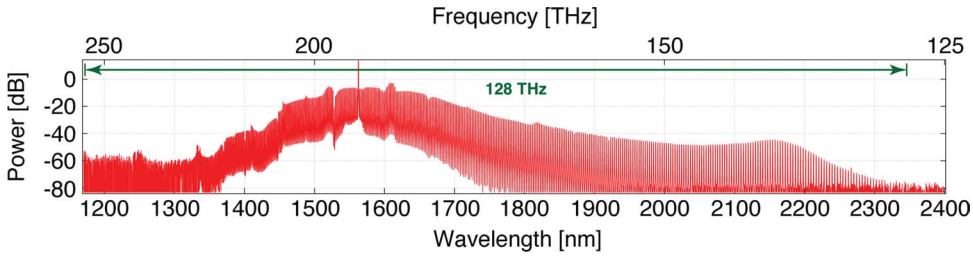

Fig. 1. Optical spectrum of an octave-spanning frequency comb in a silicon nitride resonator (from Okawachi *et al.* [44]).

generation, the wavelength of the single-frequency pump laser is red-detuned into a cavity resonance generating a signal-idler pair through FWM. As the pump wavelength is tuned deeper into resonance, the cavity power builds up further, resulting in cascaded FWM and higher-order degenerate and nondegenerate FWM processes increasing the frequency comb bandwidth and comb density. In addition, Okawachi *et al.* [44], characterize the RF amplitude noise of the comb and observe a 30 dB reduction in the noise as the comb is generated, indicating a transition to a phase-locked state. Foster *et al.* [43] characterized the comb quality and showed a comb equidistance of 3×10^{-15} relative to the optical frequency over a 115-nm bandwidth, which corresponds to a deviation 0.5 Hz over a 14.5-THz span. Since the dispersion of the resonator is highly dependent on the waveguide cross section, the dispersion and cavity free-spectral range are largely decoupled, allowing for independent control over the two parameters. This provides an advantage, as compared with whispering gallery resonators and allows for flexibility in choosing the pump wavelength, ranging from visible to midinfrared, and the comb spacing. Compared with femtosecond-laser-based frequency comb generation, parametric frequency comb generation is a technology that is not yet mature, and both theoretical and experimental studies are needed to understand the mechanisms governing the comb dynamics [45], [46]. Nevertheless, arbitrary waveform generation was achieved by Ferdous *et al.* [47] by controlling the spectral phase of each of the frequency comb lines involved in pulse shaping, and sub-ps pulses at a 230-GHz repetition rate were produced. As this technology matures over the next few years, we anticipate significant developments in on-chip frequency comb-based devices.

5. Conclusion

2011 saw significant advances in silicon-based devices utilizing the $\chi^{(2)}$ and $\chi^{(3)}$ nonlinearity at the traditional communication wavelengths and in the midinfrared. With the performance improvements shown in these devices, we anticipate the emergence of new applications utilizing chip-based nonlinear optics.

References

[1] M. A. Foster, A. C. Turner, M. Lipson, and A. L. Gaeta, "Nonlinear optics in photonic nanowires," *Opt. Exp.*, vol. 16, no. 2, pp. 1300–1320, Jan. 2008.
[2] E. Dulkeith, F. Xia, L. Schares, W. M. Green, and Y. A. Vlasov, "Group index and group velocity dispersion in silicon-on-insulator photonic wires," *Opt. Exp.*, vol. 14, no. 9, pp. 3853–3863, May 2006.
[3] A. C. Turner, C. Manolatou, B. S. Schmidt, M. Lipson, M. A. Foster, J. E. Sharping, and A. L. Gaeta, "Tailored anomalous group-velocity dispersion in silicon channel waveguides," *Opt. Exp.*, vol. 14, no. 10, pp. 4357–4362, May 2006.
[4] D. T. H. Tan, K. Ikeda, P. C. Sun, and Y. Fainman, "Group velocity dispersion and self phase modulation in silicon nitride waveguides," *Appl. Phys. Lett.*, vol. 96, no. 6, pp. 061101-1–061101-3, Feb. 2010.
[5] M. A. Foster, A. C. Turner, J. E. Sharping, B. S. Schmidt, M. Lipson, and A. L. Gaeta, "Broad-band optical parametric gain on a silicon photonic chip," *Nature*, vol. 441, no. 7096, pp. 960–963, Jun. 2006.
[6] M. A. Foster, A. C. Turner, R. Salem, M. Lipson, and A. L. Gaeta, "Broad-band continuous-wave parametric wavelength conversion in silicon nanowaveguides," *Opt. Exp.*, vol. 15, no. 20, pp. 12 949–12 958, Oct. 2007.
[7] R. Salem, M. A. Foster, A. C. Turner, D. F. Geraghty, M. Lipson, and A. L. Gaeta, "Signal regeneration using low-power four-wave mixing on silicon chip," *Nature Photon.*, vol. 2, no. 1, pp. 35–38, Jan. 2008.
[8] M. A. Foster, R. Salem, D. F. Geraghty, A. C. Turner-Foster, M. Lipson, and A. L. Gaeta, "Silicon-chip-based ultrafast optical oscilloscope," *Nature*, vol. 456, no. 7218, pp. 81–84, Nov. 2008.

[9] B. Corcoran, T. D. Vo, M. D. Pelusi, C. Monat, D.-X. Xu, A. Densmore, R. Ma, S. Janz, D. J. Moss, and B. J. Eggleton, "Silicon nanowire based radio-frequency spectrum analyzer," *Opt. Exp.*, vol. 18, no. 19, pp. 20 190–20 200, Sep. 2010.
[10] T. D. Vo, B. Corcoran, J. Schröder, M. D. Pelusi, D.-X. Xu, A. Densmore, R. Ma, S. Janz, D. J. Moss, and B. J. Eggleton, "Silicon-chip-based real-time dispersion monitoring for 640 Gbit/s DPSK signals," *J. Lightwave Technol.*, vol. 29, no. 12, pp. 1790–1796, Jun. 2011.
[11] A. Pasquazi, M. Peccianti, Y. Park, B. E. Little, S. T. Chu, R. Morandotti, J. Azaña, and D. J. Moss, "Sub-picosecond phase-sensitive optical pulse characterization on a chip," *Nature Photon.*, vol. 5, no. 10, pp. 618–623, Oct. 2011.
[12] M. Ferrera, Y. Park, L. Razzari, B. E. Little, S. T. Chu, R. Morandotti, D. J. Moss, and J. Azaña, "All-optical 1st and 2nd order integration on a chip," *Opt. Exp.*, vol. 19, no. 23, pp. 23 153–23 161, Nov. 2011.
[13] A. C. Turner-Foster, M. A. Foster, R. Salem, A. L. Gaeta, and M. Lipson, "Frequency conversion over two-thirds of an octave in silicon nanowaveguides," *Opt. Exp.*, vol. 18, no. 3, pp. 1904–1908, Feb. 2010.
[14] H. Rong, A. Liu, R. Jones, O. Cohen, D. Hak, R. Nicolaescu, A. Fang, and M. Paniccia, "An all-silicon Raman laser," *Nature*, vol. 433, no. 7023, pp. 292–294, Jan. 2005.
[15] A. D. Bristow, N. Rotenberg, and H. M. van Driel, "Two-photon absorption and Kerr coefficients of silicon for 850–2200 nm," *Appl. Phys. Lett.*, vol. 90, no. 19, pp. 191104-1–191104-3, May 2007.
[16] X. Liu, J. B. Driscoll, J. I. Dadap, R. M. Osgood, Jr., S. Assefa, Y. A. Vlasov, and W. M. J. Green, "Self-phase modulation and nonlinear loss in silicon nanophotonic wires near the mid-infrared two-photon absorption edge," *Opt. Exp.*, vol. 19, no. 8, pp. 7778–7789, Apr. 2011.
[17] K. Narayanan and S. Preble, "Optical nonlinearities in hydrogenated-amorphous silicon waveguides," *Opt. Exp.*, vol. 18, no. 9, pp. 8998–9005, Apr. 2010.
[18] B. Kuyken, S. Clemmen, S. K. Selvaraja, W. Bogaerts, D. Van Thourhout, P. Emplit, S. Massar, G. Roelkens, and R. Baets, "On-chip parametric amplification with 26.5 dB gain at telecommunication wavelengths using CMOS-compatible hydrogenated amorphous silicon waveguides," *Opt. Lett.*, vol. 36, no. 4, pp. 552–554, Feb. 2011.
[19] B. Kuyken, H. Ji, S. Clemmen, S. K. Selvaraja, H. Hu, M. Pu, M. Galili, P. Jeppesen, G. Morthier, S. Massar, L. K. Oxenlwe, G. Roelkens, and R. Baets, "Nonlinear properties of and nonlinear processing in hydrogenated amorphous silicon waveguides," *Opt. Exp.*, vol. 19, no. 26, pp. B146–B153, Dec. 2011.
[20] X. Liu, R. M. Osgood, Jr., Y. A. Vlasov, and W. M. J. Green, "Mid-infrared optical parametric amplifier using silicon nanophotonic waveguides," *Nature Photon.*, vol. 4, no. 8, pp. 557–560, Aug. 2010.
[21] S. Zlatanovic, J. S. Park, S. Moro, J. M. Chavez Boggio, I. V. Divliansky, N. Alic, S. Mookherjea, and S. Radic, "Mid-infrared wavelength conversion in silicon waveguides using ultracompact telecom-band-derived pump source," *Nature Photon.*, vol. 4, no. 8, pp. 561–564, Aug. 2010.
[22] R. K. W. Lau, M. Ménard, Y. Okawachi, M. A. Foster, A. C. Turner-Foster, R. Salem, M. Lipson, and A. L. Gaeta, "Continuous-wave mid-infrared frequency conversion in silicon nanowaveguides," *Opt. Lett.*, vol. 36, no. 7, pp. 1263–1265, Apr. 2011.
[23] B. Kuyken, X. Liu, G. Roelkens, R. Baets, R. M. Osgood, Jr., and W. M. J. Green, "50 dB parametric on-chip gain in silicon photonic wires," *Opt. Lett.*, vol. 36, no. 22, pp. 4401–4403, Nov. 2011.
[24] N. K. Hon, R. Soref, and B. Jalali, "The third-order nonlinear optical coefficients of Si, Ge, and $Si_{1-x}Ge_x$ in the midwave and longwave infrared," *J. Appl. Phys.*, vol. 110, no. 1, pp. 011301-1–011301-8, Jul. 2011.
[25] F. Gholami, S. Zlatanovic, A. Simic, L. Liu, D. Borlaug, N. Alic, M. P. Nezhad, Y. Fainman, and S. Radic, "Third-order nonlinearity in silicon beyond 2350 nm," *Appl. Phys Lett.*, vol. 99, no. 8, pp. 081102-1–081102-3, Aug. 2011.
[26] R. Soref, "Mid-infrared photonics in silicon and germanium," *Nature Photon.*, vol. 4, no. 8, pp. 495–497, Aug. 2010.
[27] G. Z. Mashanovich, M. M. Miloševi, M. Nedeljkovic, N. Owens, B. Xiong, E. J. Teo, and Y. Hu, "Low loss silicon waveguides for the mid-infrared," *Opt. Exp.*, vol. 19, no. 8, pp. 7112–7119, Apr. 2011.
[28] F. Li, S. D. Jackson, C. Grillet, E. Magi, D. Hudson, S. J. Madden, Y. Moghe, C. O'Brien, A. Read, S. G. Duvall, P. Atanackovic, B. J. Eggleton, and D. J. Moss, "Low propagation loss silicon-on-sapphire waveguides for the mid-infrared," *Opt. Exp.*, vol. 19, no. 16, pp. 15 212–15 220, Aug. 2011.
[29] M. Cazzanelli, F. Bianco, E. Borga, G. Pucker, M. Ghulinyan, E. Degoli, E. Luppi, V. Veniard, S. Ossicini, D. Modoto, S. Wabnitz, R. Pierobon, and L. Pavesi, "Second-harmonic generation in silicon waveguides strained by silicon nitride," *Nature Mater.*, vol. 11, no. 2, pp. 148–154, 2012.
[30] J. S. Levy, M. A. Foster, A. L. Gaeta, and M. Lipson, "Harmonic generation in silicon nitride ring resonators," *Opt. Exp.*, vol. 19, no. 12, pp. 11 415–11 421, Jun. 2011.
[31] J. K. Ranka, R. S. Windeler, and A. J. Stentz, "Visible continuum generation in air-silica microstructure optical fibers with anomalous dispersion at 800 nm," *Opt. Lett.*, vol. 25, no. 1, pp. 25–27, Jan. 2000.
[32] M. R. Lamont, B. Luther-Davies, D. Y. Choi, S. Madden, and B. J. Eggleton, "Supercontinuum generation in dispersion engineered highly nonlinear $(\gamma = 10\ /\mathrm{W/m})$ As_2S_3 chalcogenide planar waveguide," *Opt. Exp.*, vol. 16, no. 19, pp. 14 938–14 944, Sep. 2008.
[33] C. R. Phillips, C. Langrock, J. S. Pelc, M. M. Fejer, J. Jiang, M. E. Fermann, and I. Hartl, "Supercontinuum generation in quasi-phase-matched $LiNbO_3$ waveguide pumped by a Tm-doped fiber laser system," *Opt. Lett.*, vol. 36, no. 19, pp. 3912–3914, Oct. 2011.
[34] D. Duchesne, M. Peccianti, M. R. E. Lamont, M. Ferrera, L. Razzari, F. Légaré, R. Morandotti, S. Chu, B. E. Little, and D. J. Moss, "Supercontinuum generation in a high index silica glass spiral waveguide," *Opt. Exp.*, vol. 18, no. 2, pp. 923–930, Jan. 2010.
[35] I.-W. Hsieh, X. Chen, X. Liu, J. I. Dadap, N. C. Panoiu, C.-Y. Chou, F. Xia, W. M. Green, Y. A. Vlasov, and R. M. Osgood, "Supercontinuum generation in silicon photonic wires," *Opt. Exp.*, vol. 15, no. 23, pp. 15 242–15 249, 2007.
[36] P. Koonath, D. R. Solli, and B. Jalali, "Limiting nature of continuum generation in silicon," *Appl. Phys. Lett.*, vol. 93, no. 9, pp. 091114-1–091114-3, Sep. 2008.
[37] B. Kuyken, X. Liu, R. M. Osgood, Jr., R. Baets, G. Roelkens, and W. M. J. Green, "Mid-infrared to telecom-band supercontinuum generation in highly nonlinear silicon-on-insulator wire waveguides," *Opt. Exp.*, vol. 19, no. 21, pp. 20 172–20 181, Oct. 2011.

[38] R. Halir, Y. Okawachi, J. S. Levy, M. A. Foster, M. Lipson, and A. L. Gaeta, "Octave-spanning supercontinuum generation in CMOS-compatible silicon nitride waveguides," presented at the Conf. Lasers Electro-Optics, 2011, Paper PDPA6.
[39] S. T. Cundiff and J. Ye, "Colloquium: Femtosecond optical frequency combs," *Rev. Mod. Phys*., vol. 75, no. 1, pp. 325–342, Mar. 2003.
[40] T. J. Kippenberg, R. Holzwarth, and S. A. Diddams, "Microresonator-based optical frequency combs," *Science*, vol. 332, no. 6029, pp. 555–559, Apr. 2011.
[41] L. Razzari, D. Duchesne, M. Ferrera, R. Morandotti, S. Chu, B. E. Little, and D. J. Moss, "CMOS-compatible integrated optical hyper-parametric oscillator," *Nature Photon*., vol. 4, no. 1, pp. 41–45, Jan. 2010.
[42] J. S. Levy, A. Gondarenko, M. A. Foster, A. C. Turner-Foster, A. L. Gaeta, and M. Lipson, "CMOS-compatible multiple-wavelength oscillator for on-chip optical interconnects," *Nature Photon*., vol. 4, no. 1, pp. 37–40, Jan. 2010.
[43] M. A. Foster, J. S. Levy, O. Kuzucu, K. Saha, M. Lipson, and A. L. Gaeta, "Silicon-based monolithic optical frequency comb source," *Opt. Exp*., vol. 19, no. 15, pp. 14 233–14 239, Jul. 2011.
[44] Y. Okawachi, K. Saha, J. S. Levy, Y. H. Wen, M. Lipson, and A. L. Gaeta, "Octave-spanning frequency comb generation in a silicon nitride chip," *Opt. Lett*., vol. 36, no. 17, pp. 3398–3400, Sep. 2011.
[45] T. Herr, J. Riemensberger, C. Wang, K. Hartinger, E. Gavartin, R. Holzwarth, M. L. Gorodetsky, and T. J. Kippenberg, *Universal Dynamics of Kerr Frequency Comb Formation in Microresonators*, arXiv:1111.3071.
[46] A. A. Savchenkov, A. B. Matsko, W. Liang, V. S. Ilchenko, D. Seidel, and L. Maleki, *Transient Regime of Kerr Frequency Comb Formation*, arXiv:1111.3922.
[47] F. Ferdous, H. Miao, D. E. Leaird, K. Srinivasan, J. Wang, L. Chen, L. T. Varghese, and A. M. Weiner, "Spectral line-by-line pulse shaping of on-chip microresonator frequency combs," *Nature Photon*., vol. 5, no. 12, pp. 770–776, Dec. 2011.

Microscale Inorganic Light-Emitting Diodes on Flexible and Stretchable Substrates

Tae-il Kim, Rak-Hwan Kim, and John A. Rogers

(Invited Paper)

University of Illinois at Urbana-Champaign, Department of Material Science and Engineering,
Beckman Institute for Advanced Science and Technology,
Frederick Seitz Materials Research Laboratory, Urbana, IL 61801 USA

DOI: 10.1109/JPHOT.2012.2188998
1943-0655/$31.00 ©2012 IEEE

Manuscript received February 15, 2012; accepted February 19, 2012. Date of current version April 20, 2012. Corresponding author: J. A. Rogers (e-mail: jrogers@illinois.edu).

Abstract: Recent work involving microscale inorganic light-emitting diodes on flexible and stretchable substrates is reviewed. Techniques for materials growth, device fabrication, and assembly are summarized, along with highlights of optical, electrical, and mechanical properties that can be achieved. Some examples of emerging applications in biomedical devices illustrate the value of these methods in areas where conventional approaches are unsuitable.

Index Terms: Microscale light-emitting diodes (LEDs), organic LEDs (OLEDs), flexible electronics, stretchable electronics, biomedical devices, transfer printing.

1. Introduction

The emergence of organic light-emitting diodes (OLEDs) as a commercial technology for lighting and display has stimulated interest in devices with ultrathin, flexible, lightweight construction [1], [2]. Recent research has explored strategies for using inorganic light-emitting diodes (referred to here as ILEDs to emphasize the difference) to similar ends, and in some cases with mechanical properties that extend beyond flexibility (i.e., bendability) to full, elastic responses under large strain deformation, i.e., stretchability [3]–[5]. The appeal of this technical approach is that it exploits properties, such as life span, brightness, and efficiency in ILEDs that exceed those of currently available OLEDs [6]. The most successful schemes combine inorganic material stacks grown on nonepitaxial substrates (e.g., glass [7]), in unconventional forms (e.g., three dimensionally structured templates [8]), or processed in unusual ways to yield releasable devices [3], [9] for integration onto surfaces of interest. The last process, when implemented with advanced techniques for deterministic device assembly, has many attractive features. Here, printing methods [10], [11] deliver organized arrays of microscale inorganic optoelectronic devices to sheets of plastic or slabs of rubber where they are integrated into functional systems. This type of technology has the potential to create wide-ranging classes of application, with characteristics and modes of use that cannot be addressed in any other way. Examples in biomedicine include components for optogenetics, blood oximetry, drug delivery, advanced surgical tools, and chemical sensors.

2. Transfer Printing

Deterministic assembly techniques that use elastomeric stamps to manipulate microscale ILEDs (μ-ILEDs) represent versatile, high-throughput manufacturing strategies for the systems reviewed

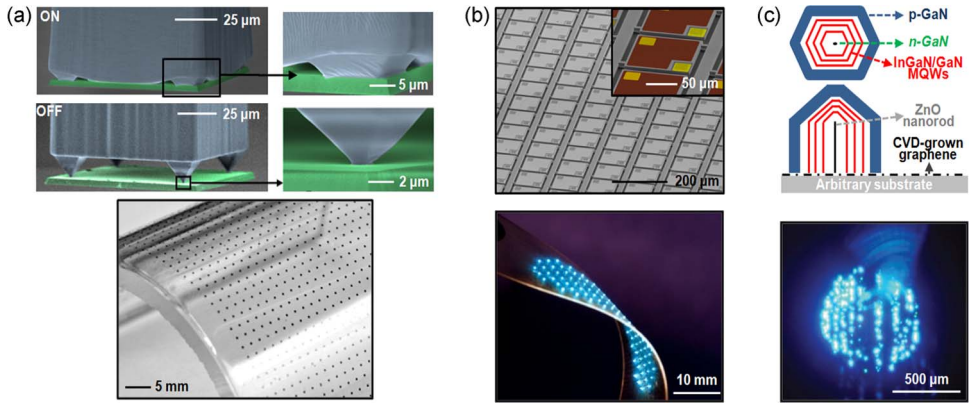

Fig. 1. (a) Deterministic assembly of microscale devices (green) using a structured elastomeric stamp (blue) with collapsible features of relief, shown here as colorized scanning electron micrographs in the adhesion ON (top) and OFF (middle) states. Reproduced with permission from [10]. Copyright National Academy of Sciences. The bottom frame shows an array of AlInGaP μ-ILEDs delivered by printing to the surface of a thin sheet of plastic that is subsequently bent around a glass cylindrical support. Reproduced with permission from [3]. Copyright American Association for the Advancement of Science. (b), (c) Unusual growth and processing strategies for InGaN LEDs and devices built with them. The top left frame shows InGaN μ-ILEDs released from an underlying silicon wafer growth substrate by anisotropic wet etching of the silicon; the frame below shows an array of such devices printed and interconnected on a thin, transparent sheet of plastic. Reproduced with permission from [4]. Copyright American Association for the Advancement of Science. The top right frame provides a schematic illustration of GaN and InGaN grown on nanorods of ZnO that form on graphene; the frame below shows a pattern of emission from a device made from such material. Reproduced with permission from [5]. Copyright Copyright WileyVCH Verlag.

here [10]. The underlying method, known as transfer printing, can be considered as a massively parallel "pick-and-place" technology that is compatible with extremely thin, fragile device components, originally developed for manipulating individual silicon transistors [10], [12], [13]. In this process, thin active layers or fully integrated devices formed on a growth wafer are released, retrieved with a stamp and then delivered to a foreign substrate. The key to successful operation is an engineered mechanism to modulate the adhesion to the stamp, from a strong state, for retrieval, to a weak one, for printing. Several approaches are available, ranging from those that use peel-rate dependent viscoelastic behaviors in the stamps [11], to pressure-modulated contact areas [10], to interfacial shear loading [14], each of which can be used for efficient transfer, even without separate adhesive layers on the target substrate. Fig. 1(a) shows, as an example of the second scheme, a contacting surface of a stamp of poly(dimethylsiloxane) (PDMS; blue) that supports compressible, pyramid-shaped features at the four corners [10]. Here, an applied preload collapses this relief to enable nearly full areal contact [adhesion ON state; Fig. 1(a) top] with a device element (green). Rapid retraction retrieves the device; shortly thereafter, elastic restoring forces push the collapsed region back into its initial, undeformed state, leaving contact only at the sharp tips of the pyramids [adhesion OFF state; Fig. 1(a) (middle)]. The adhesion is more than 1000 times stronger in the collapsed state than in the retracted one, due simply to differences in contact area for these two configurations. Fig. 1(a) (bottom) presents an image of a large array of AlInGaP μ-ILEDs printed onto a bent sheet of plastic using a related method for transfer printing [3].

3. ILEDs on Flexible Substrates

3.1. Devices in Planar Layouts

Various techniques exist for releasing planar layers of active materials grown on wafer substrates [3], [4], [15]–[18]. A recent approach that avoids cumbersome processes based on laser liftoff exploits InGaN stacks formed on silicon wafers with (111) orientation [4]. Etching through the InGaN defines

lateral dimensions of devices that form by defining contacts to the p and n regions. Immersing the processed substrate in a bath of potassium hydroxide undercuts the silicon, which leaves freely suspended, but fully formed, ultrathin μ-ILEDs, each tethered at two of their corners to unetched regions of silicon (i.e., anchor bars). Typical lateral dimensions are 100×100 μm^2 and thicknesses are $\sim$4.8 μm. Fig. 1(b) (top) shows a scanning electron micrograph of a collection of InGaN μ-ILEDs and a colorized image in the inset (yellow—ohmic contacts; brown—current spreading layer), after undercut release from the silicon substrate (gray). Transfer printing allows the assembly of selected sets of these devices into desired layouts on plastic sheets or other foreign substrates, where they can be electrically interconnected. An example appears in Fig. 1(b) (bottom). Here, the small sizes of the devices facilitate efficient passive thermal spreading, to allow operation even on plastics or other materials with low thermal conductivity. The interconnects in this case rely on a backside optical exposure technique, in which a spin-cast, photocurable layer of benzocyclobutene serves as a planarizing film that is removed in regions shadowed by the opaque p and n contact pads. This process is important because it avoids the need for device-level packaging and wire-bonding, or for demanding alignment in photolithography; the result is then scalable to large collections of devices in arbitrary layouts over large areas. These procedures are immediately applicable with μ-ILEDs that have dimensions from 150×150 μm^2 to 25×25 μm^2, with even smaller dimensions readily achievable. Color modulation from blue to white is possible using patterned films of yellow phosphor dyes.

3.2. Devices in Nonplanar Layouts

As an alternative to GaN formed using planar strategies, GaN/ZnO coaxial nanorod heterostructures, including multiple quantum wells (MQWs) can be created by growth on films of graphene, as illustrated in the top schematic illustration of Fig. 1(c) [5]. Here, GaN forms epitaxially on ZnO structures first grown on the graphene [9]. Etching away an underlying layer of SiO_2 after growth yields released nanorod ILEDs on graphene, suitable for transfer onto plastic coated with copper for backside contacts. Devices with this configuration are mechanically flexible and capable of operation without noticeable degradation after 100 cycles of bending. The bottom frame of Fig. 1(c) shows representative patterns of emission. Although less technically mature than the strategies of Section 3.1, these ideas have merit and warrant further attention, particularly in aspects of the growth. For example, initial studies suggest that the grain structure in the graphene correlates to the densities of the resultant of GaN/ZnO nanorods. As evidence, graphene grown on copper foil leads to low densities of ZnO nanorods and high degrees of crystallinity, due at least in part to the large grains observed in graphene on copper. By comparison, graphene grown on nickel has small grains, which leads to densities in ZnO nanorods that are too high for effective growth of GaN.

4. ILEDs on Stretchable Substrates and Applications in Biomedicine

The concepts of Sections 2 and 3 can yield advanced systems that offer not only the mechanics of a flexible plastic sheet but also a stretchable rubber band. This latter capability is important because it enables integration of ILED technologies directly and intimately with the soft, curvilinear surfaces of the human body, in a noninvasive fashion [19]. Potential applications range from health monitors, to oximeters and highly functional surgical tools. The following summarizes the approaches and provides several device examples.

4.1. Interconnect Strategies for Stretchable ILEDs

Flexible lighting and display systems of the type described previously follow simply from the use of thin μ-ILEDs on thin, plastic substrates, sometimes in neutral mechanical plane layouts to enhance further the degree of bendability. Stretchable characteristics demand additional attention to the mechanics in order to avoid fracture of brittle, inorganic materials during large-scale deformations, where overall strains can, in certain cases, exceed 100%. The most powerful schemes incorporate layouts in which the interconnects absorb the applied strain in a way that mechanically isolates the μ-ILEDs. Interconnects with noncoplanar geometries in straight or serpentine shapes [3], [15], [20],

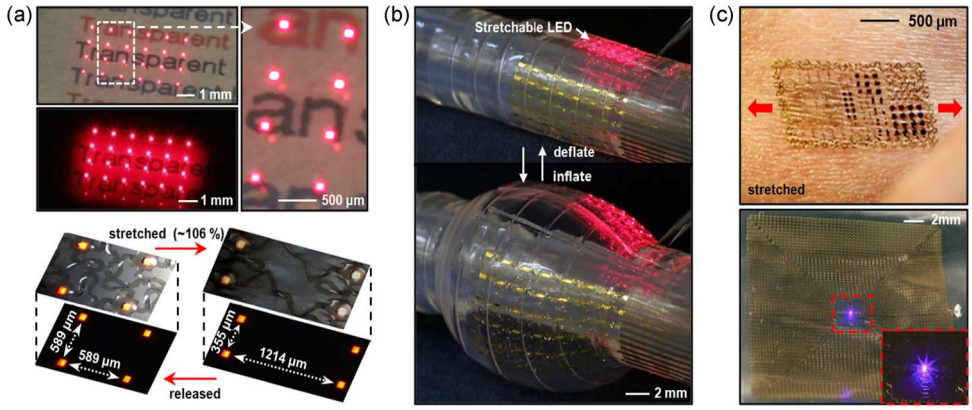

Fig. 2. (a) Collections of AlInGaP μ-ILEDs with transparent graphene interconnects on elastomeric substrates. Reproduced with permission from [20]. Copyright American Chemical Society. Applications of stretchable arrays of μ-ILEDs in advanced surgical tools (b) "instrumented" balloon catheters [23] and skin-mounted monitors as (c) "epidermal" electronic systems [24]. Reproduced with permission from [23] and [24], respectively. Copyright Nature Publishing Group for [23] and American Association for the Advancement of Science for [24].

[21], on either flat or structured elastomer supports, are effective. In these cases, controlled buckling and associated out-of-plane motions accommodate in-plane deformations, such that the strains in all of the constituent materials, except the elastomeric substrate, are small (e.g., $< 0.25\%$). Optimized designs, guided by quantitative mechanics modeling, enable stretching to 150% or more, without inducing fracture in any of the functional layers. The use of structured elastomers [22] or multilayer stacked configurations [15] enables this type of mechanics, even in systems that involve high areal coverage of active devices. In most cases, the interconnects consist of trilayer stacks of polymer/metal/polymer. Recent work shows that graphene can be used as an alternative, of interest here due to its optical transparency and its excellent mechanical properties [20]. The same concepts of buckling apply to graphene defined in narrow strips. The extremely low flexural rigidity of the graphene allows it to conform to the topography defined by the μ-ILEDs; the result facilitates efficient coverage on the contacts, over the edges of the devices. Examples of an array of AlInGaP μ-ILEDs with graphene interconnects appear in Fig. 2(a), demonstrating stretchability that exceeds 100%.

4.2. Applications in Biomedicine

Stretchable arrays of μ-ILEDs can be readily integrated into platforms that are suitable for natural, "soft" interfaces to the human body. For example, devices can be bonded to the surfaces of catheter balloons, to add advanced functionality to this otherwise conventional surgical tool. Applications for photoactivation of drugs, *in situ* spectroscopy or even optical ablation are possible, in minimally invasive modes. Fig. 2(b) shows an example that includes not only μ-ILEDs but also electrodes and various sensors, configured as a tool for monitoring and therapy in the context of cardiac surgery [23]. In another example, μ-ILEDs can be integrated with electronics in formats that have physical properties, ranging from thickness to bending rigidity, modulus and mass loading, all matched to the epidermis [24]. Mounting on the skin leads to a highly functional interface to the body, for health/wellness monitors, oximetry diagnostics, human–machine interfaces and others. Fig. 2(c) provides images of representative devices. In this case, inductive coupling provides a source of power.

5. Summary

Advanced methods in materials growth, processing, mechanics, thermal design, and system manufacturing combine to enable unusual modes of use for ILEDs. The outcomes have the potential to lead

to applications that can complement those already well addressed by conventional forms of ILEDs or OLEDs. The range of engineering opportunities and avenues for basic scientific investigations create an appealing set of circumstances for future research and development.

Acknowledgment

T. Kim and R.-H. Kim contributed equally in this paper.

References

[1] F. So, J. Kido, and P. Burrows, "Organic light-emitting devices for solid-state lighting," *MRS Bull.*, vol. 33, no. 7, pp. 663–669, Jul. 2008.
[2] S. R. Forrest, "The path to ubiquitous and low-cost organic electronic appliances on plastic," *Nature*, vol. 428, no. 6986, pp. 911–918, Apr. 2004.
[3] S.-I. Park, Y. Xiong, R.-H. Kim, P. Elvikis, M. Meitl, D.-H. Kim, J. Wu, J. Yoon, C.-J. Yu, Z. Lui, Y. Huang, K.-C. Hwang, P. Fereira, X. Li, K. Choquette, and J. A. Rogers, "Printed assemblies of inorganic light-emitting diodes for deformable and semitransparent displays," *Science*, vol. 325, no. 5943, pp. 977–981, Aug. 2009.
[4] H.-S. Kim, E. Brueckner, J. Song, Y. Li, S. Kim, C. Lu, J. Sulkin, K. Choquette, Y. Huang, R. G. Nuzzo, and J. A. Rogers, "Unusual strategies for using indium gallium nitrides grown on silicon (111) for solid-state lighting," *Proc. Nat. Acad. Sci. USA*, vol. 108, no. 25, pp. 10 072–10 077, Jun. 2011.
[5] C.-H. Lee, Y.-J. Kim, Y.J. Hong, S.-R. Jeon, S. Bae, B. H. Hong, and G.-C. Yi, "Flexible inorganic nanostructure light-emitting diodes fabricated on graphene films," *Adv. Mater.*, vol. 23, no. 40, pp. 4614–4619, Oct. 2011.
[6] P. Patel, "Solid-state lighting: The future looks bright," *MRS Bull.*, vol. 36, pp. 678–680, Sep. 2011.
[7] J. H. Choi, A. Zoulkarneev, S. I. Kim, C. W. Baik, M. H. Yang, S. S. Park, H. Suh, U. J. Kim, H. B. Son, J. S. Lee, M. Kim, J. M. Kim, and K. Kim, "Nearly single-crystalline GaN light-emitting diodes on amorphous glass substrates," *Nat. Photonics*, vol. 5, no. 12, pp. 763–769, 2011.
[8] E. C. Nelson, N. L. Dias, K. P. Bassett, S. N. Dunham, V. Verma, M. Miyake, P. Wiltzius, J. A. Rogers, J. J. Coleman, X. Li, and P. V. Braun, "Epitaxial growth of three-dimensionally architecture optoelectronic devices," *Nat. Mater.*, vol. 10, no. 9, pp. 676–681, Jul. 2011.
[9] K. Chung, C.-H. Lee, and G.-C. Yi, "Transferable GaN layers grown on ZnO-coated graphene layers for optoelectronic devices," *Science*, vol. 330, no. 6004, pp. 655–657, Oct. 2010.
[10] S. Kim, J. Wu, A. Carlso, S. H. Jin, A. Kovalsky, P. Glass, Z. Liu, N. Ahmed, S. L. Elgan, W. Chen, P. M. Ferreira, M. Sitti, Y. Huang, and J. A. Rogers, "Microstructured elastomeric surfaces with reversible adhesion and examples of their use in deterministic assembly by transfer printing," *Proc. Nat. Acad. Sci. USA*, vol. 107, no. 40, pp. 17 095–17 100, Oct. 2010.
[11] M. A. Meitl, Z.-T. Zhu, V. Kumar, K. J. Lee, X. Feng, Y. Y. Huang, I. Adesida, R. G. Nuzzo, and J. A. Rogers, "Transfer printing by kinetic control of adhesion to an elastomeric stamp," *Nat. Mater.*, vol. 5, no. 1, pp. 33–38, Jan. 2006.
[12] E. Menard, K. J. Lee, D.-Y. Khang, R. G. Nuzzo, and J. A. Rogers, "A printable form of silicon for high performance thin film transistors on plastic substrates," *Appl. Phys. Lett.*, vol. 84, no. 26, pp. 5389–5400, Jun. 2004.
[13] K. J. Lee, M. J. Motala, M. A. Meitl, W. R. Childs, E. Menard, A. K. Shim, J. A. Rogers, and R. G. Nuzzo, "Large-area, selective transfer of microstructured silicon: A printing-based approach to high-performance thin-film transistors supported on flexible substrates," *Adv. Mater.*, vol. 17, no. 19, pp. 2332–2336, Oct. 2005.
[14] A. Carlson, H.-J. Kim-Lee, J. Wu, P. Elvikis, H. Cheng, A. Kovalsky, S. Elgan, Q. Yu, P. M. Ferreira, Y. Huang, K. T. Turner, and J. A. Rogers, "Shear-enhanced adhesiveless transfer printing for use in deterministic materials assembly," *Appl. Phys, Lett.*, vol. 98, no. 26, pp. 264104-1–264104-3, Jun. 2011.
[15] R.-H. Kim, D.-H. Kim, J. Xiao, B. H. Kim, S.-I. Park, B. Panilaitis, R. Ghaffari, J. Yao, M. Li, Z. Lui, V. Malyarchuk, D. G. Kim, A.-P. Le, R. G. Nuzzo, D. L. Kaplan, F. G. Omenetto, Y. Huang, Z. Kang, and J. A. Rogers, "Waterproof AlInP optoelectronics on stretchable substrates with applications in biomedicine and robotics," *Nat. Mater.*, vol. 9, pp. 929–937, Nov. 2010.
[16] W. S. Wong, T. Sands, N. W. Cheung, M. Kneissl, D. P. Bour, P. Mei, L. T. Romano, and N. W. Johnson, "$In_xGa_{1-x}N$ light emitting diodes on Si substrates fabricated by Pd–In metal bonding and laser lift off," *Appl. Phys. Lett.*, vol. 77, no. 18, pp. 2822–2824, Oct. 2000.
[17] E. Yablonovitch, T. Gmitter, J. P. Harbison, and R. Bhat, "Extreme selectivity in the lift-off of epitaxial GaAs films," *Appl. Phys. Lett.*, vol. 51, no. 26, pp. 2222–2224, Dec. 1987.
[18] J. Yoon, S. Jo, I. S. Chun, I. Jung, H.-S. Kim, M. Meitle, E. Menard, X. Li, J. J. Coleman, U. Paik, and J. A. Rogers, "GaAs photovoltaics and optoelectronics using releasable multilayer epitaxial assemblies," *Nature*, vol. 465, no. 7296, pp. 329–334, May 2010.
[19] J. A. Rogers, T. Someya, and Y. Huang, "Materials and mechanics for stretchable electronics," *Science*, vol. 327, no. 5973, pp. 1603–1607, Mar. 2010.
[20] R.-H. Kim, M.-H. Bae, D. G. Kim, H. Cheng, B. H. Kim, D.-H. Kim, M. Li, F. Du, H.-S. Kim, D. Estrada, S. W. Hong, Y. Huang, E. Pop, and J. A. Rogers, "Stretchable, transparent graphene interconnects for arrays of microscale inorganic light emitting diodes on rubber substrates," *Nano Lett.*, vol. 11, no. 9, pp. 3881–3886, Sep. 2011.
[21] D.-H. Kim, J. Song, W. M. Choi, H.-S. Kim, R.-H. Kim, Z. Lui, Y. Huang, K.-C. Hwang, Y.-W. Zhang, and J. A. Rogers, "Materials and noncoplanar mesh designs for integrated circuits with linear elastic responses to extreme mechanical deformations," *Proc. Nat. Acad. Sci. USA*, vol. 105, no. 48, pp. 18 675–18 680, Dec. 2008.
[22] J. Lee, J. Wu, M. Shi, J. Yoon, S.-I. Park, M. Li, Z. Liu, Y. Huang, and J. A. Rogers, "Stretchable GaAs photovoltaics with designs that enable high areal coverage," *Adv. Mater.*, vol. 23, no. 8, pp. 986–991, Feb. 2011.
[23] D.-H. Kim, N. Lu, R. Ghaffari, Y.-S. Kim, S. P. Lee, L. Xu, J. Wu, R.-H. Kim, J. Song, Z. Liu, J. Viventi, B. D. Graff, B. Elolampi, M. Mansour, M. J. Slepian, S. Hwang, J. D. Moss, S.-M. Won, Y. Huang, B. Litt, and J. A. Rogers,

Materials for multifunctional balloon catheters with capabilities in cardiac electrophysiological mapping and ablation therapy," *Nat. Mater.*, vol. 10, no. 4, pp. 316–323, Apr. 2011.

[24] D.-H. Kim, N. Lu, R. Ma, Y.-S. Kim, R.-H. Kim, S. Wang, J. Wu, S. M. Won, H. Tao, A. Islam, K. J. Yu, T.-I. Kim, R. Chowdhury, M. Ying, L. Xu, M. Li, H.-J. Chung, H. Keum, M. McCormick, P. Liu, Y.-W. Zhang, F. G. Omenetto, Y. Huang, T. Coleman, and J. A. Rogers, "Epidermal electronics," *Science*, vol. 333, no. 6044, pp. 838–843, Aug. 2011.

Advances in the LED Materials and Architectures for Energy-Saving Solid-State Lighting Toward "Lighting Revolution"

S. T. Tan,[1] X. W. Sun,[1] H. V. Demir,[1,2] and S. P. DenBaars[3]

(Invited Paper)

[1]*Luminous!* Center of Excellence for Semiconductor Lighting and Displays, School of Electrical and Electronic Engineering, Nanyang Technological University, Singapore 639798
[2]UNAM-Institute of Materials Science and Nanotechnology, Departments of Electrical and Electronics Engineering and Physics, Bilkent University, Ankara 06800, Turkey
[3]Solid State Lighting and Energy Center, Department of Materials Science, University of California, Santa Barbara, CA 93106-5050 USA

DOI: 10.1109/JPHOT.2012.2191276

Manuscript received February 27, 2012; revised March 9, 2012; accepted March 13, 2012. Date of current version April 20, 2012. This work was supported by the Singapore National Research Foundation under Grant NRF-RF-2009-09 and Grant NRF-CRP-6-2010-2. Corresponding authors: X. W. Sun and H. V. Demir (e-mail: volkan@stanfordalumni.org; exwsun@ntu.edu.sg).

Abstract: In this paper, we review the recent developments (in years 2010–2011) of energy-saving solid-state lighting. The industry of white light-emitting diodes (LEDs) has made significant progress, and today, white LED market is increasing (mostly with increasing LED screen and LED TV sales). The so-called "lighting revolution" has not yet really happened on a wide scale because of the lighting efficiency at a given ownership cost. Nevertheless, the rapid development of the white LEDs is expected to soon trigger and expand the revolution.

Index Terms: Solid-state lighting, light-emitting diodes, III-nitride.

Over centuries, artificial lighting technology has made an incredible progress from candles and gas and kerosene lamps to today's incandescent and fluorescent lighting. As a result, the overall operating cost of light has been reduced by 4.3 orders of magnitude since the 1700s [1], [2]. However, this technological progress has also inevitably increased the consumption of light as the cost of light has decreased. Today, the world uses about 0.72% of its Gross Domestic Product (GDP) on light, for example, in 2010, World GDP of 63.12 T$ (current U.S. $), which means about 455 B$ for artificial lighting. Additionally, as the cost of light has decreased and GDP per capita has increased, the consumption of light per capita has also increased (almost linearly) over time. Over the last three centuries, the consumption of light per capita has increased by 5.4 orders of magnitude. Today, this has reached such a high level that an average person in a well-developed part of the world is effectively surrounded by tens of 100 W light bulbs at all times during his/her waking hours. Therefore, today, too much artificial light is consumed, which costs too much energy. According to a 2006 report by the International Energy Agency (IEA) and the Organization for Economic Co-operation and Development (OECD), lighting is responsible for $\sim$19% of electricity consumption and $\sim$6% of carbon emission. For our modern civilization today, energy-saving lighting is therefore increasingly essential. Efficient artificial lighting could save billions of dollars and reduce

greenhouse gases, while improving consumer's vision, provided that the lighting is also photometrically high quality.

Solid-state lighting (SSL) based on light-emitting diodes (LEDs) has attracted enormous interest [3], [4] and is of great importance to the development of electric lighting technologies, over a century after the early invention of incandescent bulbs (circa 1879) and over half a century after fluorescent lamps in the 1930s. The energy consumption used for lighting can be in principle reduced by 50% using LED lighting (if the targeted performance is met) and even more (if smart lighting enabled by LEDs is used). This corresponds to substantial annual carbon emission reduction of many hundreds of millions of tons per year. However, the so-called "lighting revolution" of LEDs after Thomas Edison is yet to be realized at wide scale. The lighting industry still has hurdles to clear before LED lighting penetrates the consumer market at the wide scale. Beyond the very real technical issues including device operating luminous efficacy (the efficiency droop and thermal droop) and light photometric properties, cost remains one of the main challenges for the LED lighting industry. Fortunately, recent rapid developments in LED materials and devices have brought it one step closer to the wide-scale commercialization and adaptation of general lighting.

Since the first bright blue and white LED chips were successfully demonstrated, InGaN LED has been making tremendous achievements in setting new records for luminous efficacy. In early 2010, Nichia has taken the white LED's luminous efficacy a step further, achieving values reported as high as 249 lm/W at 20 mA and 183 lm/W at 350 mA with 450×450 μm^2 blue LED die [5]. For comparison, a conventional incandescent light bulb of 60–100 W emits around 15 lm/W, and standard fluorescent lights emit up to 100 lm/W. In just one year, the LED's luminous efficacy was significantly enhanced. In March 2011, Osram Opto Semiconductors in Germany have set a new record efficacy for a warm-white LED that shows an efficacy of 142 lm/W reported at a correlated color temperature (CCT) of 2755 K and a color rendering index (CRI) of 81 at 350 mA/mm^2 [6]. Not much later, the US-headquartered LED maker Cree has set the new benchmark for the LED's luminous efficacy. The laboratory performance of the "neutral white" LED showed 231 lm/W at an operating current of 350 mA [7]. The achievement approaches the predicted maximum luminous efficacy of 260–300 lm/W [8].

In order to supply higher luminous flux, LEDs need much larger die size to handle large input power. However, a recurring problem is that the LED's luminous efficacy falls sharply under elevated current injection, and yet high current operation is necessary in SSL. This effect is known as the efficiency droop [9]. If the droop can be minimized, then the operating LED efficiency increases, which means either brighter LED is obtained, or less power is needed to run the device at the required illumination level. Though the root-cause of the droop is still debatable, various models have been adopted to explain the droop, such as junction heating [10], electron overflow [11], [12], reduced effective radiative recombination rate due to the elevated plasma temperature caused by carrier–carrier and carrier–photon collisions [12], and Auger recombination [13]. To date, several methods have been proposed to reduce the efficiency droop and enhance the optical output power of LEDs that are grown on *c*-plane sapphire substrates. For example, Schubert *et al.* proposed quaternary AlGaInN quantum barriers to suppress the polarization discontinuity between the adjacent well, and barrier demonstrates the excellency in reducing the efficiency droop [14]. Zhao *et al.* also suggested $Al_{0.83}In_{0.71}N/GaN/Al_{0.83}In_{0.71}N$ as the quantum barriers to enhance the electron injection efficiency [15]. Similarly, $Al_{0.82}In_{0.18}N$ as the electron blocking layer shows its advantage over AlGaN in preventing electron overflow [16]. Recently, it has been shown that AlGaN/GaN/AlGaN as quantum barriers is effective not only in carrier confinement but in enhancing the quantum efficiency as well, while keeping the exact emission wavelength for green LEDs [17]. Moreover, AlGaN, serving as the cap layer, has significantly reduced the strain energy and misfit dislocation density in the quantum wells [18], and this feature has been applied to the LED with AlGaN/InGaN superlattice as the quantum barriers and the electron blocking layer [19].

In addition to improving the carrier injection efficiency, it is also vital to increase the spatial overlap between the electron and hole wave functions. Staggered quantum well [20]–[23] and type-II quantum well architectures [24] were proposed for both LEDs and laser diodes for this purpose. The improved spatial overlap between electron and hole wave functions can also be achieved by

inserting a "δ" layer into the quantum wells. AlGaN [25], GaN [26], and InN [27], [28] with an optimized thickness were employed to manifest the essentiality of deepening the localized states for better carrier confinement [29], [30]. In the meantime, the lattice mismatch between InGaN and GaN can also be released in the quantum dots (QDs), which leads to a better electron–hole overlap and increased radiative recombination rates [31]. InGaN/GaN wafers grown nonpolar/semipolar orientation have eliminated the polarization-induced fields [32]–[34], therefore enabling a complete overlap between electron and hole wave functions and an increase in the optical matrix element [35], [36].

Other than the record-breaking luminous efficacy levels, LED makers also devoted great effort to bring down the fabrication cost and, hence, the cost of light. GaN-based LED epitaxial on large-area Si substrates has been a hot topic in recent years. However, the intrinsic mismatch in both lattice constant and thermal coefficient of expansion with the requisite GaN epitaxial films challenges the epitaxial growth and hence the performance of the GaN-on-Si LEDs. The threading dislocations are expected to result in poor efficiency of the resulting LEDs while the macroscopic film stresses are to yield wafer bowing and even cracks. Nevertheless, significant progress has been reported in 2011. In March 2011, California-based LED maker Bridgelux Inc. has demonstrated a 135-lm/W LED on silicon substrate that was operated at 350 mA [37]. By using low-cost silicon substrates, instead of conventionally used sapphire or silicon carbide substrates, Bridgelux claimed it can deliver a 75% reduction in cost, which is one step closer to commercialization. More recently, Osram Opto Semiconductors has also announced that it is in the pilot stage of producing LEDs on silicon. The prototypes exhibited 127 lm/W at 350 mA according to the reports [38]. Other than GaN-on-Si, recently, Zhang *et al.* proposed numerically the growth of III-nitride LEDs on InGaN ternary substrate that gives rise to higher spontaneous emission rate and reduced blue-shift of peak emission wavelength [39]. Besides, with proper indium composition, the lattice constant of InGaN substrate is matched with that of multiple-quantum-well to be grown on top of it, leading to a reduced threshold carrier density and, hence, suppressed Auger recombination [40]. This provides a possibility of applying the InGaN substrate for the development of efficient blue, green, and red high-brightness LEDs and laser diodes.

On the other hand, many LED makers started to emphasize the vertical LED architectures due to their many advantages over transverse or lateral counterparts [41]–[44]. The vertical LED architectures, involving removal of nonconductive (electrical and/or thermal) substrates, allow for better homogenous current distribution through the active region. Moreover, with the wider choice of receptor wafers (mostly metallic thin films), heat can be well dissipated and managed and, thus, can facilitate high-power LED operation. In the case of GaN LEDs on sapphire substrates, a nondestructive excimer laser-assisted lift-off of the sapphire substrates as a whole could open up the window for recycling of the sapphire substrates for epitaxial growth. This is a significant cost-saving aspect in the LED fabrication. On the other hand, instead of fully removal of sapphire substrate via excimer laser-assisted lift-off, Yang *et al.* reported the technique of thinning the substrate and etching down to the n-GaN region for metal contact, which also leads to enhanced output power and reduced forward voltage compared with the conventional lateral LED on sapphire [45]. The vertical LED architectures enable high power operation, thus increasing the maximum total flux output that can be obtained from a single chip. The latter factor also relates to cost, as it reduces the number of LED chips to achieve the same level of illumination. The aggressive device architecture advances in the GaN LEDs is expected to have an extremely beneficial impact in driving down the cost for GaN-based LEDs.

Optimization of light extraction efficiency is always a challenge for maximizing light output from the active region. Photonic crystals are one of the most commonly used techniques to solve this problem. Embedded air-gap photonic crystals show good performance in enhancing the extraction of polarized light emission as well as the polarization ratio [46]. Through pattern design of the photonic crystals, the far-field emission directionality can be controlled [47]. Meanwhile, the addition of a microlenses array on top of the device is capable of increasing the light extraction efficiency by more than two times [48]–[49] because of the increase in effective photon escape cone and a reduced level of internal reflection resulted from the grading of refractive index variation between the

GaN/SiO_2/PS/air interfaces. The surface plasmon offers another practical approach to overcome the optical output limit. The resonant coupling between the light-emitting excitons from the MQW region and the nanometer scale thickness metal layers enhance the luminescence intensity up to a factor of 5 [50]–[52].

Today, the most commonly used SSL sources are based on phosphor integrated color conversion LEDs, i.e., integrating of yttrium aluminum garnet (YAG) phosphors on blue InGaN LEDs [53]. The $Y_3Al_5O_{12} : Ce^{3+}$ phosphor emits broad yellow light when subjected to blue light. It is commonly used as a coating on blue InGaN LEDs, converting part of the blue light into yellow, which then collectively makes white. Such an arrangement, however, yields white light generation with *CCT*s of 4000–8000 K, corresponding to the neutral and cool-white intervals, and *CRI*s typically lower than 80 [4], [54]. The low *CRI*s is due to the missing of red component in the spectrum. Sulfide phosphors such as $(Ca_{1-x}, Sr_x)S:Eu^{2+}$ [55] and $Y_2O_2S:Eu^{3+}$ [56] have been used as red phosphors for white LEDs for a long time. Unfortunately, their chemical stability is not desirable. Recently, various new red phosphor systems with good stability have been reported, especially nitride-based phosphors, including $CaAlSiN_3 : Eu^{2+}$ [57], $Sr_2Si_5N_8 : Eu^{2+}$ [58], $Ba_2AlSi_5N_9 : Eu^{2+}$ [59], and β-SiAlON : Pr^{3+} [60], exhibiting great potential as efficient red phosphors. However, for high-quality and wide-scale use in indoor illumination applications, white LEDs are required to provide warm enough *CCT* (< 4000 K) with high enough *CRI* (> 80) [4], [54]. Although a red phosphor can be added (triple-color mixing), the phosphor based color conversion LED suffers from the intrinsic problem that the emission spectrum is very broad with an inventible far red emission spilling beyond the eye sensitivity curve. This problem leads to a fundamental tradeoff between the luminous efficacy of optical radiation and *CRI*.

Over the past two decades, a series of experiments sponsored by the US Department of Energy showed that rod photoreceptors responsible for scotopic (dark adapted) vision, as traditionally understood, also play an important role in vision in typical lighting conditions (e.g., offices, homes) [61]. Rods are responsible for the monochromatic vision in low light, which is called scotopic vision, as opposed to the photopic (photon adapted) vision of color perception provided by cone eye cells that are nonfunctional in low light. According to these reports, the tests showed that *a*) the rod photoreceptors are active at typical interior light levels, *b*) human eye pupil (which affects the acuity of our vision) is primarily controlled by rods (scotopic response), and *c*) the brightness of a light source is determined by both the photopic and scotopic responses. Also, according to a test carried out by Intel Corporation in Oregon [62], changing from normal lighting to scotopic enhanced lighting resulted in a total energy reduction of 57% while maintaining the same perceived brightness. However, in current practice, light sources are typically designed for photopic vision. To account for the rod response, the scotopic/photopic ratio (S/P ratio) is required. The S/P ratio of common light sources generally ranges from 0.8 to 2.5 (e.g., incandescent light with 1.41 and sunlight with 2.47) [63]. The commercially available YAG phosphor white LEDs exhibit poor S/P ratios typically ranging from 1.68 to 2.38 [64]. For single sources (including the state-of-the-art single-chip LEDs), the S/P ratio is limited to < 2.5.

The problems of low S/P ratio lighting and low CRI can be solved by modifying the phosphors. This requires design and synthesis of new phosphors, for example, by using nanophosphors of colloidal semiconductor QDs [65]. Due to the size tunability and narrow emission bandwidth ($\sim$30 nm), QD luminophors in white LEDs enable precise spectrum engineering to realize high-quality SSL tailored for different lighting requirements. Moreover, colloidal QDs feature large photoluminescence (PL) quantum yield in solution (reasonable yield in film) and increasing absorption below its emission peak toward shorter wavelengths. In fact, warm-white LEDs integrated with colloidal QDs with desirably low *CCT* < 3000 K and high *CRI* close to 90 have been achieved [66], [67].

In summary, a great opportunity for the LED-based SSL is presented to significantly impact the sociological, economic, and environmental future. Though, at present, the market demand for LED is currently dominated in flat panel display industry, given the continuous development in high-brightness LEDs, the LED-based SSL is in the limelight.

References

[1] J. Y. Tsao and P. Waide, "The world's appetite for light: Empirical data and trends spanning three centuries and six continents," *LEUKOS*, vol. 6, no. 4, pp. 259–281, Apr. 2010.
[2] R. Haitz and J. Y. Tsao, "Solid-state lighting: 'The Case' 10 years after the future prospects," *Phys. Status Solidi A*, vol. 208, no. 1, pp. 17–29, Jan. 2011.
[3] E. F. Schubert, *Light-Emitting Diodes,* 2nd ed. Cambridge, U.K.: Cambridge Univ. Press, 2006.
[4] J. Y. Tsao, "Solid-state lighting: Lamps, chips and materials for tomorrow," *IEEE Circuits Devices Mag.*, vol. 20, no. 3, pp. 28–37, May 2004.
[5] [Online]. Available: http://www.physorg.com/news202453100.html
[6] [Online]. Available: http://optics.org/news/2/3/15
[7] [Online]. Available: http://optics.org/news/2/5/8
[8] Y. Narukawa, M. Ichikawa, D. Sanga, M. Sano, and T. Mukai, "White light emitting diodes with super-high luminous efficacy," *J. Phys. D, Appl. Phys.*, vol. 43, no. 35, pp. 354 002–354 008, Aug. 2010.
[9] J. Piprek, "Efficiency droop in nitride-based light-emitting diodes," *Phys. Status Solidi A*, vol. 207, no. 10, pp. 2217–2225, Oct. 2010.
[10] A. A. Efremov, N. I. Bochkareva, R. I. Gorbunov, D. A. Lavrinovich, Y. T. Rebane, D. V. Tarkhin, and Y. G. Shreter, "Effect of the Joule heating on the quantum efficiency and choice of thermal conditions for high-power blue InGaN/GaN LEDs," *Phys. Semicond. Devices*, vol. 40, no. 5, pp. 605–610, May 2006.
[11] M. H. Kim, M. F. Schubert, Q. Dai, J. K. Kim, E. F. Schubert, J. Piprek, and Y. Park, "Origin of efficiency droop in GaN-based light-emitting diodes," *Appl. Phys. Lett.*, vol. 91, no. 18, pp. 183507-1–183507-3, Oct. 2007.
[12] W. W. Chow, M. H. Crawford, J. Y. Tsao, and M. Kneissl, "Internal efficiency of InGaN light-emitting diodes: Beyond a quasiequilibrium model," *Appl. Phys. Lett.*, vol. 97, no. 12, pp. 121105-1–121105-3, Sep. 2010.
[13] Y. C. Shen, G. O. Mueller, S. Watanabe, N. F. Gardner, A. Munkholm, and M. R. Krames, "Auger recombination in InGaN measured by photoluminescence," *Appl. Phys. Lett.*, vol. 91, no. 14, pp. 141101-1–141101-3, Oct. 2007.
[14] M. F. Schubert, J. Xu, J. K. Kim, E. F. Schubert, M. H. Kim, S. Yoon, S. M. Lee, C. Sone, T. Sakong, and Y. Park, "Polarization-matched GaInN/AlGaInN multi-quantum-well light-emitting diodes with reduced efficiency droop," *Appl. Phys. Lett.*, vol. 93, no. 4, pp. 041102-1–041102-3, Jul. 2008.
[15] H. P. Zhao, G. Y. Liu, R. A. Arif, and N. Tansu, "Current injection efficiency induced efficiency-droop in InGaN quantum well light-emitting diodes," *State Electron.*, vol. 54, no. 10, pp. 1119–1124, Oct. 2010.
[16] S. Choi, H. J. Kim, S. S. Kim, J. Liu, J. Kim, J. H. Ryou, R. D. Dupuis, A. M. Fischer, and F. A. Ponce, "Improvement of peak quantum efficiency and efficiency droop in III-nitride visible light-emitting diodes with an InAlN electron-blocking layer," *Appl. Phys. Lett.*, vol. 96, no. 22, pp. 221105-1–221105-3, May 2010.
[17] T. Shioda, H. Yoshida, K. Tachibana, N. Sugiyama, and S. Nunoue, "Enhanced light output power of green LEDs employing AlGaN interlayer in InGaN/GaN MQW structure on sapphire (0001) substrate," *Phys. Status Solidi A*, vol. 209, no. 3, pp. 473–476, Jan. 2012.
[18] H. P. Zhao, R. A. Arif, Y. K. Ee, and N. Tansu, "Self-consistent analysis of strain-compensated InGaN-AlGaN quantum wells for lasers and light-emitting diodes," *IEEE J. Quantum Electron.*, vol. 45, no. 1/2, pp. 66–78, Jan. 2009.
[19] C. L. Tsai, G. C. Fan, and Y. S. Lee, "Effects of strain-compensated AlGaN/InGaN superlattice barriers on the optical properties of InGaN light-emitting diodes," *Appl. Phys. A, Mater. Sci. Phys.*, vol. 104, no. 1, pp. 319–323, Jul. 2011.
[20] H. P. Zhao, G. Y. Liu, J. Zhang, J. D. Poplawsky, V. Dierolf, and N. Tansu, "Approaches for high internal quantum efficiency green InGaN light-emitting diodes with large overlap quantum wells," *Opt. Exp.*, vol. 19, no. S4, pp. A991–A1007, Jul. 2011.
[21] H. P. Zhao and N. Tansu, "Optical gain characteristics of staggered InGaN quantum wells lasers," *J. Appl. Phys.*, vol. 107, no. 11, pp. 113110-1–113110-12, Jun. 2010.
[22] S. H. Park, D. Ahn, J. Park, and Y. T. Lee, "Optical properties of staggered InGaN/InGaN/GaN quantum-well structures with Ga- and N-faces," *Jpn. J. Appl. Phys.*, vol. 50, no. 7, pp. 072101-1–072101-4, Jul. 2011, part 1.
[23] C. T. Liao, M. C. Tsai, B. T. Liou, S. H. Yen, and Y. K. Kuo, "Improvement in output power of a 460 nm InGaN light-emitting diode using staggered quantum well," *J. Appl. Phys.*, vol. 108, no. 6, pp. 063107-1–063107-6, Sep. 2010.
[24] S. H. Park, D. Ahn, B. H. Koo, and J. E. Oh, "Optical gain improvement in type-II InGaN/GaNSb/GaN quantum well structures composed of InGaN/and GaNSb layers," *Appl. Phys. Lett.*, vol. 96, no. 5, pp. 051106-1–051106-3, Feb. 2010.
[25] S. H. Park, J. Park, and E. Yoon, "Optical gain in InGaN/GaN quantum well structures with embedded AlGaN delta layer," *Appl. Phys. Lett.*, vol. 90, no. 2, p. 023508, Jan. 2007.
[26] J. Zhang, H. P. Zhao, and N. Tansu, "Large optical gain AlGaN-delta-GaN quantum wells laser active regions in mid- and deep-ultraviolet spectral regimes," *Appl. Phys. Lett.*, vol. 98, no. 11, pp. 171111-1–171111-3, Apr. 2011.
[27] H. P. Zhao, G. Y. Liu, and N. Tansu, "Analysis of InGaN-delta-InN quantum wells for light-emitting diodes," *Appl. Phys. Lett.*, vol. 97, no. 13, pp. 131114-1–131114-3, Sep. 2010.
[28] Y. Li, B. Liu, R. Zhang, Z. Xie, and Y. Zheng, "Investigation of optical properties of InGaN–InN–InGaN/GaN quantum-well in the green spectral regime," *Phys. E*, vol. 44, no. 4, pp. 821–825, Jan. 2012.
[29] G. Sun, G. Xu, Y. J. Ding, H. Zhao, G. Liu, J. Zhang, and N. Tansu, "Investigation of fast and slow decays in InGaN/GaN quantum wells," *Appl. Phys. Lett.*, vol. 99, no. 8, pp. 081104-1–081104-3, Aug. 2011.
[30] H. Wang, Z. Ji, S. Qu, G. Wang, Y. Jiang, B. Liu, X. Xu, and H. Mino, "Influence of excitation power and temperature on photoluminescence in InGaN/GaN multiple quantum wells," *Opt. Exp.*, vol. 20, no. 4, pp. 3932–3940, Feb. 2012.
[31] G. Liu, H. Zhao, J. Zhang, J. H. Park, L. J. Mawst, and N. Tansu, "Selective area epitaxy of ultra-high density InGaN quantum dots by diblock copolymer lithography," *Nanoscale Res. Lett.*, vol. 6, no. 1, p. 342, Apr. 2011.
[32] T. J. Prosa, P. H. Clifton, H. Zhong, A. Tyagi, R. Shivaraman, S. P. DenBaars, S. Nakamura, and J. S. Speck, "Atom probe analysis of interfacial abruptness and clustering within a single $In_xGa_{(1-x)}N$ quantum well device on semipolar $(10\overline{1}1)$ GaN substrate," *Appl. Phys. Lett.*, vol. 98, no. 19, pp. 191903-1–191903-3, May 2011.

[33] Y. Zhao, S. Tanaka, C. C. Pan, K. Fujito, D. Feezell, J. S. Speck, S. P. DenBaars, and S. Nakamura, "High-power blue-violet semipolar $(20\bar{2}1)$ InGaN/GaN light-emitting diodes with low efficiency droop at 200 A/cm^2," *Appl. Phys. Exp.*, vol. 4, no. 8, pp. 082104-1–082104-3, Aug. 2011.
[34] H. Masui, S. Nakamura, S. P. DenBaars, and U. K. Mishra, "Nonpolar and semipolar III-nitride light-emitting diodes: Achievement and challenges," *IEEE Trans. Electron. Devices*, vol. 57, no. 1, pp. 88–100, Jan. 2010.
[35] R. M. Farrell, D. A. Haeger, P. S. Hsu, K. Fujito, D. F. Feezell, S. P. DenBaars, J. S. Speck, and S. Nakamura, "Determination of internal parameters for AlGaN-cladding-free m-plane InGaN/GaN laser diodes," *Appl. Phys. Lett.*, vol. 99, no. 17, pp. 171115-1–171115-3, Oct. 2011.
[36] R. M. Farrell, P. S. Hsu, D. A. Haeger, K. Fujito, S. P. DenBaars, J. S. Speck, and S. Nakamura, "Low-threshold-current-density AlGaN-cladding-free m-plane InGaN/GaN laser diodes," *Appl. Phys. Lett.*, vol. 96, no. 23, pp. 231113-1–231113-3, Jun. 2010.
[37] K. Gatto, "Bridgelux demonstrates silicon substrate LED that produces 135 lumens per watt," PhysOrg.com, Mar. 9, 2011.
[38] "OSRAM researchers claim new white LED record," Optics.Org, Mar. 15, 2011.
[39] J. Zhang and N. Tansu, "Improvement in spontaneous emission rates for InGaN quantum wells on ternary InGaN substrate for light-emitting diodes," *J. Appl. Phys.*, vol. 110, no. 11, pp. 113110-1–113110-5, Dec. 2011.
[40] T. K. Sharma and E. Towe, "On ternary nitride substrates for visible semiconductor light-emitters," *Appl. Phys. Lett.*, vol. 96, no. 19, pp. 191105-1–191105-3, May 2010.
[41] O. B. Shchekin, J. E. Epler, T. A. Trottier, T. Margalith, D. A. Steigerwald, M. O. Holcomb, P. S. Martin, and M. R. Krames, "High performance thin-film flip-chip InGaN–GaN light-emitting diodes," *Appl. Phys. Lett.*, vol. 89, no. 7, pp. 071109-1–071109-3, Aug. 2006.
[42] "SemiLEDs: Vertical architecture boosts LED performance," *Compound Semicond.*, May 27, 2010.
[43] B. U. Ye, B. J. Kim, Y. H. Song, J. H. Son, H. K. Yu, M. H. Kim, J. L. Lee, and J. M. Baik, "Enhancing light emission of nanostructured vertical light-emitting diodes by minimizing total internal reflection," *Adv. Funct. Mater.*, vol. 22, no. 3, pp. 632–639, Feb. 2011.
[44] S. J. Lee, K. H. Kim, J. W. Ju, T. Jeong, C. R. Lee, and J. H. Baek, "High-brightness GaN-based light-emitting diodes on Si using wafer bonding technology," *Appl. Phys. Exp.*, vol. 4, no. 6, pp. 066501-1–066501-3, Jun. 2011.
[45] Y. C. Yang, J. K. Sheu, M. L. Lee, S. J. Tu, F. W. Huang, W. C. Lai, S. J. Hon, and T. K. Ko, "Vertical InGaN light-emitting diodes with a sapphire-face-up structure," *Opt. Exp.*, vol. 20, no. 1, pp. A119–A124, Dec. 2012.
[46] E. Matioli, S. Brinkley, K. M. Kelchner, S. Nakamura, S. DenBaars, J. Speck, and C. Weisbuch, "Polarized light extraction in m-plane GaN light-emitting diodes by embedded photonic-crystals," *Appl. Phys. Lett.*, vol. 98, no. 25, pp. 251112-1–251112-3, Jun. 2011.
[47] E. Rangel, E. Matioli, Y. S. Choi, C. Weisbuch, J. S. Speck, and E. L. Hu, "Directionality control through selective excitation of low-order guided modes in thin-film InGaN photonic crystal light-emitting diodes," *Appl. Phys. Lett.*, vol. 98, no. 8, pp. 081104-1–081104-3, Feb. 2011.
[48] Y. K. Ee, P. Kumnorkaew, R. A. Arif, H. Tong, H. P. Zhao, J. F. Gilchrist, and N. Tansu, "Optimization of light extraction efficiency of III-nitride LEDs with self-assembled colloidal-based microlenses," *IEEE J. Sel. Topics Quantum Electron.*, vol. 15, no. 4, pp. 1218–1225, Jul./Aug. 2009.
[49] X. H. Li, R. B. Song, Y. K. Ee, P. Kumnorkaew, J. F. Gilchrist, and N. Tansu, "Light extraction efficiency and radiation patterns of III-nitride light-emitting diodes with colloidal microlens arrays with various aspect ratios," *IEEE Photon. J.*, vol. 3, no. 3, pp. 489–499, Jun. 2011.
[50] J. Henson, J. DiMaria, E. Dimakis, T. D. Moustakas, and R. Paiella, "Plasmon-enhanced light emission based on lattice resonances of silver nanocylinder arrays," *Opt. Lett.*, vol. 37, no. 1, pp. 79–81, Jan. 2012.
[51] H. P. Zhao, J. Zhang, G. Y. Liu, and N. Tansu, "Surface plasmon dispersion engineering via double-metallic Au/Ag layers for III-nitride based light-emitting diodes," *Appl. Phys. Lett.*, vol. 98, no. 15, pp. 151115-1–151115-3, Apr. 2011.
[52] C. H. Lu, C. C. Lan, Y. L. Lai, Y. L. Li, and C. P. Liu, "Enhancement of green emission from InGaN/GaN multiple quantum wells via coupling to surface plasmons in a two-dimensional silver array," *Adv. Funct. Mater.*, vol. 21, no. 24, pp. 4719–4723, Dec. 2011.
[53] C. J. Humphreys, "Solid-state lighting," *MRS Bull.*, vol. 33, no. 4, pp. 459–470, Apr. 2008.
[54] M. R. Krames, O. B. Shchekin, R. MuellerMach, G. O. Mueller, L. Zhou, G. Harbers, and M. G. Crawford, "Status and future of high-power light-emitting diodes for solid-state lighting," *J. Display Technol.*, vol. 3, no. 2, pp. 160–175, Jun. 2007.
[55] Y. S. Hu, W. D. Zhuang, H. Q. Ye, S. S. Zhang, Y. Fang, and X. W. Huang, "Preparation and luminescent properties of $(Ca_{1-x}, Sr_x)S:Eu^{2+}$ red-emitting phosphor for white LED," *J. Lumin.*, vol. 111, no. 3, pp. 139–145, Feb. 2005.
[56] J. Thirumalai, R. Jagannathan, and D. C. Trivedi, "$Y_2O_2S:Eu^{3+}$ nanocrystals, a strong quantum-confined luminescent system," *J. Lumin.*, vol. 126, no. 2, pp. 353–358, Oct. 2007.
[57] J. Li, T. Watanabe, H. Wada, T. Setoyama, and M. Yoshimura, "Low-temperature crystallization of Eu-doped red-emitting $CaAlSiN_3$ from alloy-derived ammonometallates," *Chem. Mater.*, vol. 19, no. 15, pp. 3592–3594, Jun. 2007.
[58] S. E. Brinkley, N. Pfaff, K. A. Denault, Z. Zhang, H. T. Hintzen, R. Seshadri, S. Nakamura, and S. P. DenBaars, "Robust thermal performance of $Sr_2Si_5N_8 : Eu^{2+}$: An efficient red emitting phosphor for light emitting diode based white lighting," *Appl. Phys. Lett.*, vol. 99, no. 24, pp. 3666785-1–3666785-3, Dec. 2011.
[59] J. A. Kechele, C. Hecht, O. Oeckler, J. S. A. D. Gunne, P. J. Schmidt, and W. Schnick, "$Ba_2AlSi_5N_9$—A new host lattice for Eu^{2+}-doped luminescent materials comprising a nitridoalumosilicate framework with corner- and edge-sharing tetrahedral," *Chem. Mater.*, vol. 21, no. 7, pp. 1288–1295, Apr. 2009.
[60] T. C. Liu, B. M. Cheng, S. F. Hu, and R. S. Liu, "Highly stable red oxynitride beta-SiAlON : Pr^{3+} phosphor for light-emitting diodes," *Chem. Mater.*, vol. 23m, no. 16, pp. 3698–3705, Aug. 2011.
[61] S. M. Berman, D. J. Jewett, L. R. Bingham, R. M. Nahass, F. Perry, and G. Fein, "Pupillary size differences under incandescent and high-pressure sodium lamps," *J. IES*, vol. 16, no. 1, pp. 3–20, 1987.
[62] S. Berman, *The Coming Revolution in Lighting Practice*, 2005. [Online]. Available: http://www.lightenergysource.com/ScotopicTechnical.htm

[63] K. L. Gordon, G. P. Sullivan, P. R. Armstrong, E. E. Richman, and B. D. Matzke, *Spectrally Enhanced Lighting Program Implementation for Energy Savings: Field Evaluation*. Washington, DC: Pacific Northwest Nat. Lab. Richland, Aug. 2006, pp. 1–118.
[64] J. Van Derlofske, J. D. Bullough, and J. Watkinson, "Spectral effects of LED forward lighting," *Transp. Lighting Alliance Rep.*, pp. 1–19, Apr. 2005.
[65] T. Erdem and H. V. Demir, "Semiconductor nanocrystals as rare-earth alternatives," *Nature Photon.*, vol. 5, no. 3, pp. 126–126, Mar. 2011.
[66] S. Nizamoglu, T. Erdem, X. W. Sun, and H. V. Demir, "Warm-white light-emitting diodes integrated with colloidal quantum dots for high luminous efficacy and color rendering," *Opt. Lett.*, vol. 35, no. 20, pp. 3372–3374, Oct. 2010.
[67] H. V. Demir, S. Nizamoglu, T. Erdem, E. Mutlugun, N. Gaponik, and A. Eychmuller, "Quantum dot integrated LEDs using photonic and excitonic color conversion," *Nano Today*, vol. 6, no. 6, pp. 632–647, Dec. 2011.

Research Highlights on Organic Photovoltaics and Plasmonics

Qiaoqiang Gan,[1] Filbert J. Bartoli,[2] and Zakya H. Kafafi[3]

(Invited Paper)

[1]Department of Electrical Engineering, University at Buffalo, The State University of New York, Buffalo, NY 14150 USA
[2]Department of Electrical and Computer Engineering, Lehigh University, Bethlehem, PA 18015 USA
[3]Department of Electrical and Systems Engineering, University of Pennsylvania, Philadelphia, PA 19104 USA, on leave from the National Science Foundation, Arlington, VA 22230 USA

DOI: 10.1109/JPHOT.2012.2188886
1943-0655/$31.00 ©2012 IEEE

Manuscript received February 4, 2012; accepted February 19, 2012. Date of current version April 20, 2012. Corresponding authors: Q. Gan (e-mail: qqgan@buffalo.edu); F. Bartoli (e-mail: fjb205@lehigh.edu); Z. Kafafi (e-mail: zkafafi@nsf.gov).

Abstract: Incorporation of plasmonic nanostructures for light trapping is an attractive solution to enhance the optical absorption of the active light-harvesting layer(s) in thin-film photovoltaic cells. The latest research highlights on plasmonic-enhanced organic photovoltaics (OPVs), including metallic nanoparticles and periodic nanopatterned structures, are presented in this paper.

Index Terms: Organic photovoltaics, plasmonics, nanophotonics.

1. Introduction

As a promising clean and sustainable source of energy, photovoltaic (PV) technologies are expected to play a major role in meeting the global renewable energy challenge [1]. Considerable progress has been made recently in organic photovoltaics (OPVs). Compared with their inorganic counterparts, OPVs based on solution processable materials can be fabricated at low cost, over large areas, on rigid or flexible substrates. However, the low charge-carrier mobility and small exciton diffusion length of most organics limit the thickness of the active light-harvesting layers (30–150 nm) [2], [3] in OPVs and lead to relatively poor absorption, which results in insufficient carrier generation and low power conversion efficiency (PCE). To date the best reported PCE for solid-state OPVs is 6.7% [4] and ~8% [5] for molecular and polymer-based single and bulk heterojunctions, respectively. It is believed that the PCE has to reach at least 10% to make OPVs attractive to the marketplace. Effective light trapping schemes for thin-film PVs offer an attractive approach and are critical to ensure full absorption of the incident sunlight. Novel plasmonic nanostructures using surface plasmon polaritons (SPPs) are exciting alternatives that offer effective light trapping inside the active layer of a thin-film solar cell [6]. SPPs are collective oscillations of electromagnetic (EM) waves and free electrons at the interface of a metal and a dielectric or semiconductor material. They are strongly confined at the metal/dielectric interface, with their intensity decaying exponentially with the distance from the interface. The decay lengths of SPP modes in the visible are usually from tens to hundreds of nanometers, depending on the refractive index of the dielectric material at the interface. Incorporation of plasmonic nanostructures for light trapping using 1) random metallic nanoparticles and 2) periodic metallic nanopatterns offers a very attractive solution to enhance the optical absorption and current density in

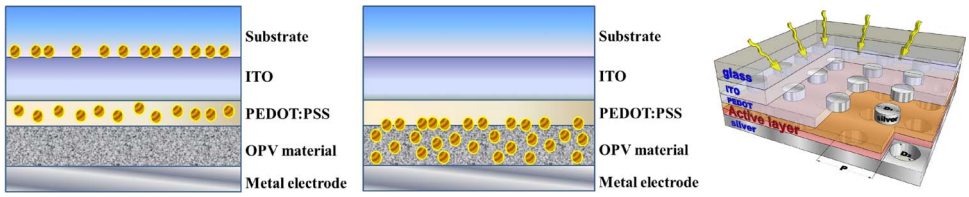

Fig. 1. Conceptual illustration of plasmonic-assisted OPV devices with random distributed metallic nanoparticles (a) outside and (b) embedded inside the active layers. (c) Conceptual illustration of plasmonic OPVs with periodic metallic nanoparticles on top and a nanopatterned metal film on the bottom interfaces of the active light-harvesting layer.

OPVs without increasing the thickness of the active layer(s). In this paper, we give a brief overview of research highlights that describe the latest progress on plasmonic-enhanced OPV devices.

2. Metallic Nanoparticles for Plasmonic-Enhanced OPVs

Metallic nanoparticles are probably the most popular nanostructures used to enhance the performance of PV devices, due primarily to the relatively ease of fabrication. General design considerations have been reviewed extensively for inorganic PVs [6]. Metallic nanoparticles using different materials, concentrations, shapes, sizes to list a few have been introduced in different layers and interfaces at various positions in OPV devices. Fig. 1(a) shows metallic nanoparticles embedded in layers outside the active light-harvesting layer(s). Low cost and simple techniques such as vapor-phase deposition [7], pulse-current electrodeposition [8], and thermal annealing [9] have been used to deposit metallic nanoparticles on indium tin oxide (ITO) electrodes or poly (3,4-ethylenedioxythiophene): poly(styrene sulfonate) (PEDOT:PSS) buffer layers. The dependence of the localized surface plasmon resonance (LSPR) on the size and composition of the nanoparticles have been studied, with reported enhancement in the PCE [8]–[12]. For instance, the PCE of OPVs using poly (3-hexylthiophene)/[6]-phenyl C61 butyric acid methyl ester (P3HT:PCBM) as the active light-harvesting layer were increased by $\sim$18.8% (PCE from 3.48% to 4.19% [10]) to $\sim$69% (PCE from 1.3% to 2.2% [7]) by blending Ag or Au nanoparticles (10 $\sim$ 15 nm in diameter [7], [8], [10] and 45 nm $\pm$ 5 nm in diameter [11]) within the PEDOT:PSS buffer layers, respectively. Au nanoparticles (15 nm) have also been introduced in the PEDOT:PSS layer of an OPV device using poly(2-methoxy-5(20-ethylhexyloxy)-1,4-phenylenevinylene (MEH-PPV) as the active layer and led to an enhancement in PCE from 1.99% to 2.36% [12]. More recently, Au nanoparticles ($\sim$72 nm) were deposited in the interconnecting layer of an inverted tandem polymer solar cell consisting of a cell based on a P3HT: indene-C_{60} bis-adduct ($IC_{60}BA$) and another based on poly[(4,4'-bis(2-ethylhexyl)dithieno[3,2-b:2',3'-d]silole)-2,6-diyl-alt-(2,1,3-benzothiadiazole)-4,7-diyl] (PSBTBT): [6,6]-phenyl-C_{71}-butyric acid methyl ester ($PC_{70}BM$) cell, and resulted in a 20% increase in PCE from 5.22% to 6.24% [13]. However, all these enhanced PCEs are still lower than the experimental records recently achieved [4], [5]. In most these reports, the nanoparticles are located relatively far from the active organic layers, and the absorption enhancement arises from light concentration/scattering from nanoparticles rather than any near-field enhanced LSPR modes.

Embedding metallic nanoparticles into the active layers of OPVs as shown in Fig. 1(b) will make full use of the strong field of the LSPR confined within the surfaces and interfaces between consecutive layers. Metallic nanoparticles are easier to disperse into the active organic layers of an OPV compared to an inorganic PV due to the ease of processability of the organic materials. By tuning the geometric parameters of the metallic nanoparticles, the interaction between the longitudinal and transverse modes supported in the nanoparticle array/chain/cluster embedded in the OPV active layer can lead to impressive absorption enhancement [14], [15]. However, it is recognized that nanoparticles embedded inside the OPV active layer may be experimentally challenging because of the fine tuning that is needed to minimize loss mechanisms such as nonradiative decay and charge-carrier recombination. For instance, it was reported that Ag nanoparticles tend to phase segregate from P3HT:PCBM polymer blends at high concentrations and when incorporated in OPVs lead to a

decrease of carrier extraction [16]. Although an enhancement of PCE from 1% to 2.4% was observed by placing Au nanoparticles at the interface between P3HT:PCBM and PEDOT:PSS [17], no study was reported on PCE enhancement when metallic nanoparticles are dispersed inside the active layer. Most studies focused on optical absorption enhancement of OPV materials containing nanoparticles of various metals (e.g., Au, Ag, Cu, Al, etc.) [18]–[20]. Cu nanoparticles (20 nm) embedded inside P3HT layers were shown to enhance the dissociation of excitons without increasing the P3HT optical absorption [21]. In summary, the roles of metallic nanoparticles dispersed inside the active layer of an OPV need to be further investigated and better understood. It remains to be seen whether the plasmon-enhanced absorption of the active light-harvesting layer will lead to an enhancement in the current density and PCE of an OPV device.

3. Periodic Nanopatterned Structures for Plasmonic-Enhanced OPVs

Although the synthesis of plasmonic metal nanoparticles seems relatively simple, it is quite challenging to control their size and shapes by thermal evaporation and electrodeposition techniques. Another approach that may lead to better tunability, employs periodic patterned metallic nanostructures to enhance the optical absorption of the organic active layers in OPVs. For instance, 1-D Ag grating nanostructures were used to design and fabricate OPVs using several different active organic layers such as P3HT:PCBM [22], PCBM [23], and copper phthalocyanine (CuPc): 3,4,9,10-perylenetetracarboxylic bis-benzimidazole (PTCBI) [24]. By tuning the geometric parameters of the 1-D metallic nanogratings for top transparent anodes [24] or back reflector cathodes [22], the resonant wavelength of the SPP modes could be tuned easily in the visible to near-IR spectral range. However, due to the polarization dependence of the 1-D grating nanostructures, the light trapping is very different for transverse-electric and transverse-magnetic polarized modes, and the simultaneous optimization of the optical absorption for both polarization modes is quite challenging. In addition, due to the intrinsic dispersive metal properties, the resonant wavelengths of SPP modes supported by optically thick metal films depend significantly on the incident light angle. Their bandwidths are also relatively narrow, which is not desirable for OPV applications. Consequently, it is critical to achieve broadband, polarization insensitive/independent, and angle-insensitive plasmonic nanostructures [see Fig. 1(c)] [25].

A straightforward solution to overcome the polarization dependence of 1-D nanostructures in the design of OPVs is to use 2-D nanopatterned structures with high-order symmetries. For instance, 2-D metallic nanovoids were proposed to enhance the coupling between localized SPP modes and J-aggregate excitons of organic semiconducting films [26]. More recently, these 2-D nanovoid plasmonic structures have been applied to an OPV device using P3HT:PCBM as the active layer and resulted in an enhancement factor of 3.5 and 4 in external quantum efficiency and in PCE (i.e., from 0.052% to 0.2%), respectively [27]. In another example, periodic and quasiperiodic 2-D nanoaperture arrays with high-order symmetries were employed as the back reflector or concentrator to enhance the optical absorption of P3HT:PCBM layers [28]. However, the enhanced absorption was demonstrated in a very narrow spectral region close to the excitation wavelength. Consequently, it is still important to achieve broadband absorption enhancement over the entire visible and part of the near-infrared solar spectrum to further improve the overall PV device efficiencies.

Although randomly distributed nanoparticles of varying size and shape received much attention [6], their resonant frequencies for periodic plasmonic nanostructures usually occur within a narrow spectral band. Physical mechanisms that lead to broadband absorption enhancement and/or a robust predictive capability for designing plasmonic nanostructures have recently been pursued [29]–[31]. Due to the dispersive nature of SPP modes, plasmonic nanostructures are usually sensitive to incident angle, which led to designs of plasmonic black bodies, perfect absorbers or omnidirectional absorbers based on 1-D grating nanostructures [32], 2-D complex metallic nanopatterned structures [33], and randomly distributed metamaterials [34], These support angle-insensitive hybrid modes in the visible and near-IR spectral region. Incorporating these nanostructures into OPV devices offers a promising approach to address the angular tolerance limitation for conventional plasmonic nanostructures. Metallic triangular/pyramid nanogratings [35] and

nanostrips [36] were designed as the back reflector in order to realize angle insensitive absorption enhancement in the active light-harvesting layer (e.g., P3HT:PCBM [35] and the donor: acceptor CuPc:C_{60} molecular heterojunction [36]).

In addition to their role in enhancing absorption in the active light-harvesting layer, the nanopatterned metal structures can also function as a device electrode. Nanopatterned metal films [29] and metallic nanowires [31] with a low fill factor have been employed as alternative electrodes to replace ITO films in organic optoelectronic devices. For example, one study introduced a 15-nm thick Au/AuO_x film to replace the ITO layer for high-performance flexible organic optoelectronics [37]. In another investigation, 40-nm thick 1-D metallic nanowires were used as anodes for organic solar cells [38], [39]. The sheet resistance of arrays of 40-nm thick nanopatterned metal electrodes (Au, Cu, Ag) varies depending on the metal and linewidth but does not exceed 20–30 $\Omega \cdot \text{sq}^{-1}$ [38]. These alternative nanomaterials for transparent electrodes are highly desirable in many optoelectronic applications due to the potential shortage in indium and other problems associated with the use of ITO, which are outside the scope of this paper. It is of interest to design metallic nanostructures for OPVs that serve concurrently for light trapping and as transparent electrodes [40]–[42].

In summary, we have reviewed the latest progress of plasmonic enhanced OPVs reported mainly in 2011. In general, most studies focused on the absorption enhancement of OPV materials, which need to be translated into improvement in current density and device efficiency. We hope that this brief overview of the research status can excite more creative research that will result in OPV devices with improved performance.

References

[1] M. A. Green, "Recent developments in photovoltaics," *Sol. Energy*, vol. 76, no. 1–3, pp. 3–8, Jan.–Mar. 2004.

[2] S. Sista, M.-H. Park, Z. Hong, Y. Wu, J. Hou, W. L. Kwan, G. Li, and Y. Yang, "Highly efficient tandem polymer photovoltaic cells," *Adv. Mater.*, vol. 22, no. 3, pp. 380–383, Jan. 2010.

[3] S. H. Park, A. Roy, S. Beaupré, S. Cho, N. Coates, J. S. Moon, D. Moses, M. Leclerc, K. Lee, and A. J. Heeger, "Bulk heterojunction solar cells with internal quantum efficiency approaching 100%," *Nat. Photon.*, vol. 3, no. 5, pp. 297–302, May 2009.

[4] Y. Sun, G. C. Welch, W. Leong, C. J. Takacs, G. C. Bazan, and A. J. Heeger, "Solution-processed small-molecule solar cells with 6.7% efficiency," *Nat. Mater.*, vol. 11, no. 1, pp. 44–48, Nov. 2011.

[5] H.-Y. Chen, J. Hou, S. Zhang, Y. Liang, G. Yang, Y. Yang, L. Yu, Y. Wu, and G. Li, "Polymer solar cells with enhanced open-circuit voltage and efficiency," *Nat. Photon.*, vol. 3, no. 11, pp. 649–653, Nov. 2009.

[6] H. A. Atwater and A. Polman, "Plasmonics for improved photovoltaic devices," *Nat. Mater.*, vol. 9, no. 3, pp. 205–213, Mar. 2010.

[7] A. J. Morfa, K. L. Rowlen, T. H. Reilly, M. J. Romero, and J. van de Lagemaat, "Plasmon-enhanced solar energy conversion in organic bulk heterojunction photovoltaics," *Appl. Phys. Lett.*, vol. 92, no. 1, pp. 013504-1–013504-3, Jan. 2008.

[8] S. Kim, S. Na, J. Jo, D. Kim, and Y. Nah, "Plasmon enhanced performance of organic solar cells using electrodeposited Ag nanoparticles," *Appl. Phys. Lett.*, vol. 93, no. 7, pp. 073307-1–073307-3, Aug. 2008.

[9] J. Lee, J. Park, J. Kim, D. Lee, and K. Cho, "High efficiency polymer solar cells with wet deposited plasmonic gold nanodots," *Organic Electron.*, vol. 10, no. 3, pp. 416–420, 2009.

[10] F. Chen, J. Wu, C. Lee, Y. Hong, C. Kuo, and M. Huang, "Plasmonic-enhanced polymer photovoltaic devices incorporating solution-processable metal nanoparticles," *Appl. Phys. Lett.*, vol. 95, no. 1, pp. 013305-1–013305-3, Jul. 2009.

[11] J. Wu, F.-C. Chen, Y.-S. Hsiao, F.-C. Chien, P. Chen, C.-H. Kuo, M. H. Huang, and C.-S. Hsu, "Surface plasmonic effects of metallic nanoparticles on the performance of polymer bulk heterojunction solar cells," *ACS Nano*, vol. 5, no. 2, pp. 959–967, Feb. 2011.

[12] L. Qiao, D. Wang, L. Zuo, Y. Ye, J. Qian, H. Chen, and S. He, "Localized surface plasmon resonance enhanced organic solar cell with gold nanospheres," *Appl. Energy*, vol. 88, no. 3, pp. 848–852, Mar. 2011.

[13] J. Yang, J. You, C. Chen, W. Hsu, H. Tan, X. Zhang, Z. Hong, and Y. Yang, "Plasmonic polymer tandem solar cell," *ACS Nano*, vol. 5, no. 8, pp. 6210–6217, Aug. 2011.

[14] W. E. I. Sha, W. C. H. Choy, Y. Wu, and W. C. Chew, "Optical and electrical study of organic solar cells with a 2D grating anode," *Opt. Exp.*, vol. 20, no. 3, pp. 2572–2580, Jan. 2012.

[15] W. E. I. Sha, W. C. H. Choy, Y. P. Chen, and W. C. Chew, "Optical design of organic solar cell with hybrid plasmonic system," *Opt. Exp.*, vol. 19, no. 17, pp. 15 908–15 918, Aug. 2011.

[16] M. Xue, L. Li, T. de Villers, J. Bertrand, H. Shen, J. Zhu, Z. Yu, A. Z. Stieg, Q. Pei, B. J. Schwartz, and K. L. Wang, "Charge-carrier dynamics in hybrid plasmonic organic solar cells with Ag nanoparticles," *Appl. Phys. Lett.*, vol. 98, no. 25, pp. 253302-1–253302-3, Jun. 2011.

[17] G. D. Spyropoulos, M. Stylianakis, E. Stratakis, and E. Kymakis, "Plasmonic organic photovoltaics doped with metal nanoparticles," *Photon. Nanostructures, Fundam. Appl.*, vol. 9, no. 2, pp. 184–189, Apr. 2011.
[18] I. Diukman, L. Tzabari, N. Berkovitch, N. Tessler, and M. Orenstein, "Controlling absorption enhancement in organic photovoltaic cells by patterning Au nano disks within the active layer," *Opt. Exp.*, vol. 19, no. Suppl 1, pp. A64–A71, Jan. 2011.
[19] A. Kulkarni, K. Noone, K. Munechika, S. Guyer, and D. Ginger, "Plasmon-enhanced charge carrier generation in organic photovoltaic films using silver nanoprisms," *Nano Lett.*, vol. 10, no. 4, pp. 1501–1505, Apr. 2010.
[20] V. Kochergin, L. Neely, C. Jao, and H. D. Robinson, "Aluminum plasmonic nanostructures for improved absorption in organic photovoltaic devices," *Appl. Phys. Lett.*, vol. 98, no. 13, pp. 133305-1–133305-3, Mar. 2011.
[21] J. Szeremeta, M. Nyk, A. Chyla, W. Strek, and M. Samoc, "Enhancement of photoconduction in a conjugated polymer through doping with copper nanoparticles," *Opt. Mater.*, vol. 33, no. 9, pp. 1372–1376, Jul. 2011.
[22] M. A. Sefunc, A. K. Okyay, and H. V. Demir, "Plasmonic backcontact grating for P3HT:PCBM organic solar cells enabling strong optical absorption increased in all polarizations," *Opt. Exp.*, vol. 19, no. 15, pp. 14 200–14 209, Jul. 2011.
[23] H. Wang, H. Wang, B. Gao, Y. Jiang, Z. Yang, Y. Hao, Q. Chen, X. Du, and H. Sun, "Surface plasmon enhanced absorption dynamics of regioregular poly(3-hexylthiophene)," *Appl. Phys. Lett.*, vol. 98, no. 25, pp. 251501-1–251501-3, Jun. 2011.
[24] C. Min, J. Li, G. Veronis, J. Lee, S. Fan, and P. Peumans, "Enhancement of optical absorption in thin-film organic solar cells through the excitation of plasmonic modes in metallic gratings," *Appl. Phys. Lett.*, vol. 96, no. 13, pp. 133302-1–133302-3, Mar. 2010.
[25] K. Aydin, V. E. Ferry, R. M. Briggs, and H. A. Atwater, "Broadband polarization-independent resonant light absorption using ultrathin plasmonic super absorbers," *Nat. Commun.*, vol. 2, p. 517, Nov. 2011, DOI:10.1038/ncomms1528.
[26] Y. Sugawara, T. A. Kelf, J. J. Baumberg, M. E. Abdelsalam, and P. N. Bartlett, "Strong coupling between localized plasmons and organic excitons in metal nanovoids," *Phys. Rev. Lett.*, vol. 97, no. 26, pp. 266808-1–266808-4, Dec. 2006.
[27] N. Lal, B. F. Soares, J. K. Sinha, F. Huang, S. Mahajan, P. N. Bartlett, N. C. Greenham, and J. J. Baumberg, "Enhancing solar cells with localized plasmons in nanovoids," *Opt. Exp.*, vol. 19, no. 12, pp. 11 256–11 263, Jun. 2011.
[28] A. Ostfeld and D. Pacifici, "Plasmonic concentrators for enhanced light absorption in ultrathin film organic photovoltaics," *Appl. Phys. Lett.*, vol. 98, no. 11, pp. 113112-1–113112-3, Mar. 2011.
[29] W. Bai, Q. Gan, G. Song, L. Chen, Z. Kafafi, and F. Bartoli, "Broadband short-range surface plasmon structures for absorption enhancement in organic photovoltaics," *Opt. Exp.*, vol. 18, no. S4, pp. A620–A630, Nov. 2010.
[30] W. Bai, Q. Gan, G. Song, L. Chen, Z. Kafafi, and F. Bartoli, "Double plasmonic structure design for broadband absorption enhancement in molecular organic solar cells," *J. Photon. Energy*, vol. 1, no. 1, p. 011121, 2011.
[31] H. Shen and B. Maes, "Combined plasmonic gratings in organic solar cells," *Opt. Exp.*, vol. 19, no. Suppl 6, pp. A1202–A1210, Nov. 2011.
[32] J. Zhang, W. Bai, L. Cai, X. Chen, G. Song, and Q. Gan, "Omnidirectional absorption enhancement in hybrid waveguide-plasmon system," *Appl. Phys. Lett.*, vol. 98, no. 26, pp. 261101-1–261101-3, Jun. 2011.
[33] T. V. Teperik, F. J. García de Abajo, A. G. Borisov, M. Abdelsalam, P. N. Bartlett, Y. Sugawara, and J. J. Baumberg, "Omnidirectional absorption in nanostructured metal surfaces," *Nat. Photon.*, vol. 2, no. 5, pp. 299–301, May 2008.
[34] M. K. Hedayati, M. Javaherirahim, B. Mozooni, R. Abdelaziz, A. Tavassolizadeh, V. S. K. Chakravadhanula, V. Zaporojtchenko, T. Strunkus, F. Faupel, and M. Elbahri, "Design of a perfect black absorber at visible frequencies using plasmonic metamaterials," *Adv. Mater.*, vol. 23, no. 45, pp. 5410–5414, Dec. 2011.
[35] A. Abass, H. Shen, P. Bienstman, and B. Maes, "Angle insensitive enhancement of organic solar cells using metallic gratings," *J. Appl. Phys.*, vol. 109, no. 2, pp. 023111-1–023111-7, Jan. 2011.
[36] W. E. I. Sha, W. C. H. Choy, and W. C. Chew, "Angular response of thin-film organic solar cells with periodic metal back nanostrips," *Opt. Lett.*, vol. 36, no. 4, pp. 478–480, Feb. 2011.
[37] M. G. Helander, Z. B. Wang, M. T. Greiner, Z. W. Liu, J. Qiu, and Z. H. Lu, "Oxidized gold thin films: An effective material for high-performance flexible organic optoelectronics," *Adv. Mater.*, vol. 22, no. 18, pp. 2037–2040, May 2010.
[38] M. G. Kang, M.-S. Kim, J. Kim, and L. J. Guo, "Organic solar cells using nanoimprinted transparent metal electrode," *Adv. Mater.*, vol. 20, no. 23, pp. 4408–4413, Dec. 2008.
[39] M. G. Kang, T. Xu, H. J. Park, X. G. Luo, and L. J. Guo, "Efficiency enhancement of organic solar cells using transparent plasmonic Ag nanowire electrodes," *Adv. Mater.*, vol. 22, no. 39, pp. 4378–4383, Oct. 2010.
[40] H. M. Stec, R. J. Williams, T. S. Jones, and R. A. Hatton, "Ultrathin transparent Au electrodes for organic photovoltaics fabricated using a mixed mono-molecular nucleation layer," *Adv. Funct. Mater.*, vol. 21, no. 9, pp. 1709–1716, May 2011.
[41] M. Elbahri, M. K. Hedayati, V. S. K. Chakravadhanula, M. Jamali, T. Strunkus, V. Zaporojtchenko, and F. Faupel, "An omnidirectional transparent conducting-metal-based plasmonic nanocomposite," *Adv. Mater.*, vol. 23, no. 17, pp. 1993–1997, May 2011.
[42] W. A. Luhman, S. Lee, T. W. Johnson, R. Holmes, and S. Oh, "Self-assembled plasmonic electrodes for high-performance organic photovoltaic cells," *Appl. Phys. Lett.*, vol. 99, no. 10, pp. 103306-1–103306-3, Sep. 2011.

Inverted Polymer Solar Cells

Song Chen,[1] Sai-Wing Tsang,[1] Cephas E. Small,[1] John R. Reynolds,[2] and Franky So,[1] *Fellow, IEEE*

(Invited Paper)

[1]Department of Materials Science and Engineering, University of Florida, Gainesville, FL 32611-6400 USA
[2]School of Chemistry and Biochemistry, School of Materials Science and Engineering, Center for Organic Photonics and Electronics, Georgia Institute of Technology, Atlanta, GA 30332-0400 USA

DOI: 10.1109/JPHOT.2012.2190274

Manuscript received February 12, 2012; revised February 23, 2012; accepted February 23, 2012. Date of current version April 20, 2012. This work was supported by the Office of Naval Research under Contract N000141110245. Corresponding author: F. So (e-mail: fso@mse.ufl.edu).

Abstract: Inverted bulk heterojunction polymer solar cells have become the preferred device architecture for roll-to-roll (R2R) processing, which allows large area devices to be fabricated on flexible substrates. Significant improvements in inverted solar cell performance have been made with novel photovoltaic polymers, along with optimized blend morphology and improved carrier extraction materials. For the first time, inverted polymer solar cells display their potential for low-cost R2R processing with power conversion efficiencies exceeding 8%.

Index Terms: Polymer solar cells, inverted structure, zinc oxide.

Polymer solar cells are attractive for next-generation photovoltaics due to their potential for low-cost roll-to-roll (R2R) processing onto flexible substrates. While the stability of polymer solar cells has been a concern in the past, Konarka has recently demonstrated that their cells have passed the critical lifetime aging tests according to IEC 61646, indicating that device stability does not appear to be an issue [1]. Because of the large exciton binding energy of organic materials, polymer photovoltaic (PPV) cells are excitonic devices wherein photogenerated electron–hole pairs are separated at the interface of an electron donating polymer and an electron accepting fullerene derivative by effective force [2], [3]. The photoactive layer consists of a polymer:fullerene blend which forms a bulk heterojunction (BHJ) [4], [5] resulting in an interpenetrating network of donor and acceptor phases, allowing dissociated holes and electrons to transport separately in the corresponding phases. To efficiently collect the photogenerated carriers, carrier extraction layers are inserted between the active BHJ layer and the electrodes.

The efficiency of PPV cells is determined by the molecular and morphological structures of the photoactive materials, wherein conjugated donor-acceptor polymers are of interest due to the tunability of the highest occupied molecular orbital (HOMO) and lowest unoccupied molecular orbital (LUMO) levels to engineer their electronic and optical properties [6]–[15]. This bandgap engineering of donor-acceptor moieties not only controls the bandgap energy to optimize light harvesting but also allows for favorable energy alignments to achieve high open circuit voltages (V_{OC}) and efficient exciton dissociation as well. By controlling these donor and acceptor energy levels, numerous groups have demonstrated significant advances in device performance. For example, the combination of dithienosilole and thienopyrrole-4,6-dione (PDTS-TPD) results in a low bandgap (1.73 eV) polymer with a low-lying HOMO level (−5.57 eV), and the resulting PPV cells

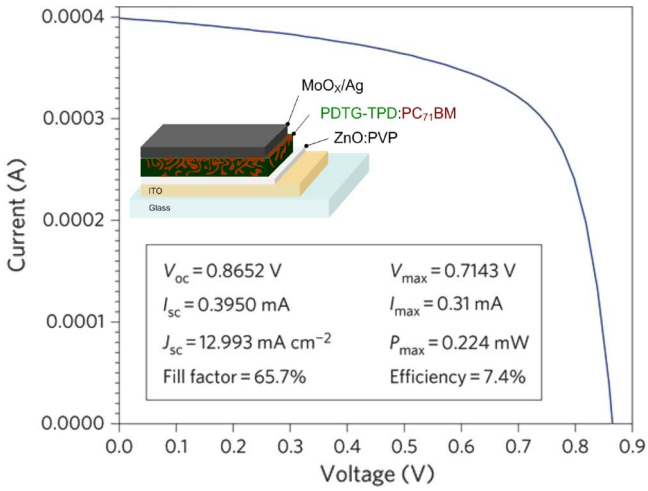

Fig. 1. Certified efficiency of PDTG-TPD: $PC_{71}BM$ cell with the inverted device structure. The figure is modified from [19].

give a high photocurrent (J_{SC}) while maintaining high open circuit voltages to realize high power conversion efficiencies (PCEs). When blended with [6,6]-phenyl-C71 butyric acid methyl ester $(PC_{71}BM)$, these PDTS-TPD polymer solar cells with an optimized BHJ morphology exhibited a PCE exceeding 7% [16]. Replacing the silicon bridging atom with germanium in the donor unit, a dithienogermole-based polymer with a bandgap of 1.69 eV and a slightly higher HOMO level was also realized, and a further enhancement in device performance was observed [8].

Achieving well-controlled nanoscale BHJ morphology is critical to the performance of PPV cells. Solvent additives provide a means to alter the miscibility of the donor and acceptor materials to control the nanoscale morphology [14], [17]. Such a strategy enables the formation of interpenetrating nanosized domains of the conjugated donor-acceptor polymers and $PC_{71}BM$ without the requirement of high temperature annealing processes, and solvent additives become a vital component to many donor-acceptor systems. In this, high carrier mobilities were achieved even without the presence of visible crystalline domains in the polymer: $PC_{71}BM$ composites. Unlike earlier donor-acceptor polymers, which suffer from recombination limited photocurrent [18], solvent additive assisted morphology control leads to high fill factors and high external quantum efficiencies in BHJ solar cells [8], [16], [19], [20]. Using this approach, a substantial enhancement in device efficiency has been demonstrated by various groups [8], [16].

While PPV cells are fabricated by solution processing, the viability to employ a R2R manufacturing process is determined by the device geometry used. In a conventional PPV cell, a top low work function metal is required for efficient electron collection while conducting polymers such as poly(3,4-ethylenedioxythiophene):poly(styrenesulfonate) (PEDOT:PSS) serve as the bottom anode interlayer for efficient hole extraction. In order to deposit the top electrode, vacuum thermal deposition is required, and this process is not compatible with R2R processes. In contrast to conventional cells, low work function metals are not necessary in inverted cells since a metal oxide electron extraction layer along with the bottom ITO electrode is used as a bottom cathode as shown in the inset of Fig. 1. For the top anode, metal oxides have also been used as hole extraction materials. Specifically, thermal evaporated MoO_3 has now become a standard material for the hole extraction layer in inverted devices fabricated in research laboratories [8], [20]–[22]. More recently, solution processed MoO_3 [23] and Ni_xO [24] have also been used in conventional polymer solar cells with good performance and these solution processed oxides can potentially be used in the inverted cells. Using these metal oxides as the charge extraction interlayer along with a top printed silver electrode, this device architecture is more compatible with the one used in the R2R printing process. The first inverted polymer solar cell was reported in 2006 [25]. Since then, a variety of

materials have been used as hole and electron transporting layers, and the efficiencies are, in general, lower than those of the conventional cells with a bottom anode. The highest efficiency reported in 2010 was 6.1%, which is a record value demonstrated with the poly[[9-(1-octylnonyl)-9H-carbazole-2,7-diyl]-2,5-thiophenediyl-2,1,3-benzothiadiazole-4,7-diyl-2,5-thiophenediyl] (PCDTBT): $PC_{71}BM$ system when MoO_3 and ZnO were used for hole and electron extraction, respectively [22]. However, most inverted cells have inferior device performance compared with their counterparts fabricated with a conventional geometry.

The poor performance of the inverted cells can be attributed to the quality of the charge extraction materials. Specifically, high density defects are present in solution processed ZnO films and they contribute to the loss of photocurrent. Modifications of solution processed ZnO films have been shown to be effective to improve the device efficiency. For example, it was shown that a thin layer of C_{60} on top of ZnO nanoparticles (NPs) helped to improve the morphology of the subsequently spin-coated polymer:fullerene layer, and significantly enhanced the J_{sc} and PCE (4.9%) of inverted poly(3-hexylthiophene) (P3HT): $PC_{71}BM$ cells [21]. This surface modification of ZnO in the inverted cells has led to PCEs comparable with the best conventional cells. The ideal solution processed ZnO films should be of low defect density and have good electric coupling with the BHJ layer. For example, the uniformity of the sol-gel derived ZnO film can be improved when the precursor is blended with an insulating polymer matrix. However, the surface of the as-spun ZnO film becomes polymer rich, and the insulating layer forms a barrier for electron extraction. Treating the ZnO-polymer composite layer with UV-ozone improves the electric coupling and enhances the PCE of inverted PDTG-TPD: PCBM cells to 8.1%. This is the first report of inverted polymer cells with efficiency exceeding 8%. The Newport certified results are showed in Fig. 1 [20].

In summary, high efficiency inverted PPV cells have been demonstrated, which illustrates the viability of PPV for R2R processing and the potential for low-cost light harvesting.

References

[1] Konarka's Next Generation Organic Photovoltaic Cells First OPV Technology to Pass Set of Individual Critical Lifetime Aging Tests According to IEC 61646 Performed by TÜV Rheinland, 2012. [Online]. Available: http://www.konarka.com/index.php/site/pressreleasedetail/konarkas_next_generation_organic_photovoltaic_cells_first_opv_technology_to

[2] C. J. Brabec, C. Winder, N. S. Sariciftci, J. C. Hummelen, A. Dhanabalan, P. A. van Hal, and R. A. J. Janssen, "A low-bandgap semiconducting polymer for photovoltaic devices and infrared emitting diodes," *Adv. Funct. Mater.*, vol. 12, no. 10, pp. 709–712, Oct. 2002.

[3] S. J. Fonash, Ed., *Solar Cells Device Physics*. New York: Elsevier, 2010.

[4] G. Yu, J. Gao, J. C. Hummelen, F. Wudl, and A. J. Heeger, "Polymer photovoltaic cells—Enhanced efficiencies via a network of internal donor-acceptor heterojunctions," *Science*, vol. 270, no. 5243, pp. 1789–1791, Dec. 15, 1995.

[5] G. Li, V. Shrotriya, J. S. Huang, Y. Yao, T. Moriarty, K. Emery, and Y. Yang, "High-efficiency solution processable polymer photovoltaic cells by self-organization of polymer blends," *Nat. Mater.*, vol. 4, no. 11, pp. 864–868, Nov. 2005.

[6] S. H. Park, A. Roy, S. Beaupré, S. Cho, N. Coates, J. S. Moon, D. Moses, M. Leclerc, K. Lee, and A. J. Heeger, "Bulk heterojunction solar cells with internal quantum efficiency approaching 100%," *Nat. Photon.*, vol. 3, no. 5, p. 297-U5, May 2009.

[7] E. G. Wang, L. Wang, L. F. Lan, C. Luo, W. L. Zhuang, J. B. Peng, and Y. Cao, "High-performance polymer heterojunction solar cells of a polysilafluorene derivative," *Appl. Phys. Lett.*, vol. 92, no. 3, p. 033307, Jan. 21, 2008.

[8] C. M. Amb, S. Chen, K. R. Graham, J. Subbiah, C. E. Small, F. So, and J. R. Reynolds, "Dithienogermole as a fused electron donor in bulk heterojunction solar cells," *J. Amer. Chem. Soc.*, vol. 133, no. 26, p. 10 062, Jul. 2011.

[9] J. Peet, J. Y. Kim, N. E. Coates, W. L. Ma, D. Moses, A. J. Heeger, and G. C. Bazan, "Efficiency enhancement in low-bandgap polymer solar cells by processing with alkane dithiols," *Nat. Mater.*, vol. 6, no. 7, pp. 497–500, Jul. 2007.

[10] Z. Li, J. F. Ding, N. H. Song, J. P. Lu, and Y. Tao, "Development of a new s-tetrazine-based copolymer for efficient solar cells," *J. Amer. Chem. Soc.*, vol. 132, no. 38, pp. 13 160–13 161, Sep. 29, 2010.

[11] N. Allard, R. B. Aich, D. Gendron, P. L. T. Boudreault, C. Tessier, S. Alem, S. C. Tse, Y. Tao, and M. Leclerc, "Germafluorenes: New heterocycles for plastic electronics," *Macromolecules*, vol. 43, no. 5, pp. 2328–2333, Mar. 9, 2010.

[12] Y. C. Chen, C. Y. Yu, Y. L. Fan, L. I. Hung, C. P. Chen, and C. Ting, "Low-bandgap conjugated polymer for high efficient photovoltaic applications," *Chem. Commun.*, vol. 46, no. 35, pp. 6503–6505, Sep. 2010.

[13] S. C. Price, A. C. Stuart, L. Q. Yang, H. X. Zhou, and W. You, "Fluorine substituted conjugated polymer of medium band gap yields 7% efficiency in polymer-fullerene solar cells," *J. Amer. Chem. Soc.*, vol. 133, no. 12, pp. 4625–4631, Mar. 30, 2011.

[14] R. C. Coffin, J. Peet, J. Rogers, and G. C. Bazan, "Streamlined microwave-assisted preparation of narrow-bandgap conjugated polymers for high-performance bulk heterojunction solar cells," *Nat. Chem.*, vol. 1, no. 8, pp. 657–661, Nov. 2009.

[15] Y. Y. Liang, Z. Xu, J. B. Xia, S. T. Tsai, Y. Wu, G. Li, C. Ray, and L. P. Yu, "For the bright future-bulk heterojunction polymer solar cells with power conversion efficiency of 7.4%," *Adv. Mater.*, vol. 22, no. 20, pp. E135–E138, May 25, 2010.
[16] T. Y. Chu, J. Lu, S. Beaupre, Y. Zhang, J. R. Pouliot, S. Wakim, J. Zhou, M. Leclerc, Z. Li, J. Ding, and Y. Tao, "Bulk heterojunction solar cells using thieno[3,4-c]pyrrole-4,6-dione and dithieno[3,2-b:2', 3'-d]silole copolymer with a power conversion efficiency of 7.3%," *J. Amer. Chem. Soc.*, vol. 133, p. 4250, 2011.
[17] J. S. Moon, C. J. Takacs, S. Cho, R. C. Coffin, H. Kim, G. C. Bazan, and A. J. Heeger, "Effect of processing additive on the nanomorphology of a bulk heterojunction material," *Nano Lett.*, vol. 10, no. 10, pp. 4005–4008, Oct. 2010.
[18] S. Chen, K. R. Choudhury, J. Subbiah, C. M. Amb, J. R. Reynolds, and F. So, "Photo-carrier recombination in polymer solar cells based on P3HT and silole-based copolymer," *Adv. Energy Mater.*, vol. 1, no. 5, pp. 963–969, Oct 2011.
[19] H. Y. Chen, J. H. Hou, S. Q. Zhang, Y. Y. Liang, G. W. Yang, Y. Yang, L. P. Yu, Y. Wu, and G. Li, "Polymer solar cells with enhanced open-circuit voltage and efficiency," *Nat. Photon.*, vol. 3, no. 11, pp. 649–653, Nov. 2009.
[20] C. E. Small, S. Chen, J. Subbiah, C. M. Amb, S. W. Tsang, T. H. Lai, J. R. Reynolds, and F. So, "High-efficiency inverted dithienogermole–thienopyrrolodione-based polymer solar cells," *Nat. Photon.*, vol. 6, no. 2, pp. 115–120, Feb. 2012.
[21] S. K. Hau, H. L. Yip, H. Ma, and A. K. Y. Jen, "High performance ambient processed inverted polymer solar cells through interfacial modification with a fullerene self-assembled monolayer," *Appl. Phys. Lett.*, vol. 9, no. 23, p. 233 304, Dec 8, 2008.
[22] Y. M. Sun, J. H. Seo, C. J. Takacs, J. Seifter, and A. J. Heeger, "Inverted polymer solar cells integrated with a low-temperature-annealed sol-gel-derived ZnO film as an electron transport layer," *Adv. Mater.*, vol. 23, no. 14, pp. 1679–1683, Apr. 12, 2011.
[23] S. R. Hammond, J. Meyer, N. E. Widjonarko, P. F. Ndione, A. K. Sigdel, A. Garcia, A. Miedaner, M. T. Lloyd, A. Kahn, D. S. Ginley, J. J. Berry, and D. C. Olson, "Low-temperature, solution-processed molybdenum oxide hole-collection layer for organic photovoltaics," *J. Mater. Chem.*, vol. 22, no. 7, pp. 3249–3254, 2012.
[24] K. X. Steirer, P. F. Ndione, N. E. Widjonarko, M. T. Lloyd, J. Meyer, E. L. Ratcliff, A. Kahn, N. R. Armstrong, C. J. Curtis, D. S. Ginley, J. J. Berry, and D. C. Olson, "Enhanced efficiency in plastic solar cells via energy matched solution processed NiO_x interlayers," *Adv. Energy Mater.*, vol. 1, no. 5, pp. 813–820, Oct. 2011.
[25] G. Li, C. W. Chu, V. Shrotriya, J. Huang, and Y. Yang, "Efficient inverted polymer solar cells," *Appl. Phys. Lett.*, vol. 88, no. 25, p. 253 503, Jun. 19, 2006.

Single-Photon and Photon-Number-Resolving Detectors

R. P. Mirin,[1] *Senior Member, IEEE*, S. W. Nam,[1] *Member, IEEE*, and M. A. Itzler,[2] *Fellow, IEEE*

(Invited Paper)

[1]National Institute of Standards and Technology, Boulder, CO 80305 USA
[2]Princeton Lightwave, Cranbury, NJ 08512 USA

DOI: 10.1109/JPHOT.2012.2190394
1943-0655/$31.00 ©2012 IEEE

Manuscript received February 15, 2012; accepted February 28, 2012. Date of current version April 20, 2012. Corresponding author: R. P. Mirin (e-mail: mirin@boulder.nist.gov).

Abstract: Several important advances were reported in single-photon detectors and photon-number-resolving detectors in 2011. New materials with smaller superconducting gaps were demonstrated for superconducting nanowire single-photon detectors (SNSPDs) that led to improved signal-to-noise ratios and infrared performance. Faster superconducting transition edge sensors (TESs) were demonstrated by using normal metal heat sinks. Both TESs and SNSPDs were evanescently coupled with waveguides as a step toward demonstrating quantum photonic integrated circuits. Photon-number resolution has been the goal in several demonstrations using semiconductor detectors, and recent results suggest a potential convergence of Geiger-mode and linear-mode avalanche diodes in exhibiting the high-gain, low-noise analog behavior necessary to reach this goal. There has also been progress focused on additional trends in single-photon avalanche diodes (SPADs) for high-rate counting and detector array scaling.

Index Terms: Single photon detectors, photon number resolving detectors, single photon avalanche diodes, superconducting single photon detectors, quantum optics.

Significant advances in both superconducting and semiconducting single-photon detectors have been achieved in recent years, and these devices have largely supplanted photomultiplier tubes for many applications because of their ease of use and especially their superior performance. There are many emerging applications that require single-photon detectors, including single-molecule fluorescence and detection, LIDAR, quantum key distribution, and linear optical quantum computing. The key performance metrics for single-photon detectors include detection efficiency (DE), dark-count rate (DCR), timing jitter, and reset time. We will describe recent advances in these metrics that enable emerging applications.

Until last year, superconducting nanowire single-photon detectors (SNSPDs) were typically made from NbN or NbTiN, with single-photon response from the UV to the near-infrared (IR). These devices operate at 2–4 K. They are very fast, with timing jitter of around 30–100 ps achieved [1]. Robust coupling to single-mode optical fiber and a cryogen-free refrigerator has enabled SNSPDs to be deployed in several interesting demonstration experiments, including QKD [2] and LIDAR [3]. SNSPDs are of particular interest for wavelengths longer than 1000 nm, where Si single-photon avalanche diodes (SPADs) are replaced by InGaAs SPADs.

Detection of photons with wavelengths longer than 1.5 μm using NbN or NbTiN is challenging because the hot spot that develops when a photon is absorbed is relatively small. This limits the

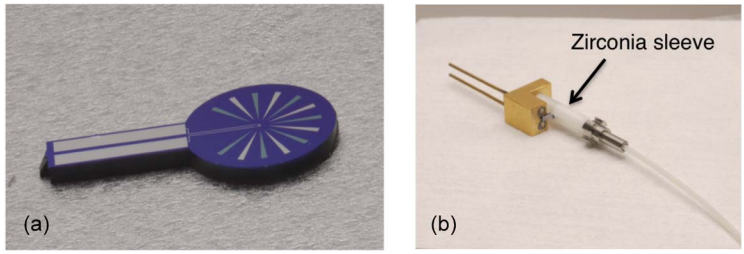

Fig. 1. (a) A completed TES chip that is freed from the wafer. The diameter of the circular part of the chip is 2.5 mm. (b) A completed assembly with a zirconia sleeve fitted over the chip and a single-mode optical fiber and ferrule.

performance of NbN SNSPDs with wire widths of $\sim$100 nm. However, recent papers [4], [5] have reported improved infrared performance, including some limited response at 3.5 μm, by using narrow wire widths ($\leq$ 50 nm). Two recent papers [6], [7] demonstrated new materials with smaller superconducting gaps to alleviate this problem. Amorphous NbSi, with nanowire widths of 160 nm, was demonstrated to have relatively better DE for wavelengths longer than 1550 nm when compared to NbTiN SNSPDs [7]. Amorphous tungsten silicide $(W_xSi_{1-x}, x \sim 0.25)$, with nanowire widths of 150 nm, demonstrated 19%–40% DE from 1280–1650 nm, with a DCR of $\sim$1 Hz [6]. Furthermore, the WSi SNSPD demonstrated a wide plateau at the maximum DE versus bias current curve. This plateau is very significant as it is indicative of saturated internal quantum efficiency, a requirement for making 100% efficient detectors. Both NbSi and WSi are deposited by room temperature sputtering, which is significantly more forgiving than the high temperature processing typically used for NbN.

Superconducting transition edge sensors (TESs) made from tungsten have demonstrated the highest system DE (SDE), i.e., $\sim$95%, of any single-photon detector [8]. The W-TES is also an outstanding photon-number-resolving detector because of this high efficiency, low DCR, and linear response function. However, the weak link between the electrons and phonons in tungsten also makes the recovery time slow, i.e., $\sim$5 μs (the recovery time is the time it takes for the TES to be able to respond to another single photon). Experimental demonstrations showed devices with the recovery time reduced to $\sim$1 μs by using a normal-metal heat sink to speed up the electron cooling in the TES [9]. It is notable that this speed-up occurs without any degradation in photon-number-resolving capability. The technique has the potential to reduce the recovery time below 50 ns.

Just as researchers in conventional optoelectronics have embraced photonic integrated circuits (PICs) for the benefits of reduced size, ease of packaging, and reduced coupling losses, the nascent field of quantum information has begun investigating quantum PICs (QPICs). Until recently, single-photon detectors were the missing component from QPICs. However, both TESs [10] and SNSPDs [11] have recently been evanescently coupled to waveguides as a stepping-stone toward complete QPICs. NbN SNSPDs have been integrated on GaAs waveguides. These devices show $\sim$20% device efficiency (3.4% SDE, including waveguide coupling loss) at a DCR of $\sim$10 kHz and timing jitter of $\sim$60 ps. These metrics are similar to normal incidence measurements from NbN devices. Photon-number-resolving W-TESs have recently been integrated onto silica waveguides. The SDE of these devices is 7.2%, somewhat lower than the predicted value of 13.2%. This discrepancy may be due to waveguide loss or fiber splice loss. Both of these devices are promising for future implementation of QPICs.

Another significant advance in packaging of superconducting detectors was introduced by Miller *et al.* [12] Differential thermal expansion can cause large dimensional shifts in components when devices are cooled from room temperature to their cryogenic operating temperature. This can lead to misalignment problems, especially when using single-mode optical fiber (mode field diameter of $\sim$9 μm). The new packaging scheme is shown in Fig. 1. The superconducting detector chips are released from the silicon wafer by etching entirely through the substrate. The chips are then placed

on a custom-designed mount and a (commercial off-the-shelf) zirconia alignment sleeve is slid over the detector chip. The single-mode optical fiber and ferrule are then attached to the open end of the zirconia sleeve until the fiber touches the chip. This arrangement enables reproducible assembly with low coupling loss ($< 1\%$) and makes the device robust to thermal cycling.

In addition to advances made in superconducting single-photon detectors, there were new reports of photon-number resolution in semiconductor-based single-photon detectors in 2011. One breakthrough [13] uses a scaled-down silicon-on-insulator (SOI) metal–oxide–semiconductor field-effect transistor (MOSFET) with photoconductive gain. In this device and similar devices in GaAs [14], photogenerated individual holes are trapped below the negatively biased gate and clearly modulate the current flowing in the small silicon nanowire conduction channel with steps as photons are absorbed. The size of the step is proportional to the number of photons absorbed. It remains an interesting challenge to raise the effective area to obtain DE useful for applications.

For Geiger-mode detectors to detect the photon number in a pulse of light, the challenge has actually been to *reduce* the effective gain and provide more highly consistent avalanches. A demonstration by the Toshiba group [15] in Cambridge, U.K., shows the feasibility of obtaining sufficient analog behavior with Geiger-mode operation to exhibit photon-number resolution. Using a conventional silicon SPAD with a self-differencing bias technique that was initially developed to achieve gigahertz-scale photon counting rates by use of InGaAs SPADs [15], [16], they were able to distinguish events with up to four photons absorbed by the detector. Interestingly, the self-difference technique also improved the DE, reduced the DCR, and reduced the afterpulsing rate compared to the conventional biasing technique for this SPAD.

Yet another approach to realizing photon-number resolution with avalanche photodiodes is the attempt to achieve single-photon sensitivity using linear-mode APDs, in which the detectors are operated below their avalanche breakdown voltage (in contrast to SPADs, which are designed for operation above the avalanche breakdown voltage). From the perspective of photon counting, it is interesting to note that advances in SPADs and linear-mode APDs are beginning to blur the distinctions between them. For inherently analog linear-mode APDs, the primary challenge has been to achieve much higher gain while maintaining low noise. The most promising detector materials system for reaching this goal is mercury cadmium telluride (HgCdTe), which exhibits very low excess noise (close to 1) when grown with an appropriate stoichiometry. Two groups recently reported [17], [18] HgCdTe detector performance with gains of 100 to 500 providing single-photon sensitivity and photon-number resolution. While these detectors are not as sensitive as SPADs operated in Geiger mode—e.g., using a metric such as noise equivalent power, SPADs exhibit two to three orders of magnitude better performance—the inherently analog response of linear-mode HgCeTe APDs makes photon-number resolution possible if the following amplifier circuitry is sufficiently low noise and if their lower operating temperatures can be tolerated. In achieving these results, the difficulty in designing the necessary amplifier circuitry is at least as challenging as that of the APD detector design.

A final example of significant recent progress in SPADs is the drive for scaling to larger formats for single-photon imaging. A Delft University group has reached a format of 160×128 pixels with 50 μm pitch by use of a deep-submicrometer (0.13 μm) CMOS process [19]. Monolithic circuit integration involving 60 million transistors on each chip provided every pixel with the ability to record photon time-of-arrival values for various medical applications employing fluorescence lifetime measurements. The trend toward even larger SPAD imaging array formats will continue as these sensors find further applications in 3-D LIDAR imaging and low-light-level imaging.

Research in single-photon detectors remains an active field with advances in both superconducting and semiconducting devices. For some performance metrics, superconducting devices exceed the performance of their semiconductor-based counterparts. However, more widespread adoption remains a challenge because of difficulties in implementation and/or integration into systems. Some of the improvements in 2011 could address these issues. Analogously, semiconducting devices continue to improve in DE and photon-number resolution, approaching the metrics achieved with superconducting devices.

References

[1] E. A. Dauler, A. J. Kerman, B. S. Robinson, J. K. W. Yang, B. Voronov, G. Goltsman, S. A. Hamilton, and K. K. Berggren, "Photon-number-resolution with sub-30-ps timing using multi-element superconducting nanowire single photon detectors," *J. Modern Opt.*, vol. 56, no. 2/3, pp. 364–373, 2009.

[2] H. Takesue, S. W. Nam, Q. Zhang, R. H. Hadfield, T. Honjo, K. Tamaki, and Y. Yamamoto, "Quantum key distribution over 40 dB channel loss using superconducting single-photon detectors," *Nat. Photon.*, vol. 1, no. 6, p. 343, Jun. 2007.

[3] R. E. Warburton, A. McCarthy, A. M. Wallace, S. Hernandez-Marin, R. H. Hadfield, S. W. Nam, and G. S. Buller, "Subcentimeter depth resolution using a single-photon counting time-of-flight laser ranging system at 1550 nm wavelength," *Opt. Lett.*, vol. 32, no. 15, pp. 2266–2268, Aug. 2007.

[4] Y. Korneeva, I. Florya, A. Semenov, A. Korneev, and G. Goltsman, "New generation of nanowire NbN superconducting single-photon detector for mid-infrared," *IEEE Trans. Appl. Supercond.*, vol. 21, no. 3, pp. 323–326, Jun. 2011.

[5] F. Marsili, F. Najafi, E. Dauler, F. Bellei, X. Hu, M. Csete, R. J. Molnar, and K. K. Berggren, "Single-photon detectors based on ultranarrow superconducting nanowires," *Nano Lett.*, vol. 11, no. 5, pp. 2048–2053, May 2011.

[6] B. Baek, A. E. Lita, V. Verma, and S. W. Nam, "Superconducting a-W_xSi_{1-x} nanowire single-photon detector with saturated internal quantum efficiency from visible to 1850 nm," *Appl. Phys. Lett.*, vol. 98, no. 25, p. 251 105, Jun. 2011.

[7] S. N. Dorenbos, P. Forn-Diaz, T. Fuse, A. H. Verbruggen, T. Zijlstra, T. M. Klapwijk, and V. Zwiller, "Low gap superconducting single photon detectors for infrared sensitivity," *Appl. Phys. Lett.*, vol. 98, no. 25, p. 251102, Jun. 2011.

[8] A. E. Lita, A. J. Miller, and S. W. Nam, "Counting near-infrared single-photons with 95% efficiency," *Opt. Exp.*, vol. 16, no. 5, pp. 3032–3040, Mar. 2008.

[9] B. Calkins, A. E. Lita, A. E. Fox, and S. W. Nam, "Faster recovery time of a hot-electron transition-edge sensor by use of normal metal heat-sinks," *Appl. Phys. Lett.*, vol. 99, no. 24, p. 241114, Dec. 2011.

[10] T. Gerrits, N. Thomas-Peter, J. C. Gates, A. E. Lita, B. J. Metcalf, B. Calkins, N. A. Tomlin, A. E. Fox, A. Lamas Linares, J. B. Spring, N. K. Langford, R. P. Mirin, P. G. R. Smith, I. A. Walmsley, and S. W. Nam, "On-chip, photon-number-resolving, telecommunication-band detectors for scalable photonic information processing," *Phys. Rev. A*, vol. 84, no. 6, p. 060301(R), 2011.

[11] J. P. Sprengers, A. Gaggero, D. Sahin, S. Jahanmirinejad, G. Frucci, F. Mattioli, R. Leoni, J. Beetz, M. Lermer, M. Kamp, S. Höfling, R. Sanjines, and A. Fiore, "Waveguide superconducting single-photon detectors for integrated quantum photonic circuits," *Appl. Phys. Lett.*, vol. 99, no. 18, p. 181110, Oct. 2011.

[12] A. J. Miller, A. E. Lita, B. Calkins, I. Vayshenker, S. M. Gruber, and S. W. Nam, "Compact cryogenic self-aligning fiber-to-detector coupling with losses below one percent," *Opt. Exp.*, vol. 19, no. 10, pp. 9102–9110, May 2011.

[13] W. Du, H. Inokawa, H. Satoh, and A. Ono, "SOI metal–oxide–semiconductor field-effect transistor photon detector based on single-hole counting," *Opt. Lett.*, vol. 36, no. 15, pp. 2800–2803, Aug. 2011.

[14] E. J. Gansen, M. A. Rowe, M. B. Greene, D. Rosenberg, T. E. Harvey, M. Y. Su, R. H. Hadfield, S. W. Nam, and R. P. Mirin, "Photon-number-discriminating detection using a quantum-dot, optically gated, field-effect transistor," *Nat. Photon.*, vol. 1, no. 10, pp. 585–588, Oct. 2007.

[15] O. Thomas, Z. L. Yuan, J. F. Dynes, and A. J. Shields, "Efficient photon number detection with silicon avalanche photodiodes," *Appl. Phys. Lett.*, vol. 97, no. 3, p. 031102, Jul. 2010.

[16] B. E. Kardynal, Z. L. Yuan, and A. J. Shields, "An avalanche-photodiode-based photon-number-resolving detector," *Nat. Photon.*, vol. 2, no. 7, pp. 425–428, 2008.

[17] M. Jack, J. Wehner, J. Edwards, G. Chapman, D. N. B. Hall, and S. M. Jacobson, "HgCdTe APD-based linear-mode photon counting components and LADAR receivers," in *Proc. SPIE Adv. Photon Counting Techn. V*, vol. 8033, M. A. Itzler and J. C. Campbell, Eds., 2011, p. 80330M.

[18] J. D. Beck, R. Scritchfield, P. Mitra, W. Sullivan, III, A. D. Gleckler, R. Strittmatter, and R. J. Martin, "Linear mode photon counting with the noiseless gain HgCdTe e-APD," in *Proc. SPIE Adv. Photon Counting Techn. V*, vol. 8033, M.A. Itzler and J.C. Campbell, Eds., 2011, p. 80330N.

[19] C. Veerappan, J. Richardson, R. Walker, D. U. Li, M. W. Fishburn, Y. Maruyama, D. Stoppa, F. Borghetti, M. Gersbach, R. K. Henderson, and E. Charbon, "A 160 $\times$ 28 single-photon image sensor with on-pixel 55 ps 10b time-to-digital converter," in *Proc. IEEE ISSCC*, 2011, pp. 312–314.

Toward On-Chip Phase-Sensitive Optical Temporal Waveform Measurements

Alessia Pasquazi,[1] José Azaña,[1] Marco Peccianti,[1,2] David J. Moss,[3] and Roberto Morandotti[1]

(Invited Paper)

[1]Ultrafast Optical Processing Group, Institut National de la Recherche Scientifique-Énergie, Matériaux et Télécommunications (INRS-EMT), Montreal, QC J3X 1S2, Canada
[2]Institute for Complex Systems—CNR, 00185 Rome, Italy
[3]CUDOS and the Institute of Photonics and Optical Science, School of Physics, University of Sydney, Sydney, NSW 2006, Australia

DOI: 10.1109/JPHOT.2012.2189759

Manuscript received February 13, 2012; accepted February 24, 2012. Date of current version April 20, 2012. Corresponding author: A. Pasquazi and R. Morandotti (e-mail: alessia.pasquazi@gmail.com; roberto.morandotti@emt.inrs.ca).

Abstract: This review summarizes the results obtained in 2011 toward the development of an "integrated optical oscilloscope," encompassing research on new technologies for the measurement of ultrafast optical pulses in both amplitude and phase through the use of integrated devices, some of which are compatible with electronic circuit technology (CMOS).

Index Terms: Coherent detection, nonlinear optics, optical waveguides, ultrafast pulse measurement.

1. Introduction

Although electronics is approaching its inherent speed limits, the increasing demand for higher bandwidths is unrelenting. In the framework of signal transport, photonics has already demonstrated its superior performances, and now, optical interconnections are spread worldwide. Photonics is called now to the big challenge to complement, and in several cases replace, electronics. For this reason, the electronic-photonic scientific community works toward the development of all-optical approaches that can lead to the integration of various, fundamental optical functionalities on electronic compatible platforms, possibly complementary metal-oxide semiconductor (CMOS) compatible, pushing electronic systems toward photonics data speeds (Terahertz range and beyond) [1]–[10]. However, the success of this approach strongly depends on the availability of efficient methods to monitor "on chip" the optical data stream. To avoid the electronic bottleneck, the information flow has to be characterized ideally in an "all-optical" way, shrinking the actual device size to fit in the electronic-friendly microscopic world. With "all optical methods" we refer to all the approaches that optically manipulate the signal in order to employ a final slow optoelectronic detection for the measurement of the ultrafast pulse.

Optical telecommunications have firmly moved to coherent modulation formats, where the information is directly encoded in the phase of the optical signal, as well as in its amplitude. Therefore, it is becoming increasingly important to be able to measure the entire complex profile (amplitude and phase) of an optical waveform. This requires phase-sensitive measurement techniques operating at milliwatt peak power levels and on time scales down to the subpicosecond regime—well beyond what is achievable via direct optoelectronic detection. With the relentless

increase in optical channel bit rates and the corresponding shortening in time of the optical pulses, standard amplitude characterization methods such as those performed using, for example, fast photodiodes, are becoming insufficient to adequately characterize the waveforms of interest; moreover, phase-sensitive measurements are needed in order to monitor optical phase-dependent phenomena, such as dispersion and nonlinear field-fiber interactions.

At the other end of the scale, photonics will undoubtedly play a fundamental role in the design of the next generation of computer processors, which very likely will implement optical methods to transport the signal to different parts of the chip. What is indeed clear to the electronics industry is that the next generation of miniaturization (the so-called *exascale* integration level [9], [10]) will in principle require an extreme density of copper-based interconnections, significantly increasing the chip power dissipation to unbearable levels. Hence, current approaches toward interconnects will need to undergo radical changes. Optics can offer high speed and low transfer energy per bit. The shift toward optical interconnects will also invariably involve increasingly significant degrees of signal processing at the optical level. Clearly, under this scenario, the ability to monitor optical signals directly on chip—particularly with phase sensitivity—will be fundamental to the success of this approach.

2. Major Achievements in 2011

A general trend in photonics in the last few years is toward developing techniques to measure or process optical pulses with increasingly more complicated amplitude and phase temporal variations, i.e., waveforms characterized by a high time-bandwidth product, often with large spectral bandwidth pulses exceeding several Terahertz, and extending over ultralong temporal durations, even beyond the nanosecond range [11]. Clever strategies have been adopted to extend the performance of coherent detection by using fast photodiodes. Fontaine *et al.* demonstrated, in 2010, the possibility of covering time durations of the order of 1 μs for signals with bandwidths as high as 160 GHz [12]. The technique they propose exploits the design principle of a novel strategy for dynamic optical arbitrary waveform generation to implement the so-called time-interleaving detection [13]–[15]. The demonstration in 2011 of a static arbitrary waveform generator integrated in InP represents an important step forward toward the full integration of this approach [15].

In a broad perspective, it is indeed natural to forecast that optical signal processing will have to be increasingly done in the optical domain to avoid the "electronic bottleneck," and therefore, all-optical approaches for pulse characterization will be undoubtedly of fundamental importance. In the last two decades, significant advances have been achieved for the characterization of ultrafast, high repetition rate optical waveforms either in a repetitive fashion or in a single shot. All of these approaches will need to meet a series of stringent sensitivity and time-bandwidth requirements, and all will invariably benefit significantly from the use of integrated approaches.

Following the comprehensive review of Wamsley and Dorrer [16], the approaches currently available for optical pulse characterization can be generally grouped into three main classes: i) *spectrographic methods*, based on the simultaneous characterization of the temporal and spectral properties of the pulse; ii) *tomographic methods,* based on the idea of temporal imaging, e.g., systems that exploit the concept of time lens and related strategies; iii) *interferometric methods* based on the encoding of the phase information of the pulse under test in a temporal or spectral interference pattern. All these strategies possess proven and effective all-optical implementations to achieve the widest photonic processing bandwidths. Frequency Resolved Optical Gating (FROG) [17], time lens based on nonlinear parametric conversion [18], and Spectral Phase Interferometry for Direct Field Reconstruction (SPIDER) [19] are prominent representatives of these three classes, and all are based on all-optical approaches that were initially demonstrated in bulk.

FROG techniques were the first to benefit from integrated waveguide implementations in order to enhance their sensitivity through the use of both quadratic and cubic nonlinearities [20], [21]. Silicon photonics has enabled very compact devices based on cross phase modulation in nanophotonic waveguides [21]. However, while implementations using bulk optics have achieved single-shot operation, approaches based on integrated geometries require multiple measurements with different pulse delays, usually controlled via a variable free-space delay line. On-chip variable

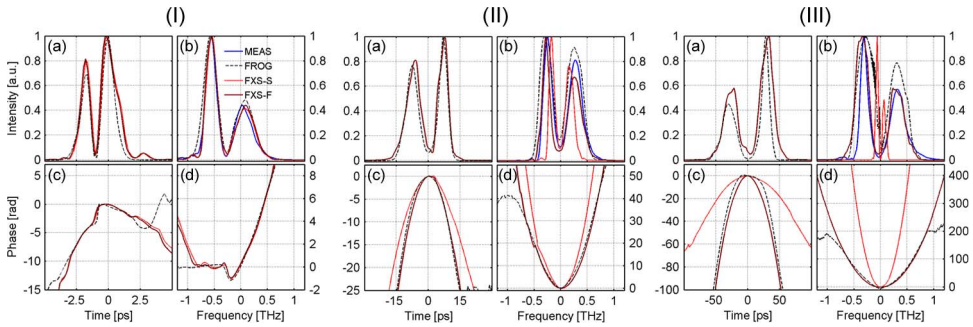

Fig. 1. Measurement of optical pulses performed with the DFWM-X-SPIDER device, for a complex waveform of ∼1 THz bandwidth: retrieved waveform and comparison with the experimentally measured FROG SHG traces. Panels (I), (II), and (III) display pulses with a time-bandwidth product 5, 30, and 100, respectively. For each panel, the amplitude (a), (b) and the phase (c), (d) are reconstructed in the temporal and spectral domains, respectively. The red and brown lines depict the results obtained through the application of the standard (FXS-S) and FLEA (FXS-F) phase-reconstruction algorithms on the measured spectral interferogram, respectively. The dashed curves are the profiles extracted from the SHG-FROG measurement. In (b), the directly measured spectrum is also shown (blue line).

delays are still unachievable with the specifications required for FROG measurements, and to date, the complete integration of FROG devices in a CMOS compatible platform has not been reported.

In 2008, Foster *et al.* presented a time lens in an integrated silicon waveguide [23], leading to the first demonstration of a silicon-based optical temporal oscilloscope. The measurement system was however insensitive to the optical phase. The demonstration of a phase-sensitive method based on a time lens in a nonlinear waveguide came from the same group in 2011 [24]. In [24] Londero *et al.* demonstrated a version of optical differential tomography in a nonlinear optical fiber, characterizing a pulse with 4 nm of bandwidth dispersed using up to 30 m of standard single mode fiber. Although this demonstration was not in an integrated platform, the technique itself is amenable for integration.

An increasingly popular group of methods for optical signal characterization is based on linear optical filtering for phase-to-intensity conversion (see [25] for a comprehensive review of these methods). These methods are purely self-referenced and they avoid the need to create an interference pattern. Li *et al.* [26] have employed an all-fiber ultrafast photonic temporal differentiator as the linear optical filter, i.e., the so-called phase reconstruction using "optical ultrafast differentiation" (PROUD) technique, demonstrating the characterization of optical pulses with durations ranging from the picosecond to the nanosecond regime. In 2009, this same group demonstrated single-shot and real-time measurements of microwatt-level continuous Gigahertz-rate data streams using an all-fiber PROUD setup [27]. The demonstration of integrated photonic temporal differentiators in CMOS compatible waveguides in 2011 by Rutkowska *et al.* [28] is promising for the full integration of this technique.

Sheared interferometry is one of the most adopted approaches for optical pulse characterization [19], especially in its all-optical implementation that has been coined SPIDER. We recently [29] revisited the so-called X-SPIDER approach (that requires a reference pump) in order to perform the measurement using degenerate four wave mixing (DFWM) [30]. SPIDER approaches have traditionally been based on difference-frequency generation (DFG)–a second-order nonlinearity. The generalization of X-SPIDER to DFWM processes allows its implementation in centrosymmetric materials supporting third-order parametric processes [29], [30], which is clearly critical if one aims to realize these devices in CMOS compatible integrated platforms. The characterization of ∼1 THz bandwidth pulses stretched up to ∼100 ps (see Fig. 1) was achieved in a nonlinear integrated glass waveguide, with the aid of a novel reconstruction algorithm that we term *Fresnel Limited Extraction Algorithm* (FLEA). This work demonstrates the feasibility of a fully integrated CMOS two-port device that only requires the pulse under test and an incoherent reference as inputs for on-chip amplitude and phase ultrafast optical waveform characterization.

3. Conclusion

Research on fully integrated techniques for the coherent measurement of ultrafast optical signals and pulses has continued to increase significantly. The results achieved in 2011 on the integration of all-optical methods in electronic compatible platforms seem promising for the development of an "integrated complex optical oscilloscope," meeting the stringent requirements demanded by coherent optical communications and related applications.

References

[1] J. Geuthold, C. Koos, and W. Freude, "Nonlinear silicon photonics," *Nature Photon.*, vol. 4, no. 8, pp. 535–544, Aug. 2010.

[2] J. Kakande, R. Slavík, F. Parmigiani, A. Bogris, D. Syvridis, L. Grüner-Nielsen, R. Phelan, P. Petropoulos, and D. J. Richardson, "Multilevel quantization of optical phase in a novel coherent parametric mixer architecture," *Nature Photon.*, vol. 5, no. 12, pp. 748–752, Dec. 2011.

[3] F. Morichetti, A. Canciamilla, C. Ferrari, A. Samarelli, M. Sorel, and A. Melloni, "Travelling-wave resonant four-wave mixing breaks the limits of cavity-enhanced all-optical wavelength conversion," *Nature Commun.*, vol. 2, p. 296, May 2011.

[4] D. T. H. Tan, P. C. Sun, and Y. Fainman, "Monolithic nonlinear pulse compressor on a silicon chip," *Nature Commun.*, vol. 1, no. 8, p. 116, Nov. 2010.

[5] A. Pasquazi, R. Ahmad, M. Rochette, M. Lamont, R. Morandotti, B. E. Little, S. T. Chu, and D. J. Moss, "All-optical wavelength conversion in an integrated ring resonator," *Opt. Exp.*, vol. 18, no. 4, pp. 3858–3863, Feb. 2010.

[6] R. Slavik, F. Parmigiani, J. Kakande, C. Lundström, M. Sjödin, P. A. Andrekson, A. D. Ellis, L. Grüner-Nielsen, D. Jakobsen, S. Herstrm, J. O'Gorman, A. Bogris, D. Syvridis, S. Dasgupta, P. Petropoulos, and D. J. Richardson, "All-optical phase and amplitude regenerator for next-generation telecommunications systems," *Nature Photon.*, vol. 4, pp. 690–695, Oct. 2010.

[7] R.-J. Essiambre, G. Kramer, P. J. Winzer, G. J. Foschini, and B. Goebel, "Capacity limits of optical fiber networks," *J. Lightwave Technol.*, vol. 28, no. 4, pp. 662–701, Feb. 2010.

[8] M. Peccianti *et al.,* "Demonstration of a stable ultrafast laser based on a nonlinear microcavity," *Nat. Commun.*, in press, DOI: 10.1038/ncomms1762 (2012).

[9] "The future of optical communication," in *Proc. Nature Photon. Workshop*, Tokyo, Japan, Oct. 2007.

[10] "OMA exascale computing: Where optics meets electronics," in *Proc. OFC/NOFC Workshop*, Los Angeles, CA, Mar. 2011.

[11] J. Cohen, P. Bowlan, V. Chauhan, P. Vaughan, and R. Trebino, "Single-shot multiple-delay crossed-beam spectral interferometry for measuring extremely complex pulses," *Opt. Commun.*, vol. 284, no. 15, pp. 3785–3794, Jul. 2011.

[12] N. K. Fontaine, R. Scott, L. Zhou, F. M. Soares, J. Heritage, and S. Yoo, "Real-time full-field arbitrary optical waveform measurement," *Nature Photon.*, vol. 4, no. 4, pp. 248–254, Apr. 2010.

[13] Z. Jiang, C.-B. Huang, D. E. Leaird, and A. Weiner, "Optical arbitrary waveform processing of more than 100 spectral comb lines," *Nature Photon.*, vol. 1, no. 8, pp. 463–467, Aug. 2007.

[14] S. T. Cundiff and A. M. Weiner, "Optical arbitrary waveform generation," *Nature Photon.*, vol. 4, no. 11, pp. 760–766, Nov. 2010.

[15] N. K. Fontaine, R. P. Scott, and S. J. B. Yoo, "Dynamic optical arbitrary waveform generation and detection in InP photonic integrated circuits for Tb/s optical communications," *Opt. Commun.*, vol. 284, no. 15, pp. 3693–3705, Jul. 2011.

[16] I. A. Walmsley and C. Dorrer, "Characterization of ultrashort electromagnetic pulses," *Adv. Opt. Photon.*, vol. 1, no. 2, pp. 308–437, Apr. 2009.

[17] R. Trebino, *Frequency Resolved Optical Gating: The Measurement of Ultrashort Optical Pulses*. Norwell, MA: Kluwer, 2002.

[18] C. V. Bennett, R. Scott, and B. H. Kolner, "Temporal magnification and reversal of 100 Gb/s optical-data with an up-conversion time microscope," *Appl. Phys. Lett.*, vol. 65, no. 20, pp. 2513–2515, Nov. 1994.

[19] C. Iaconis and I. A. Walmsley, "Spectral phase interferometry for direct electric-field reconstruction of ultrashort optical pulses," *Opt. Lett.*, vol. 23, no. 10, pp. 792–794, May 1998.

[20] S. Yang, A. M. Weiner, K. R. Parameswaran, and M. M. Fejer, "Ultrasensitive second-harmonic generation frequency-resolved optical gating by aperiodically poled LiNbO3 waveguides at 1.5 μm," *Opt. Lett.*, vol. 30, no. 16, pp. 2164–2166, Aug. 2005.

[21] P.-A. Lacourt, J. M. Dudley, J.-M. Merolla, H. Porte, J.-P. Goedgebuer, and W. T. Rhodes, "Milliwatt-peak-power pulse characterization at 1.55 micron by wavelength-conversion frequency-resolved optical gating," *Opt. Lett.*, vol. 27, no. 10, pp. 863–865, May 2002.

[22] E.-K. Tien, X.-Z. Sang, F. Qing, Q. Song, and O. Boyraz, "Ultrafast pulse characterization using cross phase modulation in silicon," *Appl. Phys. Lett.*, vol. 95, no. 5, pp. 051101-1–051101-3, Aug. 2009.

[23] M. A. Foster, R. Salem, D. F. Geraghty, A. C. Turner-Foster, M. Lipson, and A. L. Gaeta, "Silicon-chip-based ultrafast optical oscilloscope," *Nature*, vol. 456, no. 7218, pp. 81–84, Nov. 2008.

[24] P. Londero, O. Kuzucu, and A. L. Gaeta, "Spectral amplitude and phase measurement of ultrafast pulses using all-optical differential tomography," *Opt. Lett.*, vol. 36, no. 9, pp. 1686–1688, May 2011.

[25] J. Azaña, Y. Park, and F. Li, "Linear self-referenced complex-field characterization of fast optical signals using photonic differentiation," *Opt. Commun.*, vol. 284, no. 15, pp. 3772–3784, Jul. 2011.

[26] F. Li, Y. Park, and J. Azaña, "Linear characterization of optical pulses with durations ranging from the picosecond to the nanosecond regime using ultrafast photonic differentiation," *IEEE J. Lightwave Technol.*, vol. 27, no. 21, pp. 4623–4633, Nov. 2009.
[27] F. Li, Y. Park, and J. Azaña, "Single-shot, real-time frequency chirp characterization of telecommunication optical signals based on balanced temporal optical differentiation," *Opt. Lett.*, vol. 34, no. 18, pp. 2742–2744, Sep. 2009.
[28] K. A. Rutkowska, D. Duchesne, M. J. Strain, R. Morandotti, M. Sorel, and J. Azaña, "Ultrafast all-optical temporal differentiators based on CMOS-compatible integrated-waveguide Bragg gratings," *Opt. Exp.*, vol. 19, no. 20, pp. 19 514–19 522, Sep. 2011.
[29] A. Pasquazi, M. Peccianti, Y. Park, B. E. Little, S. T. Chu, R. Morandotti, J. Azaña, and D. J. Moss, "Sub-picosecond phase-sensitive optical pulse characterization on a chip," *Nature Photon.*, vol. 5, no. 10, pp. 618–623, Oct. 2011.
[30] A. Pasquazi, Y. Park, J. Azaña, F. Légaré, R. Morandotti, B. E. Little, S. T. Chu, and D. J. Moss, "Efficient wavelength conversion and net parametric gain via four wave mixing in a high index doped silica waveguide," *Opt. Exp.*, vol. 18, no. 8, pp. 7634–7641, Apr. 2010.

Integrated Optical Sensors

Vivek Singh,[1] Juejun Hu,[2] Anuradha M. Agarwal,[1] and Lionel C. Kimerling[1]

(Invited Paper)

[1]Microphotonics Center, Massachusetts Institute of Technology, Cambridge, MA 02139, USA
[2]Department of Materials Science and Engineering, University of Delaware, Newark, DE 19716, USA

DOI: 10.1109/JPHOT.2012.2192721
1943-0655/$31.00 ©2012 IEEE

Manuscript received February 15, 2012; revised March 6, 2012; accepted March 6, 2012. Date of current version April 20, 2012. Corresponding author: L. C. Kimerling (e-mail: lckim@mit.edu).

Abstract: We review important progress made in the field of integrated optical sensors in 2011. This paper focuses on key aspects of integrated sensors, including new detection mechanism developments, integration progress, and efforts toward resolving the challenges associated with surface functionalization and analyte transport.

Index Terms: Sensors, resonators, surface plasmon resonance (SPR), fluorescence, infrared spectroscopy, photonic integration.

1. Introduction

We report on the progress made in 2011 on advancing the broad field of integrated optical sensing systems. We review integrated optical sensors for detection of chemical and biological species, including a) biological macromolecules (proteins, nucleic acids, other macromolecules); b) small molecules (chemicals); and c) nanoparticles and virus particles. This paper will focus on progress in the areas of new detection mechanisms and integration schemes as well as key developments that address outstanding challenges relating to sensor surface functionalization and analyte transport. Fiber-optic sensors and sensors monitoring other physical parameters are outside the scope of this review.

2. New Detection Mechanisms

The major sensing mechanisms utilized in integrated optical sensors can be categorized under a) refractive index (RI) sensing; b) absorption sensing; and c) fluorescence sensing. Of these, the most common mechanism is RI sensing.

Index sensing typically involves detection of wavelength shift due to molecular binding which results in a change in RI. Two common types of RI sensors are surface plasmon resonance (SPR) sensors and dielectric optical resonator sensors. SPR sensors feature much higher RI sensitivity compared to resonator sensors. Yu *et al.* report that SPR sensors achieve extraordinary spectral sensitivity due to multiple optical modes involved in the detection process [1]. Unlike optical resonance peaks, these dips in transmission indicate the phase matching wavelength where the SPR mode and the excitation light beam have identical in-plane wave vectors. Index perturbation changes this phase matching condition and leads to large SPR wavelength shift. Based on this theoretical insight, the authors further show that similar extraordinary RI sensitivity can be attained in an all-dielectric system as well, with the added benefits of reduced loss and higher quality factors.

Improved cavity designs such as notched microrings [2], ultra-high-Q microtoroids [3], and active microcavities [4] have been employed to boost the detection sensitivity of optical resonator index

sensors. Novel photonic–plasmonic hybrid structures combining photonic resonance enhancement and plasmonic field concentration have also been demonstrated to significantly improve the detection sensitivity [5], [6]. Multiple ring resonators can be utilized to either leverage the Vernier effect to enable interrogation using broadband sources [7], or to improve multiplexing capabilities [8]. However, fabrication of multiple ring resonators, particularly coupled rings, can be challenging. Zhu *et al.* pioneer a new optothermal wavelength sweeping technique to improve the wavelength stability of resonator index sensors [9].

While index sensing relies exclusively on surface coatings for specific molecular recognition, absorption sensing offers inherent molecular discrimination capability by simultaneous detection of a multitude of characteristic infrared absorption lines, and is well suited for gas sensing given the sharp spectral features of gas molecules. Conventional absorption sensing resorts to benchtop instruments such as Fourier Transform InfraRed (FTIR) spectrometers. An ultra-compact chipscale spectrometer was demonstrated by Chao *et al.* which utilizes electro-optic liquid crystals to perform FTIR spectroscopy [10]. One standing challenge for on-chip absorption sensing is the limited optical path length accessible in a chipscale device; to resolve this challenge, microring resonators [11] and nanoslotted slow light photonic crystal slab waveguides [12] were employed to increase the effective path length without compromising the device footprint. Along this line, Hu *et al.* propose a photothermal detection technique where thermal confinement and double optical resonances at both pump and probe wavelengths dramatically improve the gas detection limit of on-chip devices to the sub-ppb level [13].

3. Integration

Integration of a light source and detector onto the same chip platform with the sensing element to complete the standalone "sensor-on-a-chip" platform has been a field of intensive investigation. Index sensors for protein detection usually operate in a disposable mode given the irreversible binding characteristics and short lifetime of antibody-based surface functionalization coatings, and therefore it is not practical to integrate expensive light sources and detectors with these devices.

Integration schemes involving organic components have attracted considerable interest due to their low cost and the progress made in the areas of organic light emitting diodes (OLEDs) and organic photodetectors (OPDs). One such integrated sensor platform utilizing ring-shaped OPDs is able to realize gas sensing via three different methods (fluorescence, absorption, SPR) on the same platform [14]. Vannahme *et al.* propose an integrated plastic "lab-on-a-chip" sensor relying on excitation of fluorescent markers [15]. The system employs an organic semiconductor laser, deep ultraviolet induced waveguides, and a nanostructured microfluidic channel integrated into a poly(methyl methacrylate) (PMMA) substrate and demonstrates successful detection of carboxylate-modified fluorescent microspheres and fluorescent dye-labeled antibodies. Optical biosensors comprised of a polymer-based light emitting diode (LED) acting as a light source coupled into a single mode Ta_2O_5 waveguide and a polymer photodiode array as a minispectrometer have also been demonstrated [16].

Simple, low-cost flow-through chemical sensors utilizing a chemoreceptive film as the sensing element and two LEDs—one as a light source, one as a detector—in a paired-emitter-detector-diode (PEDD) can be used for easy measurements with an ordinary voltmeter [17]. Alternatively, visible wavelength Vertical Cavity Surface-Emitting Lasers (VCSELs) have been integrated with low dark current GaAs PIN photodiodes for parallel fluorescence and RI sensing [18]. Fluorescence sensing is accomplished by a fluorescence emission filter sensitive to visible-near-IR fluorescent proteins and a nanoimprinted 2-D photonic crystal allows for RI sensing, both on the same platform.

Due to the wide use of plasmonic designs in planar sensing systems, significant efforts have been made to integrate them with appropriate sources and detectors. Designs incorporating plasmonic sensors have been integrated with MOS photodetectors on a silicon platform [19] and the plasmon resonance has also been grating-coupled with a planar photodiode [20].

Chalcogenide glasses are being widely investigated for infrared (IR) photonics applications due to their superior IR transparency [21] and work is being done on integration of lead telluride (PbTe)-based detectors with mid-IR transparent chalcogenide microdisk resonator sensors [22].

Silicon-on-insulator (SOI) microring resonator-based vapor sensors have been integrated with a 200 GHz arrayed waveguide grating (AWG) spectrometer [23] that monitors ethanol vapor concentrations by measuring intensity ratios between adjacent AWG channels.

Integrated sensors have also been demonstrated for gene expression studies with quantum dots serving as fluorescence labels on an active CMOS microarray with a sensitivity of 100 pM [24]. This approach is expected to yield even higher sensitivities with improved surface modification of the CMOS microarrays.

4. Surface Functionalization

Surface functionalization of sensors involves the application of chemical or biological agents to the surface to introduce specificity allowing only the intended target species to bind to the sensor surface. Due to the small size of planar optical sensors and the use of multiplexed arrays of resonators, this low-cost, high-throughput surface functionalization often proves to be a challenging task. Kirk *et al.* propose a functionalization process that utilizes noncontact inkjet (piezoelectric) printing to directly print the functionalizing agents on to multiplexed arrays of silicon ring resonators [25]. This method enables a high degree of scalability and parallel detection of multiple species on the same sensing platform.

If sensors are to be reused rather than discarded after one use, it is essential to have a means for the removal of attached species from sensors without damaging the surface. In an attempt to recycle sensor devices, oxygen plasma treatments have been applied to refresh the surface of silica resonator biosensors after binding events [26].

5. Analyte Transport

Analyte transport involves the movement of analyte species under investigation to the optical sensing element. While microfluidic channels are in wide use, analyte transport remains a key challenge in the realization of low concentration detection of target species. Guo *et al.* demonstrate that flow-through micro/nanofluidic channels can be placed between two reflectors to form a simple and low-cost but robust Fabry–Pérot cavity-based 3-D sensing device [27].

De Angelis *et al.* tackle analyte transport by exploiting the phenomenon of superhydrophobicity where a drop placed on a surface adopts a quasi-spherical shape with a large contact angle $(> 150^{\circ})$ instead of spreading or wetting the contact surface [28]. Evaporation of the drop can increase the concentration of the target species while maintaining the quasi-spherical shape until the drop collapses on top of the sensing surface. This approach is used in conjunction with nanoplasmonic sensors to localize and detect molecules of the target species in highly diluted solutions.

High-quality factor microring resonators have also been explored as a means to trap nanoparticles and perform sensing operations simultaneously [29]. By employing multiple ring resonators, it is possible to transport the trapped particles from one ring to another and perform velocity and particle counting measurements [30]. Analyte localization opens up the possibility of all-optical control of small particles and biological species (cells and virus particles) on an integrated platform.

6. Summary

This review summarizes new developments in detection mechanisms, integration schemes, surface functionalization methods, and analyte transport for integrated optical sensors. We envision monolithically integrated sensor systems that will be field-deployable and perform label-free, multimodal detection with high sensitivity and specificity.

References

[1] Z. Yu and S. Fan, "Extraordinarily high spectral sensitivity in refractive index sensors using multiple optical modes," *Opt. Exp.*, vol. 19, no. 11, pp. 10029–10040, May 2011.

[2] S. Wang and Y. Yi, "Single nanoparticle detection using on-chip notched ring resonator," *Proc. MRS*, vol. 1316, Mar. 2011.

[3] T. Lu, H. Lee, T. Chen, S. Herchak, J.-H. Kim, S. E. Fraser, R. C. Flagan, and K. Vahala, "High sensitivity nanoparticle detection using optical microcavities," *Proc. Nat. Acad. Sci.*, vol. 108, no. 15, pp. 5976–5979, Mar. 2011.
[4] L. He, Ş. K. Özdemir, J. Zhu, W. Kim, and L. Yang, "Detecting single viruses and nanoparticles using whispering gallery microlasers," *Nature Nanotechnol.*, vol. 6, no. 7, pp. 428–432, Jun. 2011.
[5] S. I. Shopova, R. Rajmangal, S. Holler, and S. Arnold, "Plasmonic enhancement of a whispering-gallery-mode biosensor for single nanoparticle detection," *Appl. Phys. Lett.*, vol. 98, no. 24, pp. 243 104-1–243 104-3, Jun. 2011.
[6] M. Chamanzar, E. S. Hosseini, S. Yegnanarayanan, and A. Adibi, "Hybrid plasmonic–photonic resonators for sensing and spectroscopy," in *Proc. CLEO*, Baltimore, MD, 2011, pp. 1–2.
[7] L. Jin, M. Li, and J.-J. He, "Optical waveguide double-ring sensor using intensity interrogation with a low-cost broadband source," *Opt. Lett.*, vol. 36, no. 7, pp. 1128–1130, Apr. 2011.
[8] P. Luetzow, D. Pergande, and H. Heidrich, "Integrated optical sensor platform for multiparameter bio-chemical analysis," *Opt. Exp.*, vol. 19, no. 14, pp. 13 277–13 284, Jul. 2011.
[9] J. Zhu, Ş. K. Özdemir, L. He, and L. Yang, "Optothermal spectroscopy of whispering gallery microresonators," *Appl. Phys. Lett.*, vol. 99, no. 17, pp. 171 101-1–171 101-3, Oct. 2011.
[10] T.-H. Chao, T. T. Lu, S. R. Davis, S. D. Rommel, G. Farca, B. Luey, A. Martin, and M. H. Anderson, "Monolithic liquid crystal waveguide Fourier transform spectrometer for gas species sensing," in *Proc. SPIE—Optical Pattern Recognition XXII*, Orlando, FL, 2011.
[11] A. Nitkowski, A. Baeumner, and M. Lipson, "On-chip spectrophotometry for bioanalysis using microring resonators," *Biomed. Opt. Exp.*, vol. 2, no. 2, pp. 271–277, Feb. 2011.
[12] W.-C. Lai, S. Chakravarty, X. Wang, C.-Y. Lin, and R. T. Chen, "Photonic crystal slot waveguide absorption spectrometer for on-chip near-infrared optical absorption spectroscopy of xylene in water," *Appl. Phys. Lett.*, vol. 98, no. 2, pp. 0233041-1–0233041-3, Jan. 2011.
[13] J. Hu, J. D. Musgraves, N. Carlie, B. Zdyrko, I. Luzinov, A. Agarwal, K. Richardson, and L. Kimerling, "Development of chipscale chalcogenide glass based infrared chemical sensors," in *Proc. SPIE—Quantum Sensing Nanophotonic Devices VIII*, San Francisco, CA, 2011, p. 79 452C.
[14] M. Sagmeister, B. Lamprecht, E. Kraker, A. Haase, G. Jakopic, S. Koestler, H. Ditlbacher, N. Galler, T. Abel, and T. Mayr, "Integrated organic optical sensor arrays based on ring-shaped organic photodiodes," in *Proc. SPIE—Organic Semiconductors Sensors Bioelectronics IV*, San Diego, CA, 2011.
[15] C. Vannahme, S. Klinkhammer, U. Lemmer, and T. Mappes, "Plastic lab-on-a-chip for fluorescence excitation with integrated organic semiconductor lasers," *Opt. Exp.*, vol. 19, no. 9, pp. 8179–8186, Apr. 2011.
[16] M. Ramuz, D. Leuenberger, and L. Buergi, "Optical biosensors based on integrated polymer light source and polymer photodiode," *J. Polym. Sci. B, Polym. Phys.*, vol. 49, no. 1, pp. 80–87, Jan. 2011.
[17] M. Pokrzywnicka, D. J. Cocovi-Solberg, M. Miro, V. Cerda, R. Koncki, and L. Tymecki, "Miniaturized optical chemosensor for flow-based assays," *Anal. Bioanal. Chem.*, vol. 399, no. 3, pp. 1381–1387, Nov. 2011.
[18] M. M. Lee, T. D. O'Sullivan, A. Cerruto, V. Liu, J. Zhang, O. Levi, H. Lee, S. R. J. Brueck, S. Fan, and J. S. Harris, "Integrated photonic structures for parallel fluorescence and refractive index biosensing," in *Proc. SPIE—Photonic Microdevices/Microstructures Sensing III*, Orlando, FL, 2011.
[19] L. Guyot, A. P. Blanchard-Dionne, S. Patskovsky, and M. Meunier, "Integrated silicon-based nanoplasmonic sensor," *Opt. Exp.*, vol. 19, no. 10, pp. 9962–9967, May 2011.
[20] B. Turker, H. Guner, S. Ayas, O. O. Ekiz, H. Acar, M. O. Guler, and A. Dana, "Grating coupler integrated photodiodes for plasmon resonance based sensing," *Lab Chip*, vol. 11, no. 2, pp. 282–287, Jan. 2011.
[21] B. J. Eggleton, B. Luther-Davies, and K. Richardson, "Chalcogenide photonics," *Nature Photon.*, vol. 5, no. 3, pp. 141–148, 2011.
[22] V. Singh, J. Hu, T. Zens, W. , J. Wang, P. T. Lin, J. Wilkinson, S. Novak, J. D. Musgraves, L. Kimerling, K. Richardson, and A. Agarwal, "Novel designs for on-chip mid-infrared detectors integrated with chalcogenide waveguides," in *Proc. Integr. Photon. Res., Silicon Nanophoton.*, Toronto, ON, Canada, 2011.
[23] N. A. Yebo, W. Bogaerts, Z. Hens, and R. Baets, "On-chip arrayed waveguide grating interrogated silicon-on-insulator microring resonator-based gas sensor," *IEEE Photon. Technol. Lett.*, vol. 23, no. 20, pp. 1505–1507, Oct. 2011.
[24] T.-C. D. Huang, S. Paul, P. Gong, R. Levicky, J. Kymissis, S. A. Amundson, and K. L. Shepard, "Gene expression analysis with an integrated CMOS microarray by time-resolved fluorescence detection," *Biosens. Bioelectron.*, vol. 26, no. 5, pp. 2660–2665, Jan. 2011.
[25] J. T. Kirk, G. E. Fridley, J. W. Chamberlain, E. D. Christensen, M. Hochberg, and D. M. Ratner, "Multiplexed inkjet functionalization of silicon photonic biosensors," *Lab Chip*, vol. 11, no. 7, pp. 1372–1377, Feb. 2011.
[26] H. K. Hunt and A. M. Armani, "Recycling microcavity optical biosensors," *Opt. Lett.*, vol. 36, no. 7, pp. 1092–1094, Apr. 2011.
[27] Y. Guo, H. Li, K. Reddy, H. S. Shelar, V. R. Nittoor, and X. Fan, "Optofluidic Fabry–Pérot cavity biosensor with integrated flow-through micro-/nanochannels," *Appl. Phys. Lett.*, vol. 98, no. 4, pp. 041104-1–041104-3, Jan. 2011.
[28] F. De Angelis, F. Gentile, F. Mecarini, G. Das, M. Moretti, P. Candeloro, M. L. Coluccio, G. Cojoc, A. Accardo, C. Liberale, R. P. Zaccaria, G. Perozziello, L. Tirinato, A. Toma, G. Cuda, R. Cingolani, and E. Di Fabrizio, "Breaking the diffusion limit with super-hydrophobic delivery of molecules to plasmonic nanofocusing SERS structures," *Nature Photon.*, vol. 5, no. 11, pp. 682–687, Sep. 2011.
[29] J. Witzens and M. Hochberg, "Optical detection of target molecule induced aggregation of nanoparticles by means of high-Q resonators," *Opt. Exp.*, vol. 19, no. 8, pp. 7034–7061, Apr. 2011.
[30] S. Lin and K. B. Crozier, "Planar silicon microrings as wavelength-multiplexed optical traps for storing and sensing particles," *Lab Chip*, vol. 11, no. 23, pp. 4047–4051, Dec. 2011.

VCSEL Technology for Green Optical Interconnects

A. Kasukawa

(Invited Paper)

Photonic Device Research Center, Yokohama R&D Center,
Furukawa Electric Co., Ltd., Ichihara, Chiba 290-8555, Japan

DOI: 10.1109/JPHOT.2012.2190723
1943-0655/$31.00 ©2012 IEEE

Manuscript received February 7, 2012; revised March 9, 2012; accepted March 9, 2012. Date of current version April 20, 2012. Corresponding author: A. Kasukawa (e-mail: kasukawa@yokoken.furukawa.co.jp).

Abstract: State-of-the-art vertical-cavity surface-emitting laser (VCSEL) technology will be reviewed in terms of power consumption and reliability to realize the energy-efficient high-performance computing (HPC) and data centers. Intermediate wavelength (between short and long wavelength) VCSELs emitting at 1060 nm are promising candidates for the upcoming higher performance computing with energy saving.

Index Terms: Semiconductor lasers, surface emitting lasers.

1. Introduction

Importance of green Information and Communication Technology (ICT) is expanding, especially to high-performance computing (HPC) and data center architecture for power usage effectiveness. The performance of HPC is growing rapidly with an improvement factor of 10 times in every four years, or 1000 times per 10 years, and it is predicted to reach one Exaflops in 2018 [1]. At the same time, energy consumption has to be reduced; therefore, new technologies will be needed to meet the "Next Generation HPC" system requirements. To catch up with increasing demands for higher bandwidth with lower power consumption, optical interconnect using parallel optical link called active optical cable (AOC) has been recognized as a promising solution. Arrayed vertical-cavity surface-emitting lasers (VCSELs) [2] are widely used in this application. 850-nm VCSELs have been used for these applications. On the other hand, intermediate wavelength VCSELs have been intensively investigated to meet the urgent requirements for higher speed, lower consumption, and higher reliability, which will be indispensable in the HPC with 10 Petaflops or more.

VCSELs with InGaAs/GaAs strained-layer quantum wells (SL-QW) with an emission wavelength of 980–1060 nm have been anticipated to exhibit better reliability, higher modulation speed [3], and lower power consumption [5], [6]. Power dissipations for VCSELs, for example, are shown in Fig. 1 as a function of wavelength. Lower power dissipation was achieved for InGaAs VCSELs. An extremely low power dissipation of 81 fJ/bit was reported for an 850-nm VCSEL using InGaAs SL-QW [9]. The transmitter with low power consumption using 1060 nm has also been reported from IBM [10]. In addition to the low power dissipation, thanks to inherent advantages in InGaAs/GaAs system, high modulation of 44 Gbps and high reliability of 30 Fits were reported. In this paper, 980–1060-nm VCSELs with InGaAs SL-QW will be reviewed in terms of power consumption and reliability.

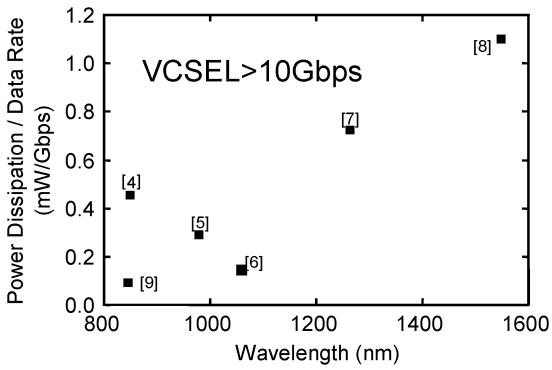

Fig. 1. Power dissipation as a function of wavelength.

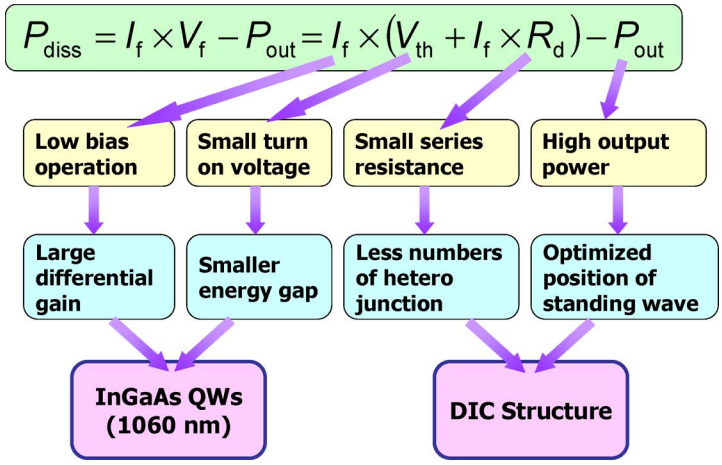

Fig. 2. Approach to achieve low power dissipation.

2. Approach for Lower Power Dissipation

The power dissipation P_{diss} is given by $P_{diss} = I_f \times V_f - P_{out} = I_f \times (V_{th} + I_f \times R_d) - P_{out}$, where I_f is the forward current, V_f is the corresponding voltage, P_{out} is the light output power at I_f, V_{th} is the threshold voltage, and R_d is the series resistance. From the above equation, the approach for power dissipation is summarized in Fig. 2.

Low power dissipation can be mainly attributed to the introduction of InGaAs SL-QW and VCSEL structure called double intracavity (DIC) [11]. High-performance laser characteristics were reported in highly strained InGaAs QW in the wavelength range of 1.1–1.2 μm [12], [13]. Large material gain as well as large differential gain can be expected from InGaAs SL-QW with an emission wavelength of 1060 nm [3], which results in lower threshold current, thus low bias current. Smaller energy gap material (InGaAs SL-QW) for lower threshold voltage, together with a current injection mechanism and low electric resistance, enables us to achieve low forward voltage. Reduced optical loss and, thus, high output power can be realized by employing DIC structure to minimize overlap volume of current path and optical mode. Throughout the careful optimization of the DIC structure, we have achieved both low optical loss and low series resistance. The detailed explanation can be found in [14].

3. VCSELs and Their Characteristics

Fig. 3 shows a schematic drawing of our VCSEL structure. We used a nondoped semiconductor bottom DBR (AlGaAs/GaAs), InGaAs/GaAs SL-QWs, an oxidation layer, and a current spreading

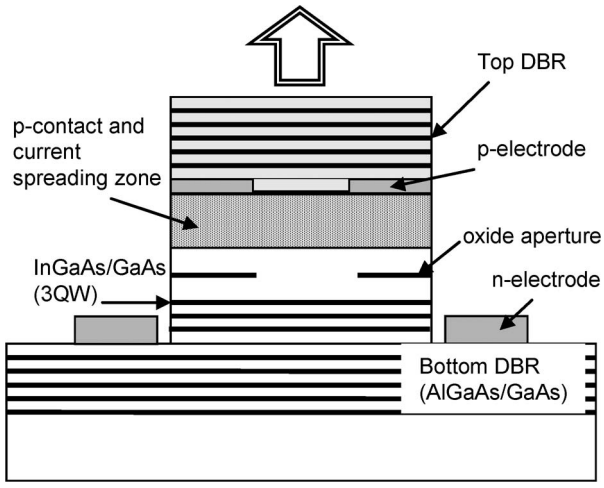

Fig. 3. Schematic drawing of a 1060-nm VCSEL.

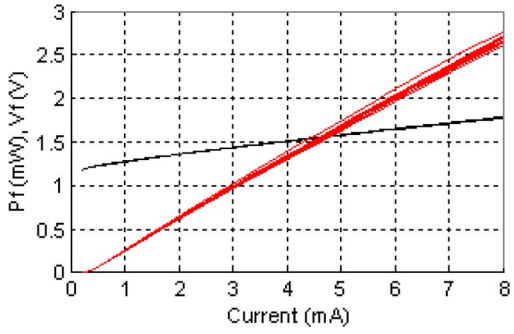

Fig. 4. I–L–V characteristics of 12ch VCSEL array.

layer. Our 1060-nm VCSEL with DIC structure consists of *aluminum-free QW active layer and n*o current flow in the DBR, which lead to both highly reliable operation and low power consumption. We have achieved a recorded power conversion efficiency of 62% among VCSELs [15]. For 10-Gbps arrayed application, we have optimized the reflectivity of top DBR to let threshold current and slope efficiency be balanced, which lead to 0.3 mA of Ith, 0.35 W/A of slope efficiency, together with 50–70 Ω of temperature independent series resistance at 3 mA. An example of *L–I–V* characteristics is shown in Fig. 4 for a 12-channel VCSEL array. A very high uniformity was obtained. It should be noted that *I–V* characteristics of our VCSEL have less temperature dependence due to the fact that no current flows in DBR region.

Reliability issue is one of the great concern in high speed (over 10 Gbps/ch) parallel application. 980-nm InGaAs SL-QW material has been proven to the telecom-grade as high power pump in-plane lasers. A systematic reliability study for the 10-Gbps 1060-nm VCSELs has been performed [12]. Table 1 shows the detail information of the aging time, number of samples, and device hours. The Estimated Failure in term (FIT) number based on the Telcordia GR-468, which used the 0.35 eV of activation energy and no current accelerated factor in calculation, was 30 FIT/ch with a confidence level of 90%. The FIT number related to the wear-out test was estimated as 0.3 FIT/ch for 10 years service time and 1.1 FIT/ch for 20 years.

Generally speaking, 2-dB degradation in the optical power is used for the definition of the lifetime under constant current drive. The definition of the lifetime is applicable for the application for 1–4 Gbps because the resonance frequency for the bias current (several milliamps) is high enough for practical application; however, in the 10-Gbps or higher speed regime, the 3-dB

TABLE 1

Aging test conditions and results

Condition (Ambient temperature)	Quantity (number of chips)	Maximum aging duration (hours)	Device hours @40°C, 6mA	Number of failures
70°C, 6mA	1,075	5,000	8.0×10^6	0
90°C, 6mA	1,121	5,000	1.6×10^7	0
120°C, 6mA	2,702	2,000	5.4×10^7	0
Total	4,898		7.8×10^7	0

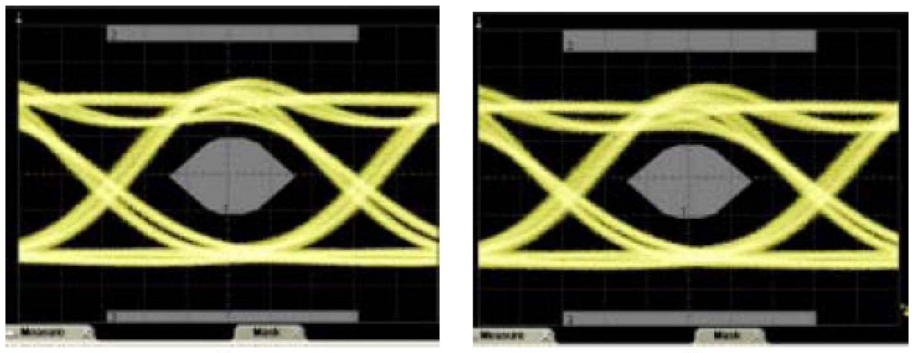

(a) (b)

Fig. 5. Eye diagrams for 10 Gbps before (a) and after (b) aging test under 120 C, 6 mA for 5000 hours.

bandwidth is close to application bandwidth and is influenced by the bias current normalized by the threshold current. If the threshold current is degraded, while the degradation of the output power is less than 2 dB, 10-Gbps operation is not always guaranteed. Therefore, the change in the threshold current as well as output power over aging time are important parameters to determine the lifetime. This would be more severe in array application, in which failure of one VCSEL leads to the failures of the products. We performed eye diagram measurement before and after the aging test at 120 C, 6 mA for 5000 hours. Identical eye patterns both 10 and 20 Gbps were confirmed at same modulation condition [14]. The eye diagrams for 10 Gbps before (a) and after (b) the aging test are shown in Fig. 5 under the identical modulation condition. No degradation in the eye diagram was observed. The threshold current change of the VCSEL during the aging test was less than 5%.

4. Summary

InGaAs 1060-nm "Double-green VCSEL" arrays definitely play an important role in the next-generation power effective HPC and data center to meet indispensable requirements of power consumption, speed, and reliability. Especially, the reliability test results verified using lots of VCSELs encourage us to promote the "new standard" as the signal source for a 100-GbE parallel solution.

Acknowledgment

The author would like to thank K. Takaki, N. Iwai, S. Kamiya, H. Shimizu, T. Nakamura, K. Hiraiwa, S. Imai, Y. Kawakita, M. Funabashi, T. Suzuki, T. Kise, T. Ishikawa, and N. Tsukiji for their contributions.

References

[1] [Online]. Available: http://www.top500.org/

[2] K. Iga, "Surface-emitting laser—Its birth and generation of new optoelectronics field," *IEEE J. Sel. Topics Quantum Electron.*, vol. 6, no. 6, pp. 1201–1215, Nov./Dec. 2000.

[3] L. A. Coldren, Y. Chang, Y. Zheng, and C. Lin, "Efficient sources for chip-to-chip to box-to-box communication within data centers," in *Proc. Photon. Soc. Summer Top. Meeting*, 2010, pp. 205–206, Paper TuD2.1.

[4] P. Westbergh, J. S. Gustavsson, B. Kogel, A. Haglund, A. Larsson, A. Mutig, A. Nadtochiy, D. Bimberg, and A. Joel, "40 GB/s error-free operation of oxide confined 850 nm VCSEL," *Electron. Lett.*, vol. 46, no. 14, pp. 1014–1015, Jul. 2010.

[5] Y.-C. Chang, C. S. Wang, and L. A. Coldren, "High-efficiency, high-speed VCSELs with 35 GB/s error-free operation," *Electron. Lett.*, vol. 43, no. 19, pp. 1022–1023, Sep. 2007.

[6] S. Imai, K. Takaki, S. Kamiya, H. Shimizu, J. Yoshida, Y. Kawakita, T. Takagi, K. Hiraiwa, H. Shimizu, T. Suzuki, N. Iwai, N. Tsukiji, and A. Kasukawa, "Recorded low power dissipation of 0.14 mW/Gbps in 1060 nm VCSELs for 'Green' optical interconnection," *IEEE J. Sel. Topics Quantum Electron.*, vol. 17, no. 6, pp. 1614–1620, Nov./Dec. 2011.

[7] Y. Onishi, N. Saga, K. Koyama, H. Doi, T. Ishizuka, T. Yamada, K. Fujii, H. Mori, J. Hashimoto, M. Shimazu, A. Yamaguchi, and T. Katsuyama, "Long-wavelength GaInNAs vertical-cavity surface-emitting laser with buried tunnel junction," *IEEE J. Sel. Topics Quantum Electron.*, vol. 15, no. 3, pp. 838–843, May/Jun. 2009.

[8] W. Hofmann, M. Muller, A. Nadtochiy, C. Melzer, A. Mutig, G. Bohm, J. Rosskopf, D. Bimberg, M. C. Amann, and C. C. Hasnain, "22-GB/s long wavelength VCSELs," *Opt. Exp.*, vol. 17, no. 20, pp. 17 547–17 554, 2009.

[9] P. Moser, W. Hofmann, P. Wolf, J. A. Lott, G. Larisch, P. Payusov, N. N. Ledentsov, and D. Bimberg, "81 fJ/bit energy-to-data ratio of 850 nm vertical-cavity surface-emitting lasers for optical interconnects," *Appl. Phys. Lett.*, vol. 98, no. 23, pp. 231106-1–231106-3, 2011.

[10] J. B. Heroux, M. Tokunari, K. Takaki, and S. Nakagawa, "Low power optical interconnect at 10 Gbps with high efficiency 1060 nm VCSEL," in *Proc. CLEO/QELS*, San Jose, CA, 2010, pp. 1–2, paper CWP3.

[11] K. Yang, C. P. Hains, J. Cheng, and A. A. Allerman, "Efficient double intracavity-contacted vertical-cavity surface-emitting lasers with very low-threshold and low-power dissipation designed for cryogenic application," *IEEE Photon. Technol. Lett.*, vol. 12, no. 2, pp. 113–115, Feb. 2000.

[12] F. Koyama, D. Schlenker, T. Miyamoto, Z. Chen, A. Matsutani, T. Sakaguchi, and K. Iga, "1.2 μm highly strained GaInAs/GaAs quantum well lasers for singlemode fiber data link," *Electron. Lett.*, vol. 35, no. 13, pp. 1079–1081, Jun. 1999.

[13] N. Tansu and J. L. Mast, "High-performance strain-compensated InGaAs-GaAsP-GaAs ($l = 1.17$ μm) quantum well lasers," *IEEE Photon. Technol. Lett.*, vol. 13, no. 3, pp. 179–181, Mar. 2001.

[14] K. Takaki, N. Iwai, K. Hiraiwa, S. Imai, H. Shimizu, T. Kageyama, Y. Kawakita, N. Tsukiji, and A. Kasukawal, "A recorded 62% PCE and low series and thermal resistance VCSEL with a double intra-cavity structure," in *Proc. 21st ISLC*, Sorrento, Italy, 2008, Paper PDP1.

[15] K. Takaki, N. Iwai, S. Kamiya, H. Shimizu, K. Hiraiwa, S. Imai, Y. Kawakita, T. Takagi, T. Ishikawa, N. Tsukiji, and A. Kasukawa, "Experimental demonstration of low jitter performance and high reliable 1060 nm VCSEL arrays for 10 G $\times$ 12 ch optical interconnection," in *Proc. SPIE*, 2010, vol. 7615, p. 761 502.

Optical Networking Beyond WDM

Peter J. Winzer, *Fellow, IEEE*

(Invited Paper)

Bell Labs, Alcatel-Lucent, Holmdel, NJ 07733 USA

DOI: 10.1109/JPHOT.2012.2189379
1943-0655/$31.00 ©2012 IEEE

Manuscript received February 15, 2012; accepted February 19, 2012. Date of current version April 20, 2012. This paper is based on a plenary talk given at the Photonics Society Annual Meeting, 2011. The paper is dedicated to Prof. Walter R. Leeb, Technical University of Vienna, Austria, on the occasion of his 70th birthday and to Dr. Herwig Kogelnik, Bell Labs, USA, on the occasion of his 80th birthday. (e-mail: peter.winzer@bell-labs.com).

Abstract: Wavelength-division multiplexing (WDM) has been the workhorse of data networks, accommodating exponential traffic growth for two decades. Recently, however, progress in WDM capacity research has markedly slowed down as experiments are closely approaching fundamental Shannon limits of nonlinear fiber transmission. Space-division multiplexing (SDM) is expected to further scale network capacities, using parallel strands of single-mode fiber, uncoupled or coupled cores of multicore fiber, or even individual modes of few-mode fiber in combination with multiple-input–multiple-output (MIMO) digital signal processing. At the beginning of a new era in optical communications, we review initial research in SDM technologies and address some of the key challenges ahead.

Index Terms: Wavelength-division multiplexing, spatial multiplexing, space-division multiplexing (SDM).

1. Exponentially Increasing Traffic Demands and the Role of WDM

Network traffic has been growing exponentially over the past two decades, at 30 to 60% per year, depending on the nature and penetration of services offered by network operators in different geographic regions [1], [2]. The growing number of applications relying on machine-to-machine traffic and cloud computing are accelerating this growth for data-centric operators as the network is increasingly taking the role of a distributed computer interface, whose bandwidth demands are proportional to the system's processing power due to Amdahl's rule of thumb [3], and are hence evolving at close to 90% per year [4].

The demand for communication bandwidth has been economically met by wavelength-division multiplexing (WDM), researched, developed, and abundantly deployed since the early 1990s [5]. At first, WDM capacities increased at around 80% per year, predominantly through improvements in optoelectronic device technologies. By the early 2000s, lasers had reached Gigahertz frequency stabilities, optical filters had bandwidths allowing for 50-GHz WDM channel spacings, and 40-Gb/s optical signals filled up these frequency slots. At this remarkable point in time where "optical and electronic bandwidths met," optical communications had to shift from physics toward communications engineering to increase spectral efficiencies, i.e., to pack more information into the limited ($\sim$5-THz) bandwidth of optical amplifiers. Consequently, the last decade has seen a vast adoption of concepts from radio-frequency communications, such as advanced modulation formats [6], coherent detection [7], considered mostly for free-space applications over the past two decades [8], and sophisticated digital signal processing (DSP) [9]. The transition to digital coherent systems was aided by the fact that coherent detection naturally enables the exploitation of both quadratures and

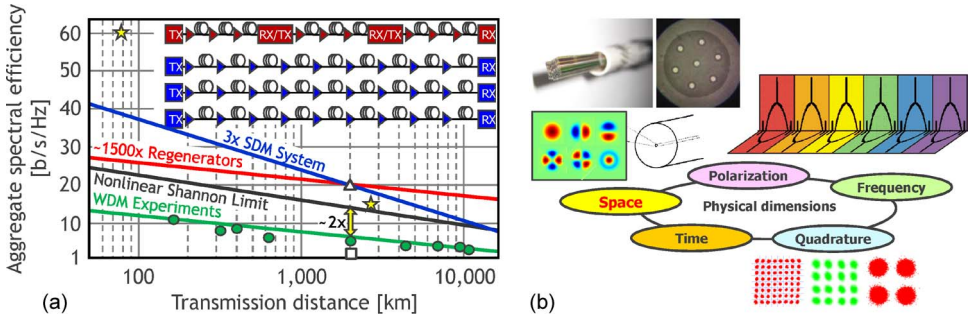

Fig. 1. (a) Tradeoff between spectral efficiency and reach of WDM experiments (green), approaching the nonlinear Shannon limit (black) to within a factor of 2. For a realistic spectral efficiency and distance target (triangle), regenerated systems (red) need about 500 times more transponders than parallel (SDM) systems (blue). (b) Today's WDM products exploit all physical dimensions but space.

polarizations of the optical field, which reduced symbol rates by a factor of 4 and brought signals within the reach of fast analog-to-digital converters (ADCs). Commercial coherent systems for fiber-optic networks were introduced at 40 and 100 Gb/s in 2008 and 2010, using polarization-division multiplexed (PDM) quadrature phase-shift keying (QPSK) at 11.5 and 28 GBaud, based on custom-designed CMOS ASICs to handle the massive required DSP functions for adaptive polarization tracking, chromatic dispersion compensation, and forward error correction (FEC).

Today's commercial WDM systems transmit close to 10 Tb/s of traffic at 100 Gb/s per wavelength. In research, interface rates of 640 Gb/s have been achieved using polarization multiplexed quadrature amplitude modulation (QAM) at a symbol rate of 80 GBaud [10]. Higher interface rates of 1 Tb/s and beyond are achieved through orthogonal frequency division multiplexed (OFDM) coherent optical superchannels [11], and the 100-Tb/s per-fiber capacity mark has recently been reached [12], [13]. However, capacities of conventional single-mode fiber systems are not expected to grow much further. Capacity increases in WDM research have slowed down from about 80% per year in the 1990s to about 20% per year since 2002, with a similar trend observed in commercial systems [1], [6]. This trend is explained by recent studies on the nonlinear Shannon capacity of optical networks [14]: Research experiments have approached their fundamental limits to within a factor of $\sim$2. This is visualized in Fig. 1(a), showing the February 2012 status of experimental WDM research spectral efficiencies (green, circles) together with the nonlinear Shannon limit [14] (black) versus transmission distance. More spectrally efficient higher-order modulation comes at the expense of reduced transmission reach due to a lower tolerance to optical amplifier noise and other signal impairments of practical importance such as laser phase noise, ADC resolution, or crosstalk. Advances in low-loss or low-nonlinearity fiber will not be able to change this picture significantly [15]. Today's commercial systems, operating at $\sim$2 b/s/Hz over $\sim$2000 km of fiber, are represented by the open square in Fig. 1(a). Assuming a 30 to 60% traffic growth per year, spectral efficiencies of 20 b/s/Hz (over the same, geography-enforced distances) will be needed in commercial systems within 5 to 10 years (open triangle), which is well beyond the Shannon limit. This observation leads to the notion of an imminent "*optical networks capacity crunch*" [16].

2. Spatial Multiplexing to Overcome the Capacity Crunch

Fig. 1(a) compares two approaches that may be taken to scale network capacities. The first option uses a concatenation of high-spectral-efficiency systems, shifting the baseline curve (green) to the right (red) by the number of regeneration spans. The scalability problem of this solution is immediately evident: With today's experimental records as a baseline, a target spectral efficiency of 20 b/s/Hz over 2000 km would require around 1500 1.3-km regeneration spans using, e.g., PDM 4096-QAM with rectangular spectral shaping and about 20% FEC overhead. In contrast, a parallel

approach may be taken. This can be done using multiple optical amplification bands or, likely more scalably, multiple parallel optical paths, referred to as *spatial multiplexing* or *space-division multiplexing (SDM)*: With just 3 parallel optical paths at 7 bits/s/Hz each (e.g., using PDM 32-QAM), the desired aggregate capacity is achieved with a total of 3 transponders. The almost 3 orders of magnitude difference in transponder count between the two solutions clearly points to SDM as the preferred solution for network capacity growth [17]. Looking at Fig. 1(b), which shows the known physical dimensions that can be exploited for optical modulation and multiplexing, SDM appears to be the *only* option to significantly scale optical system capacities.

Deploying SDM in its most trivial form by using parallel optical line systems is a scalable but not yet an economically sustainable path forward, since it still does not reduce the cost or energy per bit compared with today's systems: M parallel systems carry M times the capacity at M times the cost or energy. Commercially successful SDM technologies will be expected to scale capacity with a similar per-bit cost and energy reduction as WDM ($\sim$20% per year [18]), leveraging *integration* and sharing system components among spatial and spectral channels. Integration may take place on a system and network level, on a transponder [19], [20] and DSP level, on an optical amplifier level [21], [22], and on a fiber level [23]–[25]. Since integration generally comes at the expense of *crosstalk* among parallel paths, proper crosstalk management will be an important aspect of SDM systems. In addition, SDM will have to allow for smooth system upgrades, reusing as much as possible the deployed WDM infrastructure. Initial global efforts in SDM research are reviewed in [26] and [27].

2.1. Spatial Multiplexing in the Low-Crosstalk Regime

Whether a given level of crosstalk can be treated as a system impairment or needs to be actively compensated depends on the underlying modulation format; while QPSK tolerates as much as -15 dB of crosstalk for a 1-dB signal-to-noise ratio penalty, 64-QAM tolerates only about -30 dB [28]. A key challenge associated with nominally uncoupled SDM systems will hence be to ensure sufficiently low crosstalk over long-haul, optically networked transmission distances, including integrated transponders, amplifiers, splices, connectors, SDM fibers, and network elements such as spatial and spectral crossconnects.

Recently, low-crosstalk 7-core [29], [30] and 19-core [31] fiber for SDM has been reported, and impressive system experiments have been performed, including record per-fiber capacities of 109 Tb/s [32], 112 Tb/s [29], and 305 Tb/s [31] over up to several ten kilometers, as well as Tb/s SDM transmission over 2688 km [33] and an aggregate per-fiber spectral efficiency of 60 b/s/Hz [34]. The latter two results are visualized by yellow asterisks in Fig. 1(a), well beyond the nonlinear Shannon limit for single-mode fiber.

2.2. Spatial Multiplexing With High Crosstalk and MIMO Processing

If crosstalk rises to levels where it induces unacceptable transmission penalties, *multiple-input–multiple-output (MIMO)* techniques, originally developed for wireless systems [35], can be used. If SDM transponders are able to selectively excite and coherently detect the complete orthonormal set of modes whose propagation is supported by the transmission waveguide, and if the transmission properties of each mode in terms of fiber nonlinearities and noise are comparable with those of a single-mode waveguide, a reliable M-fold capacity gain can be achieved [36]. Some of the key challenges associated with MIMO-SDM systems are the implementation of scalable coupled-mode waveguides with differential group delays small enough to be handled by MIMO-DSP, of optical amplifiers with low mode-dependent gain and noise variations, as well as of spatial and spectral crossconnects operating outside the well-defined boundaries of single-mode optics. Importantly, tradeoffs between linear and nonlinear coupled-mode optical propagation characteristics and the need for joint optoelectronic interfacing, digitizing, and MIMO processing of M high-speed signals will limit the maximum feasible number of coupled modes. Determining the right balance between coupled and uncoupled SDM transmission paths, both from an optical and from an electronic point of view, will hence be a critical consideration in the evolution of SDM technologies.

Recently, several impressive experimental demonstrations of coupled-mode MIMO-SDM transport have been reported, including up to 4200-km transmission of six spatial and polarization modes over microstructured [37] and few-mode [38] fiber, MIMO-SDM using up to 5 partially coupled spatial modes [39], and discrete [40], [41] as well as distributed Raman [42] amplification of few-mode signals.

3. Conclusions

After a decade of physics-oriented WDM research followed by a decade of applying advanced communications engineering principles to fiber-optic systems, optical transport networks research is entering the new era of spatial multiplexing, which presents a large number of interdisciplinary challenges to develop technologies that may be able to overcome the looming optical network capacity crunch.

Acknowledgment

The author is grateful for discussions with S. Chandrasekhar, A. Chraplyvy, C. Doerr, R.-J. Essiambre, G. Foschini, A. Gnauck, H. Kogelnik, S. Korotky, X. Liu, S. Randel, G. Raybon, R. Ryf, and R. Tkach.

References

[1] R. W. Tkach, "Scaling optical communications for the next decade and beyond," *Bell Labs Tech. J.*, vol. 14, no. 4, pp. 3–9, Feb. 2010.
[2] S. K. Korotky, "Traffic trends: Drivers and measures of cost-effective and energy-efficient technologies and architectures for backbone optical networks," in *Proc. OFC/NFOEC*, Los Angeles, CA, 2012, Paper OM2G.1.
[3] J. Gray and P. Shenoy, "Rules of thumb in data engineering," Microsoft Res., Redmond, WA, Tech. Rep. MS-TR-99-100, 2000.
[4] [Online]. Available: http://top500.org/lists/2010/06/performance
[5] H. Kogelnik, "On optical communication: Reflections and perspectives," in *Proc. ECOC*, Stockholm, Sweden, 2004, Paper Mo1.1.1.
[6] P. J. Winzer, "Beyond 100G Ethernet," *IEEE Commun. Mag.*, vol. 48, no. 7, pp. 26–30, Jul. 2010.
[7] H. Sun, K. T. Wu, and K. Roberts, "Real-time measurements of a 40 Gb/s coherent system," *Opt. Exp.*, vol. 16, no. 2, pp. 873–879, Jan. 2008.
[8] W. R. Leeb, "Coherent optical space communications," in *Advanced Methods for Satellite and Deep Space Communications*, J. Hagenauer, Ed., 1992, ISBN 978-3-540-55851-4.
[9] S. J. Savory, "Digital filters for coherent optical receivers," *Opt. Exp.*, vol. 16, no. 2, pp. 804–817, Jan. 2008.
[10] G. Raybon, A. L. Adamiecki, S. Randel, C. Schmidt, P. J. Winzer, A. Konczykowska, F. Jorge, J.-Y. Dupuy, L. L. Buhl, S. Chandrasekhar, X. Liu, A. H. Gnauck, C. Scholz, and R. Delbue, "All-ETDM 80-Gbaud (640-Gb/s) PDM 16-QAM Generation and Coherent Detection," *Photon. Technol. Lett.*, 2012, submitted for publication.
[11] X. Liu and S. Chandrasekhar, "Beyond 1-Tb/s superchannel transmission," in *Proc. IEEE Photonics Conf.*, Arlington, VA, 2011, Paper ThBB1.
[12] D. Qian, M.-F. Huang, E. Ip, Y.-K. Huang, Y. Shao, J. Hu, and T. Wang, "101.7-Tb/s (370 × 294-Gb/s) PDM-128QAM-OFDM transmission over 3 × 55-km SSMF using pilot-based phase noise mitigation," in *Proc. OFC/NFOEC*, Los Angeles, CA, 2011, Paper PDPB5.
[13] A. Sano, T. Kobayashi, S. Yamanaka, A. Matsuura, H. Kawakami, Y. Miyamoto, K. Ishihara, and H. Masuda, "102.3-Tb/s (224 × 548-Gb/s) C- and extended L-band all-Raman transmission over 240 km using PDM-64QAM single carrier FDM with digital pilot tone," in *Proc. OFC/NFOEC*, Los Angeles, CA, 2012, Paper PDP5C.3.
[14] R.-J. Essiambre, G. Kramer, P. J. Winzer, G. J. Foschini, and B. Goebel, "Capacity limits of optical fiber networks," *J. Lightwave Technol.*, vol. 28, no. 4, pp. 662–701, Feb. 2010.
[15] R.-J. Essiambre, "Impact of fiber parameters on nonlinear fiber capacity," in *Proc. OFC/NFOEC*, Los Angeles, CA, 2011, Paper OTuJ1.
[16] A. R. Chraplyvy, "The coming capacity crunch," in *Proc. ECOC*, Vienna, Austria, 2009, plenary talk.
[17] P. J. Winzer, "Energy-efficient optical transport capacity scaling through spatial multiplexing," *IEEE Photon. Technol. Lett.*, vol. 23, no. 13, pp. 851–853, Jul. 2011.
[18] R. S. Tucker, "Green optical communications—Part I: Energy limitations in transport," *IEEE J. Sel. Topics Quantum Electron.*, vol. 17, no. 2, pp. 245–260, Mar./Apr. 2011.
[19] C. R. Doerr and T. F. Taunay, "Silicon photonics core-, wavelength-, and polarization-diversity receiver," *IEEE Photon. Technol. Lett.*, vol. 23, no. 9, pp. 597–599, May 2011.
[20] B. G. Lee, D. M. Kuchta, F. E. Doany, C. L. Schow, C. Baks, R. John, P. Pepeljugoski, T. F. Taunay, B. Zhu, M. F. Yan, G. E. Oulundsen, D. S. Vaidya, W. Luo, and N. Li, "120-Gb/s 100-m transmission in a single multicore multimode fiber containing six cores interfaced with a matching VCSEL array," in *Proc. IEEE Photonics Soc. Summer Topical Meeting*, 2010, Paper TuD4.4.

[21] P. M. Krummrich, "Optical amplification and optical filter based signal processing for cost and energy efficient spatial multiplexing," *Opt. Exp.*, vol. 19, no. 17, pp. 16 636–16 652, Aug. 2011.
[22] K. S. Abedin, T. F. Taunay, M. Fishteyn, M. F. Yan, B. Zhu, J. M. Fini, E. M. Monberg, F. V. Dimarcello, and P. W. Wisk, "Amplification and noise properties of an erbium-doped multicore fiber amplifier," *Opt. Exp.*, vol. 19, no. 17, pp. 16 715–16 721, Aug. 2011.
[23] T. Morioka, "New generation optical infrastructure technologies: EXAT initiative towards 2020 and beyond," in *Proc. OECC*, Hong Kong, 2009, Paper FT4.
[24] Y. Kokubun and M. Koshiba, "Novel multi-core fibers for mode division multiplexing: proposal and design principle," *IEICE Electron. Exp.*, vol. 6, no. 8, pp. 522–528, Apr. 2009.
[25] S. K. Korotky, "Price-points for components of multi-core fiber communication systems in backbone optical networks," *J. Opt. Netw.*, 2011, submitted for publication.
[26] G. Li and X. Liu, "Focus issue: Space multiplexed optical transmission," *Opt. Exp.*, vol. 19, no. 17, pp. 16 574–16 575, Aug. 2011.
[27] T. Morioka, Y. Awaji, R. Ryf, P. Winzer, D. Richardson, and F. Poletti, "Enhancing optical communications with brand new fibers," *IEEE Commun. Mag.*, vol. 50, no. 2, pp. s31–s42, Feb. 2012.
[28] P. J. Winzer, A. H. Gnauck, A. Konczykowska, F. Jorge, and J.-Y. Dupuy, "Penalties from in-band crosstalk for advanced optical modulation formats," in *Proc. ECOC*, Geneva, Switzerland, 2011, Paper Tu.5.B.7.
[29] B. Zhu, T. F. Taunay, M. Fishteyn, X. Liu, S. Chandrasekhar, M. F. Yan, J. M. Fini, E. M. Monberg, and F. V. Dimarcello, "112-Tb/s Space-division multiplexed DWDM transmission with 14-b/s/Hz aggregate spectral efficiency over a 76.8-km seven-core fiber," *Opt. Exp.*, vol. 19, no. 17, pp. 16 665–16 671, Aug. 2011.
[30] T. Hayashi, T. Taru, O. Shimakawa, T. Sasaki, and E. Sasaoka, "Design and fabrication of ultra-low crosstalk and low-loss multi-core fiber," *Opt. Exp.*, vol. 19, no. 17, pp. 16 576–16 592, Aug. 2011.
[31] J. Sakaguchi, B. J. Puttnam, W. Klaus, Y. Awaji, N. Wada, A. Kanno, T. Kawanishi, K. Imamura, H. Inaba, K. Mukasa, R. Sugizaki, T. Kobayashi, and M. Watanabe, "19-core fiber transmission of 19 $\times$ 100 $\times$ 172-Gb/s SDM-WDM-PDM-QPSK signals at 305Tb/s," in *Proc. OFC/NFOEC*, Los Angeles, CA, 2012, Paper PDP5C.1.
[32] J. Sakaguchi, Y. Awaji, N. Wada, A. Kanno, T. Kawanishi, T. Hayashi, T. Taru, T. Kobayashi, and M. Watanabe, "109-Tb/s (7 $\times$ 97 $\times$ 172-Gb/s SDM/WDM/PDM) QPSK transmission through 16.8-km homogeneous multi-core fiber," in *Proc. OFC/NFOEC*, Los Angeles, CA, 2011, Paper PDPB6.
[33] S. Chandrasekhar, A. H. Gnauck, X. Liu, P. J. Winzer, Y. Pan, E. C. Burrows, B. Zhu, T. F. Taunay, M. Fishteyn, M. F. Yan, J. M. Fini, E. M. Monberg, and F. V. Dimarcello, "WDM/SDM transmission of 10 $\times$ 128-Gb/s PDM-QPSK over 2688-km 7-core fiber with a per-fiber net aggregate spectral-efficiency distance product of 40 320 km b/s/Hz," in *Proc. ECOC*, Geneva, Switzerland, 2011, Paper Th.13.C.4.
[34] X. Liu, S. Chandrasekhar, X. Chen, P. J. Winzer, Y. Pan, T. F. Taunay, B. Zhu, M. Fishteyn, M. F. Yan, J. M. Fini, E. M. Monberg, and F. V. Dimarcello, "1.12-Tb/s 32-QAM-OFDM superchannel with 8.6-b/s/Hz intrachannel spectral efficiency and space-division multiplexing with 60-b/s/Hz aggregate spectral efficiency," in *Proc. ECOC*, Geneva, Switzerland, 2011, Paper Th.13.B.1.
[35] G. J. Foschini, "Layered space-time architecture for wireless communication in a fading environment when using multi-element antennas," *Bell Labs Tech. J.*, vol. 1, no. 2, pp. 41–59, Summer 1996.
[36] P. J. Winzer and G. J. Foschini, "MIMO capacities and outage probabilities in spatially multiplexed optical transport systems," *Opt. Exp.*, vol. 19, no. 17, pp. 16 680–16 696, Aug. 2011.
[37] R. Ryf, R.-J. Essiambre, A. H. Gnauck, S. Randel, M. A. Mestre, C. Schmidt, P. J. Winzer, R. Delbue, P. Pupalaikis, A. Sureka, T. Hayashi, T. Taru, and T. Sasaki, "Space-division multiplexed transmission over 4200 km 3-core microstructured fiber," in *Proc. OFC/NFOEC*, Los Angeles, CA, 2012, Paper PDP5C.2.
[38] S. Randel, R. Ryf, A. H. Gnauck, M. A. Mestre, C. Schmidt, R.-J. Essiambre, P. J. Winzer, R. Delbue, P. Pupalaikis, A. Sureka, Y. Sun, X. Jiang, and R. Lingle, "Mode-multiplexed 6 $\times$ 20-GBd QPSK transmission over 1200-km DGD-compensated few-mode fiber," in *Proc. OFC/NFOEC*, Los Angeles, CA, 2012, Paper PDP5C.5.
[39] C. Koebele, M. Salsi, L. Milord, R. Ryf, C. Bolle, P. Sillard, S. Bigo, and G. Charlet, "40 km transmission of five mode division multiplexed data streams at 100 Gb/s with low MIMO-DSP complexity," in *Proc. ECOC*, Geneva, Switzerland, 2011, Paper Th.13.C.3.
[40] Y. Yung, S. Alam, Z. Li, A. Dhar, D. Giles, I. Giles, J. Sahu, L. Gruner-Nielsen, F. Poletti, and D. J. Richardson, "First demonstration of multimode amplifier for spatial division multiplexed transmission systems," in *Proc. ECOC*, Geneva, Switzerland, 2011, Paper Th.13.K.4.
[41] E. Ip, N. Bai, Y.-K. Huang, E. Mateo, F. Yaman, M.-J. Li, S. Bickham, S. Ten, J. Linares, C. Montero, V. Moreno, X. Prieto, V. Tse, K. M. Chung, A. Lau, H.-Y. Tam, C. Lu, Y. Luo, G.-D. Peng, and G. Li, "88 $\times$ 3 $\times$ 112-Gb/s WDM transmission over 50 km of three-mode fiber with inline few-mode fiber amplifier," in *Proc. ECOC*, Geneva, Switzerland, 2011, Paper Th.13.C.2.
[42] R. Ryf, A. Sierra, R. Essiambre, S. Randel, A. H. Gnauck, C. Bolle, M. Esmaeelpour, P. J. Winzer, R. Delbue, P. Pupalaikise, A. Sureka, D. W. Peckham, A. McCurdy, and R. Lingle, "Mode-equalized distributed Raman amplification in 137-km few-mode fiber," in *Proc. ECOC*, Geneva, Switzerland, 2011, Paper Th.13.K.5.

Energy-Efficient VCSELs for Interconnects

Werner H. Hofmann,[1] *Member, IEEE*, Philip Moser,[1] and Dieter Bimberg,[1,2] *Fellow, IEEE*

(Invited Paper)

[1]Institute of Solid State Physics and Center of Nanophotonics, Technical University of Berlin, 10623 Berlin, Germany
[2]King Abdulaziz University, Jeddah 22254, Saudi Arabia

DOI: 10.1109/JPHOT.2012.2190500
1943-0655/$31.00 ©2012 IEEE

Manuscript received February 16, 2012; revised February 27, 2012; accepted March 6, 2012. Date of current version April 20, 2012. The lasers in the 850-nm waveband described here were developed at the Technical University of Berlin in cooperation with Vertically Integrated Systems GmbH, Hardenbergstraße 7, 10623 Berlin, Germany. Commercial samples are in progress. This work was supported by the German Science Foundation (DFG) through the Collaborative Research Centre SFB 787. Corresponding author: W. Hofmann (e-mail: Werner.Hofmann@tu-berlin.de).

Abstract: Vertical-cavity surface-emitting lasers (VCSELs) are particularly suited for energy-efficient optical interconnects in supercomputing. Consequently, several groups are developing VCSELs for energy-efficient interconnects with remarkable success. We give an overview over recent breakthroughs and present devices at the standard wavelength of 850 nm with record-low power consumption and heat dissipation per bit, achieving a value of only 69 mW/Tb/s at 17 Gb/s. This efficiency is exceeding the International Technology Roadmap for Semiconductors (ITRS) projection of 100 mW/Tb/s for 2015. If uncooled operation, ultradense arrays with smallest footprints, and highest ambient temperatures are required, the waveband around 1 μm is advantageous. At 980 nm, we could achieve an efficiency value in this waveband of 233 mW/Tb/s at an error-free 35 Gb/s.

Index Terms: Vertical-cavity surface-emitting laser (VCSEL), high-speed modulation, optical interconnects, energy-efficiency, green photonics.

1. Energy-Efficient Data Transmission

The exponential growth of Internet traffic is taken as an indicator for development and progress. On the other hand, this also means that the power consumed by data centers continues to grow exponentially. Keeping limited natural resources in mind, "green IT" is a crucial subject. As the copper-based interconnect technology is inefficient, expensive and slow, the transition to optical interconnects has become reality [1], [2]. With most of the power being consumed by sending data via interconnects within and between racks of servers, the power consumption of data centers is rapidly becoming environmentally significant [3]. According the International Technology Roadmap for Semiconductors (ITRS), lasers for future optical interconnects should highly energy efficient. In 2015, energy-efficient high-speed lasers operating at 100 mW/Tb/s (100 fJ/bit) will be required [3], [4]. These numbers refer to the *dissipated electrical energy* per bit to fit the cooling budget of the data center. We define this figure of merit as heat-to-bit rate (*HBR*) ratio [5] (in milliwatts per Terabit per second)

$$HBR = P_{diss}/BR \tag{1}$$

where P_{diss} is the dissipated heat ($P_{\text{diss}} = P_{\text{el}} - P_{\text{optical}}$) of the laser, and BR is the bit rate. We believe that "green photonics" means that the *total energy* consumed per transmitted amount of data is of

TABLE 1
Recent accomplishments in the field of energy-efficient VCSELs

Affiliation	TUB/VIS[5]	NCU/NTU[19]	Chalmers[11]	TUB[20]	UCSB[16]	Furukawa[9]
Bit rate (Gb/s)	17/25	12.5	32	35	35	10
EDR (fJ/bit)	83/117	227	470	287	357	180
HBR (mW/Tbps)	69/99	109	330	233	286	140
Wavelength (nm)	850	850	850	980	980	1060
Year of publication	2011	2011	2009	2011	2009	2010

equal importance [5]. Therefore, we define the electrical energy-to-data ratio (*EDR*, fJ/bit)

$$EDR = P_{el}/BR \tag{2}$$

where $P_{el} = V \cdot I$ is the total consumed electrical power with V and I as the laser's operating bias point. Additionally, the modulation power absorbed by the laser should be taken into account. Even though, depending on the used electronics, it might be the case that the power actually consumed in the vertical-cavity surface-emitting laser (VCSEL) is smaller than the power needed by the driving electronics, we believe that it is the most crucial one. This is due to its multiplier effect of the energy consumed by the light-source on the power consumption of the whole system. Note that efficiency per bit is not the same as the wall-plug efficiency (*WPE*), which can actually be expressed in terms of *HBR* and *EDR*

$$WPE = 1 - HBR/EDR. \tag{3}$$

Furthermore, this means that the most power-efficient lasers in terms of data transmission are not necessarily the lasers with the highest *WPE*, nor is the driving condition for best *HBR* or *EDR* identical to the point of highest *WPE*.

Having explained the need for energy-efficient interconnects and having defined the figures of merit, we would like to state, that we believe that the VCSEL technology can be a workhorse for energy-efficient links. For IBM's Terabus project the GaAs-based VCSELs with wavelengths of 985 nm and 850 nm were evaluated with the 850-nm waveband having the advantage of being commercially available at that time [6]. Efficient high-speed VCSELs have been developed in the wavebands from 850 nm to 1550 nm [7] and can be potentially optimized for highest data-transmission efficiencies. In 2011, the topic of Green Photonics has become in the focus of public and scientific interest. Conferences focusing on that topic and scientific awards acknowledging achievements in this field were initiated [8]. VCSELs operating at 10 Gb/s at 1060 nm with 140 mW/Tb/s *HBR* have been reported lately [9]. Longer wavelengths use less energy per photon and have therefore an intrinsic advantage. Furthermore, active materials with better gain properties can be used [10]. Nevertheless, 850 nm remains the current standard wavelength for fiber-based links. On the other hand, for the application in short optical interconnects also proprietary solutions with other wavelengths can address the market. Vast efforts have been made in boosting both bit rate [10]–[15], [17], [18], [20] and energy efficiency [5], [8], [9], [11], [14], [16], [19]–[21] significantly to meet the requirements of future data centers and supercomputers. The recent major accomplishments in the field of energy-efficient interconnects are summarized in Table 1. Researchers in Taiwan could demonstrate single-mode devices with high *WPEs* and a remarkable *HBR* of 109 mW/Tb/s [19]. Note that higher bit rates require a quadratic increase in current densities at a given device-technology. This makes energy-efficient devices operating at higher bit-rates more challenging. *EDR* of 500 fJ/bit or more are usually needed to achieve bit-rates of 30 Gb/s or more [11]. Consequently, at bit-rates as high as 35-Gb/s *HBR* and *EDR* values on the order of 200–300 fJ/bit are also outstanding results [16], [20].

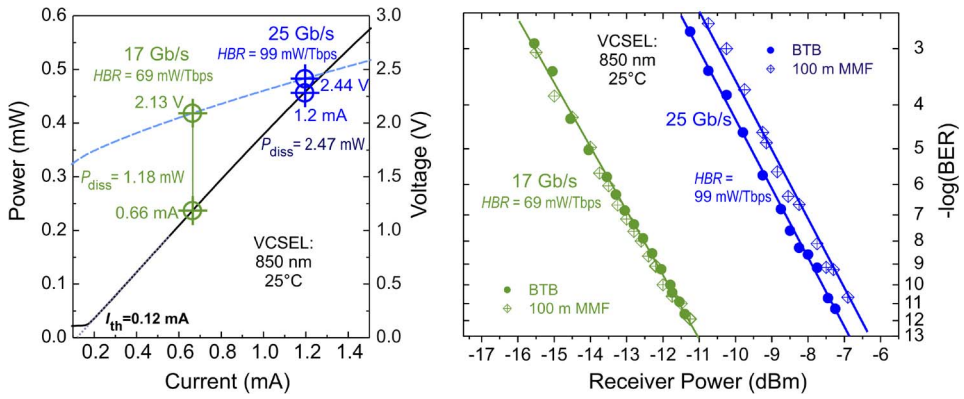

Fig. 1. Energy-efficient 850-nm VCSEL, room temperature: (Left) LIV-characteristics; the biasing point of the data-transmission experiment is indicated. (Right) Bit-error-rate measurement of that device at 17 Gb/s and 25 Gb/s. Energy efficiency: 17 Gb/s: HBR = 69 mW/Tb/s, EDR = 83 fJ/bit, Modulation energy = 10 fJ/bit 25 Gb/s: HBR = 99 mW/Tb/s, EDR = 117 fJ/bit, Modulation energy = 6 fJ/bit.

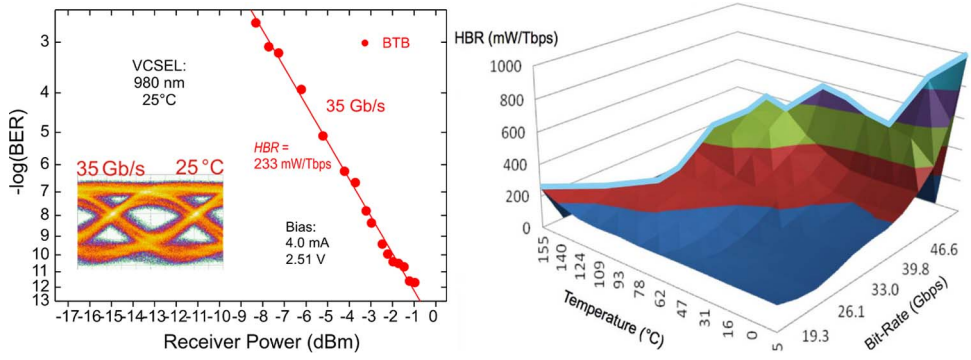

Fig. 2. Energy-efficient 980-nm VCSEL. (Left) Bit-error-rate measurement of that device at 35-Gb/s. Energy efficiency: HBR = 233 mW/Tb/s, EDR = 287 fJ/bit, Modulation energy = 26 fJ/bit. (Right) Dependence of Energy efficiency (here: HBR) on ambient temperature and bit-rate.

After having summarized the major accomplishments on energy-efficient VCSELs for optical interconnects achieved in 2011, we give some details on the achievements made at the Center of Nanophotonics at the Technical University of Berlin.

2. Energy-Efficient VCSELs for Interconnects

In a first-order approximation, for a given directly modulated VCSEL device, the resonance frequency rises with the square root of the VCSEL power. Therefore, it is trivial to understand that high-speed VCSELs typically consume more energy per bit when they are operated at higher bit rates. However, VCSELs designed to work at ultrahigh bit rates do not necessarily get more energy efficient just by simply reducing the pumping current and the bit rate. In order to realize energy-efficient high-speed performance, large resonance frequencies must be achieved at a low drive current. We characterized our latest VCSELs optimized for highest energy efficiency at different wavelengths and modulation speeds by transmission experiments characterizing the bit error rate (BER) with standard nonreturn-to-zero (NRZ) coding and a $2^7 - 1$ bit pattern length. The results for the 850-nm devices are given in Fig. 1. The *HBR* is 69 mW/Tb/s at 17 Gb/s and 99 mW/Tb/s at 25 Gb/s, respectively. A 100-m fiber link shows negligible power penalties. By heating up the device to 55 °C, we yield a record-low *EDR* of 81 fJ/bit and an *HBR* of 70 mW/Tb/s at 17 Gb/s. Data transmission over 1 km of multimode fiber is has also been accomplished [21].

In order to determine the modulation energy dissipated, we measure the true root mean square power absorbed by the VCSEL at the respective bit rate and modulation voltage.

In Fig. 2, we show the results of our 980-nm devices. The BER measurement with corresponding eye is presented in the left figure. Error-free data transmission at 35 Gb/s was accomplished at efficiencies of $EDR = 287$ fJ/bit and $HBR = 233$ mW/Tb/s. These devices also allow operation in a wide temperature range with little impact on the device performance [10]. Record-high data rates and efficiencies are not achieved at the same driving conditions, on the right-hand side of Fig. 2. On the other hand, as the efficiency of the device is not affected by ambient temperature in a wide range, uncooled systems saving large amounts energy are feasible.

3. Conclusion

In 2011, record energy-efficient directly modulated high-speed VCSELs were presented by several groups. Record error-free operation at data rates of 10 to 35 Gb/s could be achieved with NRZ coding at wavelengths ranging from 850 nm to 1060 nm. A total energy consumption within the VCSEL device of only 93 fJ/bit is sufficient for data transmission at 17 Gb/s. The devices are based on the mature GaAs-VCSEL technology and are suitable for industrial mass-fabrication in existing foundries. Based on this kind of devices, energy-efficient interconnects can be realized.

Acknowledgment

The lasers in the 850-nm waveband described here were developed in cooperation with Vertically Integrated Systems GmbH. The authors would like to acknowledge J. A. Lott and N. N. Ledentsov for contributing the vertical layer design. Commercial samples by VI-Systems are in progress. The authors also would like to thank P. Wolf, G. Larisch, and W. Unrau for their contribution in processing and measurement.

References

[1] M. Taubenblatt, "Optical interconnects for high-performance computing," *J. Lightwave Technol.*, vol. 30, no. 4, pp. 448–457, Feb. 2012.

[2] L. Huff, "State of the short-reach optics market," presented at the Optical Fiber Commun. Conf. (OFC/NFOEC), Los Angeles, CA, 2011, Paper OMV5.

[3] D. Miller, "Device requirements for optical interconnects to silicon chips," *Proc. IEEE*, vol. 97, no. 7, pp. 1166–1185, Jul. 2009.

[4] *International Technology Roadmap for Semiconductors*, 2007, Internet website accessed Jan. 2012. [Online]. Available: http://www.itrs.net/Links/2007ITRS/ExecSum2007.pdf

[5] P. Moser, W. Hofmann, W. P. Wolf, J. Lott, G. Larisch, A. Payusov, N. Ledentsov, and D. Bimberg, "81 fJ/bit energy-to-data ratio of 850 nm vertical-cavity surface-emitting lasers for optical interconnects," *Appl. Phys. Lett.*, vol. 98, no. 23, pp. 231 106-1–231 106-3, Jun. 2011.

[6] L. Schares, J. Kash, F. Doany, C. Schow, C. Schuster, D. Kuchta, P. Pepeljugoski, J. Trewhella, C. Baks, R. John, L. Shan, Y. Kwark, R. Budd, P. Chiniwalla, F. Libsch, J. Rosner, C. Tsang, C. Patel, J. Schaub, R. Dangel, F. Horst, B. Offrein, D. Kucharski, D. Guckenberger, S. Hegde, H. Nyikal, C. Lin, A. Tandon, G. Trott, M. Nystrom, D. Bour, M. Tan, and D. Dolfi, "Terabus: Terabit/second-class card-level optical interconnect technologies," *IEEE J. Sel. Topics Quantum Electron.*, vol. 12, no. 5, pp. 1032–1044, Sep./Oct. 2006.

[7] A. Larsson, "Advances in VCSELs for communication and sensing," *IEEE J. Sel. Topics Quantum Electron.*, vol. 17, no. 6, pp. 1552–1567, Nov./Dec. 2011.

[8] P. Moser, J. Lott, P. Wolf, G. Larisch, A. Payusova, G. Fiol, N. Ledentsov, W. Hofmann, and D. Bimberg, "Energy-efficient vertical-cavity surface-emitting lasers (VCSELs) for 'green' data and computer communication," presented at the SPIE, Photonics West—Green Photonics Award in Commun., San Francisco, CA, 2012, Paper 8276-18. [Online]. Available: http://spie.org/x85295.xml

[9] S. Imai, K. Takaki, S. Kamiya, H. Shimizu, J. Yoshida, Y. Kawakita, T. Takagi, K. Hiraiwa, H. Shimizu, T. Suzuki, N. Iwai, T. Ishikawa, N. Tsukiji, and A. Kasukawa, "Recorded low power dissipation in highly reliable 1060-nm VCSELs for 'green' optical interconnection," *IEEE J. Sel. Topics Quantum Electron.*, vol. 17, no. 6, pp. 1614–1620, Nov./Dec. 2011.

[10] W. Hofmann, P. Moser, P. Wolf, G. Larisch, W. Unrau, and D. Bimberg, "980-nm VCSELs for optical interconnects at bandwidths beyond 40 Gb/s," presented at the SPIE, Photonics West, San Francisco, CA, 2012, Paper 8276-4.

[11] P. Westbergh, J. Gustavsson, A. Haglund, A. Larsson, F. Hopfer, G. Fiol, D. Bimberg, and A. Joel, "32 Gbit/s multimode fibre transmission using high-speed, low current density 850 nm VCSEL," *Electron. Lett.*, vol. 45, no. 7, pp. 366–368, Mar. 2009.

[12] P. Westbergh, J. Gustavsson, B. Kögel, A. Haglund, A. Larsson, A. Mutig, A. Nadtochiy, D. Bimberg, and A. Joel, "40 Gbit/s error-free operation of oxide-confined 850 nm VCSEL," *Electron. Lett.*, vol. 46, no. 14, pp. 1014–1016, Jul. 2010.

[13] S. Blokhin, J. Lott, A. Mutig, G. Fiol, N. Ledentsov, M. Maximov, A. Nadtochiy, V. Shchukin, and D. Bimberg, "Oxide confined 850 nm VCSELs operating at bit rates up to 40 Gbit/s," *Electron. Lett.*, vol. 45, no. 10, pp. 501–503, May 2009.
[14] T. Anan, N. Suzuki, K. Yashiki, K. Fukatsu, H. Hatakeyama, T. Akagawa, K. Tokutome, and M. Tsuji, "High-speed 1.1-μm-range InGaAs VCSELs," presented at the Optical Fiber Commun. Conf. (OFC/NFOEC), San Diego, CA, 2008, Paper OThS5.
[15] Y.-C. Chang, C. Wang, and L. Coldren, "High-efficiency, high-speed VCSELs with 35 Gbit/s error-free operation," *Electron. Lett.*, vol. 43, no. 19, pp. 1022–1023, Sep. 2007.
[16] Y. Chang and L. Coldren, "Efficient, high-data-rate, tapered oxide-aperture vertical-cavity surface-emitting lasers," *IEEE J. Sel. Topics Quantum Electron.*, vol. 15, no. 3, pp. 704–715, May/Jun. 2009.
[17] W. Hofmann, P. Moser, P. Wolf, A. Mutig, M. Kroh, and D. Bimberg, "44 Gb/s VCSEL for optical interconnects," presented at the Optical Fiber Commun. Conf. (OFC/NFOEC), San Francisco, CA, 2011, Paper PDPC5.
[18] W. Hofmann, M. Müller, P. Wolf, A. Mutig, T. Gründl, G. Böhm, D. Bimberg, and M.-C. Amann, "40 Gbit/s modulation of 1550 nm VCSEL," *Electron. Lett.*, vol. 47, no. 4, pp. 270–271, Feb. 2011.
[19] J. Shi, W. Weng, F. Kuo, and J. Chyi, "Oxide-relief vertical-cavity surface-emitting lasers with extremely high data-rate/power-dissipation ratios," presented at the Optical Fiber Commun. Conf. (OFC/NFOEC), Los Angeles, CA, 2011, Paper OThG2.
[20] P. Moser, P. Wolf, A. Mutig, G. Larisch, W. Unrau, W. Hofmann, and D. Bimberg, "85 °C error-free operation at 38 Gb/s of oxide-confined 980-nm vertical-cavity surface-emitting lasers," *Appl. Phys. Lett.*, vol. 100, no. 8, pp. 081103-1–081103-3, Feb. 2012.
[21] P. Moser, J. Lott, P. Wolf, G. Larisch, A. Payusov, N. Ledentsov, W. Hofmann, and D. Bimberg, "99 fJ/(bit·km) energy to data-distance ratio at 17 Gb/s across 1 km of multimode optical fiber with 850-nm single-mode VCSELs," *IEEE Photon. Technol. Lett.*, vol. 24, no. 1, pp. 19–21, Jan. 2012.